Ventral hippocampal circuits for the state-dependent control of feeding behaviour

Ryan Wei Shien Wee

A dissertation submitted in partial fulfillment

of the requirements for the degree of

Doctor of Philosophy

of

University College London.

Neuroscience, Physiology and Pharmacology

University College London

November 9, 2020

I, Ryan Wei Shien Wee, confirm that the work presented in this thesis is my own. Where information has been derived from other sources, I confirm that this has been indicated in the work.

Abstract

The hippocampus is classically thought to support spatial cognition and episodic memory, but increasing evidence indicates that the hippocampus is also important for non-spatial, motivated behaviour. Hunger is an internal motivational state that not only directly invigorates behaviour towards food, but can also act as a contextual signal to support adaptive behaviour. Lesions to the hippocampus impair the internal sensing of hunger as a context, and hippocampal neurons express receptors for hunger-related hormones. However, it remains unclear whether the hippocampus is involved in sensing hunger and, if so, how hunger state sensing modulates hippocampal activity at the circuit and cellular levels to alter behaviour.

Using *in vivo* Ca^{2+} imaging during naturalistic and operant-based feeding behaviour, pharmacogenetics, anatomical tracing, whole-cell electrophysiology and molecular knockdown approaches, in this PhD I probed the functional role of the ventral subiculum (vS) circuitry in hunger state sensing during feeding behaviour. The results obtained implicates the vS in encoding the anticipation of food consumption. This encoding is both specific to vS projections to the nucleus accumbens (vS^{NAc}) and dependent on the hunger state; hunger inhibits the activity of vS^{NAc} neurons, and this inhibition relies on ghrelin receptor signalling in vS^{NAc} neurons. Furthermore, altering the activity of vS^{NAc} neurons shifts the probability of transitioning from food exploration to consumption. Finally, there is a distinct input connectivity to individual vS projections, providing a potential neural basis for the heterogeneous functions of projection-specific vS neurons.

Overall, this PhD advances the understanding of hippocampal function to encompass a nonspatial domain - the sensing of the hunger state – as well as clarify the cellular- and circuit-level mechanisms involved in hunger state sensing. This work presents evidence for a neural mechanism by which hunger can act as a

contextual signal and alter behaviour through defined output projections from the ventral hippocampus.

Impact Statement

Obesity and feeding disorders are important public health issues in the UK and across the world. These disorders represent unmet clinical needs that lead to reduced quality of life and loss of economic productivity. In normal health, the decision to seek and consume food depends on how the brain senses hunger, and how it uses this information to plan future behaviour. Disrupting this decision-making process is thought to underlie the maladaptive feeding behaviour observed in obesity and anorexia. One candidate brain region that is involved in the higher-order control of feeding behaviour is the hippocampus, where human and clinical imaging studies have demonstrated its role in making appropriate food consumption choices. However, how the hippocampus senses hunger and uses this information to guide behaviour remains poorly understood.

The experiments conducted in this thesis sought to test the hypothesis that the hippocampus senses hunger in mice, and to clarify the mechanisms underlying this process. My results demonstrate that a dedicated population of hippocampal neurons is involved in sensing a circulating hormone that signals hunger; in turn, the activity of these neurons depends on this hormonal signalling. Furthermore, artificially manipulating the activity of these neurons is capable of influencing the decision to investigate or to eat food. Finally, I found that this hunger-sensitive population of neurons receives distinct signals compared to neighbouring, hunger-insensitive neurons, suggesting a possible mechanism for the hunger sensing function of the hippocampus.

Until recently, the hippocampus has been thought to be important mainly for encoding memory and supporting spatial navigation. The findings of this thesis indicate that the function of the hippocampus is more wide-ranging, and involves hunger sensing and controlling feeding behaviour. Knowledge of this function of

the hippocampus will be important in not only understanding how biological organisms adapt behaviour to current metabolic needs, but also in addressing the clinical challenges posed by obesity and feeding disorders.

Acknowledgements

The completion of my PhD and this thesis would not have been possible without the help and support of many individuals who I have been fortunate to have met over the course of my training. Therefore, I would like to thank these people who have been pivotal in this work:

- To Andrew for being a supportive mentor, both personally and professionally, for providing the space and freedom to explore my interests in science, and for giving me the chance to dabble in systems neuroscience. It's been a blast.
- To Professor Tara Keck for her rigour, thoughtfulness and care. Through our discussions, she has undoubtedly made me a more confident and critical scientist.
- To Dr Tiago Branco, Professor Ainé Burns, Dr Daniel Marks, Professor David Abraham and the MBPhD clinical tutors for their training and support of my professional development.
- To Dr Marco Tripodi and Ernesto, for their mentorship and support, for introducing me to neuroscience research 5 years ago, as well as for the rabies virus!
- To members of the MacAskill lab; Karyna, Candela and Rawan – for the work- and non-work-related discussions, chilled and lovely company during our lunches on the Dickinson lab sofas, parties and many more.
- To the MBPhD programme and UCL, for their generous support of my work and PhD.
- To my parents, Mark and Irene, for their love and support, and my siblings, in

particular Rachel and Leon, who helped with artwork and machine learning advice, respectively.

- To Ernest, for too many things that can be described here.

Contents

List of Figures

List of Tables

List of abbreviations

4-AP	4-aminopyridine
AAA	Anterior amygdalar area
AAV	Adeno-associated virus
ACB	Nucleus accumbens
aCSF	Artificial cerebrospinal fluid
AP	Anteroposterior
APV	Amino-5-phosphonovalerate
AD	Anterodorsal nucleus of thalamus
AM	Anteromedial nucleus
AMY	Unannotated amygdala
ANOVA	Analysis of variance
APN	Anterior pretectal nucleus
AUC	Area under the curve
AV	Anteroventral nucleus of thalamus
BIC	Bayesian information criterion
BLA	Basolateral amygdalar nucleus
BMA	Basomedial amygdalar nucleus
BSS	Behavioural satiety sequence
BST	Bed nuclei of the stria terminalis
CA1	Field cornu ammonis 1
CA3	Field cornu ammonis 3
CEA	Central amygdalar nucleus
CL	Central lateral nucleus of the thalamus
COM	Centre-of-mass
CP	Caudoputamen

CRACM	Channelrhodopsin-2-assisted circuit-mapping
CTXβ	Cholera toxin subunit-b
D-lys	D-[Lys^3]-GHRP-6
DG	Dentate gyrus
dS	Dorsal subiculum
DV	Dorsoventral
EP	Endopiriform nucleus
EPM	Elevated plus maze
FFT	Fast Fourier transform
GP	Globus pallidus
GHSR1a	Growth hormone secretagogue receptor type 1a
GMM	Gaussian mixture model
HY	Unannotated hypothalamus
IA	Intercalated amygdalar nucleus
i.p.	Intraperitoneal
ITI	Inter-trial interval
LA	Lateral amygdalar nucleus
LDA	Linear discriminant analysis
LH	Lateral hypothalamus
LHA	Lateral hypothalamic area
LPO	Lateral preoptic area
LR	Likelihood ratio
LS	Lateral septal nucleus
MEA	Medial amygdalar nucleus
MEPO	Median preoptic area
ML	Mediolateral
MO	Somatomotor areas
mEPSC	Miniature excitatory postsynaptic current
mIPSC	Miniature inhibitory postsynaptic current
MPO	Medial preoptic area
MS	Medial septal nucleus
NAc	Nucleus accumbens

NBQX	6-Nitro-2,3-dioxo-1,2,3,4-tetrahydrobenzo[f]quinoxaline-7-sulfonamide
NDB	Diagonal band nucleus
OLS	Ordinary least squares
OT	Olfactory tubercle
P	Pons
PA	Posterior amygdalar nucleus
PB	Peanut butter
PBS	Phosphate-buffered saline
PFC	Prefrontal cortex
PVT	Paraventricular nucleus of the thalamus
PT	Parataenial nucleus
RE	Nucleus reuniens
RSP	Retrosplenial area
SC	Schaffer collateral
shRNAmir	short hairpin microRNA-adapted RNA
SI	Substantia innominata
SS	Somatosensory areas
TH	Thalamus
TRIO	Tracing the input-output relationship
TTX	Tetrodotoxin
vH	Ventral hippocampus
VIS	Visual areas
vS	Ventral subiculum

Chapter 1

Introduction

1.1 The hippocampus and its canonical computations

The hippocampus is a medial temporal lobe brain region with a diverse array of proposed functions, ranging from the encoding of episodic memory (Cohen and Eichenbaum, 1993) and spatial navigation (O'Keefe and Dostrovsky, 1971) to anxiety, motivation, planning and prediction (Moser and Moser, 1998; Bannerman et al., 2002; Strange et al., 2014; Dong et al., 2009). To date, it remains debatable what the exact function of the hippocampus is, and whether there exists a common hippocampal algorithm that may link the seemingly distinct functions of the hippocampus, e.g. the relationship between spatial navigation and anxiety. In this introduction, I will summarise the main functions of the hippocampus, and discuss the potential role of the hippocampus in resolving ambiguity, i.e. the notion that cues are associated with uncertain (probabilistic) outcomes. I will then discuss how one lesser known function of the hippocampus – interoceptive sensing and feeding behaviour – may potentially represent an instance of a nonspatial function of the hippocampus, and outline the questions related to this function that this thesis aims to address.

1.1.1 Role of hippocampus in episodic memory and spatial navigation

The hippocampus is classically thought to be the site of memory encoding. Studies in patients with lesions to the hippocampus, best exemplified by Patient H.M. and corroborated by many other studies, indicate that the hippocampus is crucial for the encoding of new memories, and in particular, episodic memory (Scoville and Mil-

ner, 1957; Vargha-Khadem et al., 1997). Episodic memory is memory for specific facts or events (as opposed to procedural memory, which is the implicit memory for stimulus-outcome-response relationships that underlie behaviours such as habits). The prominent role of the hippocampus in encoding episodic memory – which involves relating discrete features of the environment and time, and binding them into an episode – has inspired theories proposing that the hippocampus is crucial for relational processing (Cohen and Eichenbaum, 1993). More specifically, the same mechanism that allows the hippocampus to bind distinct cues into episodes also enables the hippocampus to flexibly relate together not only physical cues in space, but also non-physical quantities such as value and internal state (Behrens et al., 2018).

These insights into the mnemonic functions of the hippocampus arose almost in parallel with studies on the hippocampus' role in spatial navigation. With the discovery of place cells whose firing seemed to form a complete allocentric (without reference-to-self) representation of the environment (O'Keefe and Dostrovsky, 1971), hypotheses began to emerge that the hippocampus was the site of a cognitive map (O'Keefe and Nadel, 1978). This idea states that the hippocampus forms a complete spatial representation of the environment, including the complex relationships between objects and events which occur in the environment. Consistent with this hypothesis, as well as the role of the hippocampus in encoding memories, dorsal hippocampal lesions produce robust deficits in the Morris Water Maze task - a learned, spatial task that requires animals to remember the location of a hidden platform in an opaque pool by using extramaze cues (Morris et al., 1982). Furthermore, a whole host of spatially-selective cells that form components of the hippocampal circuit (grid cells, boundary vector cells, head direction cells etc.) have been discovered since the first description of place cells (Hafting et al., 2005; Lever et al., 2009; Taube et al., 1990), encouraging a strict view of the hippocampus as being solely involved in physical navigation through space.

However, it is increasingly recognised that hippocampal function is not restricted to physical space; rather, physical space represents just an instance of a general relational mechanism in the hippocampus that supports navigation through "memory space" – i.e. the links between elements of an experience (Cohen and

Eichenbaum, 1993; Eichenbaum and Cohen, 2014; Behrens et al., 2018). Additionally, it was noticed from early on that the hippocampus does not purely signal the spatial environment; its activity also depends on nonspatial variables. For example, in a non-match-to-sample task where odour cues are relevant, dorsal hippocampal neurons reliably encode nonspatial variables such as approach behaviour and odour identity (Wood et al., 1999). Further, the firing activity of place cells depends heavily on a variety of external sensory and internal variables that seem to depart from a purely spatial signal, including the encoding of goal locations and rewards (Hölscher et al., 2003; Lee et al., 2012; Gauthier and Tank, 2018; Ólafsdóttir et al., 2015), elapsed time (MacDonald et al., 2011), the taste and palatability of food (Herzog et al., 2018) and motivational states such as thirst and hunger (Kennedy and Shapiro, 2009; Carey et al., 2019). This sensitivity of hippocampal place cells to experience of reward, nonspatial external and interoceptive cues, require an alternative explanation beyond a purely spatial account of hippocampal function.

1.1.2 Role of hippocampus in emotional and motivated behaviour

In addition to the non-spatial determinants of hippocampal physiology in dorsal hippocampus, the specific tuning to physical space of hippocampal pyramidal neurons is not conserved throughout the entire hippocampus. More specifically, a functional gradient exists along the long-axis of the hippocampus from dorsal to ventral regions in rodents, or posterior to anterior regions in humans (Strange et al., 2014; Dong et al., 2009; Bannerman et al., 2002; Moser and Moser, 1998). The strong spatial tuning of hippocampal neurons was discovered and observed mostly within dorsal hippocampus, where the highest proportion of place cells is found (Jung et al., 1994) and from whose firing activity spatial information can be most accurately decoded (Kjelstrup et al., 2008). By contrast, further ventral in the hippocampus, hippocampal pyramidal neurons possess progressively poorer spatial tuning and have broader and larger place fields that sometimes spanned the entire behavioural chamber (Kjelstrup et al., 2008; Komorowski et al., 2013; Royer et al., 2010, **Figure 1.1**). While dorsal hippocampal neurons tend to selectively code for a particular location in space, ventral hippocampal neurons tend to generalise across spatial contexts, and instead encode for behaviourally meaningful contexts, e.g. context A means odour A is rewarded while odour B is not (Komorowski et al.,

2013). Consistent with this idea, lesions to the ventral hippocampus (vH) produce relatively little deficit in spatial memory performance in the Morris Water Maze task, while dorsal hippocampal lesions produced significant impairments in performance in the same task (Moser and Moser, 1998). Together, these studies of hippocampal physiology and lesion experiments demonstrate that information about physical space is progressively less encoded by more ventral regions of hippocampus, suggesting that other variables are more important.

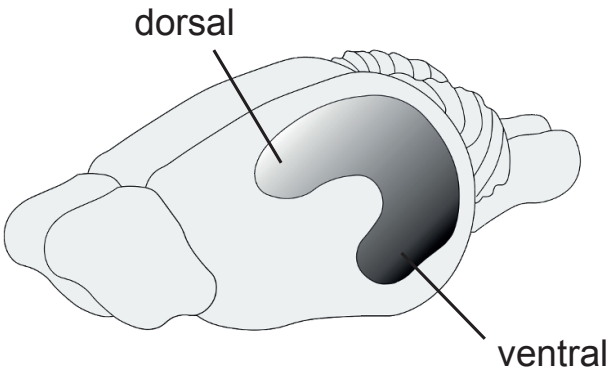

Figure 1.1: Schematic of the rodent hippocampus. Dorsal hippocampus (white) possesses strong spatial tuning, whereas vH (black) is less tuned to spatial variables.

The vH has been classically associated with nonspatial behaviour such as fear and reward learning, stress, motivation and threat processing (Strange et al., 2014; Bannerman et al., 2002; Ito et al., 2005; Ito and Lee, 2016). Lesions of the vH appear to impair behaviours involving an approach-avoidance conflict, such as social interaction with a novel conspecific, deciding to eat a novel food (hyponeophagia), or exploring potentially dangerous environments (open arm of an elevated maze). These observations suggest the hippocampus – especially its ventral component – is performing some calculation that involves a comparison between alternatives or conflicting options and resolution of this conflict (Davidson and Jarrard, 2004; Vinogradova, 2001; Bannerman et al., 2012). Another interesting observation was that lesions to vH produce inappropriate approach behaviour to ambiguous (Schumacher et al., 2015; Holland et al., 1999; Bannerman et al., 2002, 2012) and non-reinforced cues (Davidson et al., 2007) or contexts, while activating vH tends to promote avoidance behaviours (Jimenez et al., 2018; Ciocchi et al., 2015; Kheirbek et al., 2013; Adhikari et al., 2010). This negative correlation between ventral hippocampal activity and approach behaviour suggested that, under approach-

avoidance conflict, the vH is required for the inhibition of ongoing behaviour, either to attend to salient cues or to gather more information to resolve uncertainty (Gray and McNaughton, 2003; Bannerman et al., 2012). This gave rise to the behavioural inhibition hypothesis, positing that the hippocampus inhibits behaviour to resolve conflict (Gray and McNaughton, 2003). This similarity of behavioural responses of such gain- and loss-of-function studies of hippocampus also appeared to mimic the behaviour of animals provided with anxiolytic drugs (File and Gonzalez, 1996), which implicated the vH in anxiety-related behaviour.

Anxiety has been conceptualised as the 'suite of anticipatory affective, cognitive and behavioural changes in response to uncertainty' about some distal future state (Grupe and Nitschke, 2013). Under this framework, the crucial element that gives rise to the features of anxiety is the ambiguity of possible future threats. Experimentally, anxiety is probed in animal models by leveraging on ethologically-based tasks that produce approach-avoidance conflict (Calhoon and Tye, 2015). In such tasks, rodents, and in particular mice, have to balance the trade-off between exploring novel, potentially rewarding objects and environments, and hiding from the sight of predators. The prototypical examples of such tasks include the elevated plus maze (EPM) and social interaction tests. In these tasks, the ambiguity lies in the unexplored arm of the EPM, or the unfamiliarity of the novel conspecific in the social interaction test, which may represent sources of rewards or potential threats. The overall duration of avoidance from the open arms or novel rodent are used to quantify the level of anxiety in mice.

By using these 'anxiety-testing' tasks, several groups have found that inhibiting vH activity either through surgical lesions or optogenetic inhibition increase exploratory drive and reduce anxiety (Bannerman et al., 2002; Kheirbek et al., 2013; Padilla-Coreano et al., 2016). Recordings of ventral hippocampal activity in freely-behaving rodents in these tasks concomitantly showed elevated activity of vH during high anxiety states – for example, during the transitions from the closed to open arms of the EPM, the centres of the open field test, or when investigating a novel conspecific (Adhikari et al., 2010; Ciocchi et al., 2015; Jimenez et al., 2018; Padilla-Coreano et al., 2016). In humans, the balance between approach and avoidance also depends on anterior hippocampus (the ventral hippocampal analogue in hu-

mans; Bach et al., 2019; O'Neil et al., 2015). In a task that required participants to judge varying levels of uncertainty about a potential threat, patients with damage to the vH seemed to display inappropriate approach behaviour even under high uncertainty states compared to healthy controls. These and many other studies have galvanised the 'anxiety-view' of ventral hippocampal function.

One implication of this framework of anxiety as being driven by uncertainty is that the ambiguity of an outcome need not necessarily be "negative" in valence, like the possibility of threats such as predation in the open arms of the EPM or the center of the open field test. This ambiguity can be neutral or "positive", such as deliberating over the value of a reward (Lee et al., 2012; Bakkour et al., 2018), inferring where, when and how much of a reward will be available given the cue or environmental context (Riaz et al., 2017; Trouche et al., 2019; Duncan et al., 2018), or working out the location and proximity to reward or goal locations (Bannerman et al., 2012). Indeed, a key caveat of these ethologically-based 'anxiety' tasks is that they are unable to dissociate between increased exploratory drive and reward-seeking versus a reduction in anxiety levels (Calhoon and Tye, 2015).

Consistent with this view, the ventral (anterior) hippocampus appears to be involved in deliberating the value of choice (Lee et al., 2012; Bakkour et al., 2019; Jeong et al., 2018; Ólafsdóttir et al., 2015). For example, Bakkour et al. (2019) used a value-based decision-making task that required human participants to judge the value of pairs of food snacks and to choose the snacks that they preferred; they observed that longer deliberation time prior to choice – especially for snacks that were close in their value rating – was correlated with activity in the anterior hippocampus (Bakkour et al., 2019). This judgement of value also applies to food items with which subjects have had no prior experience (Barron et al., 2013), suggesting that the hippocampus is capable of searching through a model of the world and to flexibly compare the value of novel items when required (Behrens et al., 2018). Thus, ambiguity over the value of competing food items also engages the hippocampus.

This ambiguity resolution process seems to also apply in the dorsal hippocampus. For instance, Bannerman et al. (2012) found that synaptic plasticity – a cellular substrate of learning – in dorsal hippocampus was not required for successful spatial memory retrieval in the Morris Water Maze, but is instead specifically re-

quired when a spatial task introduces ambiguity in the goal location (Bannerman et al., 2012). The transgenic mice lacking functional NMDA receptors in dorsal hippocampus performed poorly only in an ambiguous variant of the Morris water maze task where the hidden platform was cued with a beacon over the platform, and an identical 'decoy' beacon placed symmetrically opposite the platform. This specific task introduced ambiguity in the form of visually identical beacons, which forced animals to rely on extra-water maze cues to solve the task. Hippocampal-lesioned rats seemed to persist in approaching the first beacon that they were closest to, regardless of the correct beacon, suggesting inappropriate approach behaviour. Thus, it appears that even dorsal hippocampus is required to resolve the ambiguity of a goal location, rather than solely encoding the explicit spatial location of goals.

1.1.3 Ambiguity resolution as a canonical hippocampal computation

As a brief summary, the dorsal hippocampus appears to be specialised in encoding space, while vH encodes approach-avoidance behaviour for both positive and negative outcomes. Ambiguity resolution occurs both in dorsal and vH. Against this backdrop is the hippocampus' relational function that is important in binding distinct features into episodes or schemas. How are all these concepts related to each other? One possibility that ties together these ideas is that the relational function of the hippocampus may be important for using past learned associations or memories to resolve decisions involving ambiguity (Biderman et al., 2020). Specifically, learned associations can be used to prospect about likely futures given the current state of the world and the actions taken from this state that lead to maximal reward. Such a computation resembles a class of decision-making strategies known as 'model-based' planning.

A classical distinction in goal-directed behaviour is the separation of behaviour into two main systems: model-free and model-based behaviour. Model-free behaviour arises from trial-and-error learning where an animal caches the value of an action after repeated trials, and generates behaviour to maximise expected future value based on this cached value. By contrast, model-based behaviour (or planning) involves making decisions based on an internal model, i.e. a tree-like model that links states with their outcomes and associated values. Choosing the action that maximises value in model-based planning involves searching through

the model and simulating future possibilities.

The development of behavioural tasks specialised to parse out model-free and model-based behaviour, namely the two-stage sequential decision-making task (Doll et al., 2015a,b), has provided insights into the neural substrates of model-based planning. Evidence from humans with hippocampal lesions and optogenetic inactivation of hippocampus in rodents indicate that the dorsal hippocampus is crucial for model-based planning (Vikbladh et al., 2019; Miller et al., 2017). Using the same task, Doll et al. (2015a) found that hippocampal activity in human subjects correlated with the degree to which they used a model-based, as compared to a model-free, strategy. More recently, novel computational models have been developed to explain a large range of experimental phenomena regarding hippocampal physiology. One notable example is the successor representation, a planning strategy that incorporates aspects of both model-based and model-free planning and is able to capture a wide range of observations regarding hippocampal place cell activity (Stachenfeld et al., 2017). Overall, there appears to be strong evidence that the hippocampus supports model-based planning.

Furthermore, the hippocampus has been implicated in the prediction of upcoming futures, a required step in deciding between competing options with ambiguous outcomes (Johnson and Redish, 2007; Buckner, 2010; Stachenfeld et al., 2017; Kay et al., 2020; Ólafsdóttir et al., 2015; Bakkour et al., 2019). For instance, Johnson and Redish (2007) observed that when rats were at a left-right decision point, hippocampal place cell activity appeared to sweep forward, down one direction and then to the other, suggesting a prospective function in the hippocampus. Such a prospective mechanism, when combined with the extensive reports of value signals within the hippocampus (Lee et al., 2012; Jeong et al., 2018; Gauthier and Tank, 2018), could potentially allow the hippocampus to simulate the future value of different options – in much the same way as model-based planning. Such forward prospection would be required for arbitrating between competing options during, for example, approach-avoidance conflict or value-based decisions.

One main assumption of model-based planning is full knowledge of what the current state is. Under naturalistic settings, the current state is often hidden or only partially observable, and this contributes to the ambiguity of the likely outcome

given the current state. Prevailing theories about the nature of ambiguity resolution propose that whenever the current state or outcome is ambiguous, the information contained within the ”context” becomes increasingly crucial to resolve the ambiguity (Bouton, 1993; Rosas et al., 2013; Gershman, 2017). In model-based planning terms, information contained within the context is required to determine which state the animal is in exactly. What precisely is meant by context depends on the given behavioural demands of a task. Context usually refers to the spatial environment surrounding the animal, such as the behavioural apparatus, the testing box and experimenter. More generally, context can be defined as the combination of external environmental factors or internal milieu that occurs at the same time as the animal is engaging in a task or behaviour (Rosas et al., 2013); thus, physical variables such as the testing box, or non-physical unobserved variables, such as task contingencies and interoceptive cues like hunger or thirst, can individually or in combination act as a context.

Gershman (2017) proposed that in tasks where ambiguity is low, such as when a tone consistently predicts an upcoming footshock or reward, context is unnecessary for successful prediction of the outcome. However, under circumstances of higher ambiguity, more information is required than is available in the external cues alone, and the context provides additional information to reduce the ambiguity. Thus, in this formalisation, what role the contextual stimuli will play depends on the degree of ambiguity between the sensory stimuli and the outcome. The hippocampus has been implicated specifically in the encoding of context and contextual retrieval – i.e. the recall of learned associations by the context that was present at the time of memory encoding (Hirsh, 1974; Good and Honey, 1991; Corcoran and Maren, 2001). Therefore, one hypothesis is that tasks involving a higher degree of ambiguity requires increasingly more information from the context and, in turn, progressively engages the hippocampus.

One specific function of a context is as an occasion setter, which is defined as a contextual or discrete stimulus that ”modulates the ability of another stimulus to control behavior” (Trask et al., 2017, **Figure 1.2A**). For example, in a task where animals are trained that a light cue is rewarded only when preceded with a tone (T $\rightarrow$ L, L+), the tone *sets the occasion* for when the light cue predicts reward

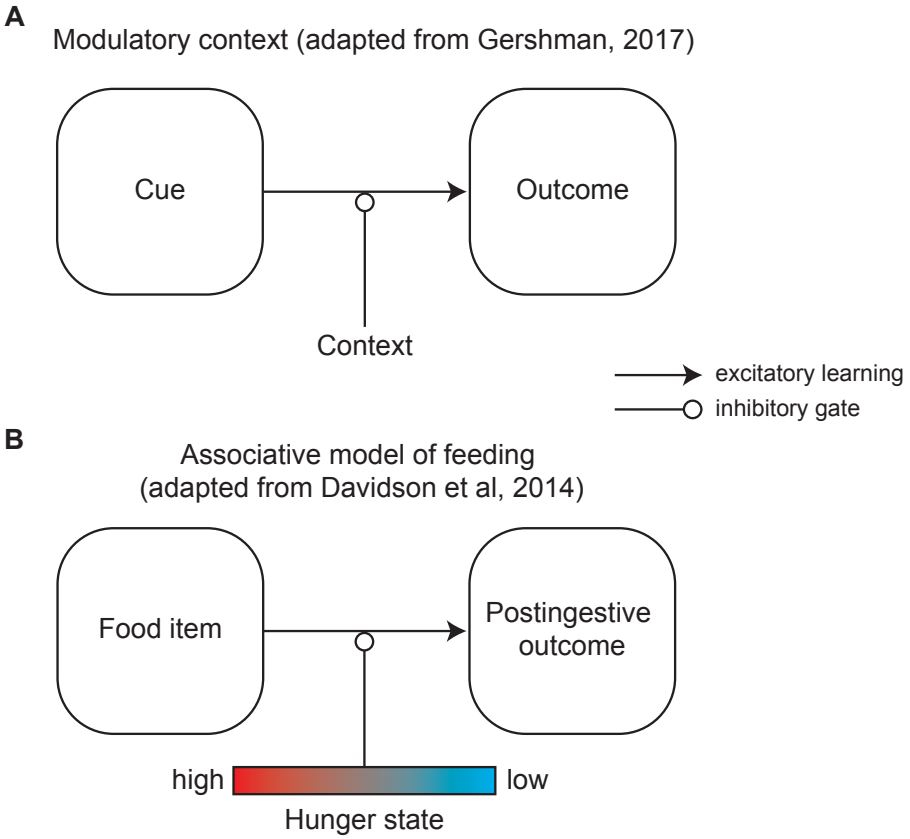

Figure 1.2: Hunger as a contextual modulator of feeding behaviour. (A) Model of context gating the behavioural responding to a cue. Adapted from Gershman (2017). The context does not influence the outcome, but rather modulates how the cue is related to the outcome. (B) Model of hormonal signals (”hunger state”) gating feeding behaviour. The model assumes that feeding will occur when food-related cues predict a rewarding postingestive outcome. However, food cues can predict both nonrewarding (when sated) or rewarding (when hungry) outcomes. In this way, food cues are ambiguous. To resolve this ambiguity, the hunger state provides the required information to determine the actual postingestive outcome, thereby gating the causal influence of food cues to rewarding postingestive outcomes.

and acts as a positive occasion setter. Conversely, a tone can set the occasion for when the light cue does *not* predict reward (T $\rightarrow$ L, L$-$), and therefore act as a negative occasion setter. In both cases, the light cue is ambiguous as it can lead to both reward and no reward, and additional information from the tone disambiguates this relationship. Thus, an occasion setter modulates the cue-outcome association (Gershman, 2017). Consistent with the role of the hippocampus in the encoding of contexts, the hippocampus is also crucial for contextual occasion setting (Yoon et al., 2011). Thus, the hippocampus is important in resolving the ambiguity by making use of information contained within the context.

Taken together, the seemingly disparate functions of the hippocampus appear

to center around a common computation: the processing and resolution of ambiguity. Tasks that involve an ambiguous outcome require deliberation over the outcome of each option, and such a deliberative process may require the model-based planning computation and the encoding of context that the hippocampus is thought to support.

1.2 Relationship of hippocampal computations to feeding behaviour

How do the functions of the hippocampus, such as planning and ambiguity resolution relate to motivated behaviours such as feeding? Firstly, model-based planning involves constructing models of relationships between distinct cues. Thus, the complex relationships between multi-modal external and internal cues are exactly what the hippocampus is thought to encode (i.e. relational and conjunctive codes) (Behrens et al., 2018). Foraging behaviours like feeding are purposeful behaviours that involve exploring an environment and locating food while avoiding danger. To select the most optimal course of action, animals need to integrate a combination of external cues such as the location and identity of the food, and internal physiological state, such as hunger (Toates, 1981; Burnett et al., 2016). This requirement of weighing up distinct cues and deliberating about future outcomes suggests that the hippocampus may be crucial in orchestrating adaptive feeding behaviour.

In the past, feeding was conceptualised as a problem of optimal control, i.e. deviations from a caloric set-point are detected as negative feedback that produces changes in behaviour to correct the deviation. Hull (1943) linked this idea of negative-feedback homeostatic control to motivated behaviour by proposing that negative feedback gives rise to an increasing drive that in turn motivates behaviours to reduce the drive (drive-reduction theory). However, evidence suggests that animals depart from a simple drive reduction strategy, and instead anticipate future changes in their hunger state to produce behaviours well in advance of shifts in caloric balance (Sterling, 2012; Andermann and Lowell, 2017). This predictive aspect of homeostatic regulation, termed allostasis, is increasingly recognised to be an important determinant of goal-directed behaviour such as feeding and drinking (Chen et al., 2015, 2016; Augustine et al., 2018, 2020). Therefore, brain regions

which contribute to prospection about future states, for example the hippocampus, may be important in regulating motivated behaviour.

Foraging and feeding behaviour have also been cast as a decision-making process that involves selecting the most optimal action given the environmental context. One key aspect of feeding is the ability to integrate external and internal cues to judge the value of a food item and decide whether or not to eat it. Davidson et al. (2014) argue that feeding behaviour, when viewed in this way, is essentially an ambiguity resolution process over the value of food (**Figure 1.2A–B**). The value of a given food item is ambiguous because the same food, depending on the hunger state, can have different values. More specifically, the food item would predict a highly rewarding post-ingestive outcome when the animal is hungry (**Figure 1.2B**), but when sated, the same food item will predict a less rewarding outcome (Yiin et al., 2005). To resolve this ambiguity, additional information about the hunger state needs to be integrated before committing to a decision (Gershman, 2017; Davidson et al., 2007, 2014). To describe the same phenomenon from a learning perspective, the decision to eat or not depends on the appropriate configuration of cues: the simultaneous presence of external food cues and hunger will drive feeding behaviour, but food cue alone will not.

Experimentally, the structure of naturalistic feeding behaviour is often studied as a set of behavioural modules comprising feeding-specific behaviours such as food-directed exploration and consumption behaviour, maintenance behaviours like grooming and resting, and general exploratory behaviour like rearing (Halford et al., 1998). More specifically, this constellation of exploratory approach, eat, rear, groom and quiet rest behaviours represents the behavioural satiety sequence (BSS) (Halford et al., 1998) that is used as a benchmark to characterise feeding behaviour. In particular, food-directed exploration is often quantified in the BSS as approaching, investigating and/or sniffing food. This particular aspect of feeding behaviour may reflect a deliberative process on deciding whether to eat or not, through sampling the sensory properties of food and combining external information with the internal state. Thus, even under naturalistic conditions with no task structure, the hippocampus may be involved in the moment-to-moment decisions on whether to eat or not. However, no study has yet examined this possibility.

Taken together, feeding behaviour can be viewed as an ambiguity resolution task that requires integration about external food-related cues and internal hunger state to decide whether or not to eat. This requirement of using information from the context to resolve ambiguity, and prediction about future metabolic states, implicates the hippocampus in controlling motivated behaviour like feeding behaviour.

1.3 Circulating hormones signalling the hunger state

Hunger is signalled by many circulating hormones that report satiety and food deprivation levels, such as leptin, cholecystokinin and ghrelin. Among these hormones, ghrelin – often termed the 'hunger' hormone – is the most well-studied hormone that is capable of stimulating appetite. Specifically, ghrelin is capable of increasing hunger levels and driving feeding when acutely injected into rodents and humans (Tschöp et al., 2000; Wren et al., 2001). Ghrelin is a 28-amino acid peptide produced by the stomach; the circulating concentration level of ghrelin closely tracks meal times during the day, where it increases with fasting, reaches a peak before a meal and falls after meal ingestion (Andermann and Lowell, 2017; Müller et al., 2015). It binds to the growth hormone secretagogue receptor 1 (GHSR1a), which is a seven-transmembrane G_q-protein coupled receptor that signals via phospholipase C activation to increase inositol phosphate and intracellular Ca^{2+} levels (Mear et al., 2013). GHSR1a is expressed both peripherally and centrally; in the brain, GHSR1a is strongly expressed in hypothalamic regions such as the arcuate nucleus, as well as 'higher-order' brain regions related to motivated behaviour such as the midbrain, striatum and hippocampus (Zigman et al., 2006; Kanoski et al., 2013; Hsu et al., 2016; Mani et al., 2014).

Although the hunger state is reported by a range of hunger- and satiety-related hormones and metabolites, there is evidence that single, individual molecules can act as principal drivers of the hunger state. One way to assess this possibility is to train animals to report the hunger state using a learned task. For example, animals can learn to associate their interoceptive hunger state – sated or hungry (after 24 hours of fasting) – with an upcoming reward or footshock, and in turn freeze or not depending on their hunger state (Davidson and Jarrard, 1993; Hock and Bunsey, 1998; Kanoski et al., 2007; Davidson et al., 2009b). Kanoski et al. (2007) demonstrated that the sated state could be mimicked with an i.p. injection of either

the hormones leptin or CCK in hungry animals, as reported through probe tests of their behavioural responding. Conversely, hunger could be mimicked by drug-induced reductions of glucose levels (Benoit and Davidson, 1996). These findings show that an individual circulating factor can mimic the internal hunger state or context to bias a learned behaviour, and supports the idea that the hunger state exists – at least partially – through the actions of individual hormones.

Although no such direct comparisons have been made between ghrelin and the fasted state, it is likely that ghrelin mimics the fasted state for several reasons. First, acute infusions of ghrelin into sated subjects are sufficient to drive feeding behaviour in both rodents and humans (Tschöp et al., 2000; Wren et al., 2001). Second, there is a tight relationship between the duration of fasting, hunger levels and circulating levels of ghrelin (Cummings et al., 2004; Natalucci et al., 2005). Third, acute infusions of ghrelin increases the perceived pleasantness (value) of food and similarly activate brain regions that are engaged by physiological fasting, such as orbitofrontal cortex, nucleus accumbens and hippocampus (Goldstone et al., 2014; Malik et al., 2008). Thus, at the behavioural and neural circuit levels, ghrelin mimics the main features of fasted behaviour.

1.4 Hunger state as a context

Over the last few decades, hunger has been conceptualised as a drive (Hull, 1943), as a gain control for the incentive value of food (Toates, 1981; Dickinson and Balleine, 1994) and as a 'discriminable interoceptive stimulus' or a Pavlovian occasion setter (Davidson, 1998). Can the hunger state act as an occasion setter or context? To function as a context that is able to provide hunger-related information to the hippocampus, and modulate behavioural response to food-related stimuli, there should be experimental support for three conditions:

1. the hunger state possesses properties of a context, for example, modulation of cue-outcome associations

2. the hippocampus uses (senses) hunger-related information

3. the hippocampus possesses the cellular components required for hunger state sensing (receptors, circuits etc.)

1.4.1 Hunger state as a context to guide behaviour

The fundamental property of a context is the ability to modulate the cue-outcome relationship (**Figure 1.2**; Rosas et al., 2013; Gershman, 2017). Traditionally, in contextual fear conditioning, the context is taken as the behavioural apparatus and behaves like a punctate cue that predicts an upcoming footshock. Early evidence demonstrated that hunger can also act as a context in this regard. Davidson and Jarrard (1993) trained one cohort of rats to predict that the fasted state was followed by a footshock while the sated state was not, and in the other cohort the reverse training contingency was applied. The inherent ambiguity in the task was the identical physical context; the only factor that differed between predicting shock or no shock was the level of hunger. Importantly, animals were able to discriminate between the hunger levels and freeze under the correct hunger state condition, demonstrating that hunger was being used as a discriminative internal stimulus to resolve the ambiguity of the upcoming footshock. However, hunger does not itself behave like a punctate cue to elicit the behavioural response. Using the same hunger discrimination task, Davidson and Benoit (1996) showed that hunger alone did not elicit freezing in a transfer test; rather, hunger modulated the physical context and footshock relationship as an occasion setter. These findings underscored the ability of hunger to function as a modulatory contextual stimulus, as opposed to directly becoming associated with the outcome (Gershman, 2017).

In addition to an aversive outcome, this modulatory function of hunger also applies to the behavioural response towards appetitive rewards (Davidson et al., 2010; Deacon et al., 2001; Hsiao and Isaacson, 1971). Davidson et al. (2010) conducted an experiment that showed that hunger levels could be used as discriminative stimuli to predict the delivery of sucrose pellets. Rats trained to predict the delivery of sucrose pellets under the fasted state predictably approached the delivery spout more in the fasted compared to the fed state. Crucially, under the reverse condition where the sated state predicted sucrose pellet delivery, rats approached the spout *more* in the sated compared to the fasted state; this counterintuive observation has been replicated in other studies (see Schepers and Bouton, 2017).

Additionally, the hunger state can act as a context to support goal-directed behaviour (Kennedy, 2004). Rats that were alternately food- or water-deprived were

able to associate goal boxes with either food or water, where one box contained water when the animal was thirsty, one contained food when the animal was hungry and the other box was left empty. This experiment demonstrated that the animals were able to use their interoceptive motivational state to choose the appropriate box to approach. These findings support the view that hunger can act as a context to modulate cue-outcome associations for both aversive and appetitive outcomes.

For such hunger-dependent discrimination tasks , an intact hippocampus is crucial for using hunger-related signals as discriminative stimuli for successful performance (Davidson and Jarrard, 1993; Hock and Bunsey, 1998; Benoit and Davidson, 1996; Kanoski et al., 2007; Davidson et al., 2009a). In the case of aversive outcomes, rats with ventral hippocampal lesions failed to freeze in the appropriate hunger state compared to controls (Davidson and Jarrard, 1993; Davidson and Benoit, 1996; Hock and Bunsey, 1998). In the case of appetitive outcomes, ventral hippocampal lesions not only impaired discriminative responding under the appropriate corresponding hunger state, rats tended to persevere and inappropriately approach the delivery spout during nonreinforced sessions (Davidson et al., 2010). Lesioning the hippocampus also prevents animals from using their internal state to select the appropriate behaviour (Kennedy, 2004). These studies indicate that the vH is not only involved in integrating hunger signals to solve ambiguous tasks, but also in inhibiting inappropriate behaviour.

1.4.2 The hippocampus senses and uses hunger-related information

Complementary evidence from lesion and neuroimaging studies from the human literature have also provided key insights into the role of the hippocampus in sensing the hunger state. Clinical observations, such as those from Patient HM and others, suggest that lesions to the hippocampus impaired the ability to report the subjective level of hunger (Scoville and Milner, 1957; Hebben et al., 1985; Rozin et al., 1998); these patients tended to persevere to eat meals regardless of having eaten a previous meal shortly before. Consistent with these case reports, studies using functional magnetic resonance imaging (fMRI) have also observed hippocampal activation after hunger state changes. For example, ghrelin infusions in sated human subjects activate the hippocampus, in addition to other reward-related regions such as nucleus accumbens (Goldstone et al., 2014; Malik et al., 2008). Gastric balloon

distention of the stomach, a procedure that stimulates the vagus nerve and induces satiety, also reliably increases the blood-dependent oxygenation level (BOLD) signal in the hippocampus in humans (Wang et al., 2006) and rodents (Min et al., 2011). Presenting food-related visual cues after physiological fasting to human subjects also increases the hippocampal BOLD signal (Wallner-Liebmann et al., 2010). Thus, manipulations of the hunger state, from physiological fasting, exogenous administration of ghrelin and stomach distension, all produce reliable activation of the hippocampus, suggesting that the hippocampus senses the hunger state.

Additionally, decades of work have demonstrated that the hippocampus is sensitive to motivational state (Kennedy and Shapiro, 2009; Carey et al., 2019). Normal hippocampal physiology – for example, place cell activity during spatial navigation – is in turn dependent on hunger. For example, the ensemble of place cell activity that span an environment is unique to that environment; when this environmental context changes, place cell activity either diminishes, switches to encode another location within the new environment or disappears entirely, a process known as remapping (Wills et al., 2005; Colgin et al., 2008). Kennedy and Shapiro (2009) found that, within the same physical environment, place cell activity remapped depending on whether the rats were hungry or thirsty. This demonstrated that even spatial representations of the physical environment were anchored to the internal motivational state.

Another signature of hippocampal physiology is the sharp wave ripple (SWR), the synchronous activation of hippocampal ensembles (Buzsáki, 2015). The content of SWRs is the compressed replay of hippocampal sequence activity from past experiences, usually during immobility and rest. Carey et al. (2019) found that SWRs were also modulated by the motivational state. They used a task where rats were alternately food- or water-restricted and trained to run down a T-maze with either food or water on both ends. They reasoned that if the hippocampus was using motivational state information to plan future goal-directed behaviour, then one might expect the SWR content to be biased towards trajectories to rewards. However, the authors found the opposite; SWRs detected when rats were on the rest platform outside the task tended to be biased towards the arm with the nonpreferred food. These findings build upon the idea that hippocampal representations are closely

tied to the motivational state, and that the hippocampus is more strongly activated during the 'devalued' or sated condition.

1.4.3 Cellular components required for hunger state sensing

In keeping with the hippocampus' role in sensing the hunger state, hippocampal pyramidal neurons express a diverse array of physiologically important receptors, for example, those involved in the signalling axes for stress, hunger and thirst (Lathe, 2001; Lathe et al., 2020). More specifically to hunger, the hippocampus is one of many regions that expresses the ghrelin receptor GHSR1a in both rodents (Guan et al., 1997; Zigman et al., 2006; Hsu et al., 2015; Diano et al., 2006; Mani et al., 2014) and non-human primates (Mitchell et al., 2000). However, the source of ghrelin mediating GHSR1a signalling in the hippocampus remains debated, and possible sources include peripherally circulating ghrelin (Banks et al., 2002; Diano et al., 2006; Rhea et al., 2018) and central ghrelin-synthesising afferents to hippocampus (Ferrini et al., 2009). There is evidence to support the entry of peripheral ghrelin through the blood-brain barrier via a saturable mechanism (Banks et al., 2002; Diano et al., 2006). For example, radioactive ghrelin administered peripherally via i.p. injection binds to hippocampal neurons in a saturable manner (Diano et al., 2006) and is capable of not only inducing structural (Diano et al., 2006) and functional (Diano et al., 2006; Ribeiro et al., 2014) plasticity, but also influencing behaviour.

Despite the presence of the blood brain barrier around the hippocampus that blocks the entry of circulating factors, it is thought that peripherally circulating hormones are nevertheless able to gain access to the hippocampus constitutively (Hamasaki et al., 2020). For example, the dye Evans blue is used to assess BBB integrity; penetration of Evans blue either indicates damage to the BBB or a region that is constantly exposed to circulating factors. Importantly, Evans blue can be detected in the hippocampus after 15 minutes post-Evans blue injection (Hamasaki et al., 2020), suggesting that the hippocampus is exposed to circulating factors from the bloodstream. Furthermore, the transport of ghrelin across the BBB appears to be dynamic; physiological fasting appears to increase the transport of ghrelin across the BBB (Banks et al., 2008). By contrast, other groups have reported that ghrelin is undetectable in the hippocampus (Furness et al., 2011) and there-

fore unable to cross the blood brain barrier; they propose alternative mechanisms for GHSR1a signalling in hippocampus, for example, indirectly through dopaminergic input to the hippocampus which then activates heterodimers of GHSR1a-dopamine receptor type 1 (D1) receptors (Kern et al., 2015), heterodimerising with other receptor subtypes (Schellekens et al., 2015), or high constitutive activity of the GHSR1a receptor independent of ghrelin binding (Damian et al., 2012). Although it remains debatable whether ghrelin actually directly penetrates the BBB to reach the hippocampus, there is nevertheless growing evidence demonstrating that blood-borne circulating factors not only bind to hippocampal pyramidal neurons, but also change their functional properties and alter behaviour.

Furthermore, the exact behavioural role of GHSR1a remains elusive. Mice with blocked signalling of GHSR1a – either through a global knockout of GHSR1a or systemic application of GHSR1a antagonists – show impaired anticipatory and 'higher-order' aspects of feeding regulation, such as appropriate feeding under a restricted feeding schedule, social learning of food preference and context-dependent feeding (Walker et al., 2012; Hsu et al., 2015; Davis et al., 2011; Gooley et al., 2006; Verhagen et al., 2011), as opposed to a pure metabolic change in feeding behaviour. Consistent with this interpretation, animals lacking the GHSR1a receptor show normal feeding behaviour and weight gain (Sun et al., 2008). Furthermore, activity in reward-related regions like striatum correlates with ghrelin levels specifically during anticipation of feeding, and not feeding itself (Simon et al., 2017). Thus, ghrelin signalling appears to mediate a higher-order, anticipatory and food-seeking behaviour, potentially through its action in the hippocampus (Hsu et al., 2016). Overall, these studies implicate the hippocampus in regulating feeding behaviour through the use of higher-order contextual information related to hunger.

1.5 Anatomical and functional components of the vH

1.5.1 Anatomical connectivity implicates the hippocampus in ingestive behaviour

The hippocampus is well-positioned based on its connectivity to regulate motivated behaviour, especially within vH. Its main output regions – in CA1 and subiculum – are comprised of pyramidal neurons with efferent projections to distinct downstream

areas, including prefrontal cortex, nucleus accumbens (NAc), lateral hypothalamus (LH), hypothalamic and preoptic areas (Naber and Witter, 1998; Hahn and Swanson, 2012; Cenquizca and Swanson, 2006, 2007; Ding et al., 2020; Wee and MacAskill, 2020). In particular, the NAc and LH are both involved in reward-seeking and ingestive behaviour. These direct, monosynaptic projections to brain regions classically thought to regulate survival and homeostatic functions highlight the potential role of the hippocampus in contributing to motivated behaviours (Risold and Swanson, 1996; Cenquizca and Swanson, 2006, 2007).

1.5.2 Hippocampus-to-nucleus accumbens projections

The nucleus accumbens is a collection of largely inhibitory cells called medium spiny neurons (MSNs) in the ventral striatum. Often described as a limbic-motor interface (Pennartz et al., 2011b), the NAc integrates heterogeneous inputs signalling context (presumably from hippocampus), valence and value (e.g. from amygdala and ventral tegmental area) (Reed et al., 2018) and translate them into overt behaviour through action selection pathways in the basal ganglia and other downstream pathways. Anatomically and functionally, the NAc is organised into the shell (the medial and ventral band that forms the borders of the nucleus accumbens) and core (the area that envelops the anterior commissure; **Figure 1.3A–D**) regions. The shell region is thought to drive goal-directed behaviour by using contextual information (Ito et al., 2008), while the core region drives reward-seeking using punctate (discrete) cues.

Ventral subicular inputs specifically target the medial shell of the NAc (**Figure 1.3C–D**, Brog et al., 1993; Britt et al., 2012) in a unilateral manner, meaning that there is little cross-hemispheric connectivity between vH and NAc. At the circuit-level, vH inputs preferentially innervate D1 dopamine receptor-expressing MSNs (MacAskill et al., 2014; Scudder et al., 2018) and parvalbumin-expressing, fast-spiking local interneurons (Scudder et al., 2018; Trouche et al., 2019). Recently, Trouche et al. (2019) demonstrated the functional significance of feedforward inhibition via local PV+ interneurons in NAc in supporting reward-driven place preference behaviour; however, it remains unclear how the balance of excitatory vH inputs to local PV+ interneurons and D1-expressing MSNs shape circuit activity *in vivo* in the NAc to alter behaviour. In turn, both D1- and D2-expressing MSNs send outputs to

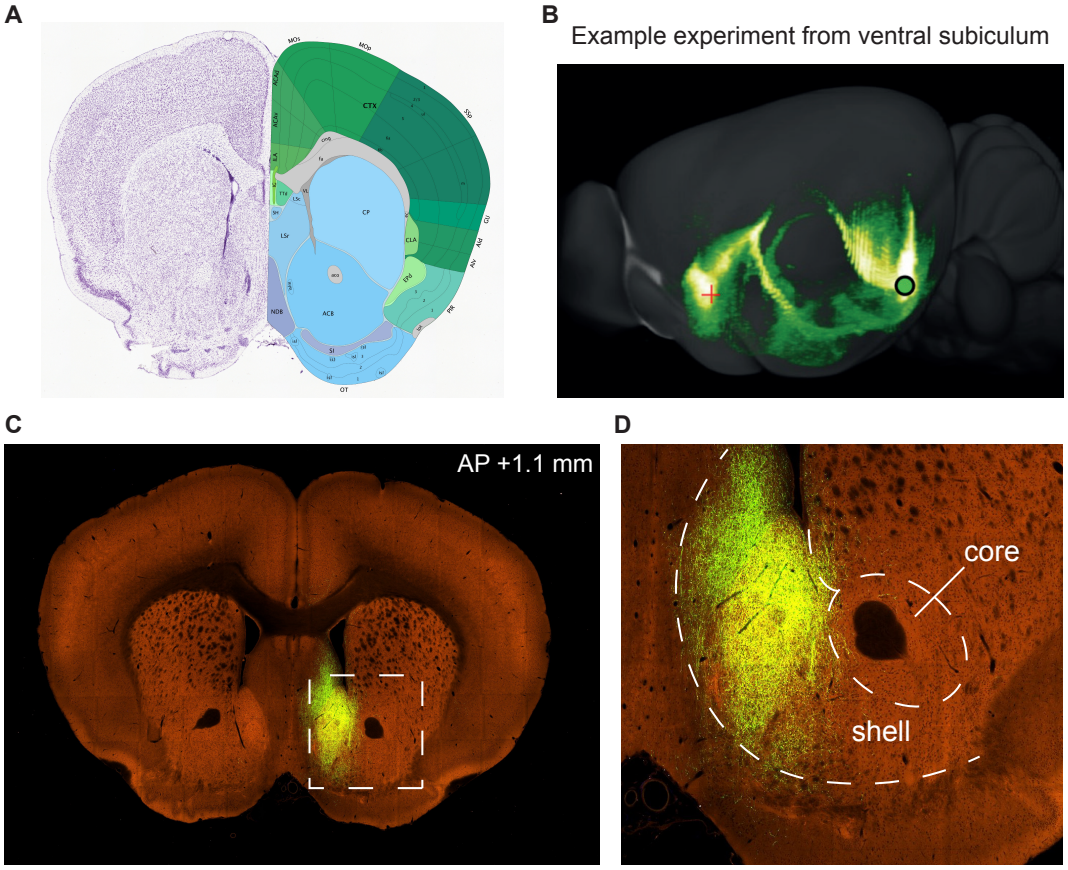

Figure 1.3: Hippocampal projections to nucleus accumbens. (A) Allen Brain Atlas coronal section around the anterior-posterior level of +1.1 mm. (B) Projection density map of experiment ID 585776749, involving GFP expression in vH (CA1, subiculum and prosubiculum) in a Ntng2-IRES2-Cre mouse. Green dot represents the site of the AAV tracer injection, and red cross represents the site of the coronal sections shown in (C–D). (C) Coronal section of the nucleus accumbens from the example experiment from (B). Boxed area indicates the zoom-in image in (D). (D) The nucleus accumbens in ventral striatum comprises the shell and core regions. The banded region with most intense axonal projection from hippocampus is the medial shell of the NAc. The core region around the anterior commissure is relatively devoid of axonal projections from hippocampus. Data taken from the Allen Brain Atlas.

a number of regions, including lateral hypothalamus (O'Connor et al., 2015), ventral tegmental area (Baimel et al., 2019), preoptic area and brainstem (Voorn et al., 2004).

These inputs and outputs of the NAc have been studied in the context of reward-seeking, goal-directed and ingestive behaviours. Recent studies have shown that NAc acts as a gate to producing consummatory behaviours. At the onset of consumption, the activity of excitatory inputs to NAc drops dramatically (Reed et al., 2018), and activity within the NAc also remains silent at the onset of reward-

driven behaviour (Taha and Fields, 2006). Additionally, non-specific inhibition via local infusions of glutamate antagonists or GABA agonists into the NAc stimulates robust food consumption behaviour (Maldonado-Irizarry et al., 1995; Stratford and Kelley, 1997), while conversely nonspecific electrical stimulation of NAc interrupts feeding behaviour (O'Connor et al., 2015; Krause et al., 2010). Specific activation of D1-expressing MSNs projecting to downstream LH, and not D2-MSNs, potently suppressed feeding behaviour (O'Connor et al., 2015) . Since the vH targets D1-expressing MSNs (MacAskill et al., 2014; Scudder et al., 2018; Baimel et al., 2019), and the vH is implicated in behavioural inhibition (Gray and McNaughton, 2003; Reed et al., 2018; Yoshida et al., 2019), one intriguing possibility is that hippocampal input to NAc may serve as a circuit mechanism for some form of feeding-related behavioural inhibition. Consistent with this idea, inhibition of hippocampal input to NAc increases the effort to consume a liquid food reward (Yang et al., 2019; Reed et al., 2018).

Another function of the vH-to-NAc projection is in forming context-reward associations – and specifically in driving reward- and goal-directed behaviour based on contextual cues (Trouche et al., 2019; Ito et al., 2008). Ito et al. (2008) used a spatial appetitive context conditioning task where the combination of a light cue *and* spatial context leads to sucrose pellet only in one of three possible spatial contexts. Disconnection of hippocampal input to NAc with asymmetric lesions impaired place preference behaviour in this task – suggesting that hippocampal input to NAc is crucial for spatial-reward associations. Furthermore, recording in dorsal CA1 neurons that project to NAc, Trouche et al. (2019) found that representations of the spatial context in CA1 was required for conditioned place preference. At the synaptic level, long-term potentiation (LTP) at the vH to NAc synapse is also required for contextual place preference (LeGates et al., 2018). These findings thus implicate the hippocampal-to-NAc projection in forming context-reward associations.

However, to date, the functional significance of the vH-to-NAc projection has mostly been examined in spatial tasks – where the conditioning box denotes the spatial context that becomes associated with reward. Given the selective role of the NAc shell in utilising contextual information to drive goal-directed behaviour, one interesting hypothesis is that the vH projection to NAc may be specifically im-

portant in relating nonspatial, internal contexts like hunger to food-related reward, and that this information may be signalled to NAc to drive feeding behaviour; this idea, however, remains untested.

1.5.3 Hippocampus-to-lateral hypothalamus projections

The lateral hypothalamus (LH) is a large, complex and heterogeneous brain region that sits between the preoptic area and the VTA (Stuber and Wise, 2016). Functionally, it contributes to a variety of motivated behaviours, including energy balance, drinking, sexual behaviour, arousal and stress and reward-seeking behaviours (Stuber and Wise, 2016; Jennings et al., 2013, 2015; González et al., 2016). It is classically the site that elicits self-stimulation, where electrode stimulation in the medial forebrain bundle (the white matter tract that courses through LHA) produces strong reinforcement of lever pressing behaviour (Olds, 1958). Specifically, electrical stimulation generates robust food consumption behaviour (Delgado and Anand, 1953), while lesioning the LHA blunts food consumption (Grossman et al., 1978), although some have proposed that it is more likely that the LH promotes a general increase in motivational drive and arousal, rather than driving a specific motivational state (Valenstein et al., 1968), likely by increasing hypothalamic input to the VTA system to promote the reinforcement of actions. Mirroring this diversity in behavioural functions, the LH is comprised of many genetically distinct cell-types that serve distinct roles (Mickelsen et al., 2019; Rossi et al., 2019). For example, glutamatergic and GABAergic neurons appear to have distinct input and output connectivity and behavioural functions (Jennings et al., 2013; Nieh et al., 2016). In turn, glutamatergic and GABAergic LH neurons also express the neuropeptides orexin, melanin concentrating hormone (MCH), galanin and neurotensin to different extents, each with seemingly distinct functions (Stuber and Wise, 2016; González et al., 2016). Thus, the LH is a highly complex region with well-described functions in motivated behaviours including feeding behaviour.

In terms of its connectivity, the LH receives diverse inputs from cortical regions such as PFC and hippocampus, and subcortical structures such as lateral septum, nucleus accumbens shell and VTA (Stuber and Wise, 2016; Cenquizca and Swanson, 2006, 2007). Specifically, ventral CA1 and subicular projections to LH are monosynaptic and focused mostly around the perifornical region, as well as other

hypothalamic regions such as dorsomedial hypothalamus, anterior hypothalamic area and ventromedial hypothalamus (Cenquizca and Swanson, 2007; Hsu et al., 2015; Petrovich et al., 2001, **Figure 1.4**). Additionally, vH sends disynaptic inputs via NAc (O'Connor et al., 2015), lateral septum (Risold and Swanson, 1996) and prefrontal cortex (Reppucci and Petrovich, 2016) to LH, producing additional complexity of the hippocampal connectivity with the LH. On its output side, LH neurons send projections to VTA (Nieh et al., 2016, 2015), lateral habenula, paraventricular thalamus (Stratford and Wirtshafter, 2013) and other effector regions. Thus, hippocampal input is well-positioned to influence motivated behaviour through the extensive connectivity between the hippocampus and hypothalamus.

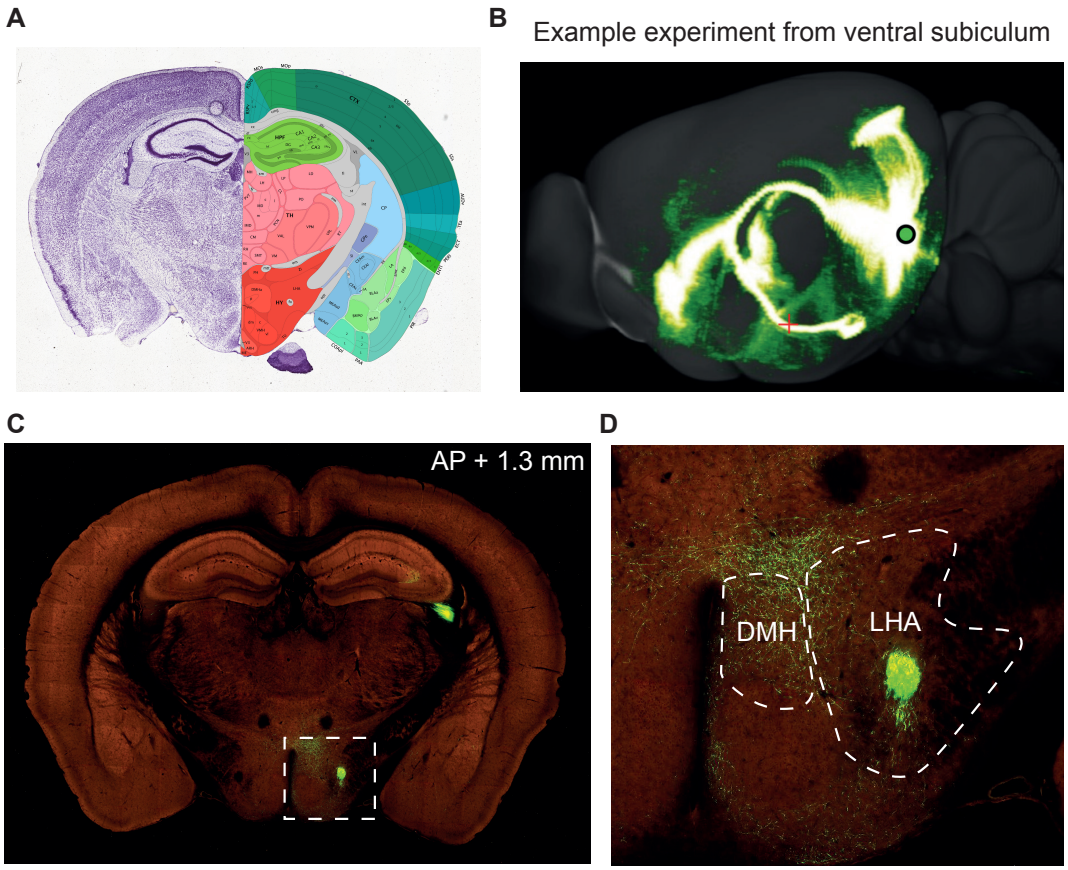

Figure 1.4: Hippocampal projections to hypothalamus. (A) Allen Brain Atlas coronal section around the anterior-posterior level of +1.3 mm. (B) Projection density map of experiment ID 152994878, involving GFP expression in vH (CA1, subiculum and prosubiculum) in a wild-type mouse. Green dot represents the site of the AAV tracer injection, and red cross represents the site of the coronal sections shown in (C–D). (C) Coronal section image of the lateral hypothalamus from the example experiment from (B). Boxed area around the region of the hypothalamus indicates the zoom-in image in (D). (D) Hypothalamus, including the dorsomedial and lateral hypothalamic area (DMH and LHA, respectively), receives dense inputs from ventral subiculum. Data taken from the Allen Brain Atlas.

Little is known about the role of these direct, monosynaptic hippocampal projections to LH; the proposed functions of this pathway range from mediating the learned aspects of feeding behaviour to anxiety (Hsu et al., 2015; Jimenez et al., 2018). Hsu et al. (2015) found that direct ghrelin signalling in ventral CA1 projections to lateral hypothalamus is critical for learned aspects of feeding behaviour. They entrained animals to feed during restricted times of the day, and found that direct cannulation of ghrelin into vH increased food consumption, but cannulating the GHSR1a antagonist potently reduced the amount of food consumed in meal-entrained rats. This effect of GHSR1a antagonism was absent in control rats not entrained to a feeding schedule, highlighting the specific role of the vH in learned aspects of feeding behaviour. The projection from ventral CA1 to the LH has also been implicated in anxiety. Jimenez et al. (2018) found increased activity of the ventral CA1 projection to LH when animals were in the open arm of the EPM and that inhibiting this projection increased open arm exploration. These few studies suggest that hippocampal input to LH may be required for behavioural avoidance and driving feeding behaviour in response to learned associations.

1.6 Thesis overview

As a brief summary of the preceding sections, I have discussed how the hippocampus is important for ambiguity resolution. Feeding behaviour can be described as a decision-making process with ambiguity surrounding the value of food, implicating the hippocampus in the control of feeding behaviour. The hippocampus can also use the hunger state as a context to guide behaviour. However, to date, no study has addressed whether the vH is sensitive to the hunger state during innate, naturalistic feeding behaviour, what behaviours its activity encodes during free-feeding behaviour, and which hippocampal projections contribute to this function. Though it is clear that motivational state affects hippocampal processing, the cellular and circuit mechanisms underlying this ability of the hippocampus in sensing the internal state remains completely unknown. Furthermore, if the hippocampus does directly sense hunger through defined hippocampal projections, it is not known what neural mechanism – whether direct hormonal sensing or processing of synaptic input – underlies this function. As a first step, an understanding of the input connectivity to the vH is crucial; however, such a description is lacking. Thus, this thesis sought to

address the following questions:

- What are the activity dynamics of the vH during feeding behaviour across different states of hunger?
- What are the ventral hippocampal circuits specifically involved in encoding feeding behaviour and the hunger state?
- What are the circuit and cellular mechanisms supporting this hunger sensitivity in vH?
- What is the input connectivity of the vS that might explain functional heterogeneity in the vH circuit?

In **Chapters 3 and 4**, I present data on the behavioural dynamics of feeding when mice are presented with food under different states of hunger, and directly relate these behavioural descriptions to vH neural activity. Using *in vivo* Ca^{2+} imaging of ventral hippocampal activity, I show that specific hippocampal projections are uniquely modulated by hunger during the anticipatory phase of feeding behaviour.

Then, in **Chapter 5**, I show that the systemic ghrelin and hippocampal ghrelin receptors mediate changes in synaptic transmission in vH *in vitro*, and that impairing ghrelin receptor signalling in vH prevents systemic ghrelin from changing circuit activity *in vivo*. I also provide evidence that pharmacogenetic manipulation mimicking the effect of ghrelin on vH is sufficient to alter the short term dynamics of feeding behaviour without affecting food consumption. This highlights the role of GHSR1a in vH projections to NAc as a mechanism for internal state sensing in hippocampus and potentially as a modulator of food-seeking behaviour.

Next, in **Chapter 6**, I present results from a series of experiments that delineates the input-output circuitry of the vH, in an attempt to identify upstream inputs that may be relaying hunger-related signals to hippocampus.

Finally, in **Chapter 7**, I summarise the main findings of my thesis and discuss the implications of my work, including how innate, motivated behaviours such as feeding may require the hippocampus.

Chapter 2

Methods

2.1 Animals

Young adult C57BL/6 male mice (behavioral and anatomical experiments: at least 7 weeks old; whole-cell electrophysiology experiments: 7 – 9 weeks old) provided by Charles River were used for all experiments. All animals were housed in cages of 2 to 4 in a temperature- and humidity-controlled environment with a 12 h light-dark cycle (lights on at 7 am to 7 pm). Food and water were provided ad libitum (except in food-restricted experiments). All experiments were approved by the UK Home Office as defined by the Animals (Scientific Procedures) Act, and strictly followed University College London ethical guidelines.

2.2 Stereotaxic surgery

Stereotaxic surgeries were performed according to previously described protocols (Cetin et al., 2007). Mice were anaesthetised with isoflurane (4% induction, 1.5 to 2% maintenance) and secured onto a stereotaxic apparatus (Kopf). A single incision was made along the midline to reveal the skull. AP, ML and DV were measured relative to bregma, and craniotomies were drilled over the injection sites. Long-shaft borosilicate pipettes were pulled and backfilled with mineral oil, and viruses were loaded into the pipettes. Viruses were injected with a Nanoject II (Drummond Scientific) at a rate of 13.8 to 27.6 nL every 10 s. Following infusion of the virus, the pipette was left in place for an additional 10 mins before being slowly retracted. Stereotaxic coordinates are listed in **Table 2.1**.

Following injection of substances into the brain, animals were sutured and recovered for 30 mins on a heat pad. Animals received carprofen as a peri-operative

Region	ML	AP	DV
Medial prefrontal cortex	0.4	+2.3	-2.4
Lateral hypothalamus	0.9	-1.3	-5.2
Nucleus accumbens (medial shell)	0.9	+1.1	-4.6
Ventral subiculum (anterior)	3.4	-3.2	-4.3
Ventral subiculum (posterior)	3.4 to 3.5	-3.7	-4.3 to -4.7
Nucleus reuniens	0.25	-0.7	-4.4

Table 2.1: Stereotaxic injection coordinates for the different brain regions. All experimental coordinates were based on the Paxinos atlas.

Virus	Viral titre (genome copies / mL)
RabiesΔG-EnvA-H2B-mCherry-2A-CLIP	1.8×10^8
pAAV-synP-FLEX-splitTVA-EGFP-B19G	3.9×10^{12}
pENN-AAV-hSyn-Cre-WPRE-hGH	1.3×10^{13}
pAAV-hSyn-hChR2(H134R)-EYFP	2.5×10^{13}
pAAV2-retro-CAG-Cre	5.3×10^{12}
AAV1-CAG-Flex-GCaMP6f-WPRE-SV40	$>1 \times 10^{13}$
AAV1-CamKII-Cre-SV40	$>1 \times 10^{13}$
AAV8-hSyn-DIO-hM3Dq	7.9×10^{12}
AAV8-hSyn-DIO-hM4Di	7.0×10^{12}
AAV8-hSyn-DIO-mCherry	3.8×10^{12}
AAV1-EF1a-DIO-mCherry-scrmb-shRNAmir	1.0×10^{13}
AAV1-EF1a-DIO-mCherry-ghsr-shRNAmir	4.1×10^{13}

Table 2.2: Viruses used for the experiments described in this thesis.

s.c. injection (0.5 mg/kg) and in their drinking water (0.05 mg/mL) for 48 hours post-surgery. The titers of viruses used in the experiments described throughout the thesis are listed in **Table 2.2**.

2.3 Behavioural studies

2.3.1 Stereotaxic surgeries

For photometry experiments, fibre cannulae were implanted following virus injection in the same surgery. The skull was roughened and two metal screws were inserted into the skull to aid cement attachment. Photometry cannulas were targeted to ventral CA1/subiculum. Cannulas were secured to the skull by applying two layers of adhesive dental cement (Superbond CB). The skin was attached to the cured dental cement with Vetbond. Animals received a subcutaneous injection

of carprofen (∼5 µL of 0.5 mg/mL stock) prior to recovery in a warm chamber for 1 hour and continued receiving carprofen in their drinking water (0.05 mg/mL) for 48 hours post-surgery. Mice were allowed to recover for a minimum of 3 weeks before starting photometry experiments. For overall vS neural activity recordings, a virus mix diluted in a ratio of 1:1:2 was used, 1 of *AAV1-CAG-Flex-GCaMP6f-WPRE-SV40* : 1 of *AAV1-CamKII-Cre-SV40* : 2 of sterile saline; total volume injected = 300 – 400 nl. The virus mix was injected into vS. This dilution protocol was used to delay excessive GCaMP expression, which could lead to reduced Ca^{2+} variance in the signal, affect cellular processes and reduce cell health (Resendez et al., 2016). For projection-specific expression of GCaMP6f, either 150 – 200 nL of *rAAV2-retro-CAG-Cre* or *rAAV2-retro-Syn-Cre* (Tervo et al., 2016) was injected into the output site (PFC, LH or NAc); in the same surgery, 300 – 400 nL of a 1:3 dilution of *AAV1-CAG-Flex-GCaMP6f-WPRE-SV40* in sterile saline was injected into vS. For combined projection-specific fibre photometry and molecular knockdown experiments, 150 – 200 nL *rAAV2-retro-Syn-Cre* was injected into NAc, and a 1:1 mix (400 - 500 nL) of *AAV1-CAG-Flex-GCaMP6f-WPRE-SV40* and *AAV1-EF1a-DIO-mCherry-ghsr-shRNAmir* or *AAV1-EF1a-DIO-mCherry-scrmb-shRNAmir* was injected into vS.

2.3.2 Free-feeding task and fibre photometry recordings

Following at least 3 weeks post-surgical recovery, animals (10 – 12 weeks old) were handled for at least 7 days before testing. During the last 3 days of habituation, empty plastic weighing boats and, in a subset of animals, a plastic tube lid and a dollop of peanut butter (Skippy) were provided in the home cage to habituate the animals to these objects. Animals were also habituated to patch cord attachment while placed in the behavioural boxes during the last 3 days of habituation. All behavioural experiments were carried out in Med Associates sound-attenuating chambers containing behavioural boxes (21.59 x 18.08 x 12.7 cm) with blank walls. Video recordings were conducted with infrared cameras (Playstation 4 Motion Camera) positioned above each chamber, and video was acquired at 15 or 25 Hz using Bonsai (Lopes et al., 2015). The different frame rates were due to a change of PS4 cameras over the course of experiments, and this difference in frame rates did not affect the resolution of capturing naturalistic behaviour given the relatively

slower time course of evolving behaviours during feeding. All experiments were performed consistently during the middle-to-end of the light cycle (from 2 pm to 7 pm) to control for circadian rhythm variables.

A typical workflow for a given animal is the following: photometry recordings of neural activity were conducted first in the Fed, Fasted and Refed states over the course of ∼3 days (**Figure 2.1A**). Then, the animal is habituated over the course of 2 to 3 days with three separate intraperitoneal (i.p.) injection of 100 µL sterile phosphate-buffered saline (PBS) to habituate them to manual scruffing and i.p. injection. Following this, the animal is tested with photometry recording of neural activity in the PBS and Ghrelin states in a counterbalanced order (**Figure 2.1B–C**). Refer to **Figure 2.1** for details of the experimental workflow.

For the Refeeding protocol (i.e. Fed/Fasted state comparison), the experiment was conducted over ∼3 days. Animals were maintained on ad-libitum food access and tested on the first day (Day 1: Fed); then, the animals were fasted overnight for 16 to 18 hours and subsequently tested (Day 2: Fasted). Finally, animals were tested again on the third day after at least 24 hours of re-feeding (Day 3: Refed). On each test day, animals were habituated to the behavioural box for 10 mins after attachment to the optic fibre patch cord. This habituation period was repeated for all days of the experimental conditions, i.e. Fed, Fasted and Refed days. The Labview programme controlling photometry signal acquisition was started at the beginning of this 10-minute habituation period. Animals were then presented with an empty weighing boat for 5 mins to habituate them to manual presentation and the weighing boat, and subsequently presented with a single 3- to 5-gram chow pellet in the weighing boat. The presentation of chow lasted for 10 mins before termination of the recording (**Figure 2.1A**).

For the Acute hormonal manipulation protocol (i.e. PBS/Ghrelin comparison), animals were habituated to patch cord attachment for a 10 minute period, as described above. At the end of this habituation period, animals were given an i.p. injection of either ghrelin (2 mg/kg; Tocris) or vehicle control (phosphate-buffered saline, PBS; pH = 7.2). The order of the injections was counterbalanced across animals. The volume of the i.p. injection was fixed at 100 µL. Animals were allowed 15 mins to recover post-injection before the presentation of non-food and food ob-

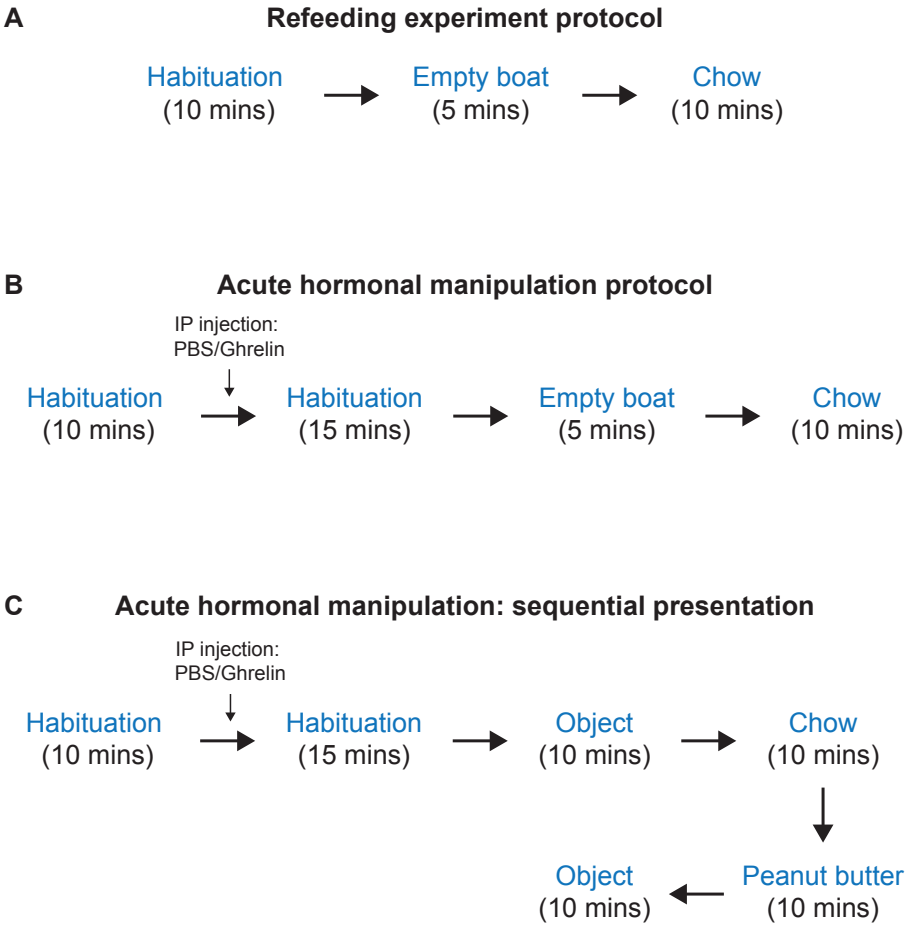

Figure 2.1: Protocol workflow for photometry experiments in the naturalistic, free-feeding setting. Animals were assessed in the Fed and Fasted states as described in (A), while PBS and Ghrelin states were assessed as described in either (B) or (C). The inclusion of non-food object ('Object') and peanut butter was chosen to assess the possibility of value coding in vS activity.

jects. Animals were then presented with a pellet of chow only (**Figure 2.1B**) or, in a subset of experiments, manually presented with items in the following sequence: a non-food plastic object (universal tube lid), standard lab chow (Envigo), peanut butter (nutritional content per 100 g: energy, 613 kcal; fat, 51.6 g; carbohydrates, 14.1 g; protein, 25.3 g; salt, 0.45 g) and non-food object again for 10 mins each, with 2 mins interval between each presentation (**Figure 2.1C**). This sequential presentation protocol was used to compare the effect of hunger state on vS activity to non-food object (tube lid) and a high-calorie food item (peanut butter). This sequence of presentations, and more specifically the ordering of chow before peanut butter presentation, was designed to avoid over-sating the animals with peanut butter before chow presentation. The inclusion of a second plastic lid presentation at

the end of peanut butter presentation was used to account for the possibility of photobleaching across the session duration. The day of ghrelin injection was selected randomly for each animal, and PBS and ghrelin injection days were spaced apart for a duration of at least 24 hours.

After termination of each testing session, the amount of chow or peanut butter consumed during the 10 min presentation was weighed; any spillage of food was recovered and subsequently weighed. The time of food or non-food presentation was noted down and used to manually synchronise the photometry recordings to the start of stimulus presentation. Photometry experiments with apparent failure in equipment or software acquisition were discarded from further analysis. Photometry signals from experiments in which the signal did not exceed $>$2 standard deviations above a 50-s preceding baseline before food presentation were excluded from subsequent analysis as these indicate poor signal (either misplaced fibres or injection sites, or inadequate expression). Data from all animals were included in the final analysis.

2.3.3 Annotation of feeding behaviour

Feeding behaviour was analysed as a composite sequence of five simple, distinct and reproducible behaviours. These elemental behaviours are: Approach (sniffing or tactile interaction with the object or food without eating), Eat (biting food or chewing movements close to food), Rear (standing on hindlegs while elevating head, can be supported on the walls i.e. thigmotaxis), Groom (licking/scratching of fur, limbs or tail, usually high-frequency movement) and Rest (motionless, usually in corner of box). These behaviours together are referred to as the Behavioural Satiety Sequence (BSS, Halford et al., 1998; **Figure 3.1A–B**). These features were manually scored offline using Ethovision XT13 (Noldus). Where possible, manual scoring was conducted in a blinded fashion to experimental groups. For a subset of videos, two independent scorers conducted manual annotation of the behaviour videos to ensure reproducibility. Manual annotation of BSS behaviours from 10-minute videos spanning the food or non-food object presentation period were conducted at 15 or 25 Hz on a frame-by-frame basis. This manual annotation produced vectors of 0s and 1s, where 0 indicates the absence and 1 the presence of the BSS behaviour.

2.3.4 Analysis of feeding behaviour as a stochastic Markov process

Each behavioural dataset exists as a sequence of BSS behaviours. In other words, the behaviour for a given animal is described by a vector of BSS behaviours occurring over time. Although the total time spent engaging in one behaviour can be computed from this vector, additional information regarding an animal's feeding strategy exists in the sequence of expression of each BSS behaviour (Burnett et al., 2019). To analyse this sequential information in more detail, I analysed the annotated behavioural patterns for each mouse as a stochastic Markov process that defined the animal's feeding strategy when presented with chow across different states of hunger. Specifically, a Markov chain is a vector of states that change as a function of time (Burnett et al., 2019). In this case, the Markov chain is comprised of 5 states corresponding to the 5 BSS behaviours. These Markov chains are described fully by a transition matrix P, where the P_{ij} term represents the transition probability from BSS behaviour i to j. As there are 5 BSS behaviours, P is a 5 $\times$ 5 transition matrix, where the rows represent the current BSS behaviour, the columns represent the BSS behaviour one-step ahead and the values in each row sums to 1. To compute the empirical transition matrices for each animal, the frequency of each possible transition from behaviour i was calculated and normalised by the total number of behavioural transitions occurring from behaviour i. These transitions are assumed to be Markovian, which simplifies the calculation of the transition probability $P(state = j|state = i)$. Specifically, the probability of transitioning from state i to state j is dependent only on the current state i and not on states preceding state i. For each animal, there were four transition matrices, P_{Fed}, P_{Fasted}, P_{PBS} and P_{Ghrelin}.

Importantly, these Markov chain vectors disregarded information relating to duration, i.e. the time spent in engaging in one behaviour and the inter-event duration (**Figure 2.2**). In other words, by focusing on transitions between BSS behaviours, this analysis was conducted time-agnostically; this method has been shown to accurately capture moment-to-moment behavioural strategies under differing contexts (Burnett et al., 2019) by focusing on the transition probability from one behavioural bout to the next. For example, the vector [Approach, Approach, Eat, Groom] represents four distinct BSS bouts of variable length within and between bouts, but only

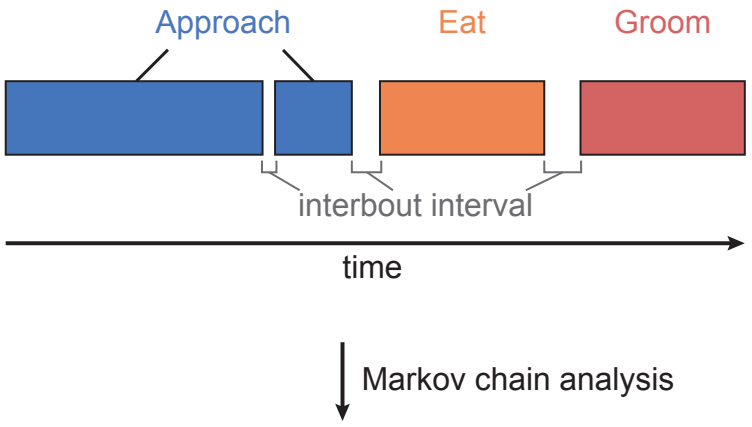

Figure 2.2: Example Markov chain analysis. Feeding behaviour unfolds as a sequence of each component (bout) of the BSS behaviour. Bouts of BSS behaviours vary in their duration within and between bouts. The Markov chain analysis disregards variability in these durations, and distills the behavioural sequence into a vector of occurrence of each BSS behaviour.

the transitions between bouts was analysed (**Figure 2.2**). Notably, frame-to-frame transitions were not considered in this analysis.

2.3.5 Analysis of transition matrix similarity

To quantify and compare the transition matrices between different states of hunger, I used the cosine distance as a similarity metric between two matrices (Burnett et al., 2016). More specifically, the transition matrices P_{Fed}, P_{Fasted}, P_{PBS} and P_{Ghrelin} contained information about the probability of transitioning from one behaviour to the next behaviour, and I used the cosine distance to make inferences about how hunger changes these transition probabilities. These 5 $\times$ 5 transition matrices were ravelled to produce 25-dimensional vectors, with each element representing a transition probability P_{ij}. Thus, for a within-subject comparison of the similarity in the transition vector between the sated and hungry states, the angle or cosine similarity between the two transition vectors u and v, i.e. Fed and Fasted state transition vectors respectively, was computed using the following formula (Burnett et al., 2019):

$$\cos\theta = \frac{u \cdot v}{\|u\| \, \|v\|} \tag{2.1}$$

$$\text{Cosine distance} = 1 - \cos\theta$$

The range of the cosine distance is bounded in the interval $[0, 1]$. Values of the cosine distance closer to 0 indicate a high similarity and a smaller angle between the two vectors, while values closer to 1 indicate low similarity and a large angle between the two vectors. For this cosine distance analysis of BSS behavioural transition vectors, 3 values were computed for each animal: ”within-subject”, ”subject-vs-mean (within state)” and subject-vs-mean (different state)” cosine distances. First, the ”within-subject” cosine distance used the ’sated’ state (Fed and PBS) as the baseline transition vector, and the cosine distance of the transition vectors for the ’hungry’ states (Fasted and Ghrelin) were compared to the baseline transition vector. Secondly, the ”subject-vs-mean (within state)” cosine distance measured the distance of the sated transition vector of *one* animal to the mean sated transition vector of *all other* animals in the cohort. This measurement provides an indication of the relative consistency of behavioural patterns in the sated state. Finally, the ”subject-vs-mean (across state)” cosine distance measured the distance of the sated transition vector of *one* animal to the mean hungry transition vector of all other animals in the cohort. This measurement provides a control analysis for the individual-to-population comparison offered by the subject-vs-mean (within state) cosine distance, and should be similar to the within-subject cosine distance if the behavioural vectors are consistent across animals.

2.3.6 Clustering of BSS behavioural transition matrices

Given the stereotyped nature of innate feeding behaviour (Berman et al., 2014; Burnett et al., 2019), it is possible that the experimental manipulations of hunger produced only a small discrete number of behavioural patterns that can be clustered into distinct groups. To identify such groupings, I first reduced the dimension of the 25-dimensional transition matrices using Fisher’s linear discrimnant analysis (LDA). LDA identifies the subspace that maximises the discriminability between the experimental manipulations of hunger, i.e Fed, Fasted, PBS and Ghrelin, by maximising the ratio of the between-class over the within-class variability. The between-

and within-class variability were scatter matrices S_B and S_W, respectively, where S_B and S_W are 25 $\times$ 25 matrices and the number of rows or columns corresponds to each behavioural transition probability. The target variable was the hunger state (labels of Fed, Fasted, PBS and Ghrelin). The projection matrix used to project the vectors to the first two LDA axes was solved by matrix factorisation using singular value decomposition (SVD) based on the LinearDiscriminantAnalysis function from the *sklearn* package.

For clustering analysis in the reduced LDA subspace, Gaussian mixture model (GMM) clustering was performed using the GaussianMixture function from the *sklearn.mixture* package. GMM was applied on the $n \times 2$ matrix containing the transformed behavioural transition probabilities in the first two LDA subspace, where n is the number of observations (60 observations) in the rows of the matrix, and LD1 and LD2 are the columns of the matrix. The parameters for GMM clustering were the following: 0.3 regularisation to the diagonal of the covariance matrix, full covariance matrix for each component and 1000 maximum iterations. The Gaussian component weights were initialised by k-means. To select the number of Gaussian components that best fit the data, the Bayesian information criterion (BIC) was calculated:

$$\text{BIC} = k \log n - 2 \log \hat{\mathcal{L}} \tag{2.2}$$

where k is the number of model parameters, n is the observation number and $\hat{\mathcal{L}}$ is the maximum likelihood of the model. The BIC value was calculated using the GaussianMixture function. A supervised random forest classifier (100 estimators and using the Gini criterion) was used to assess the robustness of the clustering (Cembrowski et al., 2018a,b). The classifier was iteratively trained with 3 random observations (0 to 39 observations) from a total of 60 observations, and the classifier was used to predict cluster identity of the remaining observations. Each training iteration was repeated 100 times with random sampling of observations to train the classifier (for example, training the classifier with 3 observations was repeated 100 times, with random sampling of 3 observations of the dataset). The accuracy of the classifier was computed as a function of the number of observations used to train the dataset.

2.3.7 Analysis of Ca^{2+} signals from fibre photometry

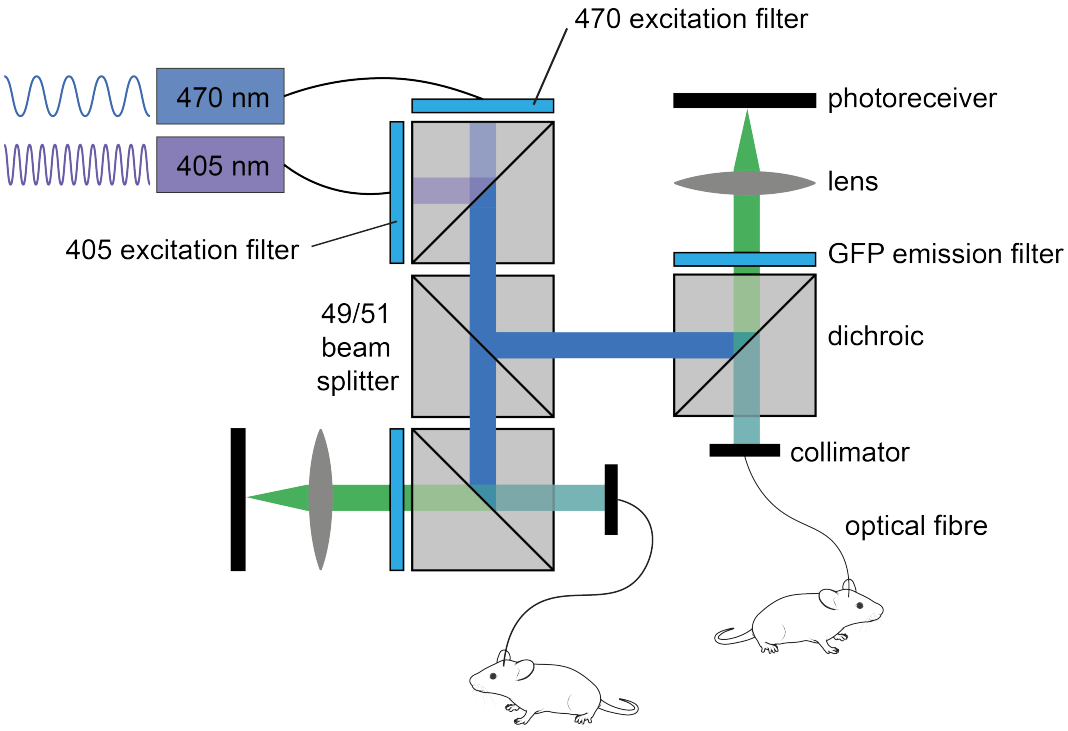

Figure 2.3: Setup of the photometry rig. See text for description.

Measurement of calcium fluorescence signals was carried out as detailed previously (Lerner et al, 2015; **Figure 2.3**). 470 nm and 405 nm LEDs were used as excitation sources, and the light amplitudes were modulated sinusoidally at 500 Hz and 210 Hz carrier frequencies, respectively. The excitation light was passed through excitation filters (for 470 nm and for 405 nm wavelengths), and a dichroic mirror to combine the two LEDs into a single beam. A 49/51 beam-splitter was used to split the beam into two independent excitation beams for simultaneous recording of two animals. The excitation light was coupled through a fibre collimation package into a fibre patch cord, and linked to a large core (200 µm), high NA (0.39) implant cannula (Thorlabs). Emitted fluorescence signals were collected through the same fibre. Fluorescence output signal was filtered through a GFP emission filter (transmission above 505 nm) and focused onto a femtowatt photoreceiver. The photoreceiver was sampled at 10 kHz, and each of the two LED signals was independently recovered using quadrature demodulation on a custom-written Labview software: this process involved using an LED channel as a signal reference, tak-

ing a 90-degree phase-shifted copy of this reference signal and multiplying these signals in quadrature. The multiplied signal was then low-pass filtered with a Butterworth filter (order = 3, cut-off frequency = 15 Hz). The hypotenuse was then computed using the square root of the sum of squares of the two channels. The result corresponds to the demodulated signal amplitude and was decimated to 500 Hz before storing to disk.

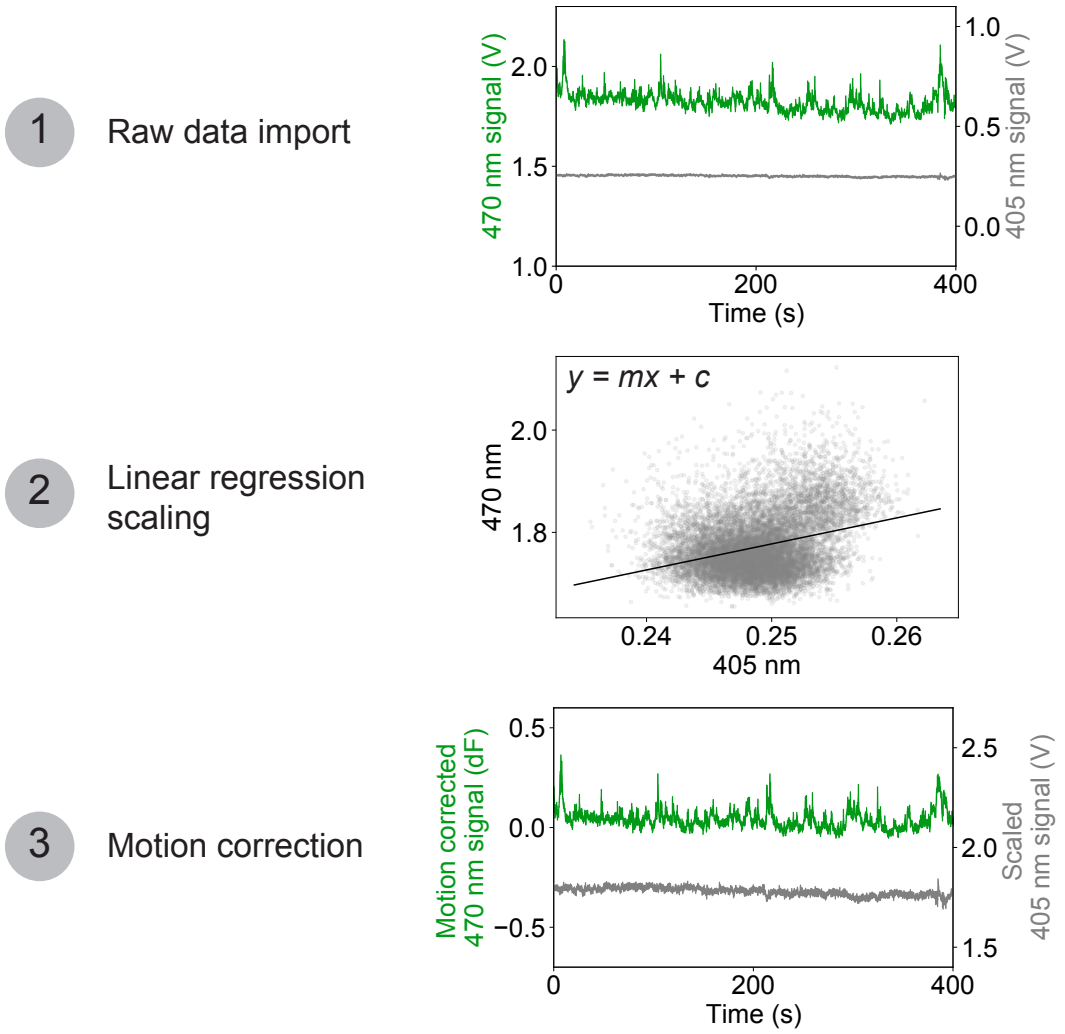

Figure 2.4: Pre-processing and motion correction of Ca^{2+} signals from fibre photometry. See text for description of the pre-processing steps.

For analysis of photometry data, the .tdms data files were analysed with custom-written scripts written in Python 3. The .tdms files containing the raw 470 nm and 405 nm signals were imported and inspected. Specifically, the 470 nm wavelength fluorescence (corresponding to the Ca^{2+}-dependent signal) was in-

spected for adequate signal-to-noise ratio in the Ca^{2+} signals (Step 1, **Figure 2.4**). To correct for artefacts resulting from Ca^{2+}-independent processes such as movement, the Ca^{2+}-independent 405 nm isosbestic wavelength signal was scaled to the 470 nm wavelength. The coefficients for the scaling was computed through a least-squares linear regression between the 405 nm and 470 nm signal (Step 2). Finally, this estimated-motion (scaled 405 nm) signal was then subtracted from the 470 nm signal to obtain a pure Ca^{2+}-dependent signal (Step 3).

Calcium activity signals time-locked to the presentation of each item (non-food object, chow, peanut butter) were extracted using the time of presentation manually determined from video recordings. The signal was decimated to either 1 Hz (for analysis of peri-presentation activity), or 15 / 25 Hz (for event-triggered and regression analysis), z-score normalised (i.e. subtracted by the mean of signal acquired during the 10-minute recording session, and divided by the standard deviation of the signal), filtered with a Gaussian filter (σ = 1.5) and baselined to the mean signal in the -50 to -10 seconds preceding the time of presentation of food or non-food object. For event-triggered analysis, the photometry signal was aligned to the onset of each BSS behavioural event obtained from the manually scored behaviour. The behavioural events were clustered into bouts (defined as continuous engagement in the behaviour), and the onset of each bout was taken as the time point to align the photometry signal. A peri-event window of 20 s surrounding the onset of the behaviour was obtained for each signal, and the resulting signal was baselined to the time period from -10 to -7.5 seconds relative to the onset of each event. All trials obtained for an animal were averaged to obtain a nested average event-triggered signal; these signals were then averaged across mice to obtain the population event-triggered average. Due to the stochastic nature of emitting a given BSS behaviour, not all BSS behaviours were present in all animals. Only Approach behaviour of bout length $>$1 second was considered for analysis, while Eat, Rear, Groom and Rest of all bout lengths were included. Animals displayed Approach behaviour consistently in all internal states of hunger, but the proportion of animals showing Eat, Groom, Rest and Rear behaviours were variable.

2.3.8 Linear encoding model relating behaviour to neural activity

To quantify the contribution of each BSS behaviour to neural activity, a multiple regression model was used. The linear model was constructed using the Python package sklearn, with the z-scored baselined photometry signal ($\frac{dF_z}{F_z}$) as the dependent variable, and a regressor matrix of BSS behavioural arrays as independent variables. The regressor matrix contained 27 regressors in total: 5 behavioural regressors (Approach, Eat, Rear, Groom and Rest), 20 behavioural transition regressors (for example, Approach $\rightarrow$ Eat), a manual presentation regressor and a velocity regressor. The 5 behavioural regressors were coded as pulses of 0s and 1s, where 1s indicate the engagement in a BSS behaviour and 0s the absence of engagement. The 20 transition regressors were included to account for any possible contribution of behavioural transitions to the photometry signal, and were derived as follows: a Markov chain vector of BSS behaviours was produced at 15 or 25 Hz and any across-BSS transitions (e.g. Approach $\rightarrow$ Eat, not Approach $\rightarrow$ Approach) occurring within 5 seconds was emitted as a temporal pulse of 1 at the onset of the next BSS behaviour. To account for temporal distortion of the behavioural transition period in the associated Ca^{2+} activity, an exponential function was first computed:

$$g(t) = Ae^{Bt} \tag{2.3}$$

where

$$A = 1$$
$$B = -\frac{\log(\frac{1}{A}) + 1}{t_{1/2}} = \frac{1}{t_{1/2}}$$

where $t_{1/2}$ is the half-life of the exponential function and set to 2 seconds. The transition regressor was convolved with the exponential function:

$$f(t) * g(t) = \int_{-\infty}^{\infty} f(\tau)g(t-\tau)d\tau \tag{2.4}$$

where $f(t)$ is the transition regressor and $g(t)$ is the exponential function. This produces a sharp peak to 1 and a decay rate of $t_{1/2}$. The exponential decay func-

tion was set to have a half-life of 2 s to approximate near-complete decay of the GCaMP6f signal. The presentation regressor was set to an exponential function with a peak time at presentation onset and a decay rate of 5 seconds to capture the salience of stimulus presentation. Finally, the velocity regressor was a continuous variable tracking the instantaneous velocity of the animal derived from position tracking using Ethovision. The velocity signal was smoothed with a rolling mean filter (window = 3 seconds), and missing values from discontinuous position tracking were imputed via linear interpolation.

The final linear encoding model was therefore the following:

$$Y = \beta_0 + \sum_{n=1}^{N_{\mathsf{B}}} \beta_n^B + \sum_{n=1}^{N_{\mathsf{Tr}}} \beta_n^{Tr} + \beta^P + \beta^V + \epsilon \tag{2.5}$$

where Y is the $\frac{\mathsf{dF}_z}{\mathsf{F}_z}$ in one animal, β_0 is the intercept (bias), ϵ is a Gaussian noise term, N_{B} and N_{Tr} are the numbers of the behavioural and transition regressors (5 and 20, respectively), β^B, β^{Tr}, β^P and β^V are the beta weights for the behavioural, transition, presentation and velocity regressors, respectively. Specifically, the beta weights β^B can be interpreted as the isolated, average neural response to engagement in that BSS behaviour. The crucial aspect of the linear encoding model is the simultaneous inclusion of possible confounding variables, for example, behavioural transitions and velocity, which may each contaminate the neural response. The linear model thus statistically disambiguates the neural response to BSS behaviour engagement from other events in close temporal proximity.

The linear model was fit using ridge regression, a version of the ordinary least-squares regression that penalises the size of the estimated β coefficients by L2 regularisation. This ensures that the β weights were constrained to avoid overfitting, and the penalty term α adjusts the degree of shrinkage of the β weights. Prior to fitting, the dataset was split into an 80% training set to estimate the β weights and 20% test set for evaluating the model predictions. On this training dataset, a nested cross-validation procedure was used: first, the training dataset was split into 5 folds for evaluation. For each fold, the α hyperparameter was tuned using leave-one-out cross-validation (GCV). GCV works analogously to a grid search by exploring the alpha parameter space, and selecting the α value that maximises the prediction accuracy of the model; the values of α tested were 10^{-3}, 10^{-2}, 10^{-1}, 10^{0}

and 10^1, using the function *RidgeCV* on Python's sklearn package. The values of α did not differ significantly between the Fed and Fasted states or the PBS and Ghrelin conditions. The photometry signal was resampled to 15 or 25 Hz to match the sampling rate of the predictor matrix, and the predictor matrix was normalised by subtracting the predictor matrix by its mean and dividing by the L2 norm of the matrix, using the function *RidgeCV*. The β weights were computed analytically using the following formula:

$$\beta = (\mathbf{X^T X} + \alpha \mathbf{I})^{-1}(\mathbf{X^T Y}) \tag{2.6}$$

where $\mathbf{X}$ is the predictor matrix, α is the ridge penalty term, $\mathbf{I}$ is the identity matrix and $\mathbf{Y}$ is the observed $\frac{\mathsf{dF}_z}{\mathsf{F}_z}$. Once fitted, the performance of the linear encoding model was assessed by using the independent test set to compute the explained variance (5-fold, cross-validated R^2) value, or the coefficient of determination, defined as:

$$R^2 = 1 - \frac{u}{v} = 1 - \frac{\sum_i (y_i - \hat{y})^2}{\sum_i (y_i - \bar{y})^2} \tag{2.7}$$

where u is residual sum of squares, v is the total sum of squares, y_i is the photometry signal at index i, $\hat{y}$ is the predicted photometry signal at index i and $\bar{y}$ is the mean amplitude of the photometry signal in the test set. Linear models were estimated separately for data from individual animals.

2.3.9 Operant feeding task

A behavioural task – referred to as the 'operant feeding task' – was designed to temporally dissociate the time leading up to food consumption. In this task, mice were trained to press a lever to obtain a liquid food droplet (20 µL per droplet of Ensure) in Med Associates behavioural boxes. In these boxes, there was a central nose port, with an infrared beam break and a syringe delivery system to dispense the liquid food. Flanked on either side of the central port was a left or right lever (counterbalanced across animals). The behavioural apparatus was controlled using custom written scripts written in MEDPC. To initiate a trial, the animal must press a lever that is presented randomly at an inter-trial interval (ITI) between 10 and 20 s in duration (Lever out). If the animal does not press the lever within 5 s, the

lever is retracted and the ITI initiated. After an animal presses the lever (Lever Press), the central nose port is illuminated (Cue Light) at a jittered time interval between 0.5 and 1.5 s to signal availability of the liquid food. Then, following the first nosepoke into the central nose port (Nosepoke), a trace interval of 0.05 to 0.25 s was added. Following the trace interval, 20 µL was dispensed (Food delivery), the trial terminates and the animal goes into the ITI. The food is delivered at a fixed-ratio of 1 lever press to 1 delivery (FR1). In this way, the delivery of food after reward is deterministic. Each behavioural session lasted 1 hour. Mice were food restricted and maintained at 90% of the baseline body weight during behavioural training.

After becoming fully trained on the task (criterion, $>$50 lever presses per session), fibre photometry recordings were performed as the animals engaged in the task. After task acquisition, the hunger state was manipulated either by alternately fasting the animals overnight (16 to 18 hours) or ensuring ad-libitum access to food for at least 24 hours. For acute hormonal manipulation of hunger, ad-libitum fed animals received either an i.p. injection of 2 mg/kg ghrelin or PBS 15 mins before the start of behavioural testing on the operant feeding task. Behavioural events corresponding to Lever out, Lever press, Cue light, Nosepoke and Food delivery were signalled via TTL pulses. For analysis of the event-triggered averages, the photometry signals were sampled at 50 Hz, filtered with a rolling mean filter (window size = 15) and baselined to the time period -1 to 0 s preceding the behavioural event onset. For analysis of time-warped signals, the latency between Cue light and Food delivery was first calculated. Only trials in which the latency was $>$0.01 s was included for analysis. Photometry signals during the latency periods were then resampled to a fixed number of samples (100 samples) using the function *resample* from the *scipy.signal* module. Thus, photometry signals during the latency periods of variable duration were resampled to produce a warped signal of fixed duration.

2.3.10 Pharmacogenetic manipulation using DREADDs

To selectively activate or inhibit neural populations at specific times, I used a type of Designer Receptors Exclusively Activated by Designer Drugs (DREADDs), i.e. the humanised muscarinic receptors. These receptors are modified G-protein coupled receptors with a high binding affinity to the inert substance clozapine-N-oxide

(CNO). The two main types of DREADDs, i.e. hM3Dq and hM4Di, are G_q-coupled receptors that, respectively, lead to neuronal activation and inhibition.

These receptors were virally expressed in specific cell types using stereotaxic viral gene delivery, as outlined above. To achieve conditional expression of hM3Dq or hM4Di in specific vS^{NAc} neurons, 150 nL of *rAAV2-retro-Syn-Cre* was injected into NAc and, in the same surgery, 500 nL of either *AAV8-hSyn-DIO-mCherry*, *AAV8-hSyn-DIO-hM3Dq* or *AAV8-hSyn-DIO-hM4Di* was injected into vS. After at least 4 weeks of expression, animals were handled for at least 7 days, including 3 days of acclimation to the testing behavioural chambers and to food presentation. Furthermore, animals were habituated to 3 days of i.p. injections with saline in the behavioural boxes.

On test days, animals were either injected i.p. with control sterile PBS or CNO (1 mg/kg; Hello Bio) 30 minutes before food presentation. These i.p. injections were conducted in their home cage. Following i.p. injection, animals were placed in the behavioural boxes and allowed at least 10 minutes of habituation to the boxes and 5 minutes to an empty weighing boat prior to food presentation. A small pellet of chow was presented to the animal in a plastic weighing boat for 10 minutes. The amount of food consumed was weighed after food presentation. Analysis of BSS behaviour was conducted offline using Ethovision XT, as outlined above under 'Feeding behaviour analysis'.

For pharmacogenetic food intake studies over the course of 24 hours, animals were singly housed and fasted for 15 hours prior to the start of experiments (i.e. remove chow at 6 pm on the first day, and reintroduce food at 9 am on the second day). Thirty minutes before the start of food intake measurements (at 8.30 am), animals received an i.p. injection of either 1 mg/kg CNO or PBS control. A pre-weighed amount of chow was reintroduced into the food hopper at 9 am, and the amount of chow consumed over 1, 2, 4, 8, 12 and 24 hours was serially measured. The i.p. injection order of CNO or PBS was counterbalanced across animals. The day of CNO injection was selected randomly for each animal, and PBS and CNO injection days were spaced apart for a duration of at least 24 hours.

2.4 Anatomical studies

The details of the methods outlined in this section have been published (Wee and MacAskill, 2020).

2.4.1 Retrograde tracing

For CTXβ retrograde tracing, 150 nL of Alexa 555- or 647-tagged CTXβ was injected into one of three output regions (PFC, NAc or LH). After at least 14 days post-surgery, animals were sacrificed for histology. For rabies monosynaptic tracing, experiments were done according to previously described protocols (Beier et al., 2015). Adult male mice were injected with 100 nL of *AAV2-retro-CAG-Cre* or *AAV2-retro-synP-Cre* into one of three output regions (PFC, NAc or LH), and in the same surgery, 250 nL of *AA2/1-synP-FLEX-split-TVA-EGFP-B19G* was injected into anterior or posterior vS. In a second surgery after at least 2 weeks, 300 – 400 nL of *EnvA-RVΔG-H2B-mCherry* was injected into vS. After 7 days of rabies expression, animals were sacrificed for histology.

2.4.2 Histology and imaging

Animals were deeply anaesthetised with a lethal dose of ketamine and xylazine (100 mg/kg) and perfused transcardially with phosphate-buffered saline (pH = 7.2) followed by 4% paraformaldehyde. Brains were dissected and post-fixed overnight at 4ºC prior to sectioning. For CTXβ tracing analysis, 60-µm sections in the horizontal plane were prepared using a vibratome (Campden Instruments). For brain-wide rabies tracing analysis, 60-µm sections were prepared in the sagittal plane with a supporting block of agar, and every second section was mounted and analysed. Sections were mounted on Superfrost Plus slides with ProLong Glass antifade mounting medium (Molecular Probes) and imaged with a 5x objective using a Zeiss Axioscan Z1 or 10x objective using a Zeiss SLM 800, using standard filter sets for excitation/emission.

2.4.3 Whole-hippocampus cell quantification and analysis

For quantification of CTXβ-labelled hippocampal neurons, consecutive 60-µm coronal sections spanning the hippocampus (approximately AP -4.3 mm to -1.0 mm) were collected. Cell counting of retrogradely labelled neurons was conducted using custom written scripts in R based around the WholeBrain package (Fürth et

al, 2018). Only sections containing labelled neurons in the hippocampus ($\sim$ -4.3 mm to -2.8 mm) were analysed. Segmentation was performed using wavelet multiresolution decomposition on the WholeBrain platform in R, and the segmentation parameters (pixel threshold, soma size, brain outline etc.) were adjusted slice by slice to achieve accurate segmentation of neurons. For the registration of coronal sections, five to six random brain sections were sampled and manually annotated with approximate AP coordinates, and the remaining sections were assigned AP coordinates based on interpolation. Registration was conducted in a semi-automated fashion, where individual coronal sections were first automatically registered based on the WholeBrain software and further refined by adding, subtracting and changing corresponding points to clear anatomical landmarks. For each injection in a given experiment, the pair of projection-specific hippocampal populations were labelled with two fluorophores (Alexa Fluor 555 and Alexa Fluor 647). Segmentation was conducted for each channel individually, while registration was conducted on one image data from one channel and an identical registration was mapped onto image data from the other channel. Cell count data were saved as .RData files, imported into Python and analysed using Python 3.6. During the coronal cell count analysis, the experimenter was blind to the assignments of fluorophore to projection cell type.

For spatial distribution, correlation and logistic regression analyses, individual sections were manually assigned AP coordinates by first estimating the posterior-most AP coordinate by referencing the ABA, and then incrementing the next anterior coronal section at 60-µm steps until the last section in the coronal section series. Only hippocampal cells in subiculum ('SUB') and CA1 residing in ventral hippocampus (vH; DV -3.5 and -4.5 mm) were analysed. Cell distributions across AP, ML and DV were determined by kernel density estimation using a Gaussian kernel function and bandwidth estimated by Scott's rule. Correlation analysis was conducted to determine which brain axis covaries most with the projection type of hippocampal neurons. For each injection pair per hemisphere, the covariation of spatial position along each axis with projection type was computed using the point biserial correlation using the scipy function *scipy.stats.pointbiserialr*. The absolute value of the correlation coefficient indicates the degree of covariation, where $|r|$ =

1 indicates perfect correlation, and $|r|$ = 0 indicates no correlation; the absolute correlation coefficient was then compared across the different axes. To analyse how the Pearson correlation coefficient changed as the positions of each cell was rotated about the AP, ML and DV axes, the spatial positions of each cell in two axes were rotated while holding the other axial position constant. The spatial position matrix M was a $2 \times n$ matrix, where n was the total number of cells, each row corresponded to a brain axis, and each column contained the elements corresponding to spatial position of one cell, i.e. $M_{1,n}$ and $M_{2,n}$. This matrix was then rotated using the following formula:

$$M_{rot} = QM_{ori} \tag{2.8}$$

$$Q = \begin{bmatrix} \cos\theta & -\sin\theta \\ \sin\theta & \cos\theta \end{bmatrix}$$

where M_{ori} is the original spatial position matrix, M_{rot} is the transformed rotated matrix and Q is the rotation matrix with the degree of rotation specified by the size of θ. Rotations were made from $-90°$ to $90°$ in bins of $10°$.

To identify which axis contributes most information to predict the projection class of hippocampal neurons, I conducted logistic regression analysis using the sklearn package in Python. For this analysis, the total vH cell counts from each hemisphere were divided into 80% training dataset to train the multinomial logistic regression model, and 20% test dataset to examine the performance of the model. The train-test-split was crucial to assess how well the linear classifiers generalised to unseen data, and thereby infer whether there was overfitting of the dataset in the correlation analysis. The 10-fold cross-validated accuracy was calculated using the LogisticCV function, and the classifiers were assessed for how much their performance degraded after removal of each brain axis (AP, ML or DV) as a predictor in the model. This reduction in accuracy after the removal of one predictor (cv. Δaccuracy) indicates the unique information that spatial position along one axis contributes to their performance. Note that 1 hemisphere out of 12 total hemispheres from 6 animals was excluded from the dataset due to poor hippocampal labelling.

Finally, LDA was used to unbiasedly identify the plane which most optimally separates the clusters of CTXβ-labelled, projection-specific hippocampal neurons in the coronal plane. The between- and within-class variability were summarised in scatter matrices S_B and S_W, respectively, where S_B and S_W are 3x3 matrices and the number of rows or columns corresponds to each brain axis (AP, ML and DV). The predictor variables for the LDA analysis were the registered spatial positions in AP, ML and DV, and the target variable was the projection type (encoded labels of NAc, PFC or LH). The entire dataset (n = 26,838 vH neurons counted from 10 experiments; 6 animals) was split into an 80% training and 20% held-out test dataset. The projection matrix used to transform the retrogradely labelled neurons to the subspace that best maximises discriminability was solved by matrix factorisation using singular value decomposition (SVD) based on the LinearDiscriminantAnalysis function from the sklearn package:

$$S_W^{-1} S_B \phi = \phi \Lambda \tag{2.9}$$

where ϕ is the eigenvector (projection) matrix where the columns correspond to the eigenvectors (linear discriminant orthonormal vectors), and Λ is the diagonal eigenvalue matrix. The spatial positions of the held-out test dataset were then transformed using the following formula:

$$X' = X\phi \tag{2.10}$$

The transformed spatial positions were plotted as a function of the first and second linear discriminants, and the distributions in the first and second linear discriminants were determined by kernel density estimation.

2.4.4 Analysis of spatial positions of vS projections along the PD axis

For a subset of CTXβ injected brains (7 out of 13 brains), brain sections were prepared in the horizontal plane to analyse the spatial positions of retrogradely labelled vS projections to PFC, NAc and LH along the PD axis. Six to eight sections spanning vS (approximately DV -3.5 to -4.5 mm) were analysed per brain hemisphere. Using ImageJ, horizontal sections of the hippocampus were digitally straightened from the dentate gyrus to the end of subiculum using the Straighten function on

ImageJ to approximate the PD axis. Labelled cells in each slice were manually counted and registered to this axis using the ImageJ CellCounter plugin. Each registered cell was collapsed in the radial axis (y-coordinate), and only the proximal-distal axis (x-coordinate) of each cell was used for spatial position analysis. The CA1/subiculum border occurs approximately at 0.7 within this normalised proximal-distal axis range and was anatomically defined as the disappearance of stratum oriens and the fanning out of the pyramidal cell layer. The spatial positions were analysed with custom Python routines.

2.4.5 Mapping and analysis of rabies-labelled inputs

Cell counting of rabies labelled inputs was conducted using WholeBrain (Fürth et al., 2018), a recently developed automatic segmentation and registration workflow in R. After acquiring the imaged sections and exporting them as 16-bit depth image files, images in the rabies mCherry channel were manually assigned a bregma coordinate (ML -4.0 to 0.0 mm) and processed using WholeBrain (Fürth et al., 2018) and custom cell counting routines written in R. The workflow comprised of (1) segmentation of cells and brain section, (2) registration of the cells to the ABA and (3) analysis of anatomically registered cells. As tissue section damage impairs the automatic registration implemented on the WholeBrain platform, sections with poor registration were manually registered to the atlas plate using corresponding points to clear anatomical landmarks. Once all cells have been registered, the cell counts were further manually filtered from the dataset to remove false-positive cells (e.g. debris). Virtually all cells were detected in the injected hemisphere, apart from a consistent set of contralateral CA3 inputs. Therefore, only the injected hemisphere up to the midline was used for cell quantification analysis.

Each cell registered to a brain region was classified as belonging to an anatomically defined region as defined by the ABA brain structure ontology. Information on the ABA hierarchical ontology was scraped from the ABA API (link: `http://api.brain-map.org/api/v2/structure_graph_download/1.json`) using custom Python routines. The coarse-level (or parent) structures to which each cell belonged were defined a priori and comprised the following: Hypothalamus, Isocortex, Hippocampal formation, Thalamus, Cortical subplate, Pallidum, Striatum, Midbrain, Pons and Medulla. All cells falling under these parent structures were

analysed. The fine-level (or child) structures represent all brain regions existing as subcategories of the corresponding coarse-level structure, e.g. nucleus reuniens and paraventricular thalamus are fine-level (child) structures relative to Thalamus (parent). For quantification of input fractions, cells residing in different layers within the same structure, e.g. CA1 stratum oriens and stratum lacunosum-moleculare, or subdivisions of nuclei, e.g. basomedial amygdala, posterior division (BMAp) and anterior division (BMAa), were agglomerated across layers and subdivisions and counted as residing in one single region (BMA).

2.4.6 Starter cell centre of mass (COM) quantification

To determine the starter cell COM, every 2nd sagittal section from both the rabies mCherry+ and TVA-G GFP+ channels that spanned the extent of the TVA-G GFP+ expression in vS was obtained and analysed. Images were collected in order from lateral to medial. Colocalised cells representing starter cells were manually registered onto digital plates from the Paxinos atlas using the ImageJ ROI Manager function. The mean x-, y- and z- coordinates (corresponding to the AP, DV and ML dimensions, respectively) represented the geometric COM along each axis. As the TVA-G construct expressed TVA and G bicistronically (i.e. the exon for TVA and G are linked by a self-cleaving 2A peptide), all cells were assumed to express TVA and G in a 1:1 stoichiometry and unlikely to express one gene without the other. Therefore, all colocalised cells were treated as starter cells.

2.4.7 Analysis of COM vs. projection dependence of inputs

To compare input fractions in the same brain (Figure 6.11), the input fractions were normalised to the total number of extrahippocampal inputs (defined as inputs from outside the *hippocampal formation*). The dataset containing cell counts from n = 20 brains were analysed according to projection or COM. Only fine-level structures exceeding 1% of extrahippocampal input were assessed (15 brain regions). For spatial-dependence visualisation, the input density for each brain region as a function of COM was visualised by first sorting the input fractions of each brain by the COM in the posterior to anterior direction. The array of input fractions was then interpolated to produce 500 data points, smoothed with a Savitzky-Golay filter (window size = 51 points, order = 3), and normalised by dividing each data point by the total area under the curve.

Multiple linear regression modelling was performed to compare the relative influence of COM and projection identity on the amount of rabies labelled inputs in a brain region of interest. For each brain region, a multiple regression model – in which the predictor variables were the COM and projection identity – was constructed using the *ols* function from the statsmodel package in Python. The overall statistical significance of full models (containing COM and projection as predictors) were assessed by ANOVA and computing the F-statistic values per brain region. All p values generated from multiple comparisons were corrected using the Benjamini-Hochberg method (false-discovery rate < 0.05). The models with adjusted p-values < 0.05 were further analysed for statistically significant coefficients using the Wald test and followed up with post-hoc pairwise Tukey multiple comparisons between vS projection populations. To further assess the importance of each predictor to the model, the likelihood ratio (LR) test was used to compare the full model to a reduced model containing only one predictor – either COM or projection. The reduced models containing either COM or projection identity as a predictor were built using the same ols function. The LR test was computed using the following formula from the statsmodel package function compare_lr_test:

$$D = -2 \log \frac{\mathcal{L}_{\text{restricted}}}{\mathcal{L}_{\text{full}}} \tag{2.11}$$

where $\mathcal{L}$ is the likelihood of the model, and D is a test statistic that follows a χ^2 distribution with degrees of freedom (df) equal to the difference in the number of predictors between the full and reduced restricted (reduced) model. The p-values generated from multiple LR tests were corrected using the Benjamini-Hochberg method (FDR < 0.05). As a complementary analysis, the projection-dependence of extrahippocampal inputs from Figure 6.11A was further analysed using multiple one-way ANOVAs, while the spatial-dependence of these inputs from 6.11B was assessed using multiple Spearman rank correlation tests of input fractions against starter cell COM. This analysis revealed similar patterns of biased connectivity to the multiple linear regression analysis, where MPO and PA were detected as projection-dependent inputs, but RE was detected as only COM-dependent.

To assess the relative goodness-of-fit of non-nested COM models or projection models, I performed linear regression models with only one predictor by using the

ols function from the Python package statsmodels. Linear models were built for each brain region, where the target variable was the input fraction observed in that brain region normalised to the total number of inputs, and the predictor variable was either the COM or projection. For each of 35 brain regions in total, there were 20 observations (n = 20 brains). The models were fitted, and goodness-of-fit was measured using the BIC. To compare model fits, the corresponding BIC values computed from COM and projection models were subtracted to obtain $\triangle$BIC.

2.4.8 ABA Mouse Brain Connectivity analysis of axonal projections

To validate the spatial targeting of rabies-labelled inputs as predicted by the multiple linear regression analysis, axonal input density arising from the input 'hits' (i.e. MPO, RE and PA) was analysed. For MPO, PVT and RE, three experiments were analysed. For PA, the only two experiments available were analysed. All images were downloaded from the ABA API using the Python package Allen SDK (2015).

The following experiments were used:

Input	Experiment ID	Transgenic line	Image sections used for analysis
MPO	158738180	C57BL/6	158738374, 158738370, 158738366, 158738362, 158738358, 158738354
	119846838	C57BL/6	119847348, 119847344, 119847340, 119847336, 119847332, 119847328
	182459635	Gal-Cre_KI87	182460001, 182459997, 182459993, 182459989, 182459985, 182459981
RE	204832205	Adcyap1-2A-Cre	204832574, 204832570, 204832566, 204832562, 204832558, 204832554
	175374982	C57BL/6	175375180, 175375176, 175375172, 175375168, 175375164, 175375160
	174957972	C57BL/6	174958286, 174958282, 174958278, 174958274, 174958270, 174958266
PA	304721447	Rbp4-Cre_KL100	304721806, 304721802, 304721798, 304721794, 304721790, 304721786
	545415593	Npr3-IRES2-Cre	545415944, 545415940, 545415936, 545415932, 545415928, 545415924
PVT	278510903	Ppp1r17-Cre_NL146	278511259, 278511255, 278511251, 278511247, 278511242, 278511238
	183225830	Grm2-Cre_MR90	183226060, 183226056, 183226052, 183226048, 183226044, 183226040
	301209502	Efr3a-Cre_NO108	301209844, 301209840, 301209836, 301209832, 301209828, 301209824

Table 2.3: ABA dataset used for TRIO validation.

For each experiment, six consecutive coronal images (spanning approximately -3.7 to -3.1 mm AP relative to bregma) of vH were downloaded and analysed using

ImageJ. Only one hemisphere per brain was analysed. The brightness and contrast values were fixed for all sections obtained from a single experiment to allow comparison of the relative fluorescence of axonal projections across slices. Images were downloaded with a downsample factor of 8, ROIs were manually drawn around the vS (defined as the region below the rhinal sulcus, between the alveus and the boundary of the CA1 stratum lacunosum moleculare and adjacent dentate gyrus or CA3 stratum radiatum border), and the mean pixel intensity within the ROIs were measured. The pixel intensity values were normalised to that from the posterior-most section, and the relative fluorescence intensities were compared across the AP axis.

2.5 Whole-cell electrophysiology

2.5.1 Slice preparation

Acute, transverse hippocampal slices were used for all electrophysiological recordings. For retrograde labelling of projection-specific vS neurons, fluorescent retrobeads (Lumafluor, Inc.) were stereotaxically injected into the target site (200 nl per injection site). Two weeks later, mice were deeply anaesthetised with a lethal dose of ketamine and xylazine (100 mg/kg), and perfused transcardially with ice-cold sucrose solution. Following perfusion, mice were decapitated, and their brains were rapidly dissected. The dissected brains were then placed in ice-cold sucrose solution and hemisected. The cerebellum was removed, and transverse slices were prepared using a vibratome (VT1200S, Leica), with a 10° angle along the ventromedial plane to obtain sections that were orthogonal to the long-axis of the hippocampus. The thickness of hippocampal sections was 300 µm. Slices were transferred to a bath containing artificial cerebrospinal fluid (aCSF) and recovered first for 30 mins at 37℃, and subsequently for 30 mins at room temperature. All recordings were performed at room temperature (22 – 24℃). All chemicals were from Sigma or Tocris. The compositions of the slicing solution and aCSF were the following (in mM) unless otherwise stated:

Whole-cell recordings were performed on retrogradely labelled hippocampal pyramidal neurons with retrobeads visualised by their fluorescent cell bodies and targeted with Dodt contrast microscopy. For sequential paired recordings, neigh-

Reagent	**Sucrose**	**aCSF**
NaCl	10	125
Sucrose	190	0
Glucose	25	22.5
$NaHCO_3$	25	25
NaH_2PO_4	1.2	1.25
KCl	2.5	2.5
Na^+ ascorbate	1	1
Na^+ pyruvate	2	3
$MgCl_2$	7	1
$CaCl_2$	0.5	2

Table 2.4: Slicing and aCSF composition. All values are indicated in mM (unless otherwise stated).

bouring neurons were identified using a 40x objective at the same depth into the slice. The recording order of neuron pairs was alternated to avoid complications due to rundown. Borosilicate recording pipettes (3 – 5 M) were filled with one of three types of internal solutions depending on the experiment (see below). The compositions of the internal solutions were the following:

Reagent	**Cs-gluconate**	**K-gluconate**	**CsCl**
Gluconate or Cl^-	135 Cs-gluconate	125 gluconate	135 CsCl
HEPES	10	0	10
KCl	7	0	0
EGTA	10	22.5	10
Na-phosphocreatine	10	25	10
MgATP	4	1.25	4
Na_2GTP	0.3	2.5	0.4
TEA	10	1	10
QX-314	2	3	2
pH	7.2	7.2	7.2 (using CsOH)
Osmolarity (mOsm)	290-300	290-300	290-300

Table 2.5: Composition of internal solutions for patch clamp recordings. All values are indicated in mM (unless otherwise stated).

2.5.2 Channelrhodopsin2-assisted circuit-mapping experiments

CRACM of projection-defined vS neurons was done according to previously described protocols (MacAskill et al., 2014). 7- to 9-week old animals were injected with 250 nL of red (1:10 dilution in sterile saline) or green (undiluted) retrobeads in

a counterbalanced order into two of three output regions (PFC, NAc or LH). In the same surgery, 250 nL of *AAV1-synP-ChR2-YFP* was injected into RE bilaterally. After at least 14 days of ChR2 expression, animals were sacrificed for electrophysiological recording.

Presynaptic release was elicited by illuminating ChR2 expressed in the presynaptic terminals of long-range inputs into the slice, as previously described (MacAskill et al., 2014). Wide-field illumination was achieved through a 40x objective with brief 10 ms pulses of blue light over the recorded neuron from an LED centred at 473 nm (CoolLED pE-4000, with corresponding excitation-emission filters). Light intensity was measured as 4 – 7 mW at the back aperture of the objective and was constant between all recorded cell pairs. When recording a cell pair, the LED power was adjusted until responses were 200 pA in a connected neuron or set to maximum in an unconnected neuron, and fixed at the same level when recording light-evoked responses in the other cell. In all experiments, the aCSF contained 1 µM TTX and 100 µM 4-AP to isolate monosynaptic connectivity and increase presynaptic depolarisation, respectively. Recordings were conducted using a Multiclamp 700B amplifier (Axon Instruments), and signals were low-pass filtered using a Bessel filter at 1 kHz and sampled at 10 kHz. Data were acquired using National Instruments boards and WinWCP (University of Strathclyde) and analysed using custom routines written in Python 3.6.

For synaptic connectivity analysis, six recording sweeps were obtained for each optical pulse duration. The signals were preprocessed by baselining the signals to the first 100 ms, low-pass filtering using a Bessel filter (cutoff = 2 Hz, order = 2), averaging across the six recording sweeps for each optical pulse duration, and decimating the averaged signal to 1 kHz. The peak amplitude response of light-evoked EPSCs was measured as averages over a 2-ms time window around the peak compared to a 2-ms baseline period preceding the optical pulse. Only paired data in which at least one cell received $>$ 5 pA were included for analysis.

2.5.3 Miniature postsynaptic current recordings

Recording of miniature inhibitory postsynaptic currents (mIPSCs) was conducted under voltage clamp with a 'high Cl^-', Cs-based internal solution. The high concentration of Cl^- in the internal solution increases the intracellular concentration of Cl^-,

thereby increasing the driving force for movement of chloride from the intracellular to extracellular space. This concentration gradient shifts the reversal potential of Cl^- to $\sim$0 mV. Therefore, mIPSCs mediated by Cl^- were recorded as inward currents when the cell was voltage clamped at -70 mV. To record mIPSCs, the aCSF bath solution contained APV (10 µM), NBQX (10 µM) and TTX (1 µM) to block synaptic excitation and spontaneous IPSCs. In a subset of experiments, miniature excitatory postsynaptic currents (mEPSCs) were recorded using a Cs-gluconate-based internal solution, and an external aCSF solution containing gabazine (10 µM) and TTX (1 µM). Recordings were filtered at 1 kHz and sampled at 10 kHz prior to storing to disk.

For analysis of mIPSCs, event detection was conducted using template matching by cross-correlation (Clements and Bekkers, 1997; Jonas et al., 1993). The raw trace was first high-pass filtered using a Bessel filter (cutoff = 1 kHz, order = 2). Next, a prototypical mIPSC event was obtained by first manually selecting five mIPSCs of differing amplitudes and kinetics from different experiments, and averaging the traces (**Figure 2.5A**). This averaged trace was then fitted with a function to obtain the final template waveform (**Figure 2.5B**), using the biexponential alpha function:

$$y = a(1 - e^{\frac{-t}{b}})e^{\frac{-t}{c}} \tag{2.12}$$

where a, b and c are constants determined by minimising the mean-squared error using the function *optimize.leastsq* from the scipy package. Then, a cross-correlation of the template was conducted by flipping the template along the time axis and conducting a convolution in the frequency domain after fast Fourier transform (FFT) of the flipped template waveform and the recorded signal (**Figure 2.5C**). The resulting signal reflects the correlation between the template waveform and the recorded signal, where peaks in the correlation indicate a high probability of synaptic events. The same template waveform was used for all recordings. The threshold for detection was set as 2$\times$standard deviation of the cross-correlation signal above the mean. The response kinetics and amplitude of each mIPSC event was calculated after fitting a biexponential function to the detected event (**Figure 2.5D**):

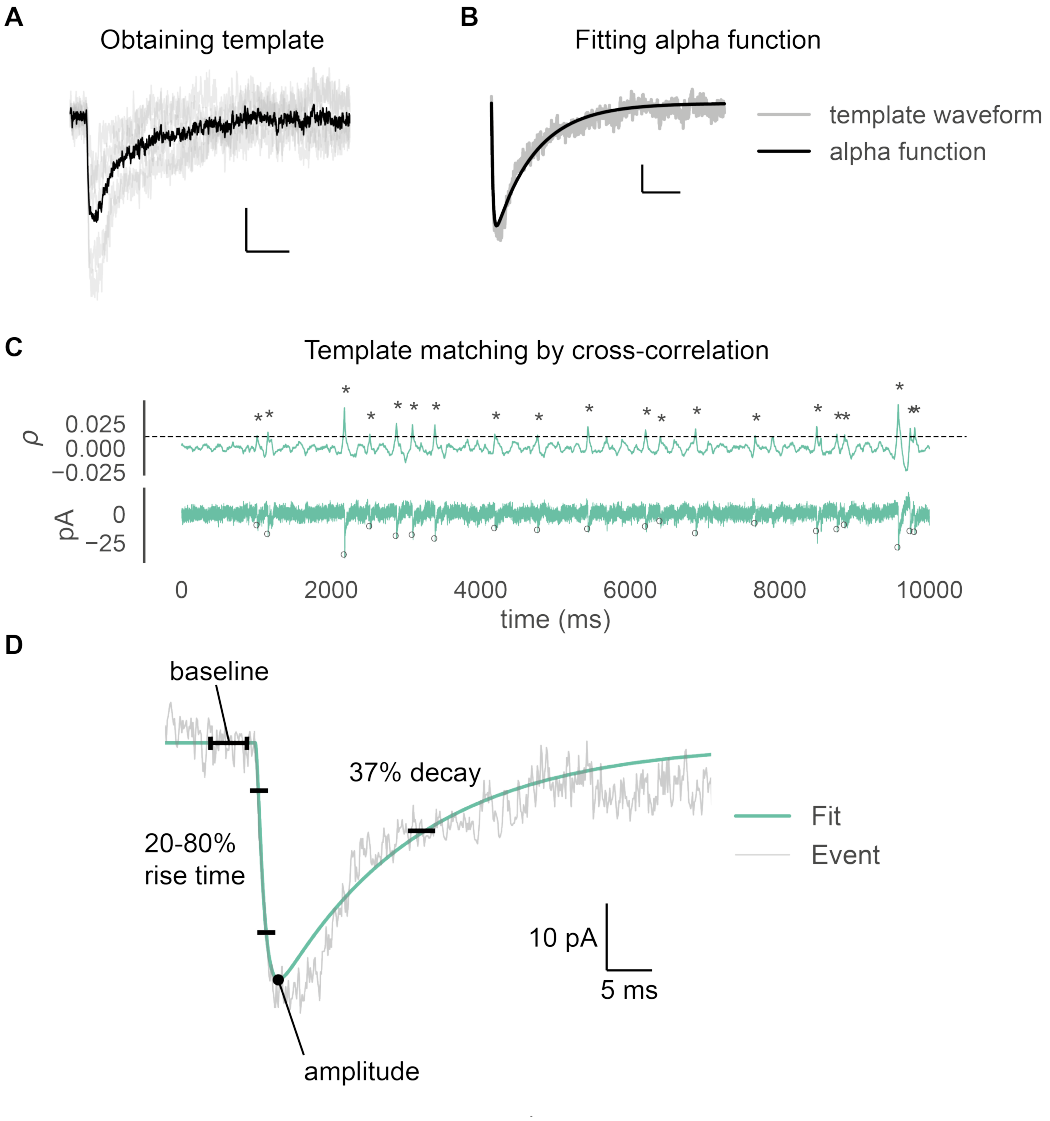

Figure 2.5: Steps for detecting and analysing mIPSC. (A) Five manually chosen mIPSC events from two different experiments (one ghrelin and one control injected animal) were used to obtain an average template waveform. Scale: 20 ms (x-axis), 10 pA (y-axis). (B) The average waveform was then fitted with a biexponential alpha function to obtain the final template waveform. Scale: 20 ms (x-axis), 5 pA (y-axis). (C) The template waveform was then used to find all events within a recorded signal, using cross-correlation by FFT-based convolution. Upper trace is the normalised cross-correlation between the template waveform with the recorded signal. Lower trace is the recorded signal. The dashed line is the 2×standard deviation of the cross-correlation signal above the mean, which was set as the threshold for detection. Asterisks (above) and circles (below) indicate detected events. (D) The kinetics and amplitude of each detected mIPSC event was analysed after fitting a biexponential alpha function with fast and slow decay components.

$$y = (1 - e^{\frac{-t}{\tau_{\text{rise}}}})(A_1 e^{\frac{-t}{\tau_{\text{fast}}}} + A_2 e^{\frac{-t}{\tau_{\text{slow}}}}) \tag{2.13}$$

where τ_{rise} is the rise time of the event, τ_{slow} and τ_{fast} are the decay constants

for the slow and fast components of the biexponential waveform respectively, and A_1 and A_2 are scaling constants. The parameters were estimated again by minimising the mean-squared error using the function *optimize.leastsq*. The amplitude was calculated by taking the minimum value of the fitted mIPSC. This value was subtracted from a 4-ms baseline amplitude preceding the event. mIPSC frequency was calculated by dividing the total number of events by the length of the recording from first to last detected mIPSC event. This method of analysis is robust to recording noise across experiments.

2.5.4 Electrical stimulation of Schaffer collaterals

Whole-cell current clamp recordings of retrogradely labelled vS^{NAc} and vS^{LH} projection neurons in CA1 and subiculum were conducted. The holding current was adjusted to maintain cells at -70 mV. While recording neurons in current clamp mode, a tungsten electrode stimular placed in stratum radiatum to stimulate volleys of synaptic input along the Schaffer collaterals. The current amplitude was adjusted such that postsynaptic potentials (PSPs) ranged from 3 to 5 mV. After a baseline recording period of 5 minutes, ghrelin (100 nM) or vehicle was washed onto the slices and recorded for 30 minutes. Slices were monitored for changes in input resistance with a current step, and input resistances that changed $>$20% were excluded from the analysis.

2.6 Quantification and statistical analyses

All statistics were calculated using the Python packages scipy, pingouin and statsmodels, as well as R. Summary data are reported throughout the text and figures as mean ± sem unless otherwise stated. For the majority of analyses presented in this thesis, normality of data distributions was determined by visual inspection of the data points. For linear model analysis of rabies labelled inputs in the TRIO experiments (Figure 6.11), the normality of the dataset was assessed with the Jarque-Bara test and equal variance with the Levene's test. The input fractions for multiple regions showed non-normality and heteroscedasticity in the input fractions across projection populations. Therefore, all analysis for Figure 6.11 were conducted after log-transformation of input fractions. Distributions of the data became more Gaussian-like after log-transformation, as assessed again by the Jarque-Bara

test and Levene's test. All data were analysed using statistical tests described in the figure legends. Correction for multiple comparisons was conducted using the Benjamini-Hochberg method, unless otherwise stated. The alpha level was defined as 0.05. No power analysis was run to determine sample size a priori. The sample sizes chosen are similar to those used in previous publications. Throughout the figures and text, the * symbol represents $p < 0.05$, unless otherwise stated, and n.s. stands for not significant.

Chapter 3

The influence of hunger state on feeding behaviour

Hunger is an internal state that not only invigorates behaviour towards feeding, but also acts as a contextual cue for the higher-order control of feeding behaviour. How hunger – and more specifically, the hunger hormone ghrelin – influences the dynamics of feeding behaviour remains poorly characterised. In this chapter, I quantify in detail the influence of physiological (through overnight fasting) and artificial (through exogenous injections of ghrelin) hunger on the dynamics of feeding behaviour. I found that hunger through physiological and artifical manipulations are behaviourally similar, allowing ghrelin to act as a proxy for physiological hunger in mice.

3.1 Introduction

Foraging in nature requires an animal to adaptively integrate external cues with the internal metabolic state. Furthermore, adaptive feeding behaviour requires an animal to predict future changes in caloric levels and therefore implement 'higher-order' feedforward processes to regulate feeding behaviour (Sterling, 2012). Viewed in this way, feeding is a decision-making process that requires the integration of external environmental cues with the internal state to initiate feeding behaviour under appropriate conditions (Saper et al., 2002; Davidson et al., 2014; Compan et al., 2015). Dysfunction of these higher-order processes is thought to underlie the maladaptive feeding behaviour observed in anorexia nervosa and depression.

Hunger is signalled by circulating hormones that report the level of satiety and food deprivation levels, such as leptin, cholecystokinin and ghrelin. Specifically, ghrelin is capable of driving feeding when acutely injected into rodents and humans (Tschöp et al., 2000; Wren et al., 2001). Levels of circulating ghrelin also closely follow the duration of fasting (Cummings et al., 2004; Natalucci et al., 2005), and infusion of ghrelin activates multiple brains regions in a pattern similar to overnight fasting. Despite these results, most studies to date have focused on the influence of ghrelin by measuring the amount of food consumed and changes in metabolic parameters. By contrast, naturalistic feeding behaviour is comprised of a sequence of feeding and non-feeding behaviours (Halford et al., 1998). It remains unclear how ghrelin influences this structure of feeding behaviour.

Therefore, in this chapter, I sought to address how hunger – both through physiological (overnight fasting) and artificial (exogenous administration of ghrelin) – influences the structure of feeding behaviour. Furthermore, I wanted to compare the behavioural patterns produced by overnight fasting and acute ghrelin administration to observe whether ghrelin could function as a behavioural proxy for overnight fasting.

3.2 Results

3.2.1 Feeding ethogram patterns depend on the hunger state

Under naturalistic settings, feeding behaviour is highly complex and is built from simpler, stereotyped behaviours. These simpler behaviours can be divided into feeding-specific behaviours, such as exploratory sniffing and investigation of food ('Approach') and eating ('Eat'), as well as non-feeding-specific behaviours (i.e. 'Rear', 'Groom' and 'Rest'). These behaviours are easily observable and reproducible, and together are collectively referred to as the behavioural satiety sequence (BSS, **Figure 3.1A–B**; Halford et al., 1998). The balance between spending preferentially more time engaging in feeding-specific, as opposed to non-feeding-specific, behaviours is critically dependent on the hunger state. Therefore, I first sought to characterise how feeding behaviour, as a composite of these five simpler behaviours, changes under different states of hunger.

First, I presented a piece of chow pellet to freely behaving mice with ad-libitum

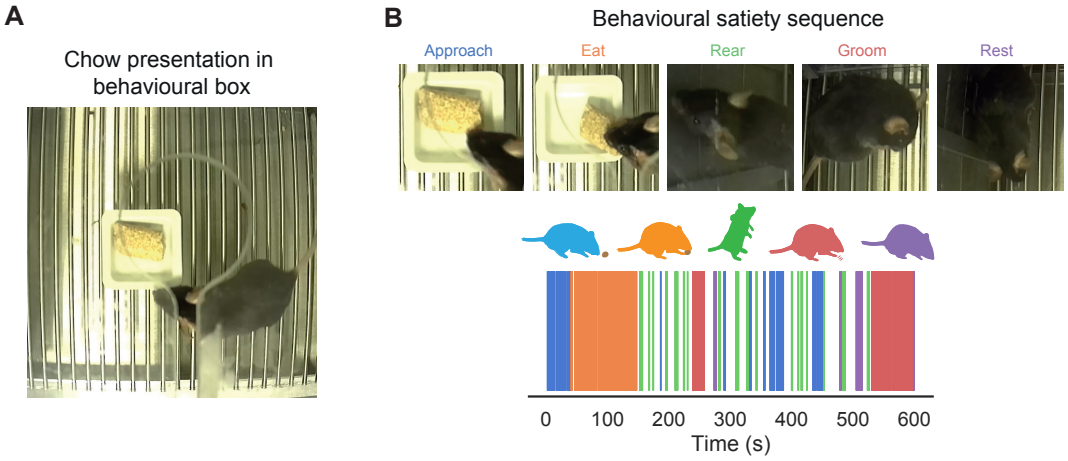

Figure 3.1: Structure of the behavioural satiety sequence (BSS). (A) Presentation of chow to a freely behaving mouse for 10 mins in a behavioural testing box. Video recordings of an animal's expression of BSS behaviours were obtained by overhead PS4 cameras. (B) *Top*: Assortment of five behaviours comprising the Behavioural Satiety Sequence (BSS). Color codes are the following: blue, Approach; yellow, Eat; green, Rear; red, Groom; purple, Rest. Example images of each behaviour are provided, where Approach and Eat represent food-specific behaviours, while Rear, Groom and Rest are non-food-specific. *Bottom*: Annotation of behaviour across the 10-minute presentation of food produced ethograms of BSS behavioural expression across time. Raster plot illustrates the ethogram of an example mouse following presentation of a piece of chow pellet.

access to food (Fed state) or after fasting overnight for 16 to 18 hours (Fasted state), and observed their behavioural patterns. These experiments were conducted during the middle of the light period (2 pm to 7 pm) of the circadian cycle. Analysis of this experiment produced feeding ethograms for these mice that changed according to the hunger state (**Figure 3.1B**). In the Fed state, animals consumed only small amounts of chow; overall consumption increased reliably after an overnight fast (amount of chow consumed in grams, fed = 0.04 ± 0.01; fasted = 0.34 ± 0.02, two-tailed unpaired t-test, t = 15.05, p = 1.1×10^{-8}, n = 12 mice; **Figure 3.2A**). Notably, sated mice spent more time approaching and investigating the food (Approach), as well as longer times in general exploratory activity (Rear) and maintenance activity (Groom; **Figure 3.2B**). With fasting, mice readjusted their strategy and spent less time approaching food, rearing and grooming, and devoted most time to eating (**Figure 3.2C**). Overall, this manifested as an increased proportion of time spent engaging in feeding-specific behaviours, and less in non-feeding specific behaviours, in the Fasted compared to the Fed state (**Figure 3.2C**). Thus, physiological hunger shifts the balance from non-feeding-specific to feeding-specific behaviours.

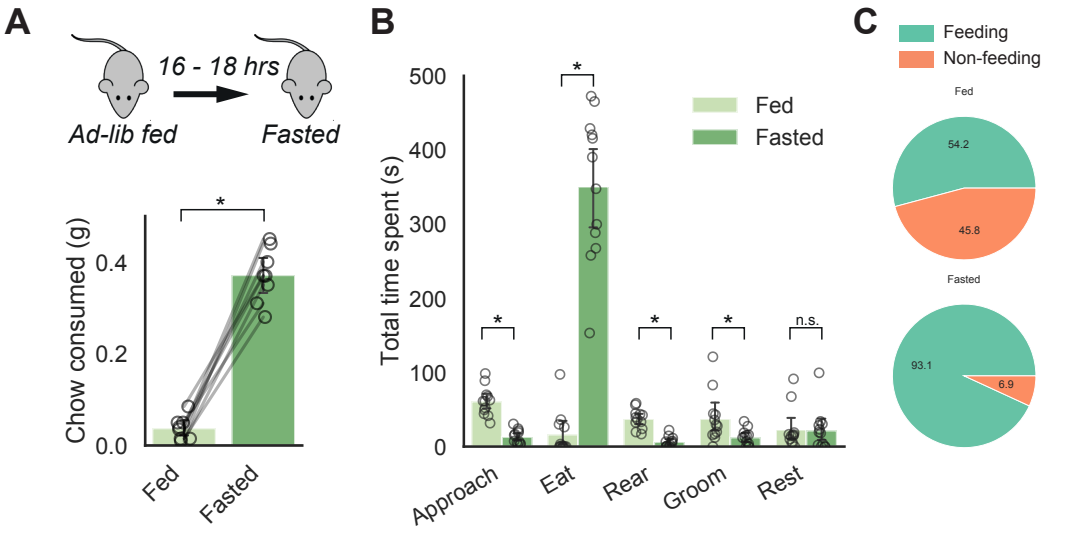

Figure 3.2: Behavioural satiety sequence expression in the ad-libitum fed state or after an overnight fast. (A) *Top*: procedure of overnight fasting. *Bottom*: Amount of chow consumed between fed and fasted states within 10 mins of chow presentation. (B) Durations of each BSS behavioural component within a 10-minute session following presentation of chow between Fed and Fasted conditions (duration of engagement of BSS behaviour in seconds: Approach, Fed = 60.7 ± 5.5, Fasted = 13.1 ± 2.7; Eat, Fed = 16.2 ± 8.4, Fasted = 350.6 ± 28.3; Rear, Fed = 37.4 ± 3.8, Fasted = 6.4 ± 2.0; Groom, Fed = 37.5 ± 9.7, Fasted = 12.3 ± 3.2; Rest, Fed = 22.9 ± 7.9, Fasted = 21.6 ± 8.0; n = 12 animals). (C) Proportion of time spent between engagement in feeding-specific BSS (Approach and Eat) and non-feeding-specific behaviours (Rear, Groom and Rest) as a function of hunger state. *p $<$ 0.05 corrected for multiple comparisons using the Benjamini-Hochberg method. Data represent mean ± sem.

The prototypical circulating factor that signals food deprivation and hunger in rodents and humans is ghrelin (Tschöp et al., 2000; Wren et al., 2001; Müller et al., 2015). Injections of ghrelin in animals robustly stimulates food intake, activates brain areas similar to physiological fasting (Goldstone et al., 2014), and increases the motivation to eat (Tschöp et al., 2000; Wren et al., 2001). However, it remains unclear how ghrelin affects the behavioural satiety sequence (BSS), and whether exogenous ghrelin accurately recapitulates physiological fasting. To determine whether exogenous ghrelin (via i.p. injection) produces a similar behavioural strategy to fasting, I delivered 2 mg/kg of ghrelin or vehicle control (phosphate-buffered saline, PBS) to sated, ad-libitum fed animals and waited 20 to 30 minutes before presenting them with a pellet of chow. I then recorded and analysed their feeding behaviour within 10 minutes of food presentation (**Figure 3.3A**). Like fasting, ghrelin elevated chow consumption compared to PBS-injected mice (chow consumption within 10 mins in grams, PBS = 0.03 ± 0.01; Ghrelin = 0.22 ± 0.02,

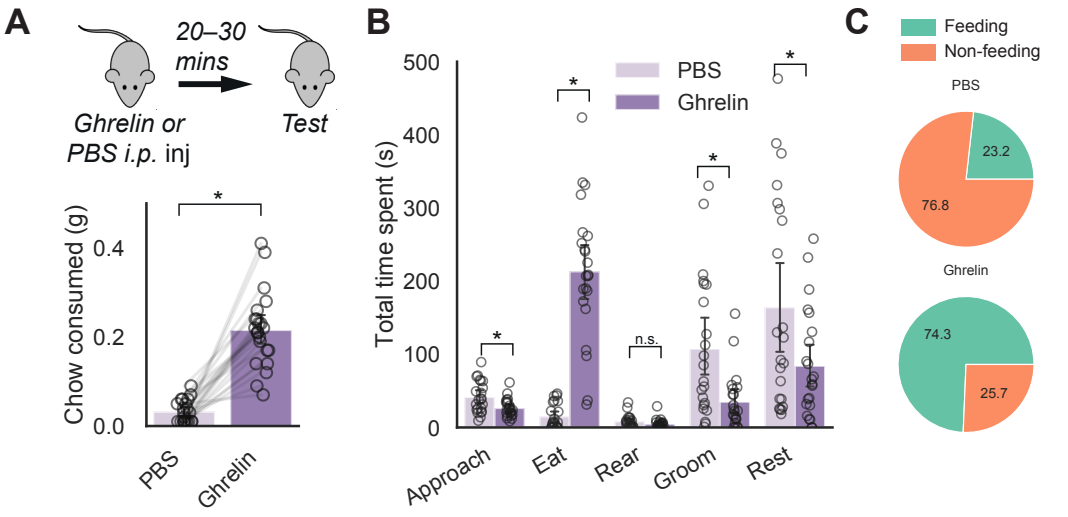

Figure 3.3: Behavioural satiety sequence expression after acute administration of ghrelin. (A) *Top*: procedure of artificially-induced hunger via intraperitoneal (i.p.) injection with ghrelin. Animals were given i.p. injections of with either 2 mg/kg of ghrelin or vehicle control (PBS), allowed to recover for 20 to 30 minutes, and presented with a pellet of chow. Injection order was counterbalanced across behavioural sessions. *Bottom*: Amount of chow consumed following i.p. injections of PBS and ghrelin. (B) Durations of each BSS behavioural component within a 10-minute session following presentation of chow following i.p. injections of either PBS of 2 mg/kg ghrelin (duration of engagement of BSS behaviour in seconds: Approach, PBS = 41.5 ± 4.6, Ghrelin = 26.4 ± 2.7; Eat, PBS = 14.9 ± 3.7, Ghrelin = 213.3 ± 20.2; Rear, PBS = 8.1 ± 1.8, Ghrelin = 4.9 ± 1.3; Groom, PBS = 107.7 ± 20.7, Ghrelin = 35.1 ± 8.3; Rest, PBS = 164.1 ± 30.8, Ghrelin = 84.2 ± 16.0; n = 22 animals). (C) Proportion of time spent between engagement in feeding-specific BSS (Approach and Eat) and non-feeding-specific behaviours (Rear, Groom and Rest) following administration of 2 mg/kg of ghrelin. *p $<$ 0.05 corrected for multiple comparisons using the Benjamini-Hochberg method. Data reported as mean ± sem.

two-tailed unpaired t-test, t = 9.85, p = 2.5 $\times$ 10^{-9}, n = 22 animals; **Figure 3.3A**). Sated, PBS-treated mice spent more time approaching food and engaging in non-feeding specific behaviours such as grooming and resting (**Figure 3.3B**), consistent with a Fed state-like behavioural pattern. By contrast, artificially inducing hunger by ghrelin injection made mice spend less time engaging in Approach, Groom and Rest behaviours, and, like the Fasted state, these mice devoted most time in Eating behaviour (**Figure 3.3A–C**). Taken together, both physiological (through overnight fasting) and non-physiological hunger (through i.p. ghrelin injections) shift the balance of behaviours from non-feeding-specific to feeding-specific behaviours.

3.2.2 Feeding behavioural sequences are dynamic and depend on the hunger state

However, the above measurements are whole-session quantifications and do not capture an animal's choice to engage in one BSS behaviour to the next. This information about behavioural sequence represented an additional source of information regarding an animal's feeding strategy (Burnett et al., 2019). To analyse this sequential information in more detail, I analysed the annotated behavioural patterns for each mouse as a behavioural sequence that defined the animal's feeding strategy when presented with chow across different states of hunger. Specifically, the sequence of scored behaviours were analysed as a discrete-time Markov chain, a vector of behavioural states that change as a function of time (Burnett et al., 2019). In this analysis, the set of states that defined the Markov chain were the five BSS behaviours, yielding a total of 25 pairs of possible combinations of behavioural transitions. Like similar analyses of innate behaviour that have been reported (Carola et al., 2011; Burnett et al., 2019), this analysis assumed that the feeding behavioural sequence exhibited the Markov property (i.e. a 'memory-less' process in which the future BSS behaviour that an animal will transition to depends only on the current BSS behaviour and not on previous behaviours; see Discussion). For any given behavioural Markov chain, a transition matrix P_{ij} fully defines an animal's probability of transitioning from behaviour i to behaviour j, i.e. its overall behavioural strategy. Thus, I computed the transition matrices for each animal in each hunger state, and compared these matrices across different states of hunger.

This analysis revealed that marked differences in transition probabilities across hunger occurred in the feeding-specific transitions (transitions between Approach and Eat; **Figure 3.4A–C**). In the Fasted state, animals displayed increased Approach-Eat and Eat-Eat transitions compared to the Fed state, indicating that animals were more likely to transition to consuming chow when investigating food and continue to revisit the Eating state. Fasted animals were also less likely to engage in Approach-Approach transitions, indicating that once they engage in Approach, they were more likely to transition towards other behaviours, most notably Eat behaviour. There were also reductions in transition probabilities in non-feeding-specific behaviours, such as reduced Rear-Rear and Rear-Groom transitions, pos-

sibly to reduce general exploratory behaviour in the service of increasing Eat behaviour. Thus, animals in the Fasted state prioritise eating by biasing transitions towards Eating, and remaining in the Eat state, at the expense of Approach and non-feeding specific behaviours.

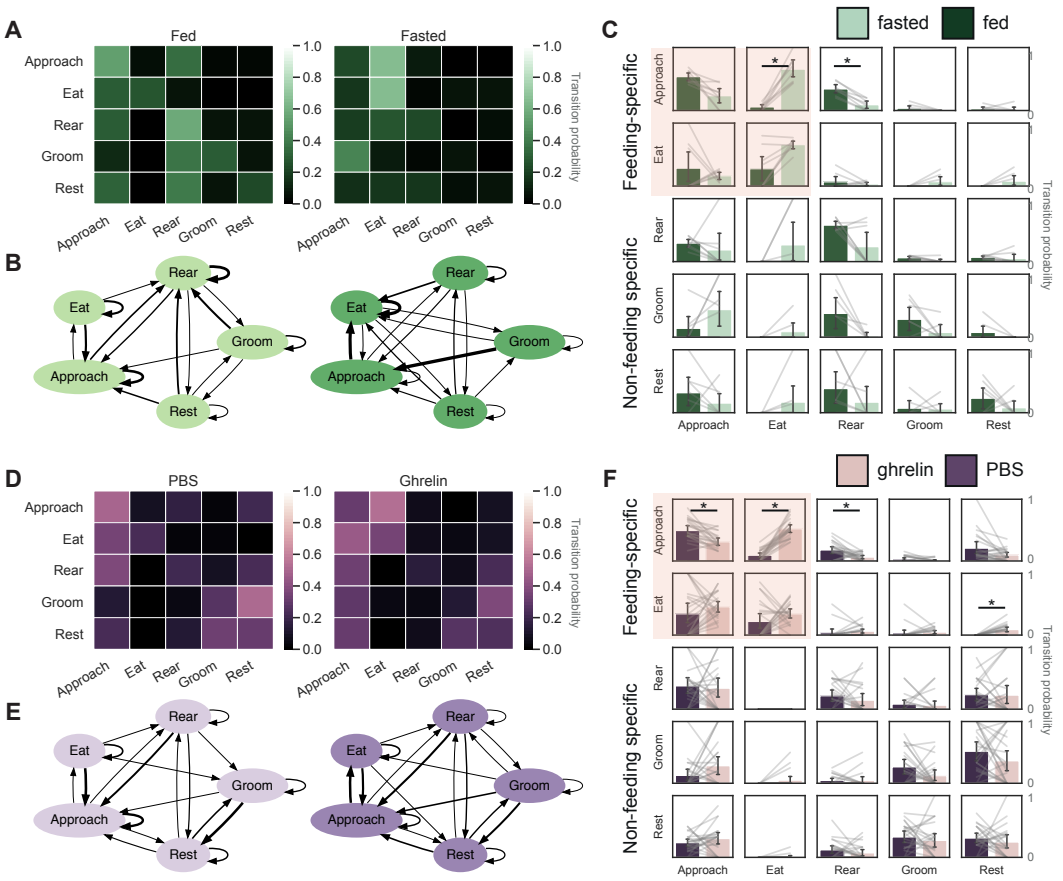

Figure 3.4: Markov chain analysis of BSS behavioural transitions across different states of hunger. (A) Transition matrices for Fed and Fasted animals. Each row represents the current BSS behaviour, and each column represents the next upcoming BSS behaviour. (B) Graph diagrams of the transition matrices from (A), where each node represents a BSS behaviour and each arrow (edge) represents the transition to another node. The width of the edges are weighted by the transition probability such that thicker edges represent a higher transition probability, and vice versa. Note that transition probabilities < 0.05 have been omitted as edges. (C) Matrix of transition probabilities and their modulation by overnight fasting. The bar plots for each row share the same y-scale, and each pair of bar plots represent the transition probability from behaviour i to behaviour j, where i is the current BSS behaviour (row) and j is the next BSS behaviour (column). Pink box highlights the feeding-specific behavioural transitions. (D) Transition matrices for PBS and ghrelin-injected animals. (E) Graphs of transition matrices from (D). (F) Matrix of transition probabilities and their modulation by ghrelin. All data represented as mean ± sem. *p < 0.05 (two-tailed paired t-tests, corrected for multiple comparisons with the Benjamini-Hochberg method).

Ghrelin injections in sated mice produced a qualitatively similar behavioural

pattern to the Fasted condition. Firstly, animals displayed a reduced probability of Approach-Approach transitions and increased probability of Approach-Eat and Eat-Eat transitions compared to PBS-injected animals (**Figure 3.4D–F**). These patterns, like the Fasted state, indicates that animals were unlikely to continue approaching food, and were more likely to transition to eating, and remain eating, the pellet of chow. Furthemore, similar to the Fasted state, there were generalised reductions in transitions towards non-feeding specific behaviours, such as reduced Approach-Rear and Approach-Rest transitions. Thus, the effect of exogenous ghrelin on the animal's strategy was qualitatively similar to the Fasted state by prioritising changes in transitions towards feeding-specific behaviours.

3.2.3 Experimental manipulations of hunger produce two states: the hungry and sated states

Next, I sought to quantify and make inferences about the similarity of the behavioural patterns (i.e. the transition matrices) between different states of hunger. For this analysis, I used each 5×5 transition matrix as a 25-dimensional vector, and computed the similarity of these behavioural vectors using the cosine distance. Briefly, the cosine distance measures the angle between two vectors, producing an absolute scalar value ranging from 0 to 1, where values close to 0 indicate high similarity of two vectors, and values close to 1 indicate low similarity. This analysis was carried out for each animal's behavioural transition matrix in each hunger state (i.e. Fed, Fasted, PBS, Ghrelin; **Figure 3.5A**). Specifically, an animal's 'sated' state (Fed and PBS) was taken as the baseline condition, and the 'hungry' state (Fasted and Ghrelin) as the experimental condition; these two vectors for each animal were then compared to produce a cosine distance metric (i.e. a Within-subject measurement). Furthermore, to compare the similarity of the baseline conditions across the entire cohort, an animal's sated behavioural vector was compared to the mean sated behavioural vector of all other animals in the cohort (i.e. Subject-vs-mean, same baseline state). In this way, this analysis produced a within-subject comparisons of the similarities and differences of BSS behavioural sequences across different states of hunger.

Using this analysis for the Fed and Fasted conditions, I observed that the Fed and Fasted states produced highly dissimilar behavioural vectors, thus producing

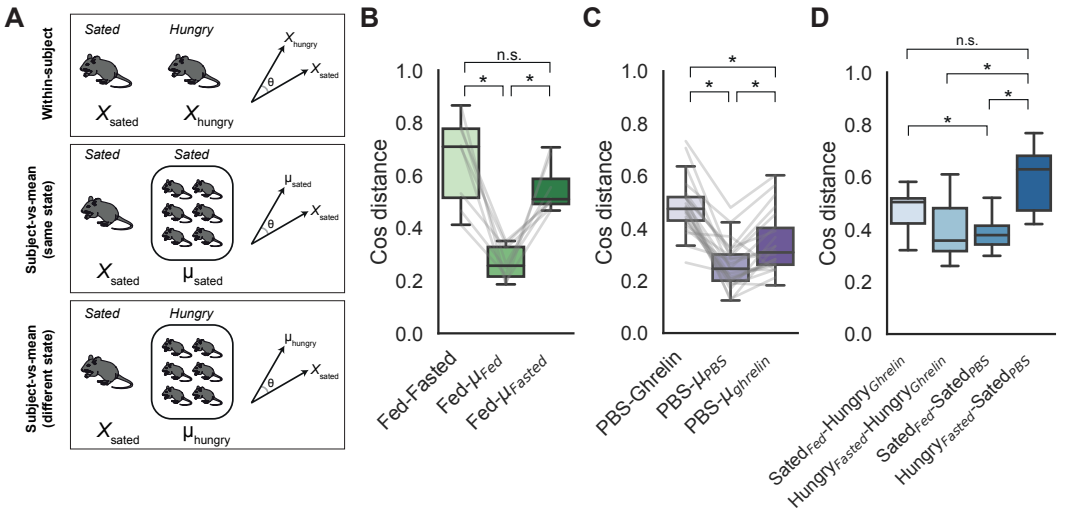

Figure 3.5: Comparisons of transition matrices across hunger states using the cosine distance analysis. (A) Each 5×5 transition matrix for each animal in each hunger state was ravelled to produce a vector of 25 features, with each feature being a transition probability. Three cosine distance values were computed for a single animal. *Top*: within-subject comparison, where an animal's vector in the sated state (e.g. Fed) was compared to its corresponding vector in the hungry state (e.g. Fasted) by calculating the angle between the two vectors. *Middle*: subject-vs-mean comparison (same state), where the transition matrix of one animal in the sated state was compared to the average transition vector of all animals in the cohort (excluding the animal being compared) in the same sated state. The subject-vs-mean comparison would be low as the two vectors being compared arose from the same state. *Bottom*: subject-vs-mean comparison (different state) which acts as a control measure of comparing individual vs. mean effect. This subject-vs-mean angle compares one animal in the sated state to the mean of whole cohort in the hungry state, which would produce a large cosine distance similar to the within-subject comparison. (B) Cosine distance analysis for the Fed and Fasted conditions. (C) Cosine distance analysis for the PBS and Ghrelin conditions. (D) Across-animal comparisons of the Fed, Fasted, PBS and Ghrelin conditions. Boxplots show median and the whiskers represent 1.5 times the interquartile range. *p $<$ 0.05, pairwise t-tests after correction for multiple comparisons with the Benjamini-Hochberg method. Data represented as median ± 1.5 times the IQR.

a high cosine distance. In other words, the Fed and Fasted vectors had a large angle. As control measurements, the individual subject-vs-mean comparison was used, where the Fed vector of one animal was compared to the mean Fed vector of all other animals (Fed-μ_{Fed}). When comparing the Fed-Fasted vectors to the Fed-μ_{Fed} vectors (**Figure 3.5B**), the Fed-μ_{Fed} vectors were more similar and thus had a lower cosine distance compared to the Fed-Fasted vectors. This indicates that the behavioural vectors produced by the Fed and Fasted states were more dissimilar than when then Fed state was compared to itself (**Figure 3.5B**). This is consistent with the shift from non-feeding towards feeding behaviours by overnight fasting.

Next, I compared the Fed vector of one animal to the mean Fasted vector of

all other animals in the cohort (Fed-μ_{Fasted}). This measurement acts as a control to the subject-vs-mean vector comparison. I found that the Fed-μ_{Fasted} angle was larger compared to the Fed-μ_{Fed} angle, indicating that the Fed state behavioural strategy of a given animal was more dissimilar to the mean Fasted vector (repeated-measures one-way ANOVA, $F_{2,14} = 20.3$, $p = 7.4 \times 10^{-5}$, n = 12 mice, **Figure 3.5B**). Notably, the Fed-Fasted and Fed-μ_{Fasted} angles were similar, indicating that the dissimilarity between Fed and Fasted states was consistent within- and across-animals.

A similar analysis was conducted for the PBS and Ghrelin conditions. The PBS behavioural vector was highly dissimilar compared to the Ghrelin behavioural vector (i.e. the PBS-Ghrelin vectors had a high cosine distance). When comparing the PBS behavioural vector of one animal to the mean PBS behavioural vector of the cohort (i.e. PBS-μ_{PBS}), the PBS-μ_{PBS} vectors resulted in low cosine distances, indicating a high similarity of behaviour between PBS conditions across animals (**Figure 3.5C**). Finally, when comparing the PBS behavioural vector of one animal to the mean Ghrelin behavioural vector of the cohort (i.e. PBS-μ_{Ghrelin}), I observed a high PBS-μ_{Ghrelin} cosine distance. Thus, the similarity of the behavioural patterns overall depended on the hunger state mediated by ghrelin (repeated-measures one-way ANOVA, cosine distance measurements across different hunger state pairs, $F_{2,42} = 51.5$, $p = 4.96 \times 10^{-12}$, n = 22 mice). Together, these findings indicate that sated animals injected with PBS had a consistent behavioural pattern, and that ghrelin reliably increased the cosine distance from the PBS state by altering the pattern of feeding behaviour. Notably, the cosine distance was higher for PBS-Ghrelin vectors than PBS-μ_{Ghrelin} vectors (**Figure 3.5C**). This suggests that while ghrelin produced a behavioural pattern that was dissimilar to PBS injections, ghrelin injections may produce subject-specific differences in feeding behaviour that lowered the overall cosine distance across animals (see Discussion).

Lastly, I made across-animal comparisons of the similarities of the behavioural vectors between all 'sated' and 'hungry' states (**Figure 3.5D**). This analysis revealed that Fasted-PBS and Fed-Ghrelin vectors were more dissimilar compared to the within-state Fasted-Ghrelin and Fed-PBS pairs. Notably, the cosine distance

between Fed-Ghrelin and Fasted-PBS was not significantly different, indicating that in spite of the subject-specific variability produced by ghrelin injections, the Ghrelin state produced a reliably different behavioural pattern to the Fed state (**Figure 3.5D**). Taken together, the cosine distance analysis indicates that the experimental manipulations of hunger produced largely stereotyped behavioural patterns, such that hungry and sated states were associated with highly similar behavioural patterns when compared within each state, but very dissimilar when compared across state.

The behavioural strategy of a given animal is likely limited to only a small part of the whole feeding behavioural space, given the stereotyped nature of innate feeding behaviour (Berman et al., 2014; Burnett et al., 2019). Therefore, it is possible that within my experimental manipulations, only a small discrete number of behavioural patterns exist. Thus, I next hypothesised that feeding behaviour can be clustered into distinct groups.

To answer this question, I first reduced the 25-dimensional behavioural transition vectors to 2-dimensions using Fisher's linear discriminant analysis (LDA). These 2 dimensions (i.e the first and second linear discriminants) maximised the separability between each of the hunger states: Fed, Fasted, PBS and Ghrelin (**Figure 3.6**). The LDA showed that the first and second LD axis had discriminability ratios of 0.73 and 0.19, respectively, meaning that $>$90% of the discriminability between the hunger states could be explained by the first two LDA components. Next, I ran unsupervised clustering of the dataset in LDA space using Gaussian mixture modelling (GMM), which aims to identify clusters in an unsupervised manner by modelling subgroups of data as independent Gaussian components (clusters). To determine the number of Gaussian components which best fit the data, I iteratively fitted GMM models with increasing number of Gaussian components and computed the Bayesian information criterion (BIC) as a metric for model comparison. The most likely number of behavioural patterns was fitted with two Gaussians (**Figure 3.6A**), corresponding perfectly to the hungry and sated states. Importantly, the results of the GMM clustering was robust as a supervised random forest classifier only required 6 observations (10% of the dataset) to predict the correct GMM cluster with $\sim$90% accuracy (**Figure 3.6B**). This finding means that the Ghrelin state

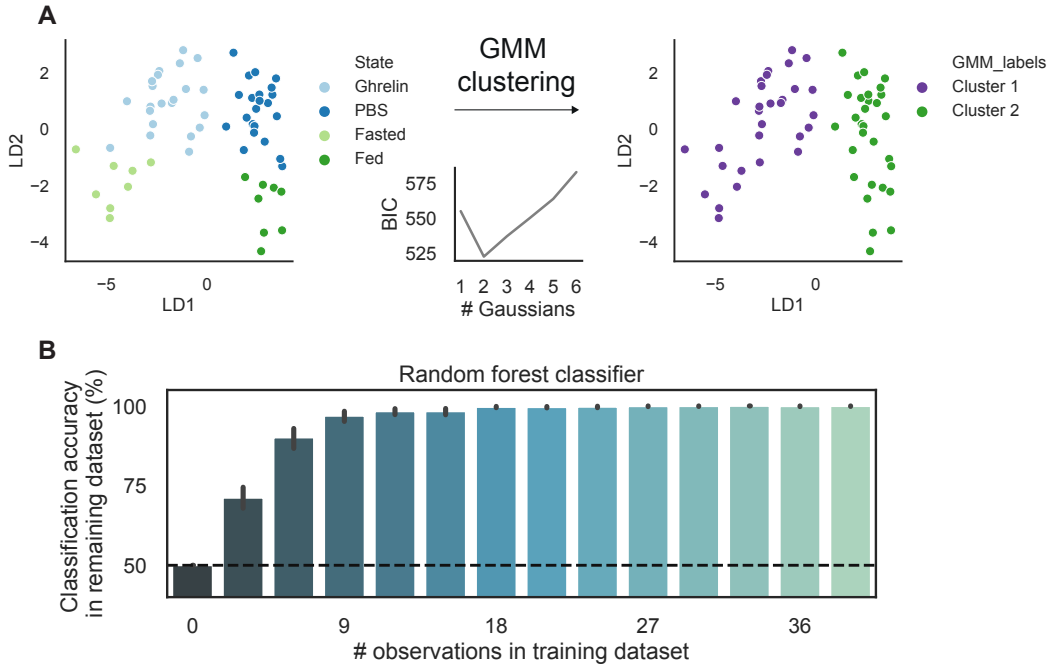

Figure 3.6: Clustering of behavioural transitions produces two states: the hungry and sated states. (A) Each 5×5 transition matrix was ravelled to produce a vector of 25 features. *Left*: Dimensionality reduction using Fisher's linear discriminant analysis (LDA) was conducted to find the first two linear discriminants which best separated the hunger state conditions: Fed, Fasted, PBS and Ghrelin. The 25-dimensional vectors were then projected onto this 2-dimensional subspace. *Middle*: A Gaussian mixture model was fitted to the dataset in LDA space. The Bayesian information criterion (BIC) was used to select the number of components, with the lowest BIC score occurring with two components (clusters). *Right*: The dataset was clustered according to the two-component GMM, and show that the two components perfectly represented the hungry and sated states, where cluster 1 is comprised of all Ghrelin and Fasted data points, and cluster 2 is comprised of all Fed and PBS data points. (B) Robustness of GMM clustering as assessed by the accuracy of a supervised random forest classifier trained with increasing number of observations in the training dataset, and tested on the remaining dataset. Data plotted as mean ± 95% confidence interval.

produced a behavioural pattern similar enough to the Fasted state to be clustered together, consistent with the similarity of the BSS behavioural sequence produced by the Fasted and Ghrelin states.

Taken together, the behavioural analysis presented in this section indicates that sated and hungry animals have divergent behavioural strategies that are stereotyped and dependent on the hunger state. Furthermore, manipulating states of hunger produced at most two behavioural patterns: the hungry and sated conditions.

3.3 Discussion

Foraging in nature for food is a complex behaviour that is built from simpler, stereotyped modules of behaviour (Halford et al., 1998; Burnett et al., 2019). The behavioural sequence that is expressed depends upon a multitude of external environmental cues, such as the location and availability of food sources, and internal cues, principally hunger but also other competing motivational states (Burnett et al., 2016, 2019). In my experiments, I elected to manipulate hunger as the main factor that alters the feeding strategy. As most studies usually focus on examining feeding behaviour through measurements of food consumption, body weight or changes in metabolic components (Uchida et al., 2013), the results described in this chapter build upon the idea that hunger, and specifically ghrelin, alters feeding behaviour through changes in the expression of simpler behaviours as a sequence, i.e. the anticipatory and other maintenance behaviours that accompany the entire feeding repertoire (Halford et al., 1998).

One expected finding of this behavioural analysis was that the time spent engaging in feeding-specific behaviours (Approach and Eat) was most strongly modulated by hunger; hunger – both physiological and through ghrelin i.p. injections – reduces the time spent investigating food (Approach) and increases the time spent eating (Eat). Notably, I found that the time spent engaging in Eating occurred at the expense of the maintenance or 'non-feeding-specific' behaviours (Groom and Rest). Thus, expression of feeding-specific behaviours competed with the expression of non-feeding-specific behaviours. Additionally, Rearing behaviour is a general exploratory behaviour (Lever et al., 2006) that provided an important comparison to Approach, enabling the dissociation of a generalised increase in exploratory drive with food-specific investigation. I found that the time spent Rearing did not differ between ghrelin- and control-injected mice (**Figure 3.3**), indicating that ghrelin promoted food-specific investigation and not overall exploratory drive.

By taking into account the transition dynamics from one behaviour to the next, the Markov chain analysis of feeding behaviour also provided higher granularity of behavioural information beyond a simple frequency description of feeding behaviour. Specifically, strong hunger-dependent modulations in transitions dynamics occurred between Approach and Eat behaviours, where hunger promoted an in-

creased transition probability from Approach to Eat. Moreover, general changes in transition probabilities across the other BSS behaviours demonstrates that hunger biases the expression of feeding-specific behaviour at the expense of non-feeding-specific behaviours. This applied to both overnight fasting, and exogenous injections of ghrelin.

Building upon this analysis, the transition dynamics matrices provided snapshots of feeding behavioural patterns across different hunger states that allowed me to compare the similarity and difference of behaviours under different states of hunger. This was achieved using the cosine distance between the transition probability matrix. In particular, this analysis revealed that, as expected, the sated states (Fed and PBS-injected) and hungry states (Fasted and Ghrelin-injected) were highly similar to each other; however, while the Fasted state was highly dissimilar compared to the sated states, the Ghrelin-injected state was dissimilar to a lower extent compared to the sated states, although this subtle difference was not significant (see Figure 3.5). This subtle difference is likely due to variability in the subject-specific response to ghrelin inherent in the method, for example, the variable accuracy of i.p. injections. Furthermore, ghrelin-injected animals also displayed more 'Fed'-like features (Approach, Groom and Rest time profiles), whereas overnight fasting brings about a stronger drive to eat at the expense of the other behaviours. Another further difference between the Fasted and Ghrelin states was their effects on velocity; animals on average moved with greater velocity after overnight fasting compared to after receiving an i.p. injection of ghrelin (compare Figure 4.5F and Figure 4.17A in Chapter 4). This suggests that while fasting strongly modulates arousal, the behavioural effect of ghrelin appears to be more specific to influencing Approach behaviour with less of an effect on arousal.

Despite these subtle differences between the Fasted and Ghrelin states, these hungry states still produced highly similar profiles such that they could be clustered together using an unsupervised Gaussian mixture clustering method, with the sated states (Fed and PBS-injected) forming the other cluster. Therefore, one additional finding from this behavioural analysis is that ghrelin recapitulates with high fidelity the key behavioural features of the Fasted state. This means that ghrelin acts as a reliable proxy of physiological hunger (at least behaviourally), which provided me

with acute experimental control over hunger.

One assumption of the Markov chain analysis is that the BSS conforms to the Markov property, i.e. previous behaviour does not affect future behaviour. Thus, feeding behaviour under the Markov assumption is a stochastic process in which any of the five main BSS behaviours (Approach, Eat, Rear, Groom and Rest) has some probability of expression that is not dependent on past behaviour. Although not explicitly tested for the Markov property, the Markov assumption is usually made for behavioural observations occurring at a short timescale (minutes to hours, Carola et al., 2011; Burnett et al., 2019). By contrast, feeding behaviour observed on longer timescale (for example, days to weeks) are more likely to rely on longer-term memory processes to regulate feeding behaviour, thereby violating the Markov assumption (Davidson et al., 2014; Allcroft et al., 2004). Given that the period of observation of feeding behaviour was short (10 mins in my experiments), the expression of each component of the BSS behaviour is likely stochastic and conditionally independent from previous behaviours. However, future analysis could directly examine the history dependence of feeding behaviour by comparing history-independent models, such as the Markov decision process model, and models which take into account varying degrees of history, such as semi-Markov or autoregressive models, and compare the fit of these models to feeding behaviour.

In summary, this chapter has outlined that the structure of feeding behaviour is crucially dependent on the hunger state, and that physiological fasting and hunger brought about by ghrelin injections are highly similar. This observation also yields the important implication that i.p. injections of ghrelin can be used as an experimental proxy for hunger, a fact that is leveraged in subsequent experiments outlined in this thesis.

Chapter 4

Ventral hippocampal neural dynamics during feeding behaviour

The hippocampus is a brain region important in encoding contexts, but how internal contexts such as the hunger state is represented in hippocampal circuits is not known. In this chapter, I present data from a series of experiments that investigated the neural dynamics of ventral subiculum (vS) during feeding behaviour across different states of hunger. I used *in vivo* Ca^{2+}-based fibre photometry in freely feeding mice, and manipulated their hunger either physiologically (by overnight fasting) or artificially (by exogenous injections of the hunger hormone ghrelin). I found that the vS was most activated when animals approach and investigate food, and that hunger reduces neural activity during this anticipatory phase of feeding behaviour. Furthermore, this effect could be specifically mapped to vS projections to the nucleus accumbens, and likely encodes the value of food. Hunger therefore shifts the encoding of value during food approach in hippocampal neurons that project to nucleus accumbens, suggesting a projection-specific logic in the hunger state modulation of hippocampal circuitry.

4.1 Introduction

The hippocampus is classically known to support the encoding of memory and spatial navigation. By contrast, its ventral region is important in regulating emotional and motivated behaviour (Strange et al., 2014). As discussed in the Introduction, this dissociation of function across hippocampal regions suggest that perhaps the

hippocampus is performing a more general computation in forming internal representations about the relationships between discrete features of the environment to predict outcomes and guide future behaviour (Stachenfeld et al., 2017; Pennartz et al., 2011a; van der Meer and Redish, 2011; Biderman et al., 2020; Bannerman et al., 2014).

In particular, the ventral hippocampus (vS) appears to be an important candidate brain region in directing the higher-order control of feeding behaviour (Davidson et al., 2007; Kanoski and Grill, 2017). Human patients with lesions to the medial temporal lobe are impaired in describing their internal state and persist in eating multiple consecutive meals (Hebben et al., 1985; Rozin et al., 1998; Higgs et al., 2008). Lesioning the hippocampus in rats also disrupts the ability of animals to use the hunger state as a contextual cue to disambiguate between uncertain outcomes (Davidson and Jarrard, 1993; Hock and Bunsey, 1998), suggesting that the hippocampus senses hunger-related signals for pattern completion.

The hippocampus also expresses diverse receptors for circulating feeding-related peptides (Lathe, 2001; Lathe et al., 2020), such as the hunger hormone ghrelin (Diano et al., 2006; Zigman et al., 2006; Guan et al., 1997; Hsu et al., 2015), and the satiety hormone glucagon-like peptide 1 (Hsu et al., 2014; Kanoski et al., 2016); direct cannulation of these hormones into the vS is sufficient to modulate feeding (Kanoski et al., 2013; Hsu et al., 2015). Furthermore, hunger as a motivational state influences hippocampal physiology, such as place cell representations (Kennedy and Shapiro, 2009) and sharp wave ripple activity (Carey et al., 2019). Finally, activating vS projections suppresses feeding behaviour (Sweeney and Yang, 2015; Reed et al., 2018; Yoshida et al., 2019) while inhibiting the vS increases time spent feeding (Henderson et al., 2012). Together, these studies strongly suggest that the hippocampus detects the internal hunger state to guide behaviour. However, it remains less clear what aspect of feeding behaviour is being served by the vS, and whether vS is integrating hunger-related signals during the course of naturalistic free-feeding behaviour.

Anatomically, the output region of the vS – the CA1 and subiculum area – is critical in governing affective and motivated behaviours (Cooper et al., 2006; Ciocchi et al., 2015; Jimenez et al., 2018; Ding et al., 2020). It is believed to perform this

function through intermingled and largely non-overlapping subpopulations of projection neurons with parallel output targets to diverse reward-related brain regions (Naber and Witter, 1998; Wee and MacAskill, 2020), including the lateral hypothalamus (LH; Cenquizca and Swanson, 2006, 2007; Swanson and Cowan, 1975) and nucleus accumbens shell (NAc; Britt et al., 2012; MacAskill et al., 2012, 2014). In particular, the LH is the classical site of intracranial self-stimulation, and manipulating LH circuit activity can promote or suppress appetitive behaviours such as feeding (Stuber and Wise, 2016; Jennings et al., 2013, 2015). The NAc shell forms part of the ventral striatum and is known to integrate a multitude of signals relating to context and value to produce actions (Pennartz et al., 2011b). Importantly, the NAc is also known to control feeding behaviour (Maldonado-Irizarry et al., 1995; Stratford and Kelley, 1997; O'Connor et al., 2015; Reed et al., 2018; Yang et al., 2019). However, it remains unknown how each of these hippocampal-subcortical pathways contributes to goal-directed feeding behaviour under naturalistic and unrestrained settings.

In this chapter, I sought to address these questions by relating vS population activity to the descriptions of feeding behaviour outlined in the previous chapter.

4.2 Results

4.2.1 Ventral hippocampal encoding of feeding behaviour across hunger states

Having characterised feeding behaviour in detail in the previous chapter, I next asked how the vS may be involved in the course of the BSS, and whether the ventral subiculum (vS) in particular encodes a specific aspect of the BSS. To address this question, I used Ca^{2+}-based fibre photometry to monitor the neural activity of populations of excitatory vS neurons as a bulk fluorescence signal. In wild-type mice, I stereotaxically injected two viruses, *AAV1/2-CamKII-Cre* and *AAV1/2-FLEX-GCaMP6f-WPRE*, into vS; this dual viral strategy ensured that the expression of the calcium indicator GCaMP6f was preferentially restricted to excitatory neurons in vS.

Following at least 4 weeks of expression, animals were presented with a pellet of chow for 10 mins in the Fed and Fasted states – as described previously – while tethered to the fibre optic cable during testing sessions (**Figure 4.1A**). There was a

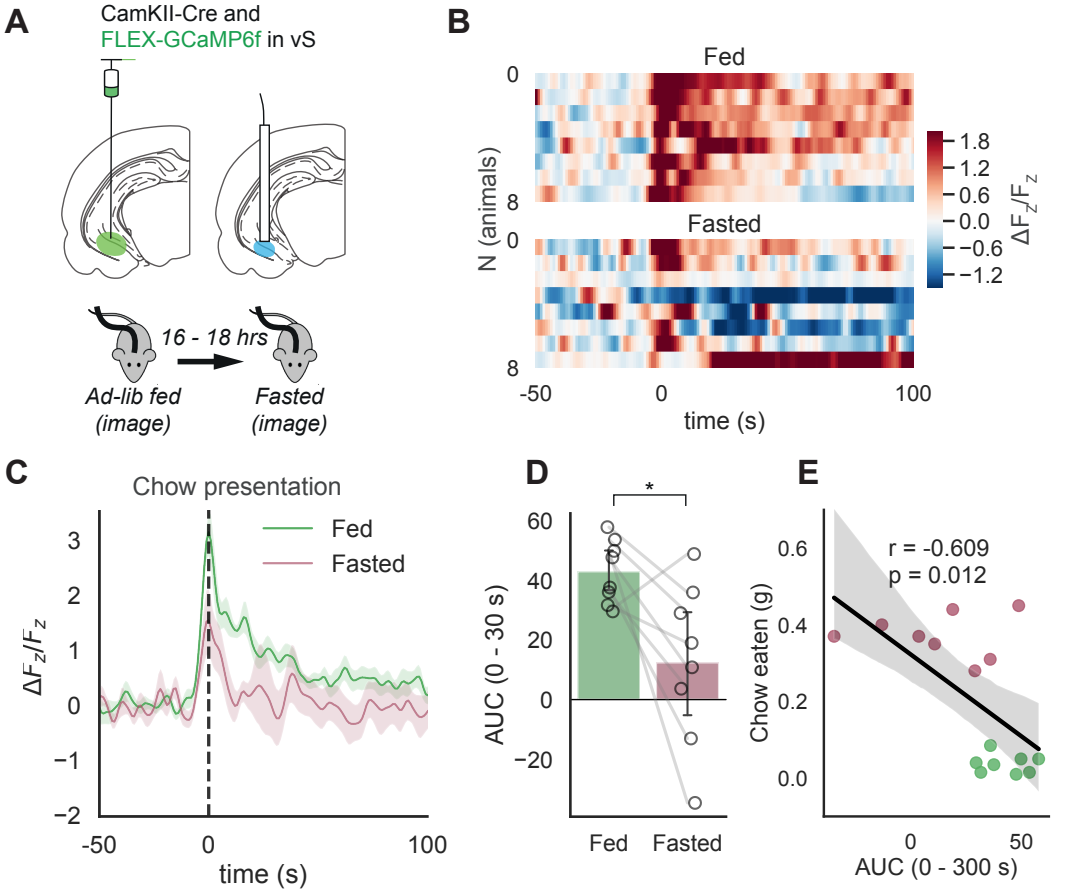

Figure 4.1: Neural dynamics of excitatory vS neurons to presentation of chow across Fed and Fasted states. (A) Schematic of stereotaxic injections to express the calcium indicator GCaMP6f in excitatory vS neurons. After at least 4 weeks of expression, ad-libitum fed animals were imaged by fibre photometry during a 10-minute presentation of a chow pellet in a behavioural testing box. Mice were then fasted overnight, and the experiment was repeated. (B) Heatmap demonstrating the $\frac{\Delta F_z}{F_z}$ (z-scored Ca^{2+} activity) as a function of time, aligned to the moment of chow presentation, and baselined to the period -50 to -10 s prior to chow presentation. Each row represents 1 mouse, and the signals have been sorted by area under the curve (AUC) in the period 0 to 30 s. (C) Averaged z-scored neural activity as a function of time, aligned to the moment of chow presentation. (D) The AUC from 0 to 30 s between the Fed and Fasted conditions were compared (t = 2.89, p = 0.023, n = 8 animals). (E) Linear regression of AUC against the amount of chow consumed during the 10-minute chow presentation (Pearson correlation coefficient, r = -0.61, p = 0.012). Data represent mean ± sem.

time-locked increase in Ca^{2+} activity at the moment of chow presentation (**Figure 4.1B–C**). Compared to the Fed state, vS activity in the Fasted state quickly dropped to baseline levels, while in the Fed state vS activity remained elevated (AUC from 0 to 30 s in $\frac{\Delta F_z}{F_z} s^{-1}$, Fed = 42.97 ± 3.75, Fasted = 12.43 ± 9.57, two-tailed paired t-test, t = 2.89, p = 0.023, n = 8 mice; **Figure 4.1D**). Furthermore, I observed that there was a negative correlation between the overall activity of vS following chow

presentation and the total amount of chow consumed within 10 mins (Pearson correlation coefficient, r = -0.61, p = 0.012; **Figure 4.1E**). Importantly, the order of the Fed (day 1) and Fasted (day 2) conditions could not alone explain the reduction in vS activity, as vS activity following 24 hours of refeeding state (Refed; day 3) was comparable to that in the Fed state (AUC from 0 to 30 s between Fed and Refed states, paired t-test, t = 0.74, p = 0.48, data not shown). Therefore, physiological hunger produced by overnight fasting led to a reduction in overall vS activity immediately following food presentation to chow, and this reduction correlated with the amount of chow consumed.

Qualitatively, when directly examining the z-scored Ca^{2+} activity in vS during the occurrence of feeding-specific BSS behaviours (i.e. Approach and Eat), vS activity appeared to closely track Approach bouts with sharp increases in the Ca^{2+} signal (**Figure 4.2A**), whereas eating bouts appeared unrelated (**Figure 4.2B**). This suggested that vS may be specifically encoding Approach behaviour as opposed to Eating.

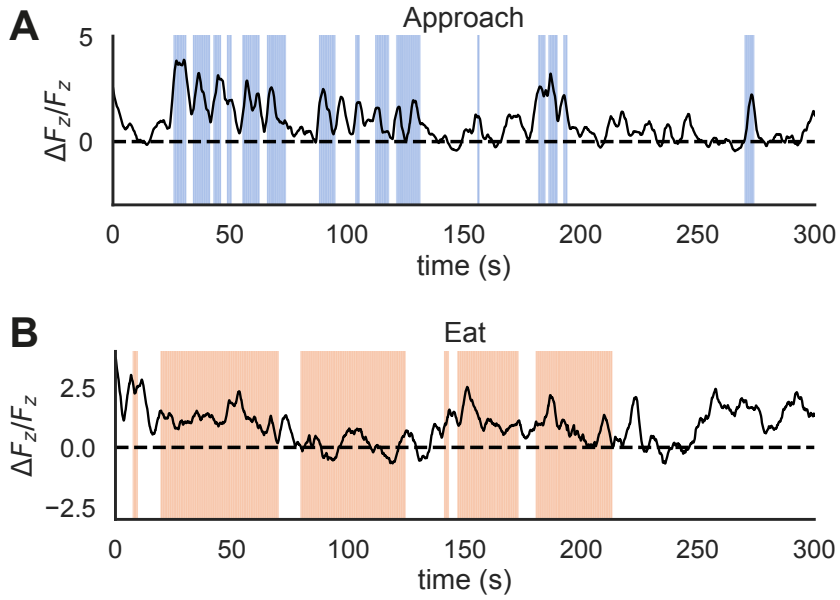

Figure 4.2: Neural dynamics of excitatory vS neurons during Approach and Eat events. (A) Example Ca^{2+} activity recording in one animal during (A) Approach and (B) Eat bouts.

To directly relate the vS activity to specific components of the BSS, and hence determine which behaviour is encoded by vS, I first annotated the occurrence of the BSS behaviours of the animals during the 10-minute presentation period – as

described previously. I then aligned the photometry signals to the onset of each BSS behaviour, and obtained event-triggered averages of the Ca^{2+} signals around the time of each event. This analysis revealed qualitatively that Approach and Eat resulted in the largest increases in vS activity, followed by Rear, Groom and Rest (**Figure 4.3**). vS activity also appeared to be suppressed by hunger during Approach and Eat.

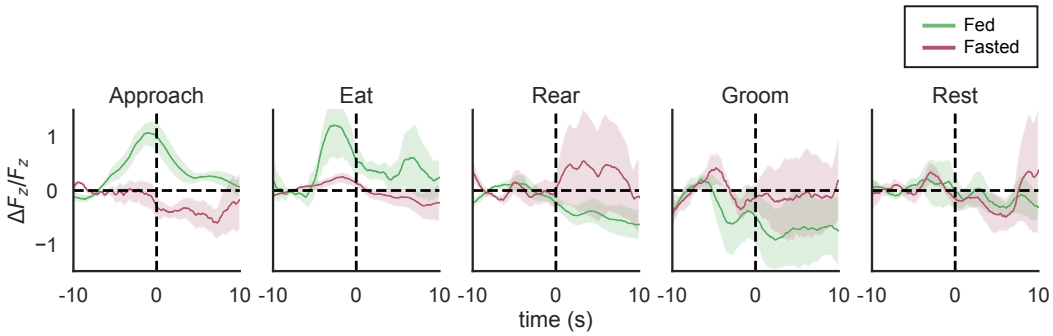

Figure 4.3: Event-triggered responses of excitatory vS neurons to each BSS behaviour. The $\frac{\Delta F_z}{F_z}$ signal was aligned to the onset of each BSS event and baselined to the period -10 to -7.5 s relative to the event onset. Approach and Eat events were associated with positive modulation of vS activity, while Rear, Groom and Rest events were variable and on average unchanged. Data represented as mean ± sem.

However, one caveat of the event-triggered average analysis is that the photometry signals may be contaminated by more than one behavioural event. For example, Approach and Eat behaviours often occur close in time together, and these behavioural events may each bleed into the other event's signal. To more accurately quantify the level of vS activity during each event, I built a linear encoding model that modelled vS activity as a linear combination of each component of the BSS (see Methods for details; **Figure 4.4A–B**). This linear encoding model is able to statistically separate the contributions of each BSS event to the recorded neural activity. Briefly, the dependent variable of the linear model was the z-scored Ca^{2+} activity, and the predictor variables were comprised of 27 regressors in total: 5 main behavioural regressors (Approach, Eat, Rear, Groom and Rest), 20 behavioural transition regressors (for example, Approach $\rightarrow$ Eat transitions), a stimulus presentation regressor and a velocity regressor. The 5 behavioural regressors represented the 5 core BSS behaviours, and were vectors of 1s indicating the engagement in a BSS behaviour and 0s elsewhere. The 20 transition regressors were pulses of exponential decays with a half-life of 2 seconds to capture any vS activity that may

be related to transitions between BSS behaviours. To control for the salience of the actual food presentation and the influence of animal movement (velocity), I further included a stimulus presentation regressor as a pulse of an exponential decay with a half-life of 5 seconds from the onset of chow presentation, and a velocity regressor as a continuous analog signal of the instantaneous velocity of the animal. Together, this linear encoding model approach allowed me to statistically dissociate the photometry signals from neighbouring behavioural events and to capture any dependence of the photometry signal to each BSS behaviour.

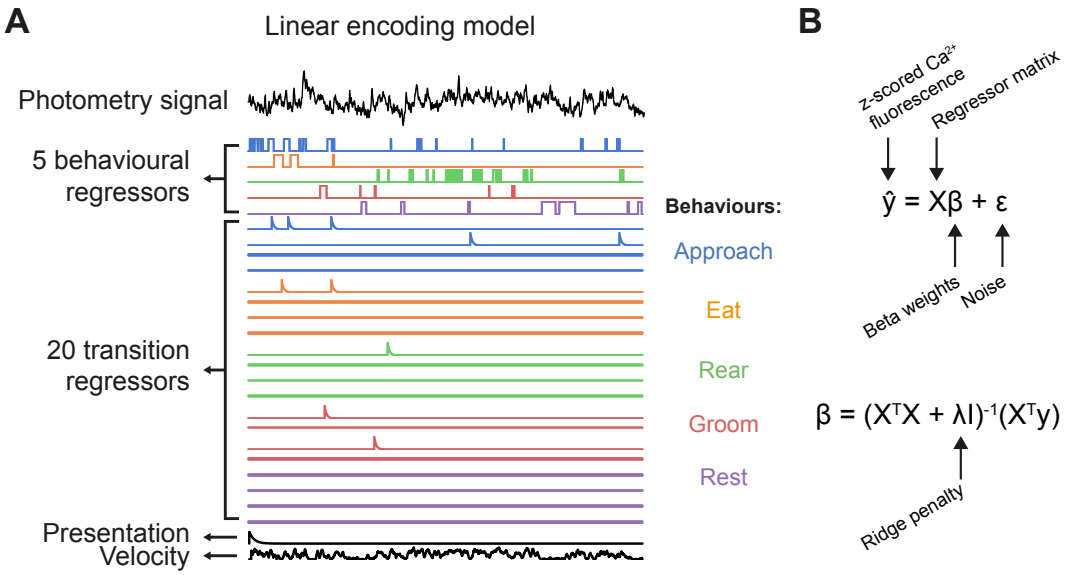

Figure 4.4: Linear encoding model to quantify neural activity during each BSS behaviour. (A) Example regressor (design) matrix comprising 27 regressors in total: 5 behavioural regressors, 20 transition regressors, a stimulus presentation regressor and a velocity regressor. Each BSS behavioural regressor was coded as temporal pulses of 0s and 1s, where 1s indicate engagement in the BSS behaviour and 0s elsewhere. Transition regressors (e.g approach to eat) were defined as behaviours that changed to another BSS behaviour within a 5-second window. Transition regressors were convolved with an exponential decay function with a half-life of 2 s to capture the decay of GCaMP6f. The presentation regressor was a pulse of an exponential decay with a half-life of 5 s. The velocity regressor is the smoothed, tracked velocity of the animal during the 10-minute food presentation. (B) *Top*: A multiple linear regression model was fitted with the dependent variable being the $\frac{\Delta F_z}{F_z}$ and the independent variable being the regressor matrix defined in (A). *Bottom*: The β weights were computed using ridge regression, which implements an L2 regularisation to prevent overfitting of the β weights.

In this analysis, I focused on how the vS neural activity was related to the five main behavioural regressors (i.e. Approach, Eat, Rear, Groom and Rest), and use the other regressors to control for any confounding contribution to the vS signal (**Figure 4.4A**). The estimated β coefficients of the 5 behavioural regressors after

model fitting can be interpreted as the isolated, average neural activity of vS in the presence of each BSS behaviour, and thus signified how strongly each behaviour was related to the calcium signal. In turn, the size of these β coefficients can be used to infer the extent of up- or down-modulation of the Ca^{2+} signal by the presence of each behaviour. The model was fit using ridge regression with penalisation (**Figure 4.4B**) and a cross-validation procedure (see **Figure 2.1C** in Methods). Using this procedure, the model captured substantial amount of the variance in the Ca^{2+} signal (5-fold cross-validated R^2 of models, Fed, = 0.38 ± 0.03; Fasted = 0.25 ± 0.04).

To compare the extent of vS encoding of each BSS behaviour, I analysed the fitted β weights for each BSS behaviour across the Fed and Fasted states. Firstly, the β weights for each BSS behaviour depended on the hunger state (two-way repeated-measures ANOVA, interaction between BSS behaviour and the hunger state, $F_{4, 28} = 8.27$, $p = 1.56 \times 10^{-4}$; **Figure 4.5A**). In addition to this significant interaction, there was a significant main effect of behaviour ($F_{4, 28} = 5.62$, $p = 0.002$), indicating that vS activity is differentially encoding each BSS behaviour. In the Fed state, Approach behaviour produced the largest β weights, followed by Rear, Eat, Groom and Rest behaviour; this finding indicates that Approach behaviour was most robustly encoded by vS activity. When analysing each BSS behaviour separately, Approach behaviour was associated with a reduced β weight in the Fasted compared to the Fed state, and more subtly Eat behaviour, while Rest behaviour was associated with a reduced β weight in the Fed compared to the Fasted state (**Figure 4.5A**). Interestingly, feeding- and non-feeding-specific exploratory behaviours (Approach and Rear) were associated with positive β weights for vS activity, suggesting that exploration was encoded by the vS; by contrast, consummatory behaviours such as Eat, Groom and Rest were lower compared to the exploratory behaviours. Importantly, there was no significant main effect of hunger state ($F_{1, 7} = 2.45$, $p = 0.16$), indicating that hunger did not lead to a suppression of activity irrespective of the type of BSS behaviour.

Next, I sought to identify which BSS behaviour-associated neural activity correlated most with food consumption. Furthermore, I asked which of the estimates of vS activity during each BSS component significantly correlated with the micro-

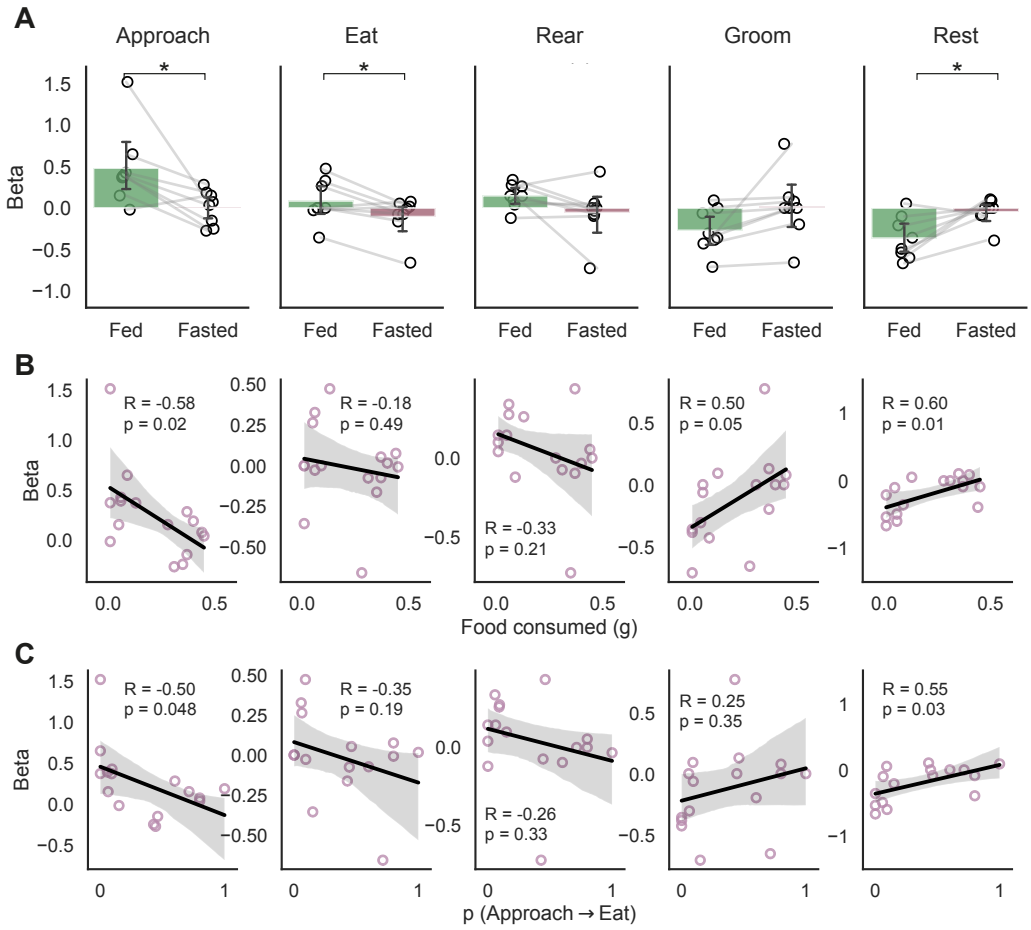

Figure 4.5: Linear regression of vS activity to the BSS. (A) The fitted β weights of the ridge regression model for each BSS behaviour (Approach, Fasted = 0.02 ± 0.08, Fed = 0.51 ± 0.14, t = -3.33, p = 0.013; Eat, Fasted = -0.11 ± 0.10, Fed = 0.12 ± 0.12, t = -2.64, p = 0.033; Rear, Fasted = -0.03 ± 0.11, Fed = 0.18 ± 0.06, t = -1.97, p = 0.089; Groom, Fasted = -0.01 ± 0.14, Fed = -0.29 ± 0.11, t = 2.25, p = 0.059; Rest, Fasted = -0.06 ± 0.06, Fed = -0.39 ± 0.10, t = 2.90, p = 0.023; paired t-tests, n = 8 mice). Note that the values of the L2 regularisation penalty were unchanged between the Fed and Fasted conditions (Wilcoxon signed-rank test, W = 1.5, p = 1.0) and thus cannot explain the differences in the fitted β weights across hunger state. (B) Linear regression of the estimated β weights with the amount of food consumed. Approach-related activity is significantly correlated with subsequent food consumption, while Eat-related activity is not. (C) Linear regression of the β weights with the transition probability from Approach to Eat (i.e. the normalised frequency of Approach events that are followed by Eat events). Data represented as mean ± sem.

structure of feeding behaviour, and specifically the transition probability from Approach to Eat (the phase of feeding behaviour that is strongly modulated by hunger, see Figure 3.4). By regressing the amount of food consumed within the 10 minutes session against the estimated β weights, I found that Approach-related activity was specifically correlated with the subsequent amount of chow consumed, while Eat-related activity was not (**Figure 4.5B**). Notably, Rest-related activity was

positively correlated with food consumed, suggesting that low activity during Rest might promote engagement in non-food-specific behaviour (see Discussion). Similarly, by regressing the probability of Approach-to-Eat transitions to the estimated β weights, I found that Approach-related activity was specifically correlated with the probability that animals will transition to Eat bouts once they start approaching and investigating food (**Figure 4.5C**). This finding further suggests that vS activity may be important in gating the transition from Approach to Eat. Overall, the regression analysis demonstrates that the vS most strongly encoded Approach behaviour, and that hunger reduced Approach-related activity in a manner that negatively correlated with the amount of food consumed and transition probability from Approach to Eat.

As a control analysis, I analysed the effect of food presentation and velocity on vS activity to determine if changes in the encoding of presentation or velocity by hunger could have produced the changes in the encoding of BSS behaviours. Hunger by overnight fasting did not modulate the coupling between chow presentation and velocity with vS activity (two-way repeated-measures ANOVA, interaction between regressor type and hunger state, $F_{1,7} = 1.07$, $p = 0.34$, main effect of regressor (presentation or velocity), $F_{1,7} = 33.08$, $p = 6.98 \times 10^{-4}$; main effect of hunger state, $F_{1,7} = 1.09$, $p = 0.33$; **Figure 4.6A**). Crucially, the β weight for food presentation was high, indicating that vS encodes the salience of food presentation, while the β weight for velocity was minimal; this was important as the overall velocity was reduced in the Fasted state (velocity in cm/s, Fed = 1.70 ± 0.08, Fasted = 1.32 ± 0.11, two-tailed paired t-test, $t = 2.80$, $p = 0.03$; **Figure 4.6B**), corresponding to the increased food investigation and consumption – with concomitant decreases in locomotion – that accompany fasting. Furthermore, velocity specifically during food approach was unchanged by hunger (velocity during approach in cm/s, Fed = 2.00 ± 0.08, Fasted = 2.11 ± 0.15, two-tailed paired t-test, $t = -0.60$, $p = 0.57$; **Figure 4.6C**). Together, these observations argue against the idea that changes in salience encoding or movement contributes to the differential encoding of BSS behaviours, and specifically Approach behaviour, in vS activity across different hunger states. Lastly, the fibre placements for all experiments involving imaging of the vS were examined and confirmed to be localised within vS (**Figure 4.7**).

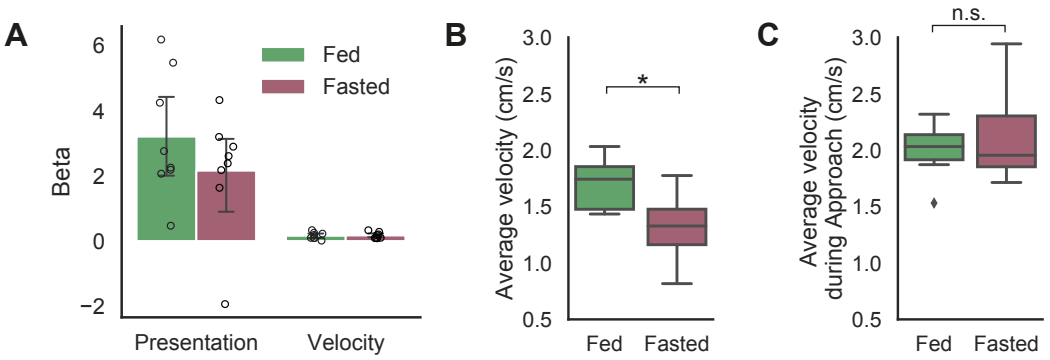

Figure 4.6: Stimulus presentation or velocity cannot account for the differential encoding of behaviour in vS activity. (A) β weights for presentation and velocity. (B) Average velocity for the entire 10 minute period of chow presentation. (C) Average velocity during Approach boats. Data represented as mean ± sem in bar plots, and median ± 1.5 times the IQR in box plots.

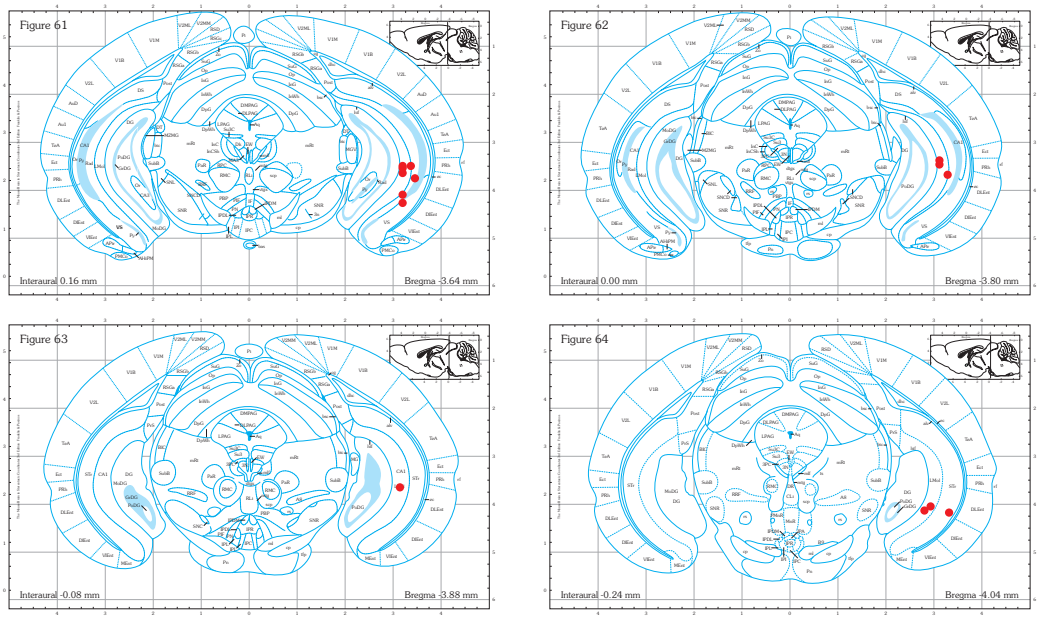

Figure 4.7: Fibre implant locations for vS photometry experiments. Red dots indicate the location of the fibre tips.

Combined, these data indicate that vS activity is highest during exploratory behaviours such as Approach and lowest during consummatory behaviours such as Eat and Rest, and that hunger changes the encoding of feeding behaviour in vS population activity.

4.2.2 Ghrelin inhibits vS activity following chow presentation

The next question I sought to address was what signalling mechanism might underlie the hunger state dependence of the vS signal. In particular, ghrelin is an impor-

tant circulating hormone signalling the hunger state; the hippocampus expresses the ghrelin receptor (growth hormone secretagogue receptor 1a; GHSR1a; Zigman et al., 2006; Kanoski et al., 2013; Diano et al., 2006). Additionally, I showed that exogenous ghrelin can not only act as a reliable proxy to overnight fasting (**Figure 3.6**), but it also influences feeding behaviour by markedly changing the probability of transitioning between Approach and Eat behaviours (**Figure 3.4**) – the phase of behaviour that the vS seems to encode (**Figure 4.5**). Therefore, I chose to use i.p. injections of ghrelin to gain acute experimental control over the hunger state. This is important as the hunger manipulations used thus far – i.e. overnight fasting – changes a panoply of satiety- and hunger-related hormones (Morton et al., 2014), and many of these circulating hormones bind to receptors expressed in the hippocampus (Diano et al., 2006; McNay, 2007; Harvey, 2013; Kanoski et al., 2013).

Therefore, in animals expressing GCaMP6f in excitatory neurons in vS, I delivered i.p. injections of 2 mg/kg ghrelin or PBS (control) and recorded vS activity during presentation of chow (**Figure 4.8A**). Like the Fasted state, vS activity was reduced following chow presentation in the Ghrelin condition compared to the PBS condition (AUC from 0-30 seconds, PBS = 58.49 ± 10.92; Ghrelin = 25.91 ± 9.99; paired t-test, t = 2.57, p = 0.03, n = 10 mice; **Figure 4.8B–D**). Mirroring the Fed and Fasted conditions, vS activity was furthermore negatively correlated with the amount of chow eaten (Pearson correlation coefficient, r = -0.508, p = 0.02; **Figure 4.8E**). Thus, Ghrelin recapitulated the gross overall reduction in vS activity observed in the Fasted condition.

To clarify at exactly what phase of behaviour ghrelin may be modulating vS activity, I manually annotated the BSS behavioural events for animals injected with either ghrelin or PBS and aligned the photometry signals to the onset of these events (**Figure 4.9A**). This event-triggered average analysis revealed qualitatively that the predominant reduction in activity occurred during the Approach phase of the BSS (**Figure 4.9A**).

To isolate the average neural activity during each BSS event, I used multiple linear regression to directly relate the photometry signal to behaviour. The resulting linear models captured substantial variance in the photometry signal (model 5-fold cross-validated R^2, PBS = 0.29 ± 0.05, Ghrelin = 0.27 ± 0.05). This analysis

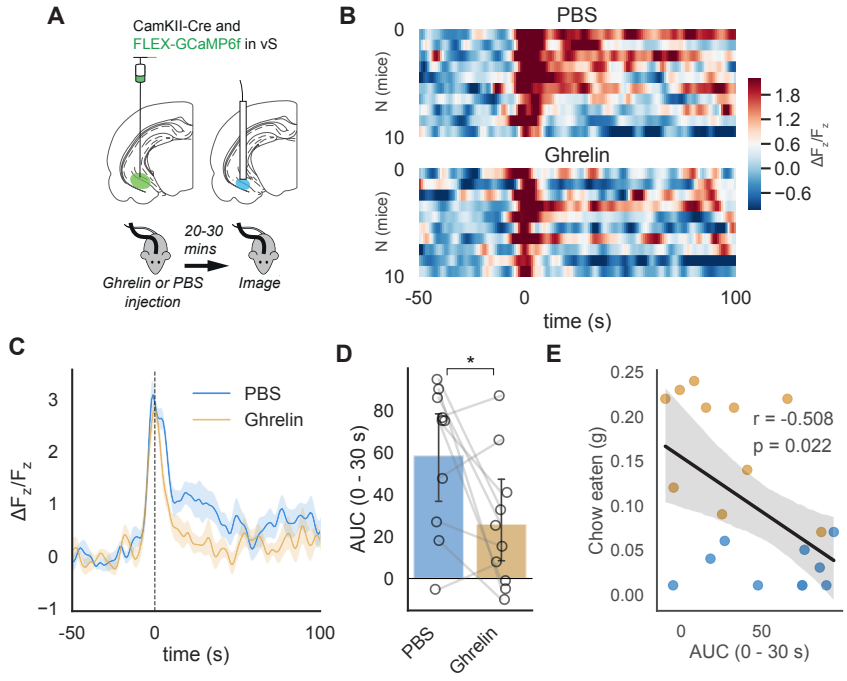

Figure 4.8: Ghrelin inhibits vS activity in response to chow presentation. (A) Schematic of stereotaxic injections to express the calcium indicator GCaMP6f in excitatory vS neurons. After at least 4 weeks of expression, ad-libitum fed animals were given i.p. injections of 2 mg/kg ghrelin or PBS prior to imaging using fibre photometry. (B) Heatmap demonstrating the $\frac{dF_z}{F_z}$ (z-scored Ca^{2+} activity) as a function of time, aligned to the moment of chow presentation, and baselined to the period -50 to -10 s prior to chow presentation. Each row represents one animal, and the signals have been sorted by area under the curve in the period 0 to 30 s. (C) Averaged z-scored neural activity as a function of time, aligned to the moment of chow presentation. (D) The area under the curve (AUC) was computed for the period between 0 and 30 s across hunger states (AUC in the period from 0 to 30 seconds, PBS = 58.49 ± 10.92; Ghrelin = 25.91 ± 9.99; paired t-test, t = 2.57, p = 0.03, n = 10 mice). (E) Linear regression of AUC against the amount of chow consumed during the 10-minute chow presentation (Pearson correlation coefficient, r = -0.508, p = 0.02). Data represent mean ± sem.

showed that, like the Fed and Fasted conditions, vS qualitatively encoded the BSS behaviours differentially across hunger state. Exploratory behaviours (Approach and Rear) were encoded as positive modulations in the photometry signal, consummatory behaviours (Groom and Rest) and negative modulations of the signal, and Eat behaviour is related to fluctuations in the photometry signal around 0 (**Figure 4.9B**). Notably, while there was a trend of a reduction in Approach-related activity in Ghrelin compared to the PBS condition, this was not statistically significant (**Figure 4.9B**), while Eat-related activity showed a slight reduction with ghrelin. The encoding of Rear, Groom and Rest were unaltered by ghrelin (**Figure 4.9B**). Thus, while vS activity reliably encodes Approach-related behaviour, overall vS activity appears

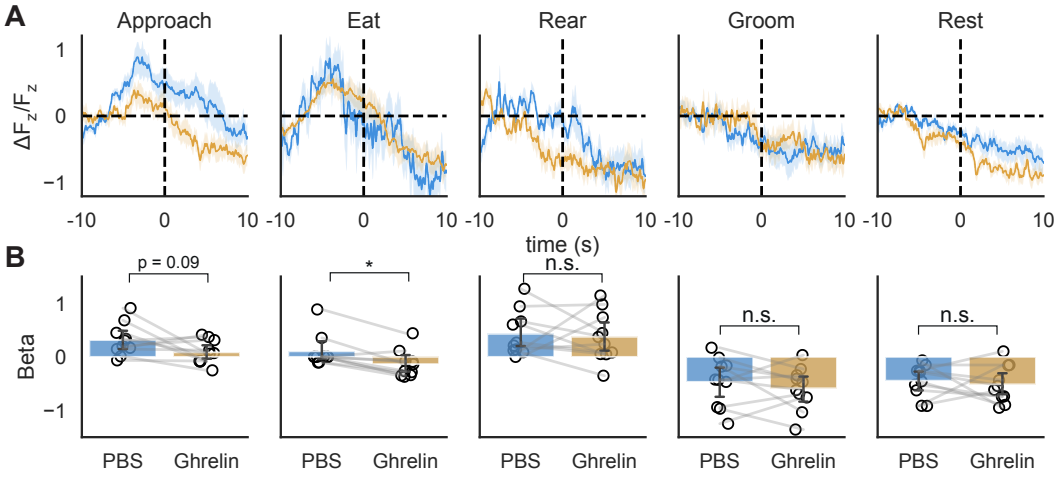

Figure 4.9: Ghrelin does not globally inhibit vS activity during Approach behaviour. (A) Event-triggered photometry traces aligned to the onset of the event. The signal was baselined to the -10 to -7.5 s period. (B) The β coefficients for each BSS behaviour obtained from multiple linear regression analysis. The β coefficient for the behavioural regressors can be interpreted as the isolated, independent neural response in the presence of that behaviour (β coefficients, Approach, Ghrelin = 0.09 ± 0.07, PBS = 0.31 ± 0.09, t = -1.93, p = 0.086; Eat, Ghrelin = -0.14 ± 0.08, PBS = 0.10 ± 0.10, t = -4.15, p = 0.002; Rear, Ghrelin = 0.37 ± 0.15, PBS = 0.43 ± 0.13, t = -0.31, p = 0.765; Groom, Ghrelin = -0.59 ± 0.13, PBS = -0.47 ± 0.14, t = -0.86, p = 0.411; Rest, Ghrelin = -0.51 ± 0.11, PBS = -0.45 ± 0.09, t = -0.47, p = 0.648). Data represent mean ± sem.

to be invariant to the effect of ghrelin during Approach behaviour.

Taken together, systemic ghrelin appears to inhibit vS activity immediately following food presentation, but ghrelin injection is insufficient to inhibit the whole population activity of excitatory vS neurons during Approach.

4.2.3 Ghrelin-mediated inhibition during food approach is specific to vS projections to nucleus accumbens

One potential reason for the lack of a reduction of vS activity during Approach is that i.p. ghrelin injections represent a more specific manipulation of hunger than overnight fasting. This is coupled with the fact that vS neurons are heterogeneous; most notably, vS is comprised of populations of pyramidal neurons that send projections to distinct brain regions such as the nucleus accumbens (vS^{NAc}) and lateral hypothalamus (vS^{LH}), and each of these projections uniquely contributes to behaviour (Cembrowski et al., 2018b; Ciocchi et al., 2015; Jimenez et al., 2018). This raises the possibility that the effect of ghrelin may be specific to a particular vS projection, as opposed to globally affecting the activity of all vS projections. I hypothesised that either vS^{NAc} or vS^{LH}, or both these projections, may be specif-

ically modulated by ghrelin, as both NAc and LH have been implicated in feeding behaviour (Hsu et al., 2018; O'Connor et al., 2015; Nieh et al., 2016; Yang et al., 2019; Reed et al., 2018; Stuber and Wise, 2016).

To address this question, I recorded the neural activity of vS^{NAc} or vS^{LH} neurons in freely feeding mice (**Figure 4.10A,E**). To specifically express the calcium indicator GCaMP6f in projection-defined neurons, I injected *AAV2-retro-CAG-Cre* or *AAV2-retro-Syn-Cre* into either NAc or LH, which are taken up by the presynaptic terminals and retrogradely transported to the soma of vS neurons to express Cre (Tervo et al., 2016). Within the same surgery, a Cre-dependent construct harbouring the calcium indicator (*AAV1-CAG-FLEX-GCaMP6f-WPRE-SV40*) was injected into vS. This viral expression strategy ensured that GCaMP6f is expressed only in vS neurons that projected to either NAc or LH.

Using this method, I recorded vS^{NAc} and vS^{LH} activity after animals had been i.p. injected with either 2 mg/kg of ghrelin or PBS and presented with a piece of chow in the testing box. Immediately following chow presentation, both vS^{NAc} and vS^{LH} neurons showed time-locked increases in Ca^{2+} activity at the time of chow presentation (**Figure 4.10B–C, F–G**). vS^{NAc} neurons did not show differences in the activity levels following food presentation (AUC from 0 to 30 s, PBS = 48.12 ± 5.78, Ghrelin = 52.05 ± 9.96, t = -0.34, p = 0.75; **Figure 4.10B–C**); by contrast, vS^{LH} neurons showed an increased Ca^{2+} activity in the Ghrelin compared to the control condition (AUC from 0 to 30 s, PBS = 8.04 ± 14.81, Ghrelin = 51.53 ± 7.03, t = -4.33, p = 0.01; **Figure 4.10F–G**). These activity dynamics in vS^{NAc} and vS^{LH} neurons therefore showed distinct time courses compared to the overall vS recordings, highlighting prominent projection-specific heterogeneity in vS.

To determine more specifically if ghrelin was modulating vS^{NAc} and vS^{LH} activity during a particular phase of behaviour, I once again annotated the behaviours of animals during the 10-minute chow presentation, and aligned the corresponding Ca^{2+} to the onset of each BSS behaviour. Surprisingly, and in contrast to the signals aligned to chow presentation, the event-triggered average analysis revealed that the vS^{NAc} neurons showed prominent changes in activity levels at the onset of Approach and Eat bouts that appeared to be inhibited by ghrelin (**Figure 4.11A**), while their activity surrounding the onset of the non-feeding-specific behaviours

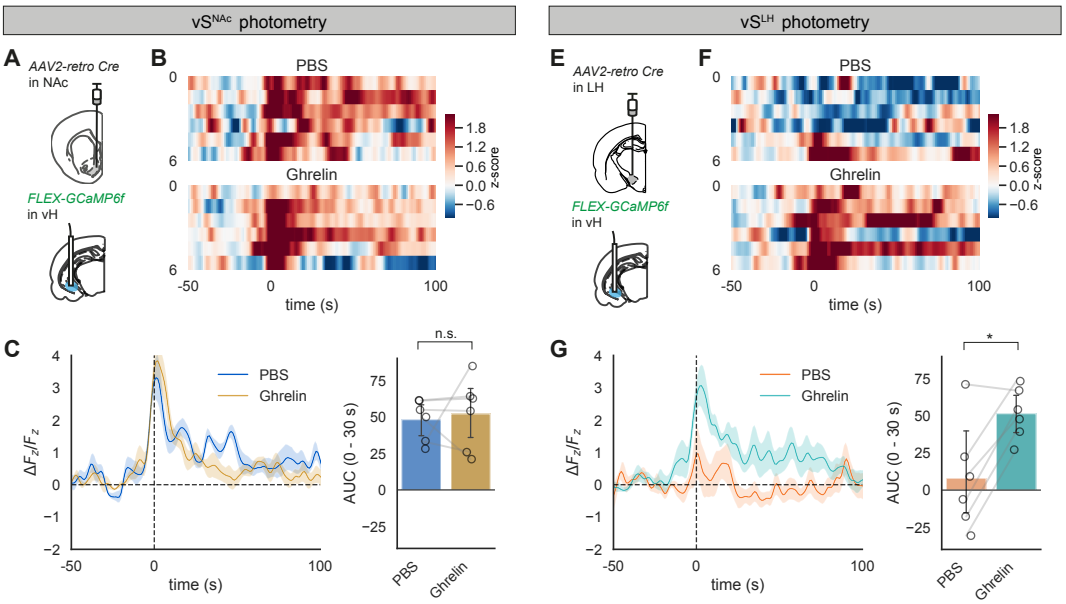

Figure 4.10: Time-locked Ca^{2+} activity in projection-specific vS neurons during food presentation. (A,E) Conditional expression of GCaMP6f in either vS^{NAc} (A) or vS^{LH} (E) neurons. To achieve conditional expression, *AAV2-retro-CAG-Cre* or *AAV2-retro-Syn-Cre* was injected into either NAc or LH. In the same surgery, *AAV1-CAG-FLEX-GCaMP6f-WPRE-SV40* was injected into vS. The retrograde expression of Cre in neurons that project to either NAc or LH, and the expression of Cre-dependent GCaMP6f in soma of vS neurons, allows projection-specific expression of GCaMP6f. Fibre cannulae were implanted in the same surgery. After at least 4 weeks, animals underwent imaging and behavioural testing. (B, F) Heatmap illustrating the z-scored Ca^{2+} activity aligned to the moment of chow presentation. Each row represents 1 animal. The signals were baselined to the period -50 to -10 s. (C, G) *Left*: Averaged z-scored Ca^{2+} activity across animals, aligned to chow presentation. *Right*: Quantification of the AUC from 0 to 30 s. Data represent mean ± sem.

were variable and on average unchanged. By contrast, vS^{LH} neurons appeared to exhibit minimal changes in activity at the onset of both feeding and non-feeding specific BSS behaviours; crucially, vS^{LH} activity during these behaviours appeared to be invariant to ghrelin (**Figure 4.11C**). The absence of vS^{LH} activity encoding of Approach or Eat behaviours, coupled with their significant response to the manual presentation of chow (**Figure 4.10F–G**), suggests that the ghrelin-mediated increase in vS^{LH} activity following chow presentation may reflect increased salience as opposed to a hunger state-dependent encoding of feeding behaviour (Gonzalez et al., 2016).

To quantify the encoding of each BSS behaviour by vS^{NAc} and vS^{LH} neurons, I conducted the linear encoding model analysis where the vS^{NAc} and vS^{LH} activity were modelled as a linear combination of the BSS behaviours (5-fold cross-validated R^2, vS^{LH} = 0.16 ± 0.03, vS^{NAc} = 0.23 ± 0.03). Strikingly, for vS^{NAc} neural

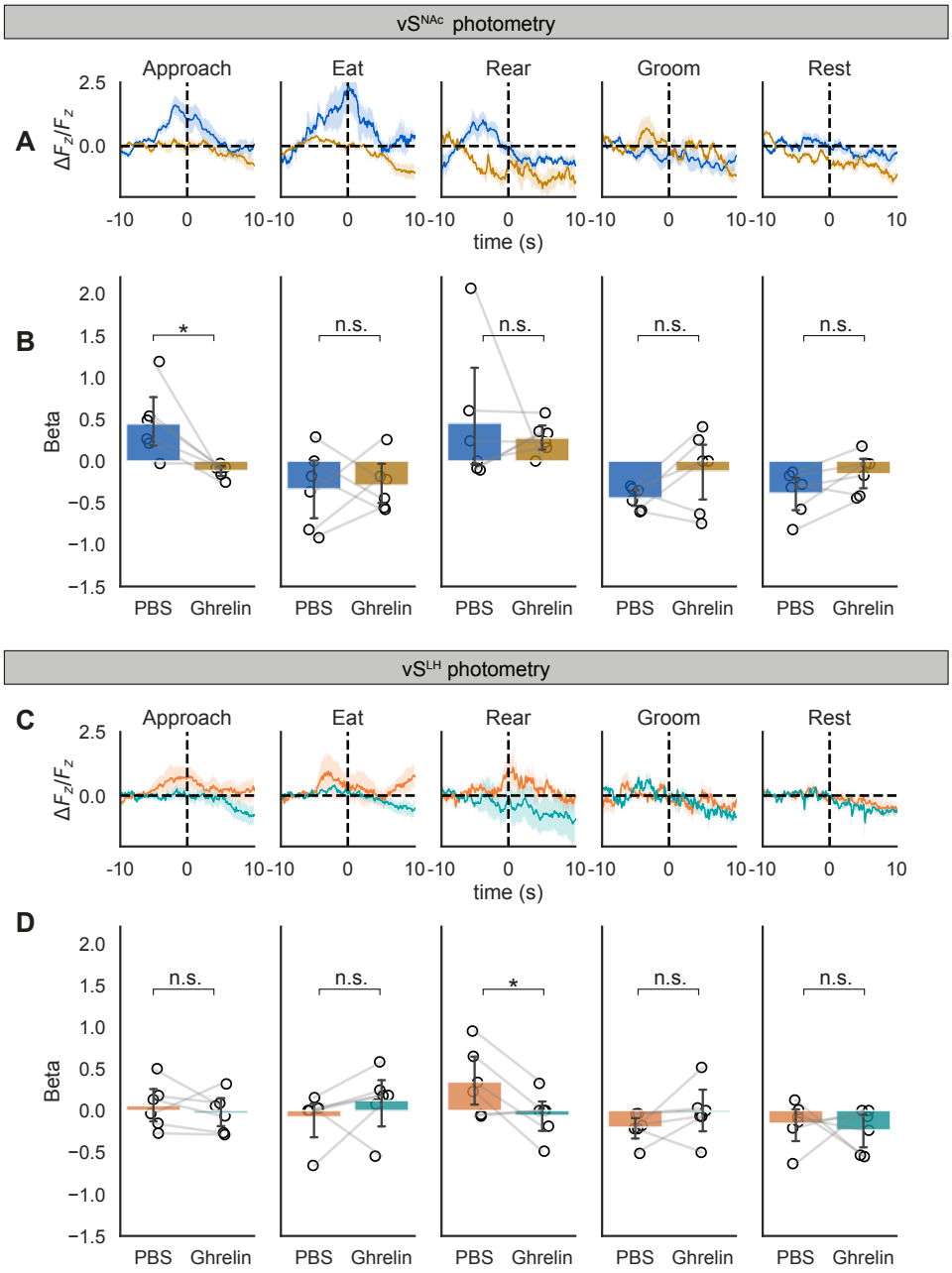

Figure 4.11: Ghrelin shifts the encoding of feeding- and non-feeding-specific predominantly in vS^{NAc} neurons. (A,C) Event-triggered average of (A) vS^{NAc} or (C) vS^{LH} neural activity when aligned to the onset of each BSS behaviour. (B, D) The β weights obtained from multiple linear regression for each BSS behaviour in (B) vS^{NAc} or (D) vS^{LH} neurons. (B) The β weights for each behaviour depended on hunger state (two-way repeated-measures ANOVA, interaction between behaviour and hunger state, $F_{4,20} = 3.30$, $p = 0.03$; main effect of behaviour, $F_{4,20} = 14.51$, $p = 3.2 \times 10^{-4}$); main effect of hunger state, $F_{1,5} = 0.04$, $p = 0.86$, $n = 6$ mice). Approach β was significantly modulated by ghrelin. (D) as in (B) for vS^{LH} neurons. Approach β was not modulated by ghrelin (two-way repeated-measures ANOVA, interaction between hunger state and behaviour, $F_{4,20} = 2.12$, $p = 0.12$; main effect of behaviour, $F_{4,20} = 3.06$, $p = 0.04$; main effect of hunger state, $F_{1,5} = 0.41$, $p = 0.55$, $n = 6$ mice). Data represented as mean ± sem. *$p<0.05$.

activity, the encoding of feeding behaviour in vS^{NAc} activity depended on both the hunger state and type of BSS behaviour (two-way repeated-measures ANOVA, interaction between behaviour and hunger state, $F_{4,20} = 3.30$, $p = 0.03$, $n = 6$ mice; **Figure 4.11B**) and the direction of the β coefficients was highly specific to each behaviour (main effect of behaviour, $F_{4,20} = 14.51$, $p = 3.2 \times 10^{-4}$). Importantly, ghrelin did not globally reduce vS^{NAc} activity across all BSS behaviours (main effect of hunger state, $F_{1,5} = 0.04$, $p = 0.86$). Notably, the β coefficient for Approach behaviour was reduced with ghrelin, while that for Rear was unchanged, indicating that vS^{NAc} activity encoding food-specific exploratory behaviour was uniquely modulated by ghrelin. Ghrelin also did not modulate the β coefficient for Eat, Rest and Groom behaviours (β weight of vS^{NAc} activity encoding of each BSS behaviour, Approach, Fed = 0.46 ± 0.18, Fasted = -0.08 ± 0.03, t = 2.92, p = 0.03; Eat, Fed = -0.34 ± 0.19, Fasted = -0.32 ± 0.13, t = -0.09, p = 0.93; Rear, Fed = 0.48 ± 0.35, Fasted = 0.27 ± 0.08, t = 0.53, p = 0.62; Groom, Fed = -0.48 ± 0.07, Fasted = -0.14 ± 0.19, t = -1.92, p = 0.11; Rest, Fed = -0.42 ± 0.11, Fasted = -0.18 ± 0.10, t = -2.24, p = 0.07, n = 6 mice; **Figure 4.11B**).

In contrast to vS^{NAc} population activity, the encoding of feeding behaviour in the vS^{LH} neural activity was not modulated by ghrelin across the different behaviours (two-way repeated-measures ANOVA, interaction between hunger state and behaviour, $F_{4,20} = 2.12$, $p = 0.12$; **Figure 4.11D**). vS^{LH} activity depended on the type of BSS behaviour (main effect of behaviour, $F_{4,20} = 3.06$, $p = 0.04$), and most notably Rear behaviour (**Figure 4.11D**). Furthermore, vS^{LH} activity was not changed overall by ghrelin (main effect of hunger state, $F_{1,5} = 0.41$, $p = 0.55$). Analysing each BSS behaviour individually revealed that only Rear-related activity was subtly modulated by ghrelin in vS^{LH} activity (β weight of vS^{NAc} activity encoding of each BSS behaviour, Approach, Fed = 0.07 ± 0.11, Fasted = 0.04 ± 0.11, t = 0.23, p = 0.83; Eat, Fed = -0.07 ± 0.12, Fasted = 0.12 ± 0.16, t = -1.01, p = 0.36; Groom, Fed = -0.21 ± 0.08, Fasted = -0.05 ± 0.14, t = -1.04, p = 0.35; Rear, Fed = 0.36 ± 0.16, Fasted = -0.07 ± 0.11, t = 2.86, p = 0.04; Rest, Fed = -0.17 ± 0.10, Fasted = -0.26 ± 0.11, t = 0.47, p = 0.66, n = 6 mice, **Figure 4.11D**). Taken together, ghrelin modulates the activity of vS^{NAc}, and not vS^{LH}, neural activity during Approach behaviour.

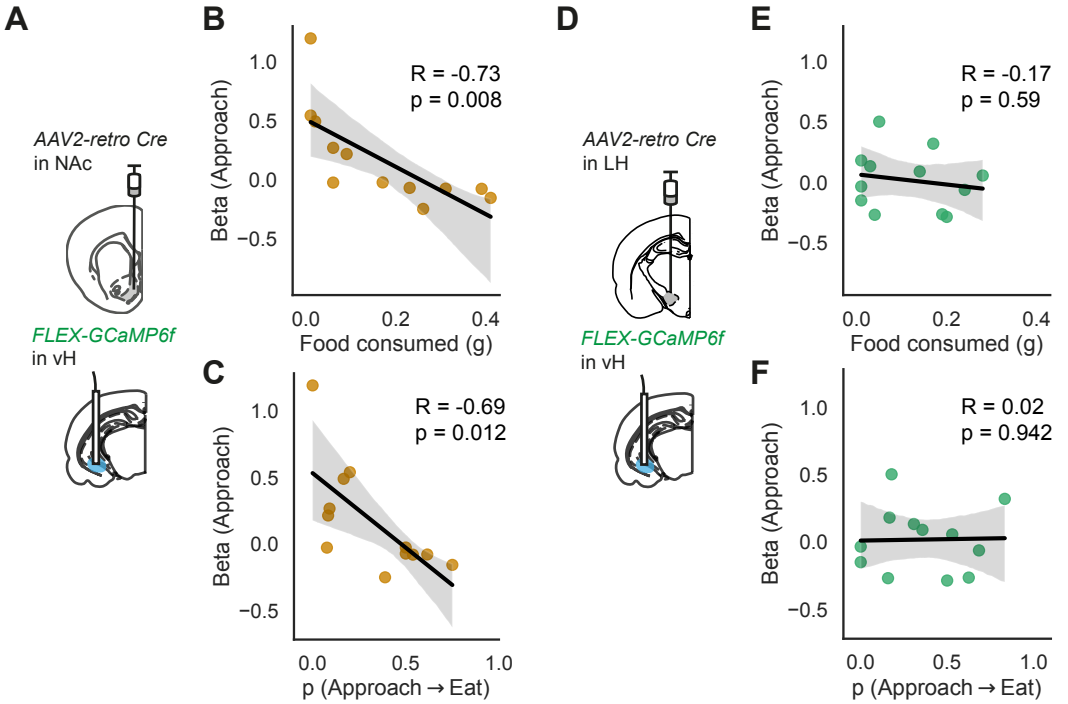

Figure 4.12: Approach-related vS^{NAc} activity correlates with subsequent food consumption. (A) Photometry of vS^{NAc} neurons. (B–C) Linear regression analysis of the β weights for Approach in vS^{NAc} neurons against (B) the amount of chow consumed within the 10 minute presentation session and (C) the transition probability from Approach to Eat. (D–F) as in (A–C) for vS^{LH} neurons. Data represent mean ± sem.

Next, to determine whether the Approach-related vS^{NAc} activity was predictive of food seeking and consummatory behaviour, I explored the relationship between the Approach β weight and both the amount of food that the animal consumed within the 10-minute food presentation and its probability of transitioning from Approach to Eat. This analysis revealed that vS^{NAc} activity during food approach was strongly and inversely correlated with the amount of chow consumption (Pearson correlation between vS^{NAc} β for Approach bouts and amount of chow consumed, Approach, r = -0.73, p = 0.008; **Figure 4.12A–B**). Furthermore, vS^{NAc} activity during Approach was negatively correlated with the transition probability from Approach to Eat (Pearson correlation between vS^{NAc} β for Approach bouts and Approach-Eat transition probability, Approach, r = -0.69, p = 0.012; **Figure 4.12C**). By contrast, no significant correlation existed for the Approach-related β weight with the amount of chow consumed in vS^{LH} activity, indicating that vS^{LH} activity during Approach cannot explain the corresponding changes in consumption (Pearson correlation between vS^{LH} β for Approach bouts and food consumed;

Approach, r = -0.17, p = 0.59; **Figure 4.12D–E**) and Approach-Eat transition probability (Pearson correlation between vS^{LH} β for Approach bouts and Approach-Eat transition probability, Approach, r = 0.02, p = 0.94; **Figure 4.12F**). This observation highlights that vS^{NAc} activity, and not vS^{LH} activity, during food Approach is uniquely coupled to Approach-Eat transitions and subsequent food consumption in a hunger state-dependent manner.

This unique sensitivity of vS^{NAc} population activity to ghrelin during feeding behaviour was initially surprising, given previous findings of vS^{LH} involvement in driving food consumption (Hsu et al., 2015). However, it is well recognised that vS^{NAc} neurons support context-dependent, reward-related behaviour (LeGates et al., 2018; Trouche et al., 2019; Ito et al., 2008). This suggests that the activity of vS^{NAc} neurons may also encode food-related value in a hunger-dependent manner. If vS^{NAc} activity only encoded Approach behaviour irrespective of food value, then Approach-related activity to food items differing in value would be expected to be equivalent; by contrast, if vS^{NAc} activity does encode value, then Approach-related activity would vary depending on the item presented to the animal.

To distinguish between these possibilities, the previous experiment described in **Figure 4.10–4.11** used a behavioural task that involved a sequential presentation of qualitatively distinct items in this order: a non-food object (plastic tube lid), a pellet of chow and a dollop of peanut butter (PB), which acted as a high-calorie and hedonic food item (Chen et al., 2015). This sequential presentation design enabled a comparison of the vS^{NAc} activity during presentation and investigative Approach towards distinct food and non-food items.

First, I examined the activity of vS^{NAc} and vS^{LH} populations to the presentation of the non-food object and PB. In both vS^{NAc} and vS^{LH} neurons, the population activity exhibited a time-locked increase in activity during both non-food object and PB presentations. Notably, vS^{NAc} population activity showed no change in the overall levels of activity following non-food object presentation (AUC from 0 to 30 s, PBS = 21.58 ± 10.46, Ghrelin = 27.46 ± 9.65, t = -0.84, p = 0.44, **Figure 4.13A**), but did exhibit a modest reduction in activity during the PB presentation in the ghrelin compared to PBS condition (AUC from 0 to 30 s, PBS = 35.44 ± 10.67, Ghrelin = 13.01 ± 12.97, t = 5.55, p = 0.003, **Figure 4.13B**). By contrast, vS^{LH} neurons showed a

larger increase in activity with ghrelin injections during presentation of the non-food object compared to PBS injections (AUC from 0 to 30 s, PBS = 5.08 ± 9.25, Ghrelin = 40.98 ± 9.56, t = -4.04, p = 0.01, **Figure 4.13C**), while no change was observed in their activity levels across drug conditions during PB presentations (AUC from 0 to 30 s, PBS = 12.93 ± 12.57, Ghrelin = 30.25 ± 6.31, t = -1.02, p = 0.35, **Figure 4.13D**). These data indicate that the activity dynamics of vS^{NAc} and vS^{LH} neurons is dependent on hunger and the perceived value of the food in a complex manner. More specifically, the data show that ghrelin alters the response of vS^{NAc} population activity to the presentation of a high-value and high-calorie food item (PB) and not to a less-salient, familiar non-food item, while ghrelin elicits a larger vS^{LH} response to less-salient items and not to a high-value food item.

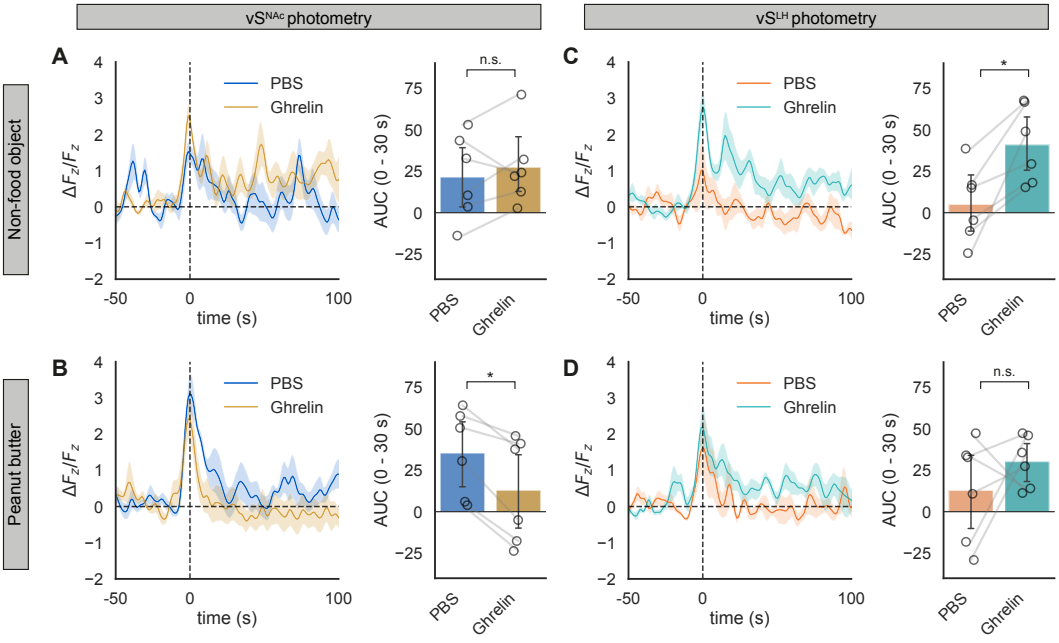

Figure 4.13: vS^{NAc} and vS^{LH} population activity aligned to presentation of a non-food object and peanut butter. (A–B) vS^{NAc} popoulation activity aligned to the time of (A) non-food object (plastic tube lid) and (B) peanut butter presentation. (C-D) as for (A–B) for vS^{LH} photometry. Data represent mean ± sem.

To examine the potential for food-related value coding in the vS^{NAc} and vS^{LH} circuit activity more directly, I next examined the activity aligned to the onset of each Approach bout towards the non-food object and PB. This event-triggered analysis showed that event-triggered increases in population activity was observed in primarily the vS^{NAc} population, while the vS^{LH} population activity remained relatively unchanged during Approach events (**Figure 4.14**).

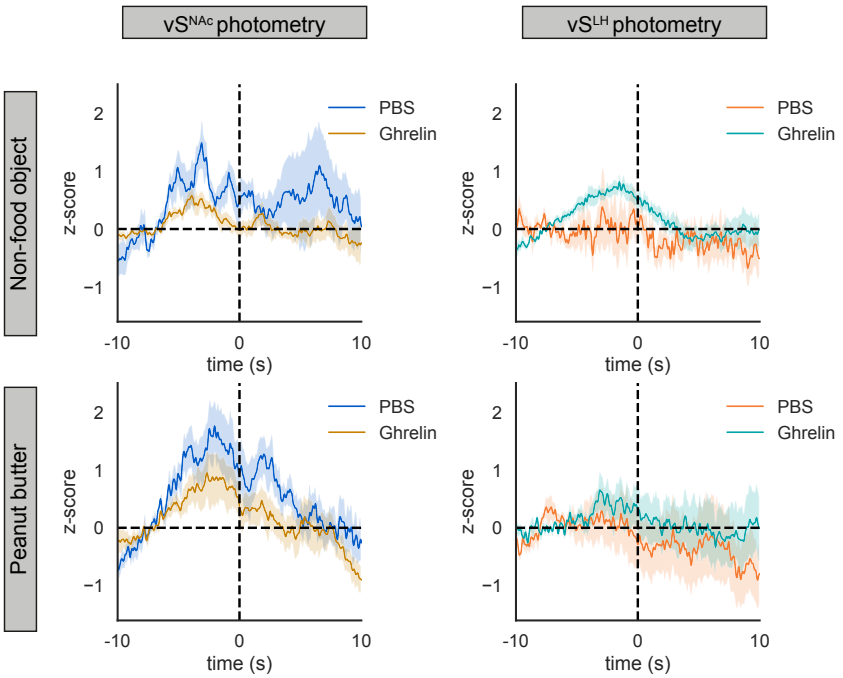

Figure 4.14: vS^{NAc} and vS^{LH} population activity aligned to Approach bouts to a non-food object and peanut butter. (A–B) vS^{NAc} popoulation activity aligned to the time of Approach bouts towards (A) a non-food object (plastic tube lid) and (B) peanut butter. (C-D) as for (A–B) for vS^{LH} photometry. Data represent mean ± sem.

To quantify the magnitude of these signals more accurately, I again used the multiple linear encoding approach to compute the β weights for Approach across food items and hunger state, and compared the Approach β weights during Approach towards the non-food object, chow and PB. Consistent with value-encoding in vS^{NAc} activity, in the sated state (PBS injection), Approach-related vS^{NAc} activity was highest during the presentation of a non-food object, followed by chow and then PB (one-way repeated-measures ANOVA, $F_{2,10} = 13.12$, $p = 0.0016$, $n = 6$ mice; **Figure 4.15A**). This relationship was present only in the sated PBS condition, as ghrelin injection suppressed Approach-related vS^{NAc} activity for all items presented compared to the PBS condition and thus did not encode the type of food or non-food presented (one-way repeated-measures ANOVA, $F_{2,10} = 0.53$, $p = 0.61$). By contrast, vS^{LH} activity did not reliably encode Approach behaviour nor the value of food in both the PBS and Ghrelin conditions (**Figure 4.15B**). Notably, the reduction in vS^{NAc} Approach-related activity cannot be explained by potential photobleaching across the testing session, as a second object presentation after the PB presentation showed a similar β weight for Approach compared to the first object presenta-

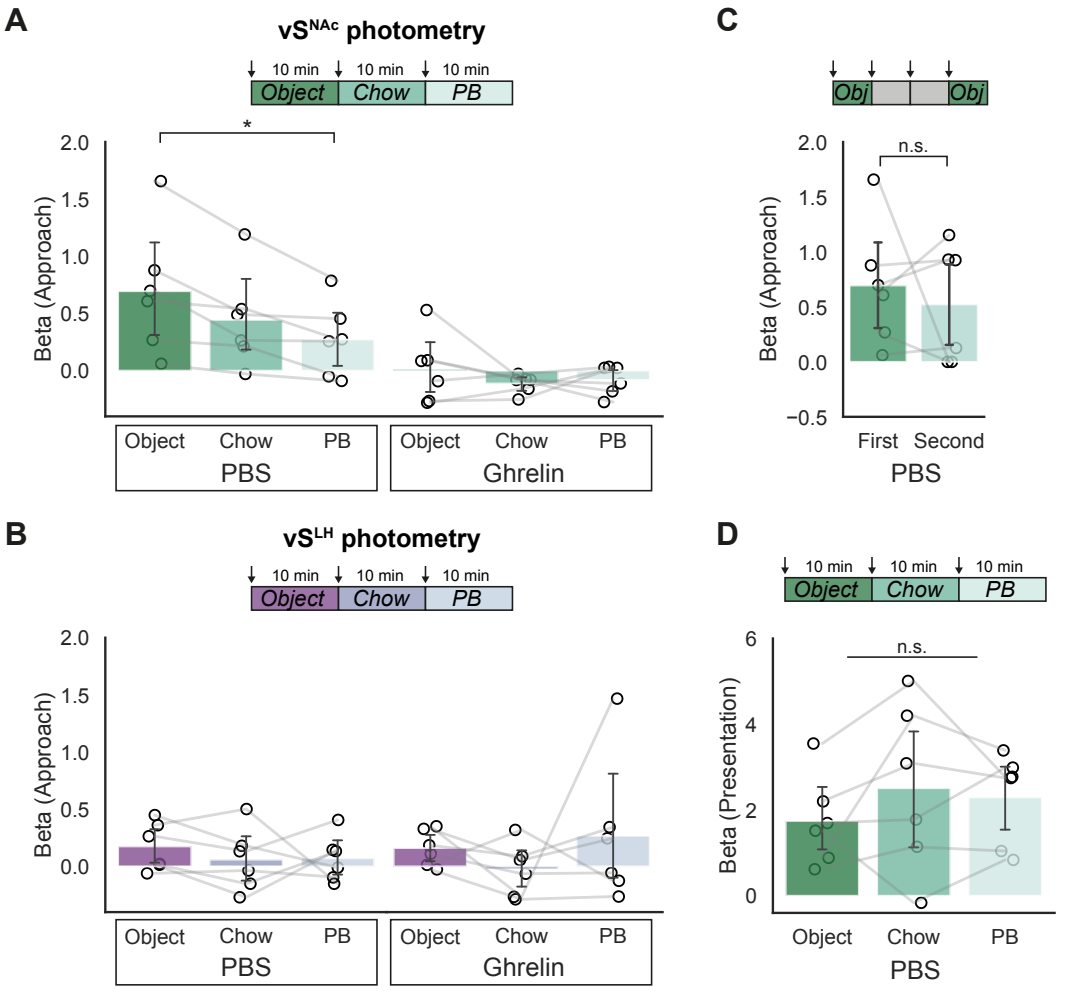

Figure 4.15: vS^{NAc} population activity depends on food identity. (A) The β weights for Approach events towards a non-food Object (plastic tube lid), a pellet of chow and a dollop of peanut butter (PB) in vS^{NAc} recordings. The Approach β weight depends on the food item identity only in the sated PBS condition, and not in the Ghrelin condition. (B) as in (A) for vS^{LH} neural activity. (C) The β weight for Approach during the first and last presentation of the non-food object. (D) The β weight for the salience of presentation across the different items presented. Data represent mean ± sem. *p$<$0.05

tion (Approach β for object, First = 0.69 ± 0.52; Second = 0.23 + 0.22, paired t-test, t = 0.55, p = 0.61; **Figure 4.15C**). Furthermore, the salience of presentation did not decrease with the presentation of each time, making a decrement in the size of the photosignal due to photobleaching unlikely (one-way repeated-measures ANOVA, $F_{2,10}$ = 0.96, p = 0.42, **Figure 4.15D**).

Next, I asked how this encoding of value relates to the amount of food that animals consumed for each food item. In the PBS condition, animals consumed significantly larger amounts of PB compared to chow (amount of food consumed in grams, Chow = 0.03 ± 0.01, PB = 0.21 ± 0.03, paired t-test, t = 5.51, p = 0.0002,

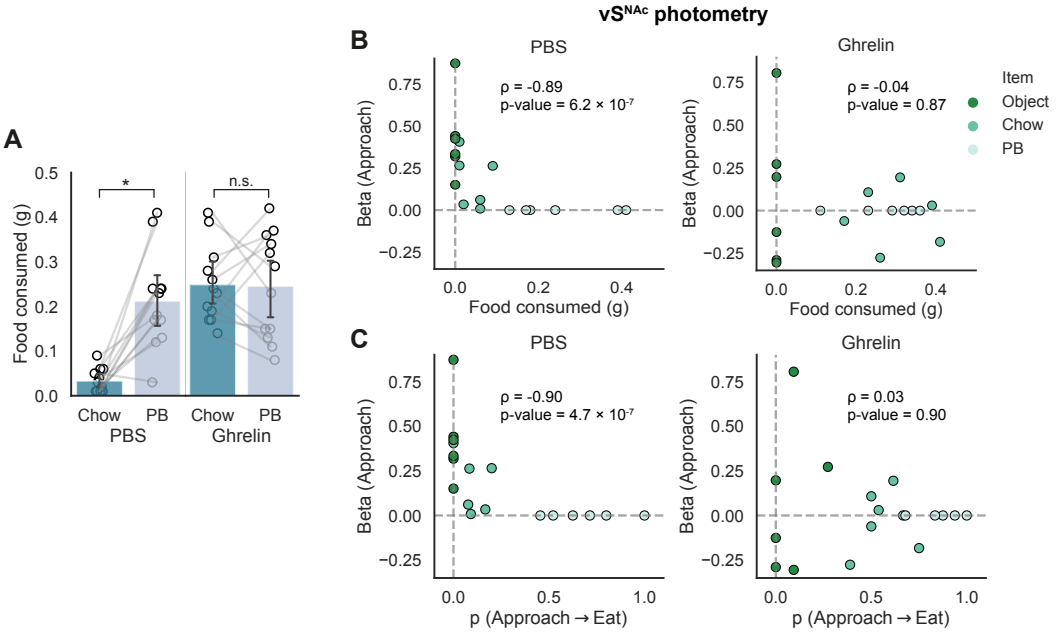

Figure 4.16: vS^{NAc} population activity encodes the value of food. (A) Amount of chow and PB consumed in the PBS and Ghrelin conditions (n = 12 mice in total; 6 vS^{NAc} and 6 vS^{LH} animals). (B) Correlation of the amount of each food type consumed against the β for Approach for the PBS (left) and Ghrelin (right) conditions. Note that the for the PBS and Ghrelin datasets, the PB presentation was considered the baseline by subtracting the β for Approach of all animals to their corresponding Approach β during the PB presentation. Non-food object consumption was set to 0 grams. (C) as for (B), now correlating the transition probability from Approach to Eat against the β for Approach. Data represent mean ± sem.

n = 12 mice), but not in the Ghrelin condition (amount of food consumed in grams, Chow = 0.25 ± 0.02, PB = 0.25 ± 0.03, paired t-test, t = 0.10, p = 0.92, n = 12 mice; **Figure 4.16A**). This difference in the scale of food consumption for the different food items could explain the value coding present in the PBS, but not the ghrelin, condition. Indeed, Approach-related activity in vS^{NAc} neurons reliably encodes the value of food in the sated PBS condition, corresponding to the condition where chow and PB were consumed to different extents (**Figure 4.16A–B**). Furthermore, the β weights for Approach was significantly correlated with the transition probability from Approach to Eat, suggesting a link between vS^{NAc} population activity and the transition dynamics between Approach and Eat behaviour (**Figure 4.16C**). By contrast, the encoding of value was not apparent in the Ghrelin condition, where the ghrelin-associated β weights were related to neither the level of food consumption nor the Approach-Eat transition probability (**Figure 4.16B-C**); this suggests that i.p. injections of ghrelin may reduce Approach-related activity irrespective of food

consumption (see Discussion). Together, these findings suggest that Approach-related activity in vS^{NAc} neurons encode the value of item at the time of investigation in the sated state.

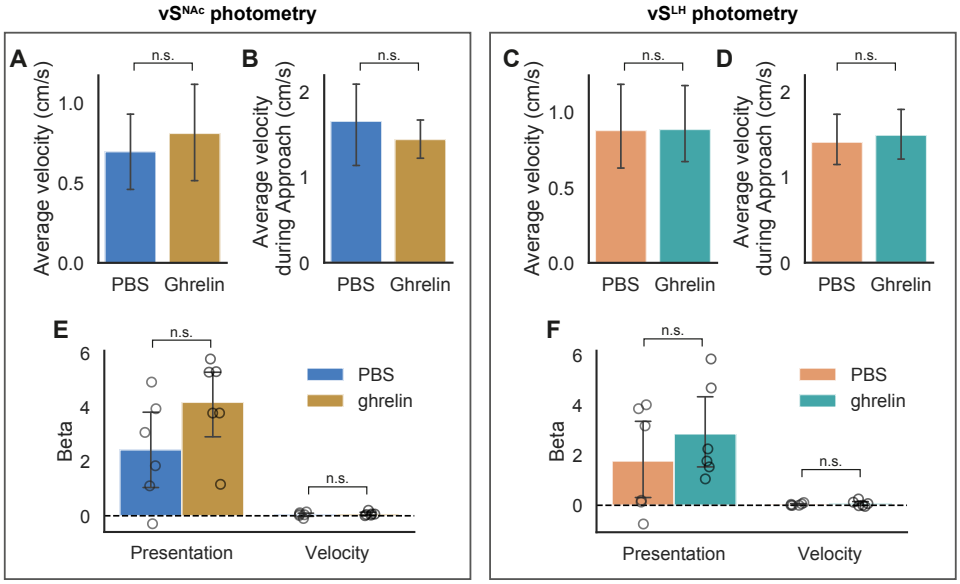

Figure 4.17: Lack of contribution of velocity and salience to vS activity modulation by ghrelin. (A) Average velocity of vS^{NAc} animals within the 10-minute period of chow presentation (n = 6 animals). (B) Average velocity during Approach behaviour for the same animals in (A). (C and D) as in (A) and (B) for vS^{LH} animals (n = 6 animals). (E) β weights for the salience of presentation and velocity for vS^{NAc} animals. (F) as in (E) for vS^{LH} animals. Data represent mean ± sem.

As a set of complementary analyses, I examined whether changes in velocity or the encoding of salience could explain the variation in vS^{NAc} activity during Approach with food value, or the differences between the encoding of behaviour in vS^{NAc} and vS^{LH} activity. Firstly, there was no change in the average velocity of animals across hunger state during the presentation of chow, in both vS^{NAc} and vS^{LH} recordings (average velocity in cm/s, vS^{NAc} animals, PBS = 0.70 ± 0.13, Ghrelin = 0.81 ± 0.16, t = -0.73, p = 0.50; vS^{LH} animals, PBS = 0.88 ± 0.15, Ghrelin = 0.89 ± 0.14, t = -0.05, p = 0.97; **Figure 4.17A,C**). Furthermore, the velocity of animals specifically during food Approach did not change with the hunger state (average velocity during food approach in cm/s, vS^{NAc}, PBS = 1.66 ± 0.27, Ghrelin = 1.45 ± 0.12, t = 0.61, p = 0.57 ;vS^{LH}, PBS = 1.42 ± 0.18, Ghrelin = 1.50 ± 0.16, t = -0.33, p = 0.76; **Figure 4.17B,D**), indicating that changes in movement during food investigation could not explain the differences in the encoding of food approach in vS projections across hunger states. Finally, the encoding of salience or velocity

during chow presentation was not modulated by ghrelin in vS^{NAc} (β weight, Presentation, PBS = 2.44 ± 0.79, Ghrelin = 4.20 ± 0.70, t = -1.88, p = 0.12; Velocity, PBS = 0.04 ± 0.03, Ghrelin = 0.07 ± 0.03, t = -0.85, p = 0.43; **Figure 4.17E**) nor in vS^{LH} neurons (β weight, Presentation, Fed = 1.77 ± 0.87, Fasted = 2.85 ± 0.79, t = -1.49, p = 0.20; Velocity, Fed = 0.03 ± 0.02, Fasted = 0.06 ± 0.05, t = -0.59, p = 0.58; **Figure 4.17F**). Finally, the fibre location of these photometry experiments were confirmed post-hoc to be localised within the vS for both vS^{NAc} (**Figure 4.18**) and vS^{LH} experiments (**Figure 4.19**).

Taken together, the data from fibre photometry of projection-specific vS neurons demonstrate that vS^{NAc}, as opposed to vS^{LH}, activity is uniquely sensitive to ghrelin, where ghrelin reduces the activity of vS^{NAc} neurons during food approach and anticipation of upcoming food consumption; additionally, vS^{NAc} activity during food approach encoded the value of food and was mostly tightly correlated with the amount of food subsequently consumed and the Approach-Eat transition probability.

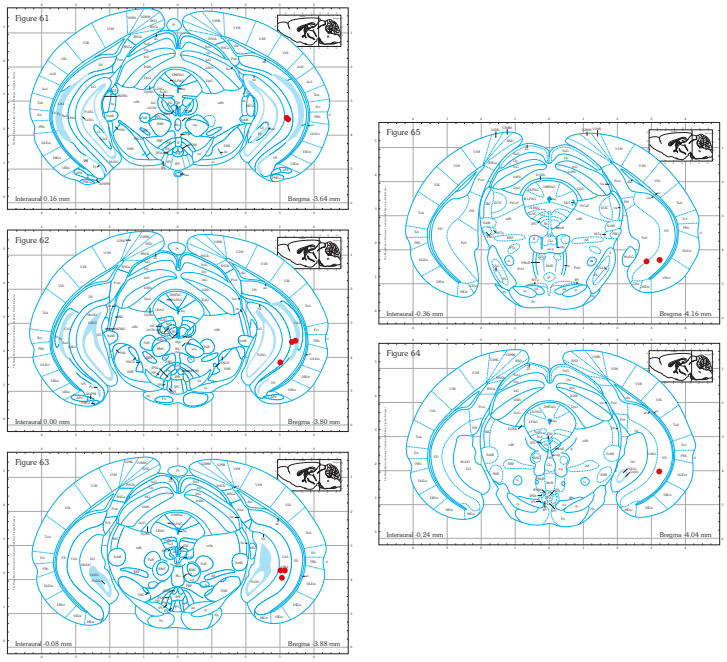

Figure 4.18: Fibre locations for vS^{NAc} photometry experiments.

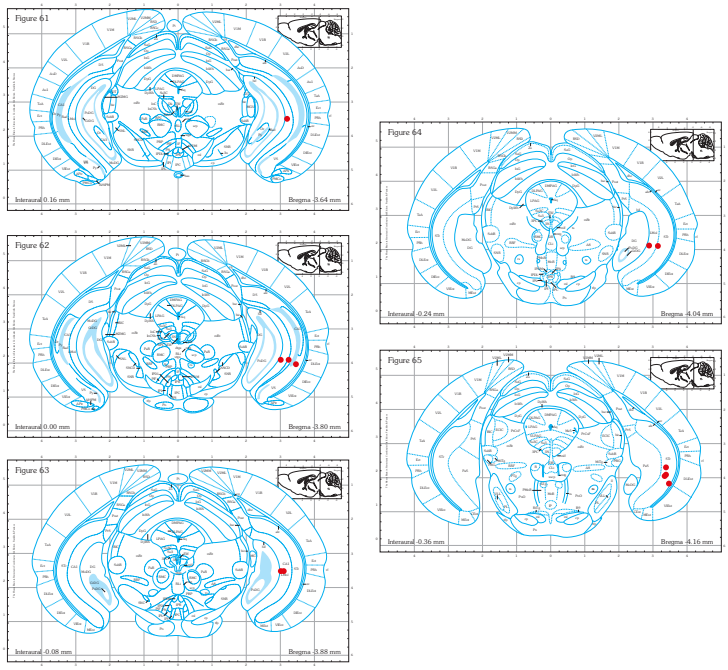

Figure 4.19: Fibre locations for vS^{LH} photometry experiments.

4.2.4 Ventral hippocampal activity signals food expectation in a hunger-state dependent manner

The finding that vS activity is reduced by hunger and is most activated during Approach behaviour is similar to previous reports of anticipatory hippocampal activation during the time preceding a goal (Deadwyler et al., 1996; Hampson et al., 2000; Hampson and Deadwyler, 2003). Furthermore, the fact that vS activity is higher during the Fed state and the well-documented role of the vS in encoding anxiety (Bannerman et al., 2002; Ciocchi et al., 2015; Jimenez et al., 2018) makes it possible that vS may be encoding anxiety in the form of an anxiogenic response to food (hyponeophagia), rather than Approach behaviour. However, if vS was signalling purely anxiety in response to novelty, then vS activity during a well-learned, goal-directed action, such as waiting in anticipation for a reward during a delay period, should be minimal. Therefore, to address this potential confound and to temporally dissociate the anticipation and consummatory phases of feeding behaviour, I trained animals on an operant-based feeding task in which animals learn to press a lever to obtain a liquid food droplet (Ensure strawberry milkshake; **Figure 4.20A**).

In this task, goal-directed effort, read out by the number of lever presses and nose pokes (entries into central port) that the animals made, depended critically on the hunger state. Animals worked harder for food by pressing the lever and nose-poking more during the Fasted state (number of lever presses, Fed = 18.97 ± 3.66; Fasted = 95.07 ± 17.22, paired t-test, t = -4.053, p = 0.007; number of nose pokes, Fed = 173.00 ± 26.49, Fasted = 824.50 ± 124.62, two-tailed paired t-test, t = -5.604, p = 0.001; **Figure 4.20B**). Crucially, animals worked for Ensure even in the Fed state, allowing a comparison of vS activity between the Fed and Fasted states. Consistent with the vS being most engaged during Approach behaviour, the most marked activation of vS occurred during the Cue light phase of the task, i.e. the period immediately preceding actual food consumption (AUC for each event from 0 to 5 s, Lever out, Fed = 2.06 ± 3.33, Fasted = 6.91 ± 20.78, t = 0.239, p = 0.819; Lever press, Fed = 42.99 ± 8.90, Fasted = -0.23 ± 22.65, t = -2.012, p = 0.114; Cue light, Fed = 45.33 ± 8.78, Fasted = 6.25 ± 9.22, t = -4.969, p = 0.012; Nosepoke, Fed = -16.65 ± 13.43, Fasted = -54.70 ± 18.54, t = -2.681, p = 0.06; Food delivery, Fed = -20.11 ± 12.42, Fasted = -58.08 ± 17.95, t = -3.117, p = 0.05; n = 7 mice;

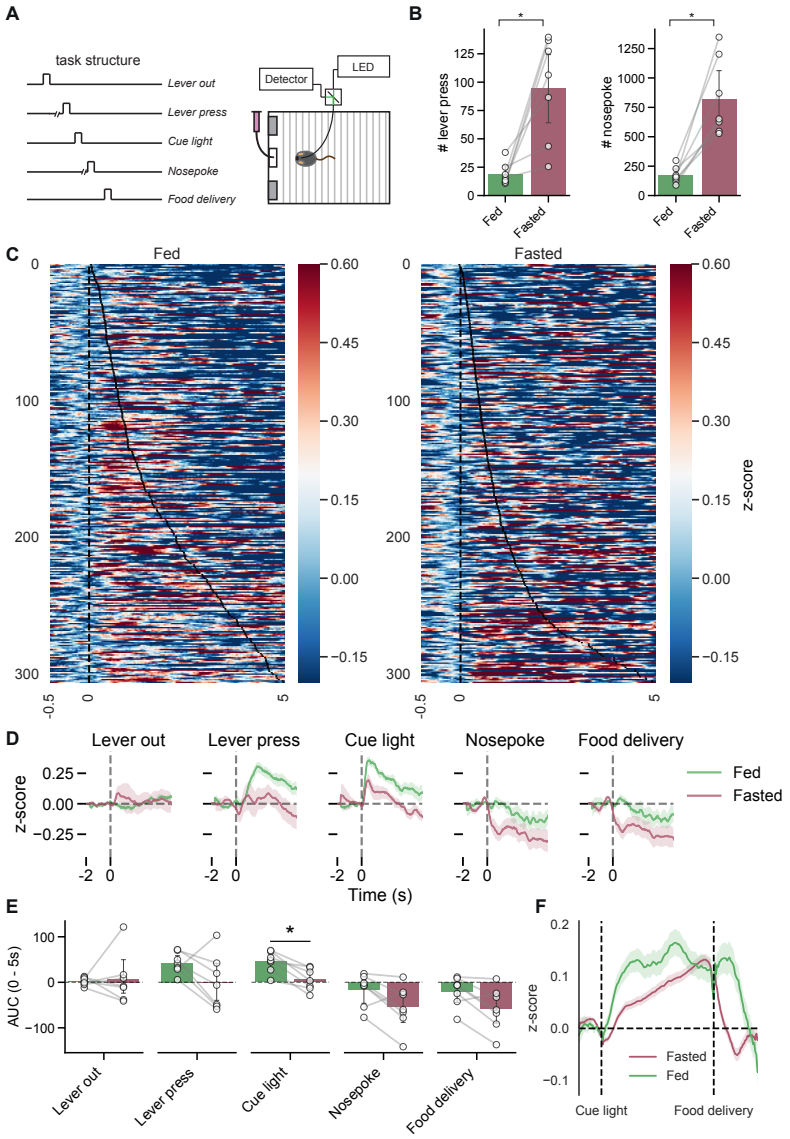

Figure 4.20: Anticipatory vS activity modulated by hunger state. (A) Schematic of operant feeding task. During a trial, a lever is presented (Lever out). Animals then press the lever (Lever press). A Cue Light is illuminated above the central nose port to signal the availability of food, and after a delay following Nosepoke, a drop of liquid food is delivered (Food delivery). Animals then enter the ITI. (B) The number of lever presses and nosepokes are sensitive to the hunger state. (C) Example trials pooled from 7 animals aligned to Cue Light onset and sorted by the latency to food delivery. The heatmap indicates the $\frac{\Delta F_z}{F_z}$ baselined to the period -1 to 0 s. Vertical ticks indicate the time of food delivery. As the Fed state contained fewer trials compared to the Fasted state, Fasted trials were randomly sampled to obtain the same number of trials for qualitative comparison. (D) Event-triggered average of vS activity aligned to the onset of each behavioural event, baselined to the -1 to 0 s time period. (E) AUC between 0 and 5 s for each behavioural event. Only paired t-tests between Cue light remained significant after correction for multiple comparisons using the Benjamini-Hochberg method. (F) The $\frac{\Delta F_z}{F_z}$ signals corresponding to the cue light-to-food delivery intervals were warped to a common interval duration. Data represent mean ± sem.

Figure 4.20C–E). This activation of vS during the anticipatory phase of feeding behaviour is consistent with the vS activation during Approach in the naturalistic feeding task.

To examine the cue light-to-food delivery period in more detail, I analysed the photometry signals during this interval and warped the signals to a fixed interval duration (**Figure 4.20F**). This analysis showed that vS activity began rapidly at the onset of cue light, and steadily ramps to the onset of food delivery (**Figure 4.20F**), albeit at a lower magnitude for the Fasted compared to the Fed state. Immediately following food delivery, the vS activity dipped for the Fasted state, but remained elevated for a longer while before falling for the Fed state. The Fasted condition reduced the overall vS activity during the ramp towards food delivery. Thus, the operant feeding task revealed that the vS activity does not signal food consumption, but rather the anticipatory period preceding it.

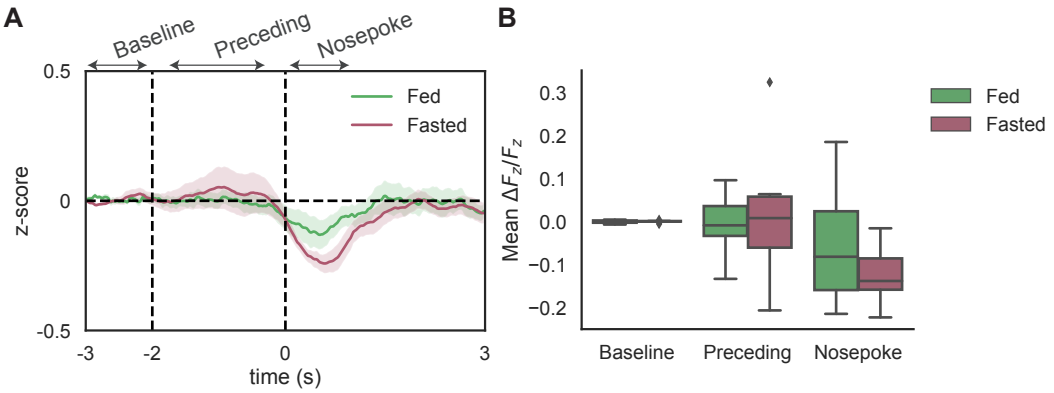

Figure 4.21: Task-unrelated movements during nose port entries cannot explain the anticipatory vS ramping signal. (A) Event-triggered average signal aligned to the moment of nose pokes during the ITI interval. The signal was baselined to the -3 to -2 s period. A small dip in activity occurs during nose poke events. (B) The mean $\Delta F_z/F_z$ during each of the periods outlined in (A). Data represented as mean ± sem, and box plots indicate the median and whiskers 1.5 times the interquartile range.

To confirm that task-independent, movement-related signals did not contribute to the ramping signal in vS, I analysed the stochastic nose port entries that animals made during the inter-trial interval (ITI) period (**Figure 4.21A**). vS activity exhibited a small dip at the onset of nosepokes during the ITI interval, but this was variable and not significantly different across hunger state and ITI period (two-way repeated-measures ANOVA, interaction between period and hunger state, $F_{2,12}$ = 1.23, p = 0.325, n = 7 mice; **Figure 4.21B**). Crucially, however, no ramping signal was ob-

served in the periods preceding the nosepoke, in contrast to the activity preceding nose poke and food delivery during the trials. Thus, the movements that accompany the preceding periods during a nosepoke cannot explain the vS ramping signal during the anticipatory period of food consumption.

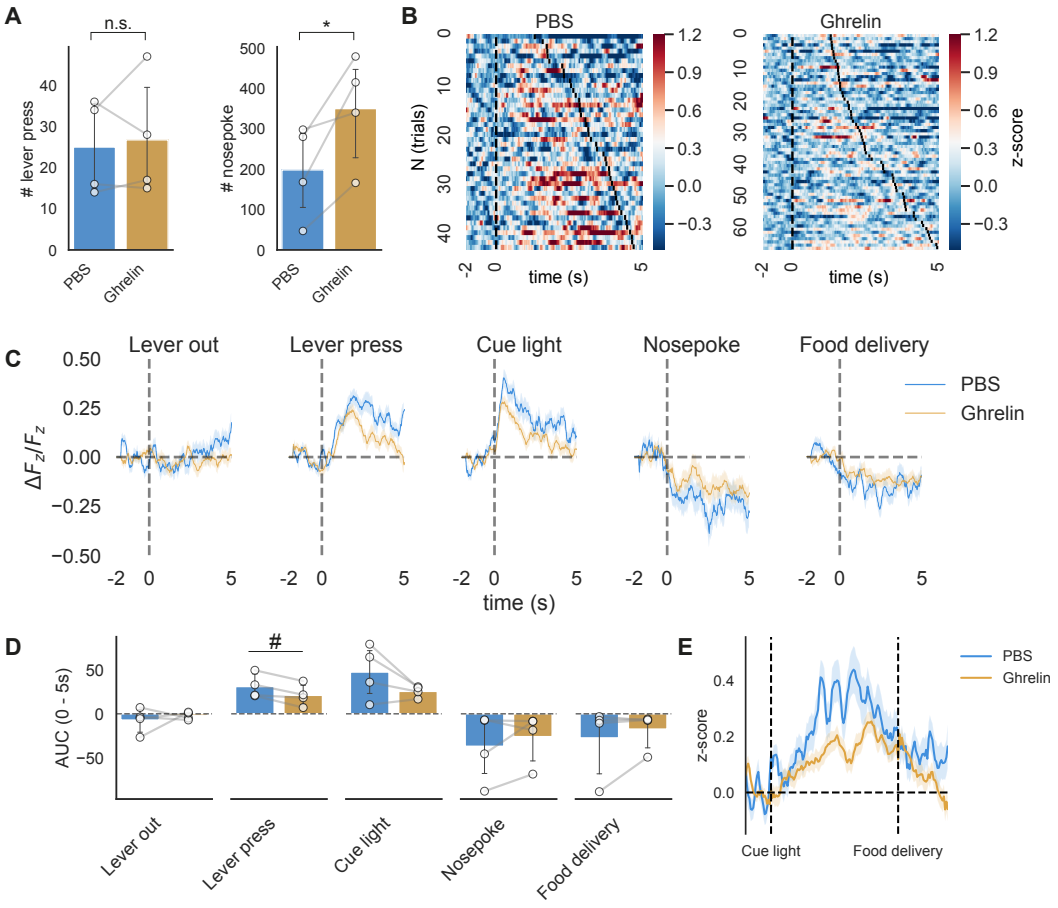

Figure 4.22: Anticipatory vS activity modulation by ghrelin. (A) Measures of effort in goal-directed behaviour, i.e. lever press and nose poke. Ghrelin increases the number of nose pokes and not lever presses. (C) Example trials pooled from 4 animals aligned to cue light onset and sorted by the latency to food delivery. The color map indicates the $\frac{dF_z}{F_z}$ baselined to the period -2 to 0 s before cue light at time 0 s. Vertical ticks after cue light indicate the time of food delivery. (D) Event-triggered average of vS activity aligned to the onset of each behavioural event: Lever out, Lever press, Cue light, Nosepoke and Food delivery. (E) Area under the curve between 0 and 5 s for each behavioural event. Only paired t-tests between Lever press was significant ($\# < 0.05$, uncorrected). (F) Cue light-to-food delivery Ca^{2+} signal where the time period between the events was warped (normalised). Data indicate mean ± sem.

Finally, I asked whether ghrelin inhibits the anticipatory vS signal in the period preceding food delivery. Using the operant feeding task, I observed that animals trained on the operant feeding task expressed goal-directed behaviour (lever press and nose poke) that depended differently on hunger state brought about by ghrelin.

Whereas the total number of nose pokes was increased by ghrelin, the number of lever presses remained unchanged (number of lever presses, PBS = 25.00 ± 5.80, Ghrelin = 26.75 ± 7.33, t = -0.40, p = 0.72; number of nose pokes, PBS = 198.25 ± 58.04, Ghrelin = 350.00 ± 67.59, t = -3.36, p = 0.04; **Figure 4.22A**). In contrast to the Fasted condition, ghrelin had relatively modest effects on vS activity around the lever press and cue light periods (AUC from 0 to 5 s for each event, Lever out, PBS = -7.19 ± 7.09, Ghrelin = -2.26 ± 2.16, t = 0.565, p = 0.612; Lever press, PBS = 31.10 ± 6.80, Ghrelin = 21.09 ± 6.22, t = -4.165, p = 0.025; Cue light, PBS = 47.58 ± 15.32, Ghrelin = 25.61 ± 3.18, t = -1.776, p = 0.174; Nosepoke, PBS = -37.05 ± 19.30, Ghrelin = -26.07 ± 14.41, t = 1.015, p = 0.385; Food delivery, PBS = -27.48 ± 20.46, Ghrelin = -17.46 ± 10.65, t = 1.012, p = 0.386, n = 4 mice, **Figure 4.22B–D**). This effect was more readily apparent when observing the period between the cue light-to-food delivery; vS activity ramps towards the food delivery timepoint, but this ramping signal appeared to be reduced in the Ghrelin state (**Figure 4.22E**).

Overall, the results indicate that vS is signalling food expectation most markedly during lever press and cue light; this signal is modulated by hunger and and ramps towards food delivery in both the Fed and Fasted states. The fact that vS is activated during anticipation of a food reward makes it unlikely that vS encodes a pure anxiety signal; instead, vS appears to signal the anticipation of future choice (during Approach in the naturalistic task) and food consumption (during the delay prior to food delivery in the operant task) in a hunger state-dependent manner.

4.3 Discussion

Using a combination of behavioural analysis and bulk *in vivo* Ca^{2+} imaging the activity of excitatory and projection-specific neuronal populations in vS during free feeding behaviour, here I present data that describe the specific encoding of approach behaviour (in the unrestricted, naturalistic task) and anticipation (in the operant feeding task) by the vS. Further, I show that vS is reduced by hunger (both fasting and ghrelin injections), and that this inhibition is specific to vS^{NAc} as opposed to vS^{LH} neurons.

4.3.1 vS encodes the approach towards food and the anticipation of upcoming food

By recording bulk fluorescence from populations of excitatory vS neurons during free feeding behaviour, I found that vS was most strongly activated during the sated state – i.e. Fed and PBS-injected states. In turn, this activation was focused mostly on the phase of behaviour around Approach, while food consumption during Eat was associated with low vS activity. Due to the unrestrained and stochastic nature of the free-feeding task, I then used a learnt, operant-based feeding task to gain more experimental control over each step of feeding behaviour and to observe vS activity during temporally dissociated windows around behavioural events. Again, I observed that vS activity was driven mostly during the phases preceding food consumption. This finding is important as it demonstrates for the first time that vS activity is specific in its encoding of food investigation, and builds upon similar recent work looking at the contribution of vS to feeding behaviour (Reed et al., 2018; Yoshida et al., 2019; Sweeney and Yang, 2015). In particular, these previous studies examined the activity dynamics of distinct parts of the hippocampal circuit, e.g. ventral CA1 or brain regions downstream of vS. In this study, recordings were targeted to vS, and I observed qualitatively distinct activity dynamics of vS compared to these previous studies, most notably the anticipatory rise in vS activity preceding food intake. Moreover, this vS encoding of the anticipation of food consumption, and not food consumption per se, ties in well with ideas about how the hippocampus provides a predictive representation about future states and its role in value-based decision-making (Stachenfeld et al., 2017; Buckner, 2010; Bakkour et al., 2019; Kay et al., 2020; Voss et al., 2011), rather than the overt consummatory phase of behaviour.

The modulation of vS activity by hunger during the anticipatory phase of behaviour suggests that the vS is integrating hunger-related signals during food anticipation. This sensitivity to changes in the value of reward by motivational state is one facet of hippocampal function that has been known for a while (Kennedy, 2004; Kennedy and Shapiro, 2009), but only recently becoming increasingly studied (Yoshida et al., 2019; Carey et al., 2019). Notably, these previous studies observed motivational state-dependent processing using tasks that required animals

to learn to obtain rewards, e.g. press a lever to obtain food or learn that one path leads to a reward while the other does not. The experiments conducted in this thesis contribute to the idea that the hippocampus is surprisingly also sensitive to hunger in an unlearned, freely feeding behaviour devoid of any task structure and where animals are constantly exposed to food.

Hunger inhibits vS activity during the anticipatory phase of feeding behaviour in both innate and learned behavioural tasks. One speculation is that the hippocampus performs a general computation in both 'innate' and 'learned' feeding tasks, i.e. the sensing of hunger signals to set the occasion that provides value to eating (Holland et al., 1999; Davidson et al., 2014). This may be occurring constantly, regardless of whether or not a task structure is present that necessitates an animal to perform some action to obtain food, or whether to simply choose to eat a food that is already present and available. Furthermore, it is also possible that the detection of hunger signals may be a more general mechanism to support flexible behaviour (Davidson and Jarrard, 1993; Kennedy, 2004; Kennedy and Shapiro, 2009), as has been suggested in previous experiments. Thus, it will be important in future studies to examine mechanistically whether hormonal signals like ghrelin are used in the hippocampus to flexibly guide decision-making behaviour.

Given the rich literature of the role of the vS in mediating anxiety-like and defensive behaviour (Dong et al., 2009; Strange et al., 2014; Maren, 1999; Xu et al., 2016), an alternative account of the findings of these experiments is that the vS activity represents an anxiety signal in response to food presentation, and that the corresponding hyponeophagia (defined as novelty-suppressed feeding, or reduced feeding behaviour in an unfamiliar context or in response to an unfamiliar food item) instead drives the vS activity. In turn, hunger competes with anxiety as a motivational drive, thereby reducing the vS signal.

In contrast to this pure 'anxiety' interpretation, I argue that this is unlikely for the following reasons: (1) the activation of vS activity to food occurs even in a self-paced, operant-based task with a deterministic delivery of food reward upon lever press, (2) vS activity also encodes Rearing, a general exploratory behaviour in response to environmental novelty and not specific to anxiety (Lever et al., 2006), and (3) the food item (a single chow pellet) presented to animal was familiar and

constantly provided in their home cage (except under the Fasted state) and that animals were well habituated to the testing box.

Firstly, the operant feeding task, in addition to providing tight experimental control over observation of vS activity, also acted as an important control for this anxiety interpretation. The signals of anxiety observed in vS (Adhikari et al., 2010; Ciocchi et al., 2015; Jimenez et al., 2018) have mostly been observed in tests such as the elevated plus-maze (EPM) and open field test (OFT), where animals avoid aversive portions of the task, such as the open arms of the EPM and centers of the OFT, that produce the corresponding anxiety signals. By contrast, I observed strong vS activation in a self-paced, appetitive task where animals press the lever to obtain food, in both the hungry and sated states. That vS activation occurs most strongly during Cue Light, a phase of the task that precedes food consumption, makes it more likely that the vS is signalling an upcoming reward, reminiscent of ramping signals observed in the ventral striatum (Howe et al., 2013; Hamid et al., 2016).

Secondly, vS appeared to encode Rearing behaviour, a behavioural marker of information gathering in response to environmental novelty (Lever et al., 2006). Rearing behaviour has been shown to be invariant to anxiolytic drugs, and under states of high anxiety animals do not reliably change the amount of rearing behaviour (Lever et al., 2006). This argues that vS activity is more closely tied to general exploration than anxiety. Lastly, animals were well-habituated to both food item and context, having been habituated to food presentation on three separate days prior to test day. This procedure thus minimises any potential of novelty-induced suppression of behaviour due to anxiety. Together, these reasons challenge the view that vS is encoding purely anxiety in our task.

Instead, I propose that the higher vS activity during the feeding tasks may be related to a putative role of the hippocampus in resolving uncertainty (Bannerman et al., 2012, 2014; Biderman et al., 2020; Grupe and Nitschke, 2013), and in the case of the free-feeding task, the uncertainty surrounding the value of food (Davidson et al., 2014; Gershman, 2017). This uncertainty over the value of food arises from the time-varying value of food as a function of hunger (Davidson et al., 2014); when an animal is hungry, the value of food is high and will lead to a positive postingestive outcome. By contrast, when the animal is sated, the value of food

is low and would lead to a low postingestive outcome. This association of food with multiple outcomes is the source of food-related uncertainty, and could explain why the vS is required in feeding behaviour. Resolving this uncertainty also requires integrating signals about the hunger state in addition to other sensory cues to reach conclusions about the value of food, which is another reason why the vS is known to be sensitive to hunger as motivational state and to use hunger-state related information (Davidson and Jarrard, 1993; Hock and Bunsey, 1998; Benoit and Davidson, 1996; Kanoski et al., 2007; Kennedy and Shapiro, 2009; Carey et al., 2019; Momennejad et al., 2018). This interpretation of vS as being involved in resolving uncertainty can potentially explain how the vS is involved both in anxiety (i.e. the uncertainty about novel, potentially dangerous parts of the environment) and uncertainty about appetitive outcomes, such as the value of food (Davidson et al., 2014).

By honing down on ghrelin as a cellular substrate of hunger, which not only stimulates robust feeding behaviour when acutely administered to rodents and humans (Tschöp et al., 2000; Wren et al., 2001) but also recapitulates the key features of hunger-related feeding behaviour, I found that i.p. injections of ghrelin not only reduced vS activity in the free-feeding task, but also activity during anticipation of the food reward in the operant task. This corresponds well with ideas about the putative functions of ghrelin, which has been increasingly viewed as mediating anticipatory feeding behaviour rather than food consumption itself (Hsu et al., 2016). Studies in which ghrelin signalling is disrupted in rodents, either through knockouts of the GHSR1a receptor, demonstrate that ghrelin signalling is required for the normal anticipatory increase in locomotion preceding a meal, especially in animals entrained to feed within a restricted 4-hour time window (Drazen et al., 2006; Gooley et al., 2006; Blum et al., 2009; Verhagen et al., 2011). These putative roles of ghrelin in influencing anticipatory feeding is also consistent with the role of the hippocampus in prediction and the hunger-state modulation of vS activity described in this chapter. Moreover, the effect of ghrelin on anticipatory behaviour has mostly been examined on an operational timescale of multiple hours. The results presented in this chapter suggest that the effect of ghrelin on vS activity during anticipation – defined in my experiments as the Approach phase in the free-feeding task, or the delay interval

preceding delivery of food reward in the operant feeding task – is fast and occurs acutely within a second-to-second or minute-to-minute timescale, suggesting that the hippocampus may be constantly sampling hunger-related signals.

4.3.2 Circuit-specificity of behavioural encoding in vS

Increasingly, circuit elements in the vS defined by their output projections are proposed to serve distinct functions in emotional and motivated behaviour (Ciocchi et al., 2015; Jimenez et al., 2018; Cembrowski et al., 2018a). In my experiments, I observed a similar dissociation of function in vS^{NAc} and vS^{LH} neurons. By using intersectional methods to restrict expression of calcium indicators to projection-defined vS neurons, I observed that (1) vS^{NAc} neurons reliably encoded Approach behaviour, (2) their activity during Approach was most predictive of the amount of food animals consumed, and (3) their activity also negatively correlated with the Approach-Eat transition probability. This stands in contrast to vS^{LH} neurons, whose activity appeared to be invariant to hunger state and more related to the the immediate sensory detection upon food presentation. This heterogeneity in projection-specific encoding of feeding behaviour could also explain the lack of an effect of ghrelin on overall vS (non-projection-specific) activity during Approach behaviour. Future experiments could employ temporally precise optogenetic manipulation of vS activity during Approach bouts to observe its influence on subsequent food consumption and Approach-Eat transition probability.

In addition to the negative correlation between Approach-related vS^{NAc} activity, food consumption and Approach-Eat transition probability, vS^{NAc} activity during food approach appears to encode the value of food. More specifically, the presentation of qualitatively distinct food items elicited different degrees of vS^{NAc} activation during Approach behaviour in the sated state and correlated with behavioural preference (amount consumed). This finding is in keeping with previous observations of the role of the vS^{NAc} circuit in reward-driven behaviour (LeGates et al., 2018; Ciocchi et al., 2015; Britt et al., 2012), and suggests that vS^{NAc} activity encodes the hedonic properties of food only in the state where hunger-derived value is low. Another interesting observation is that ghrelin indiscriminately reduced vS^{NAc} Approach-related activity to the presentation of all item types, irrespective of behavioural preference. Together, these results suggest the existence of two modes

of operation in vS^{NAc} activity: a 'sensory-driven' and 'hunger-driven' regime of encoding. In other words, reward value derived from both the metabolic state (ghrelin) and hedonic properties of food are jointly encoded in vS^{NAc} activity; however, when sated, the hedonic properties of food dictates the level of vS^{NAc} activity (sensory-driven), but under increasing hunger levels, the response of vS^{NAc} activity becomes progressively dependent on hunger state (hunger-driven). Beyond a certain point, hunger inhibits vS^{NAc} activity in a manner that is independent of food consumption. This framework could potentially explain why the vS^{NAc} activity was reduced by ghrelin even during Approach towards the non-food object. Thus, the data suggest that the vS^{NAc} circuit encodes anticipated value, and ghrelin modulates vS^{NAc} circuit activity in response to the object currently being investigated. In the future, experiments employing behavioural tasks with better experimental control over the value of the same food item would be able to further clarify value encoding in the vS^{NAc} circuit.

Moreover, the reduction in vS^{NAc} activity by ghrelin is consistent with similar studies looking at the activity of vS and its inputs to NAc during consummatory behaviour (Reed et al., 2018; Yoshida et al., 2019). For example, food consumption is associated with reduced vS terminal activity in NAc (Reed et al., 2018). This finding is consistent with our results, although the study by Reed et al. (2018) only investigated Ca^{2+} activity baselined to food port entry and would have thus missed the anticipatory ramp in vS activity. Furthermore, activation of D1-MSNs is known to potently reduce food intake (O'Connor et al., 2015), consistent with our finding of a negative correlation vS^{NAc} activity with food consumption, and the fact that vS^{NAc} appears to specifically project to D1-MSNs (MacAskill et al., 2014; Scudder et al., 2018; Baimel et al., 2019). This circuit motif fits with the data presented in this chapter, where vS^{NAc} activity during Approach is negatively correlated with Approach-Eat transitions and food consumption, and suggests that excitatory vS inputs to D1-MSNs are well-placed to suppress food intake.

By contrast, vS^{LH} activity appeared to be less well-explained by feeding behaviour, where its activity was invariant across each BSS behaviour and hunger state. This was surprising, given the well-established role of the LH in feeding behaviour (Stuber and Wise, 2016; Jennings et al., 2013, 2015) and the reported

roles of ghrelin signalling in vS^{LH} neurons in promoting feeding (Hsu et al., 2015). A previous study found that, in a meal entrainment task, ghrelin signalling potentiated food consumption and this was attributed to direct vS projections to LH (Hsu et al., 2015). However, due to methodological limitations, the study could not exclude the possibility that their behavioural effect of direct cannulation of ghrelin into vS may have occurred through separate vS pathways, for example, through the NAc (O'Connor et al., 2015) or lateral septum (Risold and Swanson, 1996; Carus-Cadavieco et al., 2017), before being conveyed to LH. In my results, I found that it was the vS^{NAc} neurons that were uniquely sensitive to ghrelin, and more tightly encoded features of feeding behaviour, in contrast to vS^{LH} activity. Thus, the observation by Hsu et al. (2015) that ghrelin signalling required an intact LH to produce potentiated feeding in their task could alternatively be explained by the relay of hippocampal signals to the NAc before reaching the LH.

One limitation of these experiments is that the annotation of feeding behaviour was conducted manually. While there has been a rise in open-source software for behavioural pose estimation based on deep learning (Mathis et al., 2018; Berman et al., 2014; Markowitz et al., 2018), the clustering of pose data into defined behavioural modules based on the statistical properties of behavioural poses, such as approach, rest and eat, remains challenging and prone to noisy observations (Berman et al., 2014; Markowitz et al., 2018). To mitigate potential biases in such manual annotation, the scoring of behaviour was conducted blindly and, in a subset of video data, two scorers independently annotated the behaviours to ensure reproducibility. Nevertheless, the development of newer software that will allow robust behavioural classification with higher throughput will provide deeper insights into the micro-architecture of feeding behaviour and its neural correlates.

Another drawback of the present experiments is the inability to resolve single-cell activity with fibre photometry, which limits an understanding of how single-neuron activity changes during the anticipation of food. For instance, the ramping signal observed in the fibre photometry recordings in the operant feeding task could be produced by hippocampal neurons whose activity tiles the time points from action to the food outcome, reminiscent of 'time cells' that have been reported in the hippocampus (MacDonald et al., 2011). Bulk fluorescence imaging is un-

able to dissociate this possibility from other mechanisms of ramping, for example, through ensemble activity in attractor networks (Inagaki et al., 2019; Rolls, 2013). Furthermore, vS projections to NAc are not uniform and target specific cell-types, such as parvalbumin-expressing interneurons, and may represent distinct subpopulations with dissociable functions (Reed et al., 2018; Trouche et al., 2019). Thus, future experiments incorporating single-cell imaging using microendoscopic imaging methods, with more specific intersectional approaches to monitor vS projections to specific NAc cell types, would be able to tease apart these different possibilities.

In conclusion, I found that the vS signals the anticipation of food in a hunger-state dependent manner, and this encoding of food anticipation is specific to subpopulations of vS projecting to NAc. This finding clarifies an important neural mechanism through which the hunger state could be sensed by the hippocampus.

Chapter 5

Cellular and circuit mechanism of hunger sensing in the ventral hippocampus

Following the observation that vS encodes food approach behaviour in a hunger state-dependent manner, in this chapter I provide *in vitro* and *in vivo* evidence for the functional role of ghrelin signalling in ventral hippocampus (vS), using a combination of whole-cell electrophysiology, pharmacology, pharmacogenetics and molecular knockdown together with Ca^{2+}-based fibre photometry. Through a series of experiments, I found that one functional role of ghrelin *in vitro* is to increase inhibitory synaptic transmission onto vS^{NAc} neurons. *In vivo*, impairing ghrelin signalling through molecular knockdown of the ghrelin receptor GHSR1a prevents the ghrelin-mediated inhibition of vS^{NAc} activity during Approach behaviour. Together, this suggests that ghrelin signalling inhibits vS^{NAc} activity during Approach. Lastly, manipulating vS^{NAc} activity *in vivo* bidirectionally modulates the short-term dynamics of investigative approach and eating behaviour without affecting food consumption. These results indicate that ghrelin signalling promotes synaptic inhibition onto vS^{NAc} that may be crucial for the regulation of food-seeking behaviour.

5.1 Introduction

The hippocampus is important in sensing the internal metabolic state, such as hunger and thirst, to guide behaviour (Kennedy and Shapiro, 2009; Carey et al., 2019). One hypothesis of the underlying mechanism of metabolic sensing is the binding of peripherally circulating hormones and ligands to receptors expressed on hippocampal neurons (Lathe, 2001; Harvey, 2013; Kanoski et al., 2013; Diano et al., 2006). The hippocampus expresses a wide array of functional receptors for circulating hormones, such as receptors for hunger- and satiety-related hormones (Harvey, 2013; Lathe, 2001; Lathe et al., 2020). These hormones are capable of inducing structural and functional plasticity (Diano et al., 2006; Ribeiro et al., 2014; Berrout and Isokawa, 2012), suggesting that these receptors are able to modulate circuit function and behaviour.

In particular, the receptor for ghrelin, the growth hormone secretagogue receptor (GHSR1a), is expressed in the ventral hippocampus (vS) (Guan et al., 1997; Zigman et al., 2006; Hsu et al., 2015; Diano et al., 2006). Several studies have shown that ghrelin is capable of passing through the blood-brain barrier (Banks et al., 2002; Rhea et al., 2018), binding to hippocampal neurons (Diano et al., 2006), inducing structural and functional plasticity (Diano et al., 2006; Berrout and Isokawa, 2012; Ribeiro et al., 2014) and altering ongoing behaviour (Hsu et al., 2015; Carlini et al., 2008, 2002). However, while the ability of ghrelin to modulate synaptic plasticity and circuit function has been well-characterised in the hypothalamus (Yang et al., 2011; Zeltser et al., 2012), relatively little is known about how ghrelin affects the function of hippocampal circuits. Across extra-hypothalamic regions, ghrelin signalling is known to modulate excitatory (Diano et al., 2006; Ribeiro et al., 2014) and inhibitory (Cruz et al., 2013) synaptic transmission, suggesting that the mechanism of ghrelin signalling may be region- and cell-type specific. An additional layer of complexity exists in the hippocampus, as pyramidal neurons are made up of heterogeneous and intermingled projections to distinct downstream brain areas (Naber and Witter, 1998; Cembrowski and Spruston, 2019). Thus, one possibility is that ghrelin signalling might be specific to a certain subpopulation of projection neurons. This has been suggested in recent work investigating vS projections to hypothalamus (Hsu et al., 2015), as well as the findings of the previous chapter showing the

unique sensitivity of ghrelin in vS^{NAc} projections. However, *in vitro* evidence for a projection-specific effect of ghrelin on hippocampal circuit function is lacking.

In addition to its metabolic actions, ghrelin signalling also contributes to a variety of different functions, including hippocampal-dependent learning and memory (Diano et al., 2006; Tian et al., 2019), approach-avoidance behaviour (Carlini et al., 2002, 2004, 2008) and motivated feeding (Kanoski et al., 2013; Hsu et al., 2015; Suarez et al., 2019, 2020). In particular, studies using GHSR1a-null mice show that animals are impaired in anticipating upcoming meals (Drazen et al., 2006; Gooley et al., 2006; Verhagen et al., 2011). While these studies provide insights into the role of ghrelin signalling in hippocampus, their scope was limited owing to their main use of perturbation techniques, such as genetic knockout or pharmacological manipulation of ghrelin signalling, without neural activity recording; this limits the ability to relate how ghrelin signalling may be involved in shaping hippocampal activity *in vivo* during free behaviour.

Therefore, in this Chapter, I sought to address three main questions: (1) how does ghrelin signalling alter synaptic transmission in vS circuits; (2) what is the role of ghrelin signalling in shaping hippocampal neural activity during behaviour? and (3) how does manipulating vS activity alter feeding behaviour? To answer these questions, I used a combination of complementary techniques, including *in vitro* whole-cell electrophysiology, molecular knockdown with fibre photometry and pharmacogenetics to reveal the underlying *in vitro* and *in vivo* mechanisms of ghrelin sensing within vS.

5.2 Results

5.2.1 Ghrelin incubation *in vitro* does not change synaptic transmission and intrinsic neuronal properties

The ventral subiculum (vS) is comprised of heterogeneous projection populations that contribute distinctly to behaviour (Naber and Witter, 1998; Ciocchi et al., 2015; Jimenez et al., 2018). In the previous chapter, I showed that ghrelin selectively reduced the activity of the projection from vS to nucleus accumbens (vS^{NAc}), as opposed to lateral hypothalamus (vS^{LH}) during food approach. To identify a mechanism that could explain the reduction in the *in vivo* activity of vS^{NAc} neurons, I asked

whether ghrelin could mediate this effect *in vitro* through a synaptic mechanism. More specifically, a recent study identified that increased inhibition onto ventral CA1 neurons was required to produce goal-directed, feeding behaviour (Yoshida et al., 2019). Therefore, I first focused on studying inhibitory synaptic transmission by conducting *in vitro* whole-cell recordings of miniature inhibitory postsynaptic currents (mIPSCs) in vS^{NAc} and vS^{LH} neurons after acute incubation in different concentrations of ghrelin.

In this experiment, I first stereotaxically injected green and red retrobeads in a counterbalanced order into either NAc or LH (**Figure 5.1A**) to retrogradely label vS^{NAc} or vS^{LH} neurons. This fluorescent tag enabled visually-guided patch clamp recordings of projection-specific vS neurons in the same slice. Two weeks later, animals were perfused with sucrose solution, and slices from the same animal were alternately incubated in either control, 10 nM or 100 nM ghrelin (Shi et al., 2013) for 30 minutes prior to recording. For these mIPSC recording experiments, the bath contained artificial cerebrospinal fluid (aCSF) with tetrodotoxin (TTX; 1 mM), 2-amino-5-phosphonopentanoic acid (APV; 10 µM) and 6-Nitro-2,3-dioxo-1,2,3,4-tetrahydrobenzo[f]quinoxaline-7-sulfonamide (NBQX; 10 µM). These drugs served to block action potentials and excitatory glutamatergic transmission, thereby isolating inhibitory transmission. Further, a high Cl^- internal solution was used to shift the reversal potential of Cl^- to $\sim$0 mV, thereby allowing the recording of mIPSCs as inward currents at the resting membrane potential of -70 mV and minimising space-clamp issues (especially in large hippocampal pyramidal neurons).

Using this method, I found that there was no change in the amplitudes of mIPSCs of vS^{NAc} neurons in response to different concentrations of ghrelin (mIPSC amplitudes in pA; PBS = -29.40 ± 1.68; 10 nM ghrelin = -34.01 ± 2.53; 100 nM ghrelin = -30.20 ± 1.99; one-way ANOVA, $F_{2,29}$ = 1.44, p = 0.25, n = 12 cells in PBS, 11 cells in 10 nM ghrelin, 9 cells in 100 nM ghrelin; **Figure 5.1B, D**). There was also no change in the frequency mIPSC events across different concentrations of ghrelin, despite the increasing trend of mIPSC frequency at higher ghrelin levels (mIPSC frequency in Hz, PBS = 1.52 ± 0.11; Ghrelin 10 nM = 1.70 ± 0.07; Ghrelin 100 nM = 1.82 ± 0.05; one-way ANOVA, $F_{2,\ 29}$ = 2.97, p = 0.07, n = 12 cells in PBS, 11 cells in 10 nM ghrelin, 9 cells in 100 nM ghrelin; **Figure 5.1D**). Similar to vS^{NAc}

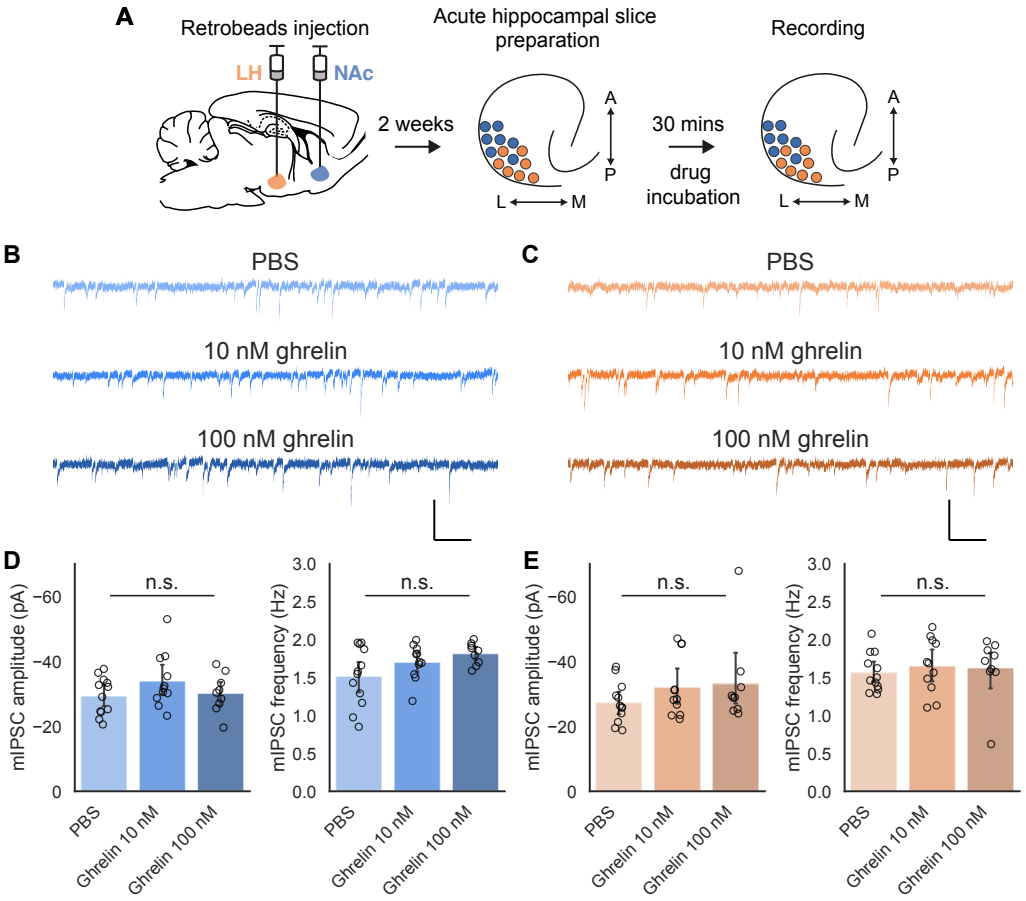

Figure 5.1: mIPSC recordings in vS projections after slice incubation with ghrelin. (A) Retrobeads were stereotaxically injected into either NAc or LH. After 2 weeks post-surgery, animals were perfused and horizontal sections of vS were prepared for whole-cell recording. Prior to recordings, each slice was incubated in aCSF in the bath containing either control (PBS), 10 nM or 100 nM ghrelin. A: anterior, P: posterior, M: medial, L: lateral. (B) Example traces of mIPSC recordings in vS^{NAc} neurons. (C) as in B for vS^{LH} neurons. Scale bar for (B) and (C): 500 ms (x-axis), 40 pA (y-axis). (D) mIPSC amplitudes (Left) and frequency (Right) of vS^{NAc} neurons in the different drug conditions (n = 12 cells in PBS, n = 11 cells in 10 nM ghrelin, n = 9 cells in 100 nM ghrelin, each from 3 animals). (E) as in B for vS^{LH} neurons (n = 12 cells in PBS, n = 11 cells in 10 nM ghrelin, n = 9 cells in 100 nM ghrelin, each from 3 animals). Data represent mean ± sem.

neurons, no change in either mIPSC amplitude or frequency was observed for vS^{LH} neurons (mIPSC amplitude, PBS = -27.30 ± 1.82, 10 nM ghrelin = -32.05 ± 2.84, 100 nM ghrelin = -33.12 ± 4.54, $F_{2, 29}$ = 1.088, p = 0.350; mIPSC frequency, PBS = 1.56 ± 0.07, 10 nM ghrelin = 1.65 ± 0.11, 100 nM ghrelin = 1.63 ± 0.14, $F_{2, 29}$ = 0.218, p = 0.806, n = 12 cells in PBS, 11 cells in 10 nM ghrelin, 9 cells in 100 nM ghrelin; **Figure 5.1C, E**). Therefore, direct application of ghrelin onto vS slices is insufficient to alter inhibitory synaptic transmission.

Next, I asked whether incubation with ghrelin modulated excitatory synaptic

transmission (i.e. in the absence of APV and NBQX). Because miniature excitatory synaptic currents (mEPSCs) were technically challenging to record in the vS owing to the low mEPSC event rate (∼0.1 Hz, data not shown, see Discussion), I used instead electrical stimulation of axons in the Schaffer collateral (SC) to evoke excitatory synaptic inputs (**Figure 5.2A**). One reason I focused on the SC pathway was the existing reports of the influence of ghrelin on the plasticity of the SC input to CA1 neurons (Ribeiro et al., 2014). In these experiments, I switched to a potassium gluconate-based internal solution to record in current clamp mode, thus enabling the simultaneous assessment of excitatory postsynaptic potentials (EPSPs) before and after 100 mM ghrelin incubation, as well as changes in the intrinsic properties of neurons after exposure to ghrelin.

In these experiments, a stimulus electrode was placed in the stratum radiatum layer between CA3 and CA1 (**Figure 5.2A**), and the amount of current was adjusted to achieve an evoked EPSP of 3 to 5 mV in the recorded neuron. The SC was stimulated at 0.1 Hz for 30 minutes, and 100 nM ghrelin was applied to the bath after obtaining a 5-minute stable baseline. Although there was a trend in vS^{NAc} neurons of increasing EPSP amplitude following ghrelin incubation, this was not statistically different from the control condition (percentage change of the EPSP amplitude in the last 5 minutes of recording compared to the first 5 minutes, Ghrelin = 18.17 ± 15.76%; PBS = -8.33 ± 21.95%, Mann-Whitney test, U = 46.0, p = 0.159, n = 18 cells in Ghrelin, n = 7 cells in PBS; **Figure 5.2B–D**). This was also the case for EPSP recordings in vS^{LH} neurons, where no change in EPSP was detected (Ghrelin = 0.48 ± 7.43, PBS = 8.79 ± 18.85, Mann-Whitney test, U = 14.0, p = 0.288, n = 6 cells in Ghrelin, n = 6 cells in PBS; **Figure 5.2E–G**). Therefore, at least with SC-driven excitatory synaptic inputs, ghrelin does not modulate the level of synaptic excitation in vS^{NAc} and vS^{LH} neurons.

In this SC excitation experiment, current steps were also applied before and after drug incubation to examine if ghrelin influenced the intrinsic properties of neurons. First, I examined if neuronal excitability was influenced by ghrelin (**Figure 5.3A–D**). To quantify this, I examined the number of action potentials as a function of injected current (i.e. the input-output curve). Incubating the slices in 100 nM ghrelin did not appreciably shift the input-output curve in vS^{NAc} neurons (two-way

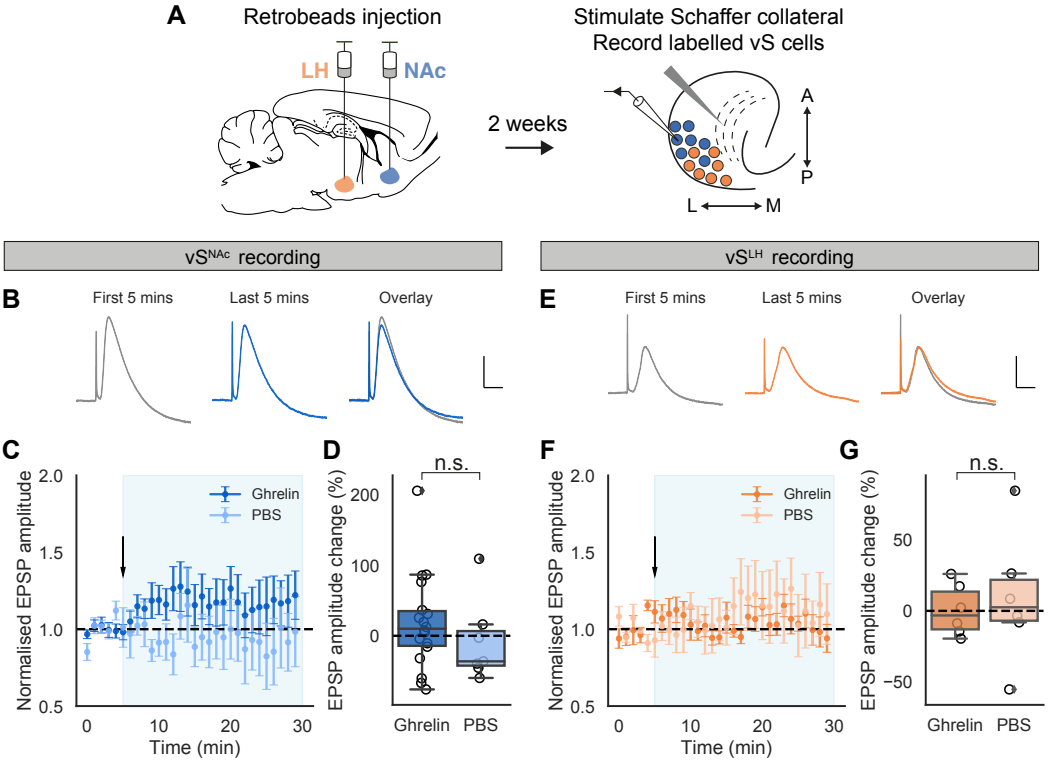

Figure 5.2: Synaptic excitation from CA3 is not modulated by ghrelin incubation. (A) Protocol of stereotaxic surgery, where green and red retrobeads were injected into NAc or LH (counterbalanced). Two weeks later, hippocampal slices were prepared and whole-cell recordings were made from vS^{NAc} or vS^{LH} during ghrelin wash-ins while stimulating the Schaffer collateral (SC) at a rate of 0.1 Hz. (B) Example traces of EPSPs evoked by SC stimulation in vS^{NAc} neurons. The EPSP traces are averages of responses from the first 5 minutes (left) or last 5 minutes (right). Scale bar: 20 ms (x-axis), 1.5 mV (y-axis). (C) EPSP amplitude normalised to the 5-minute baseline period before ghrelin wash-in (arrow). Normalised EPSP amplitudes were averaged in 1-min bins. (D) Change in EPSP amplitude in the last 5 mins of recording relative to the first 5 mins (n = 18 cells in Ghrelin, n = 7 cells in PBS). (E–G) as in (B–D) for vS^{LH} neurons (n = 6 cells in Ghrelin, n = 6 cells in PBS). Error bars represent mean ± sem. Box plots represent median and whiskers represent 1.5 times the interquartile range.

repeated-measures ANOVA, interaction between injected current and incubation, $F_{16,80} = 0.980$, $p = 0.368$, n = 5 cells and 4 cells for the ghrelin and PBS conditions, respectively; **Figure 5.3A–B**) as well as vS^{LH} neurons (interaction, $F_{16,64} = 3.241$, $p = 0.108$, n = 5 cells and 4 cells for the ghrelin and PBS conditions, respectively; **Figure 5.3C–D**). No change in the number of spikes was detected in the control conditions for both vS^{NAc} (interaction, $F_{16,80} = 1.789$, $p = 0.269$) and vS^{LH} neurons (interaction, $F_{16,48} = 0.460$, $p = 0.628$). Therefore, acute exposure of vS^{NAc} and vS^{LH} neurons *in vitro* to ghrelin did not change their excitability. Finally, I examined whether ghrelin changed the input resistance of the recorded vS^{NAc} and vS^{LH}

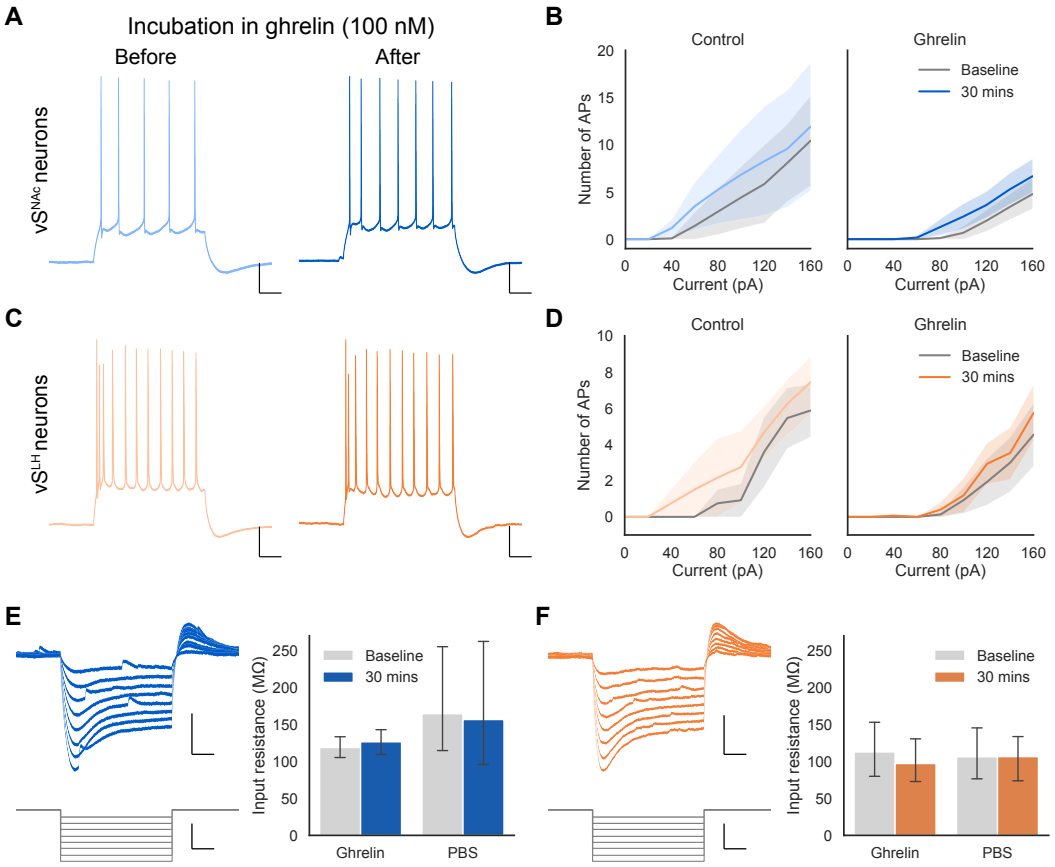

Figure 5.3: Intrinsic properties of vS neurons are not modulated by ghrelin incubation. (A and C) Example spiking profile of vS^{NAc} (A) and vS^{LH} (C) neurons in response to a +160 pA current injection. vS^{NAc} neurons are predominantly regular-spiking, whereas vS^{LH} are mostly burst firing. (B and D) Current input-spike output curves for (B) vS^{NAc} (ghrelin wash-ins, n = 6 cells from 5 animals; PBS wash-ins, n = 4 cells from 4 animals) and (D) vS^{LH} neurons (ghrelin wash-ins, n = 5 cells from 3 animals; PBS wash-ins, n = 4 cells from 3 animals), demonstrating the number of action potentials as a function of injected current. (E) *Left*: Example voltage responses of vS^{NAc} neurons in response to negative current injections (from -160 to -20 pA). Scale bar (top): 100 ms (x-axis), 10 mV (y-axis). Scale bar (bottom): 100 ms (x-axis), 80 pA (y-axis). *Right*: input resistance of vS^{NAc} neurons at baseline (before drug wash-in) and 30 mins after drug wash-in (ghrelin wash-ins, n = 6 cells from 5 animals; PBS wash-ins = 4 cells from 4 animals). (F) as in (E) for vS^{LH} neurons (ghrelin wash-ins, n = 5 cells from 3 animals; PBS wash-ins, n = 4 cells from 3 animals). Data presented as mean ± sem.

neurons before and after ghrelin incubation (**Figure 5.3E–F**). I found no change in input resistance in either vS^{NAc} neurons (input resistance in MΩ, ghrelin incubation, 30 mins = 126.57 ± 8.91, Baseline = 118.87 ± 7.90; PBS incubation, 30 mins = 156.69 ± 53.38, Baseline = 164.62 ± 45.44, interaction between drug and incubation period, $F_{1,8}$ = 3.720, p = 0.089, n = 6 cells and 4 cells for the ghrelin and PBS conditions, respectively; **Figure 5.3E**) or vS^{LH} neurons (input resistance

in MΩ, ghrelin incubation, 30 mins = 97.19 ± 17.02, Baseline = 112.85 ± 20.88; PBS incubation, 30 mins = 106.51 ± 16.32, Baseline = 106.36 ± 19.34; interaction between drug and incubation period, $F_{1,8}$ = 2.821, p = 0.137, n = 5 cells and 4 cells for the ghrelin and PBS conditions, respectively; **Figure 5.3F**).

Taken together, these data indicate that ghrelin incubation alone is insufficient to change the levels of synaptic inhibition (in the form of mIPSCs), excitation (in the Schaffer collateral pathway) and the intrinsic properties such as neuronal excitability and membrane input resistance in vS^{NAc} and vS^{LH} neurons.

5.2.2 Ghrelin enhances inhibitory synaptic transmission in a cell-type specific manner

The data from the ghrelin incubation experiments suggest that ghrelin signalling alone is insufficient to change synaptic transmission in vS. However, these ghrelin incubation experiments differed from the results observed *in vivo*, where exogenous ghrelin delivered via i.p. injection in animals led to changes in vS activity during behaviour.

Thus, to more faithfully mimic the *in vivo*-like conditions that produced the changes in vS circuit activity, I manipulated the hunger state of animals by giving them i.p. injections of ghrelin *in vivo* before perfusion and acute slice preparation for electrophysiological recording. Specifically, two weeks after surgery, during the early light cycle (9 am), animals were given an i.p. injection of 2 mg/kg ghrelin or vehicle control to manipulate their hunger state and perfused 30 minutes later. Hippocampal slices with retrogradely labelled vS^{NAc} and vS^{LH} neurons were then prepared to record mIPSCs from projection-specific vS neurons in the same slice using a high Cl^- internal solution (**Figure 5.4A**).

Strikingly, I observed that the amplitudes of mIPSCs in vS^{NAc} were higher in ghrelin-injected animals compared to PBS-injected animals (mIPSC amplitudes of vS^{NAc} neurons in pA, injections with ghrelin = -21.02 ± 2.36; Injections with PBS = -11.81 ± 1.48, two-tailed unpaired t-test, t = -3.00, p = 0.004, n = 37 cells for Ghrelin, n = 26 cells for PBS; **Figure 5.4B, D–E**). Concomitantly, there was no change in mIPSC frequency (mIPSC frequency of vS^{NAc} neurons in Hz, injections with ghrelin = 1.22 ± 0.05; injections with PBS = 1.17 ± 0.07; two-tailed unpaired t-test, t = 0.61, p = 0.547, n = 37 cells for Ghrelin, n = 26 cells for PBS; **Figure 5.4B, F–G**).

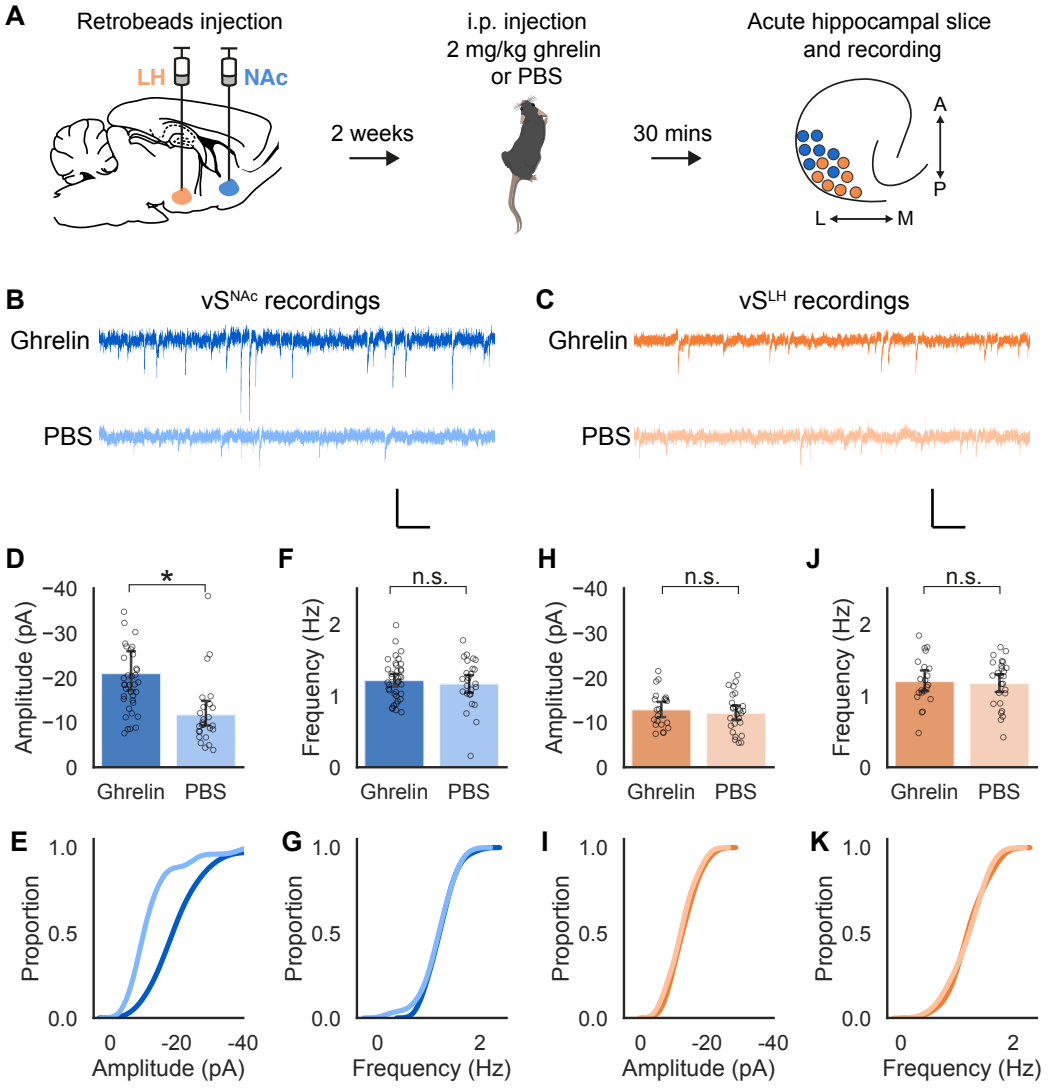

Figure 5.4: High *in vivo* ghrelin selectively increases synaptic inhibition onto vS^{NAc} neurons. (A) Retrobeads were stereotaxically injected into either NAc or LH. After 2 weeks post-surgery, animals wer given an i.p. injection of either 2 mg/kg ghrelin or PBS control 30 minutes before perfusion and slicing. (B and C) Example traces of mIPSCs after injecting animals with either ghrelin or PBS in vS^{NAc} (B) or vS^{LH} (C) neurons. Scale bar: 500 ms (x-axis), 30 pA (y-axis). (D and E) mIPSc amplitudes of vS^{NAc} neurons (ghrelin-injected, n = 37 cells from 5 animals; PBS-injected, n = 26 cells from 3 animals, two-tailed unpaired t-test, t = -3.00, p = 0.004) expressed as a bar plot (D) and a cumulative proportion. (F and G) vS^{NAc} neuron mIPSC frequency (two-tailed unpaired t-test, t = 0.61, p = 0.547) as a bar plot in (F) and cumulative proportion in (G). (H and I) mIPSC amplitudes as in (D and E) for vS^{LH} neurons (ghrelin-injected = 21 cells from 3 animals, PBS-injected = 26 cells from 3 animals, two-tailed unpaired t-test, t = -0.62, p = 0.539). (J and K) mIPSC frequency as in (F and G) for vS^{LH} neurons (two-tailed unpaired t-test, t = 0.28, p = 0.782). Error bars represent mean ± sem. Illustration downloaded from SciDraw.

This effect of ghrelin was absent in vS^{LH} neurons, where neither the amplitude nor frequency of mIPSCs was altered by ghrelin (mIPSC amplitudes of vS^{LH} neurons in pA, injections with ghrelin = -12.92 ± 0.90; injections with PBS = -12.15 ± 0.84;

two-tailed unpaired t-test, t = -0.62, p = 0.54,; mIPSC frequency in Hz, mIPSC frequency in Hz, injections with ghrelin = 1.20 ± 0.07; injections with PBS = 1.18 ± 0.06; two-tailed unpaired t-test, t = 0.28, p = 0.782, n = 21 cells for Ghrelin, n = 26 cells for PBS; **Figure 5.4C, H–K**). Thus, by systemically increasing ghrelin levels in the periphery, which thus mimicked the *in vivo* conditions in which I observed a ghrelin-mediated reduction in vS^{NAc} activity, I found that peripheral ghrelin is sufficient to selectively increase inhibitory synaptic transmission onto vS^{NAc}, but not vS^{LH}, neurons.

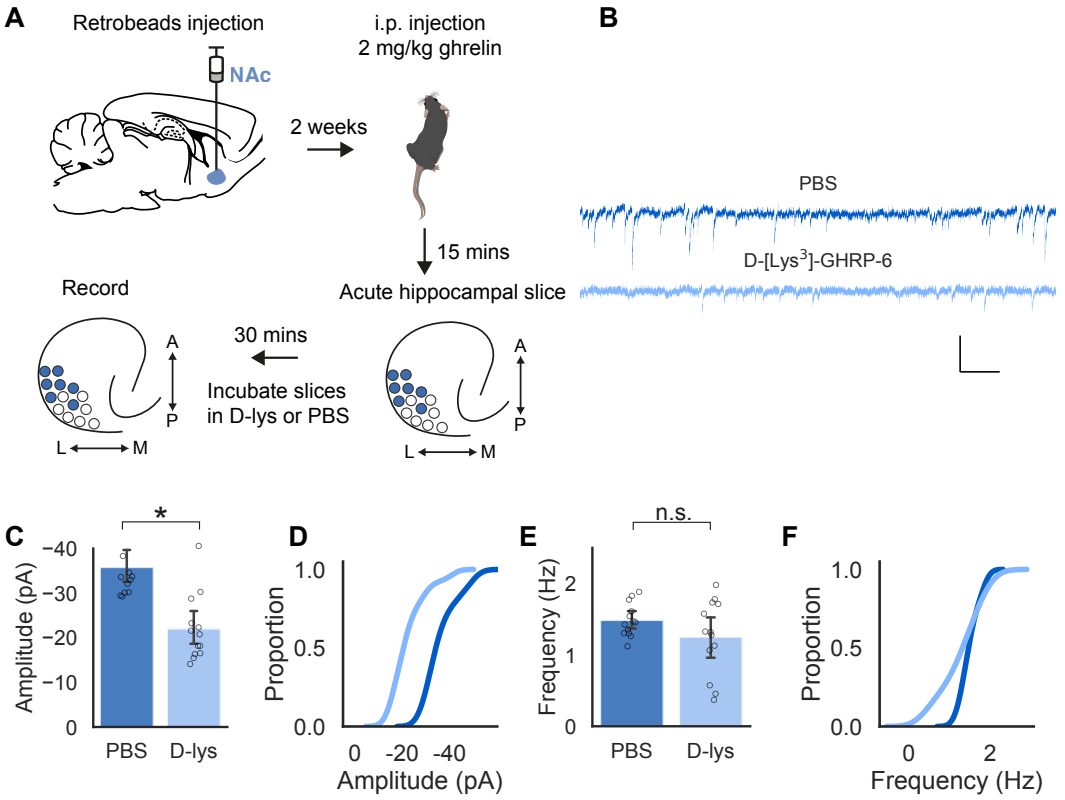

Figure 5.5: GHSR1a antagonism reduces mIPSC amplitude in vS^{NAc} neurons. (A) Retrobeads were stereotaxically injected into NAc. After 2 weeks post-surgery, animals were injected with 2 mg/kg, perfused and sliced. Half of the prepared slices were incubated in aCSF containing 50 µM D-[Lys^3]-GHRP-6, and the other half in aCSF containing vehicle control. 30 mins later, mIPSCs were recorded from vS^{NAc} neurons. (B) Example recordings from vS^{NAc} neurons in PBS and D-lys. Scale bar: 500 ms (x-axis), 40 pA (y-axis). (C–D) mIPSC amplitude as a (C) bar plot and (D) cumulative fraction (D-lys, n = 12 cells from 2 animals; PBS, n = 12 cells from 2 animals). (E and F) mIPSC frequency as in (C–D). Error bars represented as mean ± sem. Illustration downloaded from SciDraw.

To determine whether this effect of ghrelin on synaptic inhibition onto vS^{NAc} neurons was dependent on the ghrelin receptor GHSR1a, I repeated the experiments and focused on recording mIPSCs from vS^{NAc} neurons (**Figure 5.5A**).

Retrobeads were injected into NAc, and two weeks later, animals were given i.p. injections of ghrelin prior to slicing. In these animals, I prepared vS slices and incubated one half of the slices in aCSF containing the GHSR1a antagonist D-[Lys^3]-GHRP-6 (D-lys; 50 µM) and the other half in vehicle control. 30 minutes later, I recorded mIPSCs from vS^{NAc} neurons. Incubating the slices in the bath containing D-lys led to a specific reduction in the mIPSC amplitude (mIPSC amplitude in pA, incubations in D-lys = -22.03 ± 2.06, incubations in PBS = -35.81 ± 1.95; two-tailed unpaired t-test, t = 4.87, p = 0.0001, n = 12 cells in D-lys, n = 12 cells in PBS; **Figure 5.5B–D**), without a simultaneous change in the mIPSC frequency (mIPSC frequency in Hz, incubations in; D-lys = 1.25 ± 0.15; incubations in PBS = 1.49 ± 0.06; two-tailed unpaired t-test, t = -1.47, p = 0.16, n = 12 cells in D-lys, n = 12 cells in PBS; **Figure 5.5E–F**). This finding demonstrates that ghrelin signalling via the GHSR1a in vS^{NAc} neurons modulates the level of inhibitory synaptic transmission.

Taken together, these results indicate that ghrelin mediates a projection-specific increase in inhibitory transmission onto vS^{NAc} neurons, and that GHSR1a antagonism reverses the increase in inhibitory synaptic transmission.

5.2.3 Knockdown of ghrelin receptors in vS^{NAc} neurons impairs the encoding of Approach behaviour

Thus far, the evidence presented indicates that systemic ghrelin promotes an increased inhibitory drive onto vS^{NAc} neurons *in vitro*. These results suggest that ghrelin signalling in vS^{NAc} neurons may be important in producing the inhibition of vS^{NAc} activity *in vivo*. Given that hippocampal neurons express GHSR1a (Hsu et al., 2015; Diano et al., 2006; Zigman et al., 2006), I therefore asked how GHSR1a signalling influences vS^{NAc} population activity in different hunger states, and hypothesised that reducing ghrelin signalling in vS^{NAc} neurons would prevent the reduction in vS^{NAc} activity brought on by ghrelin. To test this idea, I needed to simultaneously impair ghrelin signalling in vS^{NAc} neurons and record their neural activity. Thus, I used a molecular knockdown approach that involves virally transducing vS^{NAc} neurons with both a knockdown construct for the microRNAi-adapted short-hairpin RNA intereference of the GHSR1a (shRNAmir; **Figure 5.6A–C**), as well as the calcium indicator GCaMP6f. This approach allows the simultaneous imaging of vS^{NAc} neurons with reduced GHSR1a signalling.

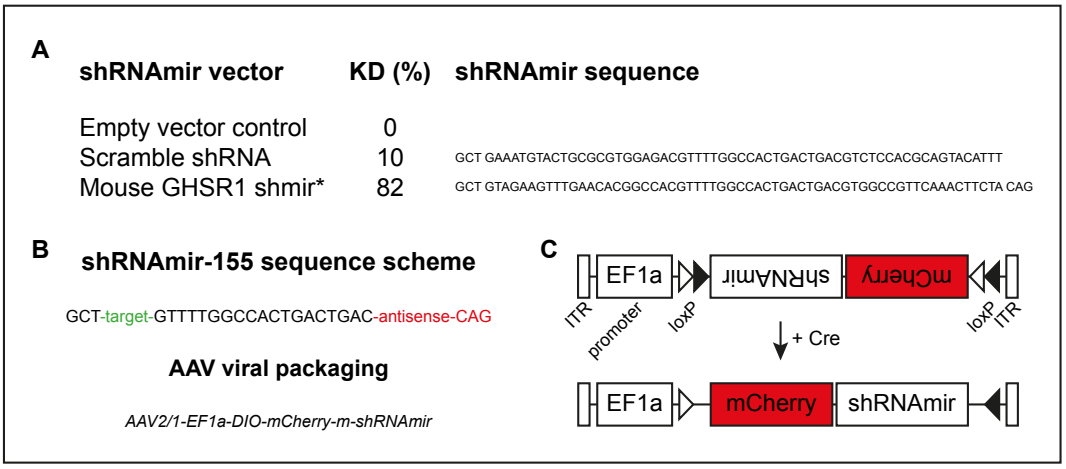

Figure 5.6: Design of shRNAmir sequence and viral construct. (A) Knockdown of GHSR1a by plasmids harbouring the shRNAmir sequence targeting the growth hormone secretagogue receptor 1a (GHSR1a), as assayed in a HEK293 cell culture. The percentage of knockdown was assessed using qT-PCR to measure the relative expression compared to the empty vector control. Note that data presented in (A) are taken from validation experiments conducted by Vector Biolabs. (B) The shRNA sequence against GHSR1a was inserted into a mir-155 backbone, and packaged into an AAV under the elongation factor 1α promoter, and made Cre-dependent through a double inverted open reading frame (DIO) design. The mCherry fluorophore allows confirmation of shRNAmir expression. (C) In the presence of Cre, the ORF becomes inverted into the forward orientation, thus enabling functional transcription of the shRNAmir and mCherry sequence.

Briefly, the shRNAmir molecular knockdown approach makes use of a construct that incorporates both natural microRNAi and artificial short-hairpin RNAi to achieve efficient knockdown of the the ghrelin receptor GHSR1a. First, the shRNAmir sequence targeting the GHSR1a protein was validated *in vitro* in a HEK293 cell line and shown to reduce the expression of GHSR1a by 82% relative to an empty vector (**Figure 5.6A**). A scrambled control – in which the shRNAmir sequence targeting the GHSR1a was shuffled and therefore cannot base-pair with the mRNA for GHSR1a – achieved by comparison 10% knockdown (**Figure 5.6A**).

This shRNAmir sequence targeting GHSR1a was then placed in a cassette and subsequently packaged into a recombinant adeno-associated virus (AAV) vector that expresses both the shRNAmir and an mCherry reporter (**Figure 5.6B**). Crucially, the rAAV was made Cre-dependent by inverting the open reading frame (ORF; **Figure 5.6C**). Upon Cre recombination, the ORF is inverted, switching the cassette into the forward sequence and allowing for the functional transcription of the shRNAmir.

Using this viral construct, I first injected *AAV2-retro-Syn-Cre* into NAc, which

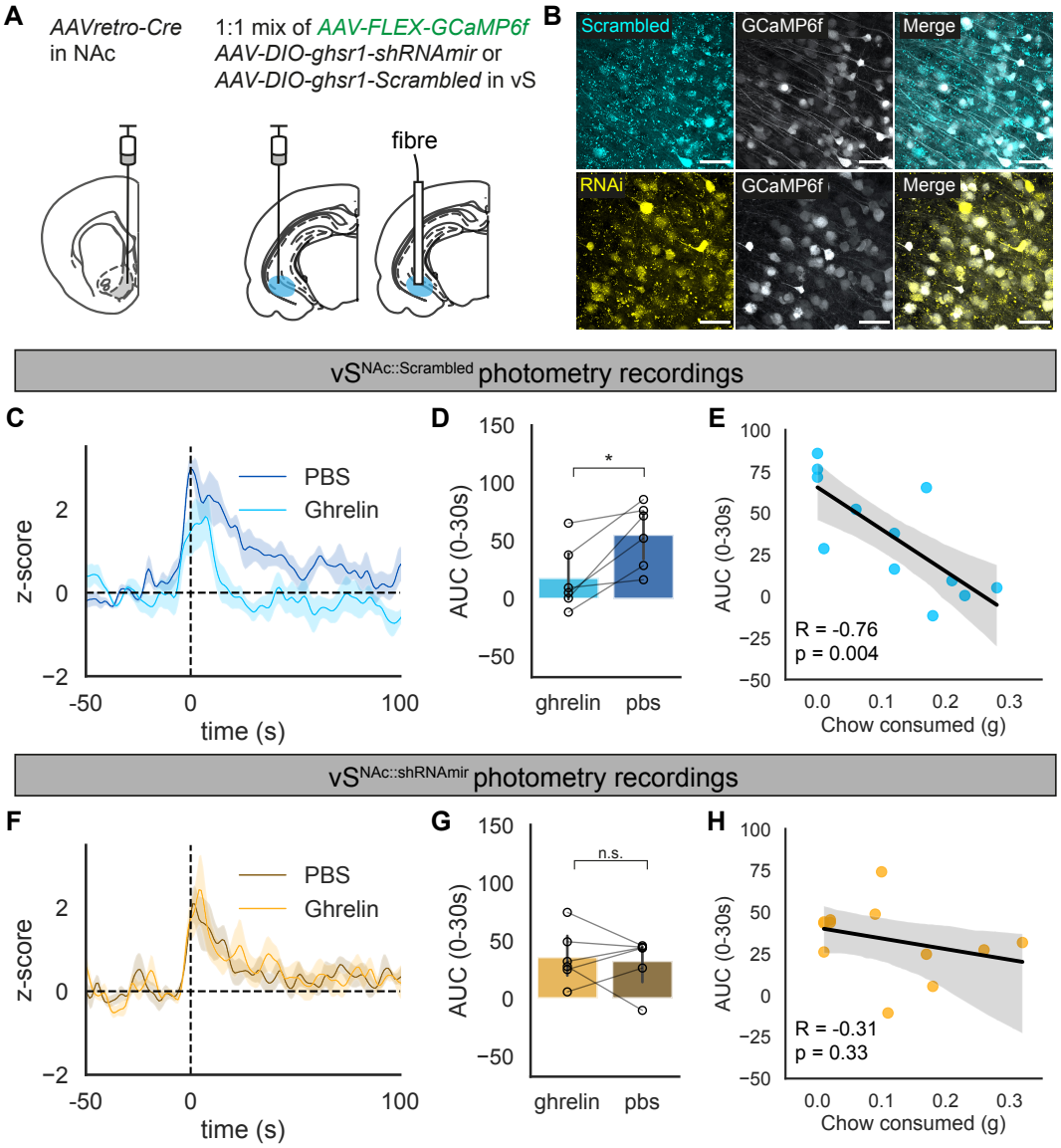

Figure 5.7: GHSR1a knockdown in vS^{NAc} neurons impairs hunger-driven circuit inhibition during chow presentation. (A)Viral strategy for simultaneous Ca^{2+} imaging and molecular knockdown of GHSR1a in vS^{NAc} neurons in freely feeding mice. The virus *AAV2-retro-Syn-Cre* was injected into NAc, thereby retrogradely expressing Cre in vS neurons. In the same surgery, a 1:1 mix of the Cre-dependent viruses expressing GCaMP6f (*AAV1-CAG-FLEX-GCaMP6f-WPRE-SV40*) and shRNAmir (*AAV1/2-EF1a-DIO-m-ghsr1-shRNAmir*) or scrambled constructs (*AAV1/2-EF1a-DIO-m-ghsr1-Scrambled*) was injected into vS. (B) 20x confocal images of vS demonstrating colocalisation of shRNAmir or Scrambled constructs with GCaMP6f. Scale bar: 50 µm. (C, F) Averaged z-scored Ca^{2+} activity of all (D) vS$^{NAc::Scrambled}$ or vS$^{NAc::shRNAmir}$ animals, aligned to chow presentation (n = 6 vS$^{NAc::shRNAmir}$ animals, 6 vS$^{NAc::Scrambled}$ animals). (D, G), Area under the curve from 0 to 30 s for (D) vS$^{NAc::Scrambled}$ and (G) vS$^{NAc::shRNAmir}$ animals. (E, H) Linear regressions of the amount of chow consumed within the first 10 minutes with the AUC of (E) vS$^{NAc::Scrambled}$ or (H) vS$^{NAc::shRNAmir}$ activity. Data represent mean ± sem.

retrogradely expresses Cre in vS (**Figure 5.7A**). In the same surgery, the Cre-dependent AAV harbouring the shRNAmir against GHSR1a (*AAV1/2-EF1a-DIO-m-ghsr1-shRNAmir*) was injected into vS, thus expressing the shRNAmir specifically in vS^{NAc} neurons ($vS^{NAc::shRNAmir}$ animals). In parallel, and as a control, littermate animals were injected with the control virus *AAV1/2-EF1a-DIO-m-ghsr1-scrambled* in vS to express a scrambled version of the shRNAmir targeting GHSR1a ($vS^{NAc::Scrambled}$ animals). Either of these viruses was mixed in a 1:1 ratio with *AAV1-CAG-FLEX-GCaMP6f-WPRE-SV40* to allow for the specific imaging of Ca^{2+} activity preferentially in vS neurons co-expressing either the shRNAmir or scrambled construct (**Figure 5.6B**). All injections were conducted unilaterally to avoid possible behavioural impairments resulting from bilateral knock down of GHSR1a in vS^{NAc}, thereby decoupling behaviour from the neural encoding of behaviour in the vS^{NAc} circuit. After at least 4 weeks post-surgery, animals were subjected to behavioural testing.

Animals were injected with either 2 mg/kg ghrelin or PBS 30 mins before presentation of chow. At the moment of chow presentation, $vS^{NAc::Scrambled}$ activity in the ghrelin condition was markedly reduced to a lower level of Ca^{2+} fluorescence compared to the PBS condition (AUC from 0 to 30 s for $vS^{NAc::Scrambled}$ mice, Ghrelin = 17.73 ± 11.63, PBS = 55.18 ± 11.37, two-tailed paired t-test, t = -3.76, p = 0.01, n = 6 mice; **Figure 5.7C–D**). By contrast, the Ca^{2+} fluorescence in $vS^{NAc::shRNAmir}$ animals exhibited no change in overall activity across Ghrelin and PBS conditions (AUC from 0 to 30 s for $vS^{NAc::shRNAmir}$ mice, Ghrelin = 35.35 ± 9.63, PBS = 32.01 ± 9.02, two-tailed paired t-test, t = 0.33, p = 0.76, n = 6 mice; **Figure 5.7F–G**). Consistent with this differential activity across hunger states, $vS^{NAc::Scrambled}$ activity significantly correlated with ghrelin-driven food intake (Pearson correlation between amount of chow consumed and AUC 0-30 s, r = -0.76, p = 0.004; **Figure 5.7E**). This was not the case for $vS^{NAc::shRNAmir}$ activity, which appeared decorrelated from food consumption (Pearson correlation between amount of chow consumed and AUC 0-30 s, r = -0.31, p = 0.33; **Figure 5.7H**). Thus, molecular knockdown of GHSR1a in vS^{NAc} neurons impairs the ability of ghrelin to inhibit vS^{NAc} neurons following chow presentation.

Notably, the above results indicated that ghrelin signalling was required for in-

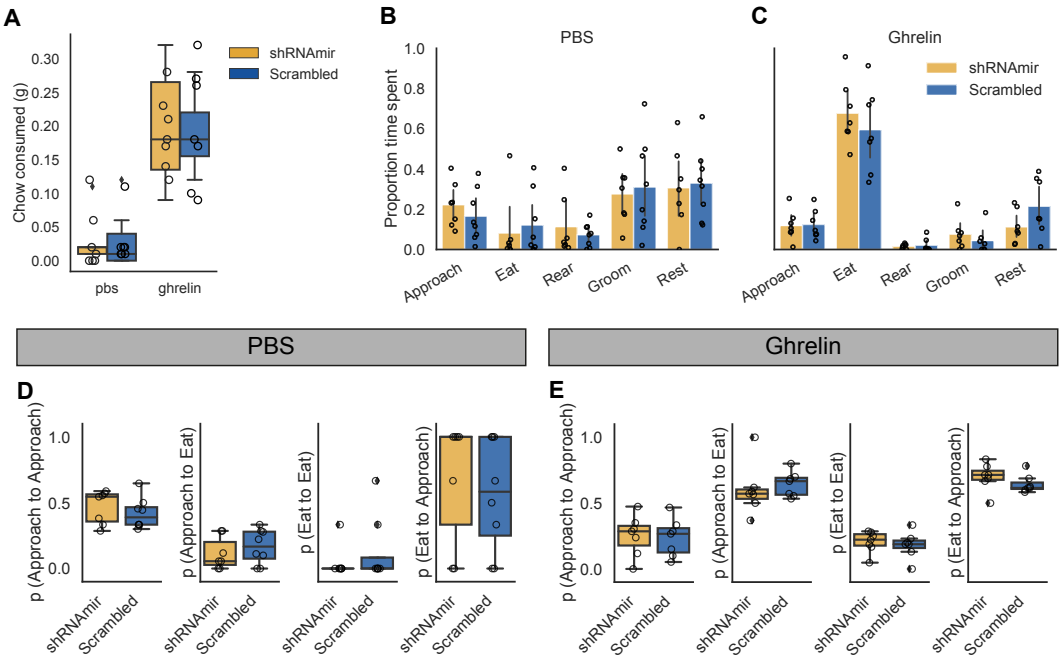

Figure 5.8: Unilateral GHSR1a knockdown does not influence hunger state-dependent behaviour. (A) The amount of chow consumed within the 10-minute chow presentation period between $vS^{NAc::shRNAmir}$ and $vS^{NAc::Scrambled}$ animals. (B, C) Distribution of time spent engaging in a BSS behaviour after (B) PBS or (C) ghrelin injection, normalised by the total amount of time spent in any BSS behaviour. (D, E) Markov chain transition probability analysis in the sequence of BSS behaviours following (D) PBS or (E) ghrelin injection. Bar plots show mean ± sem, and boxplots demonstrate the median and 1.5 times the interquartile range.

hibiting the vS^{NAc} circuit following chow presentation. However, it remained possible that this effect was indirect; impaired ghrelin signalling may have influenced the expression of certain feeding behaviours, e.g. reduced approach or increased eating, thereby shifting vS^{NAc} activity accordingly. To exclude this possibility, I manually annotated the behaviour of $vS^{NAc::shRNAmir}$ and $vS^{NAc::Scrambled}$ animals in a blinded manner, and analysed the feeding patterns between these two conditions (**Figure 5.8**). No difference was detected in the overall amount of chow consumed between $vS^{NAc::shRNAmir}$ and $vS^{NAc::Scrambled}$ animals (two-way mixed effects ANOVA, interaction between hunger state and virus injected, $F_{1,10} = 0.10$, $p = 0.76$; **Figure 5.8A**). Furthermore, no difference was detected in the amount of time spent engaging in a BSS behaviour in either the ghrelin condition (two-way mixed effects ANOVA, interaction between virus injected and BSS behaviour, $F_{4,40} = 0.45$, $p = 0.78$) or PBS condition (two-way mixed effects ANOVA, interaction between virus injected and BSS behaviour, $F_{4,40} = 0.59$, $p = 0.67$; **Figure 5.8B–C**). When focusing specifically

on Approach behaviour, there was no interaction between the hunger state and virus injected (two-way mixed effects ANOVA, interaction between virus injected and hunger state, $F_{1,10} = 3.13$, $p = 0.11$); instead, Approach behaviour was dependent solely on the hunger state and not on whether shRNAmir or Scrambled was expressed in vS^{NAc} (main effect of hunger state, $F_{1,10} = 5.08$, $p = 0.047$; main effect of virus injection, $F_{1,10} = 0.57$, $p = 0.46$). Lastly, analysis of the transition probabilities from each BSS behaviour to the next behaviour revealed no differences in the feeding-specific (**Figure 5.8D–E**) and non-feeding-specific (data not shown) BSS behavioural sequences in both the PBS and ghrelin states. Thus, unilateral knockdown of GHSR1a in vS^{NAc} does not affect overall feeding behaviour, and effectively decouples behaviour from the encoding of behaviour in vS^{NAc} activity. This also means that the lack of an inhibition in $vS^{NAc::shRNAmir}$ population activity could not have resulted from an altered behavioural pattern in the feeding sequence.

Does this impairment of vS^{NAc} circuit inhibition by shRNAmir-mediated knockdown of GHSR1a occur specifically during food approach? Using the annotated BSS behaviours across the 10-minute behavioural session, I aligned the photometry signals from $vS^{NAc::shRNAmir}$ and $vS^{NAc::Scrambled}$ animals to the onset of Approach events (**Figure 5.9**). Consistent with previous vS^{NAc} activity recordings, the z-scored Ca^{2+} signal in $vS^{NAc::Scrambled}$ neurons appeared to be inhibited at the onset of Approach in the ghrelin condition (**Figure 5.9A**). This is consistent with the analysis of vS^{NAc} activity (**Figure 4.11**, Chapter 4) where vS^{NAc} activity showed ghrelin-dependent modulation predominantly at food approach. By contrast, knockdown of GHSR1a in $vS^{NAc::shRNAmir}$ animals made the Ca^{2+} signal invariant to ghrelin during Approach (**Figure 5.9D**). This suggested that molecular knockdown of GHSR1a in vS^{NAc} impairs the ability of ghrelin to inhibit vS^{NAc} circuit activity during food approach.

To quantify the reduction in vS^{NAc} activity during Approach, I used multiple regression analysis to estimate the β weight for Approach – as described in the previous chapter. This β value for Approach is a measure that represents the isolated, average neural activity during Approach, after taking into account possible contributions from other BSS behaviours, presentation and velocity (see Methods). These linear models captured significant variance in the z-scored Ca^{2+} activity (5-

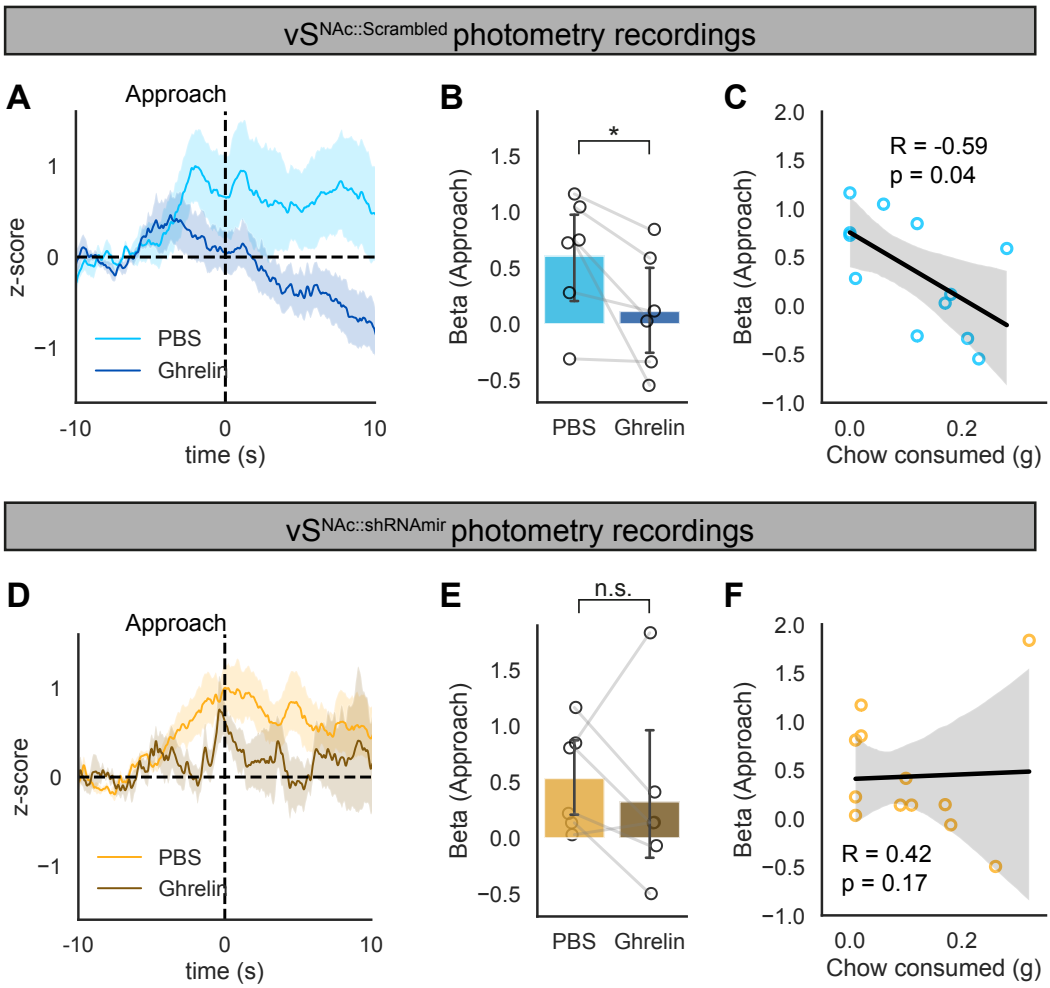

Figure 5.9: GHSR1a knockdown decouples the relationship between Approach-related activity and food consumption. (A, D) Event-triggered averages of the z-scored Ca^{2+} activity, aligned to the onset of Approach behaviour, for (A) $vS^{NAc::Scrambled}$ and (D) $vS^{NAc::shRNAmir}$ animals. (B, E) Multiple linear regression was used to quantify the average vS^{NAc} neural response during engagement in Approach behaviour. (B) $vS^{NAc::Scrambled}$ activity during Approach was significantly reduced in the Ghrelin condition compared to control (β weight for Approach, PBS = 0.61 ± 0.22, Ghrelin = 0.12 ± 0.22, two-tailed t-test, t = 2.67, p = 0.04, n = 6 mice), in contrast to $vS^{NAc::shRNAmir}$ activity (β weight for Approach, PBS = 0.54 ± 0.19, Ghrelin = 0.33 ± 0.33, Approach, two-tailed t-test, t = 0.77, p = 0.48, n = 6 mice). (C, F) Linear regressions of the β weights and amount of chow consumed for Approach behaviour. Only the Approach β weights in (C) $vS^{NAc::Scrambled}$ animals were negatively correlated with and predictive of food consumption, while the Approach β weights in $vS^{NAc::shRNAmir}$ animals were not. Photometry traces represent mean ± sem, and boxplots represent median and 1.5 times the interquartile range.

fold cross-validated accuracy, $vS^{NAc::shRNAmir}$ = 0.16 ± 0.02; $vS^{NAc::Scrambled}$ = 0.23 ± 0.02). Consistent with the Approach-aligned Ca^{2+} signals, the β weight for Approach was significantly reduced in the Ghrelin condition compared to PBS only in $vS^{NAc::Scrambled}$ animals, and not $vS^{NAc::shRNAmir}$ animals ($vS^{NAc::Scrambled}$ β weight

for Approach, PBS = 0.61 ± 0.22, Ghrelin = 0.12 ± 0.22, two-tailed t-test, t = 2.67, p = 0.04; $vS^{NAc::shRNAmir}$ β weight for Approach, PBS = 0.54 ± 0.19, Ghrelin = 0.33 ± 0.33, Approach, two-tailed t-test, t = 0.77, p = 0.48; n = 6 mice each; **Figure 5.9B, E**).

Finally, I asked how GHSR1a knockdown in vS^{NAc} neurons affected the relationship between Approach-related activity and amount of chow consumed. I previously demonstrated that vS^{NAc} activity during food approach was predictive of subsequent food consumption (**Figure 4.12**, Chapter 4). I hypothesised that molecular knockdown of GHSR1a would decouple the relationship between Approach-related vS^{NAc} activity and subsequent food consumption. To answer this question, I regressed the β weights obtained for Approach against the amount of chow consumed within the 10 minute presentation period. I found that while the β weight for Approach in $vS^{NAc::Scrambled}$ animals was highly correlated with chow consumption, the β weight for Approach in $vS^{NAc::shRNAmir}$ was decorrelated from chow consumption (Pearson correlation between for Approach β and chow consumption $vS^{NAc::Scrambled}$, r = -0.59, p = 0.04; $vS^{NAc::shRNAmir}$, r = 0.42, p = 0.17; **Figure 5.9C, F**). Therefore, impairing ghrelin signalling in vS^{NAc} projections reduced the ability of ghrelin to inhibit vS^{NAc} activity at the time of food approach.

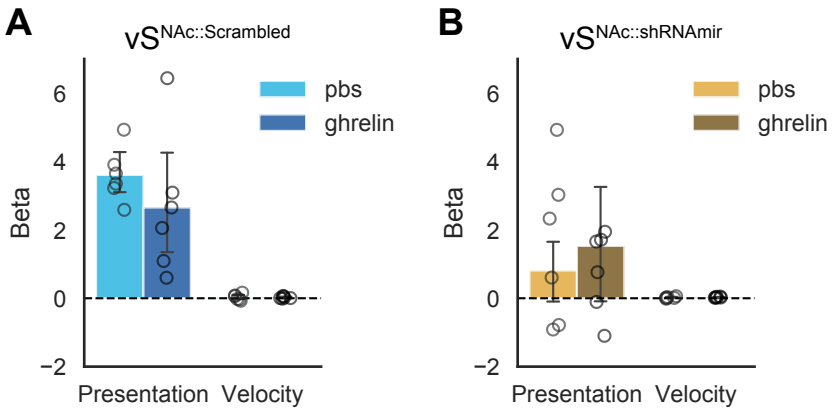

Figure 5.10: Changes in Ca^{2+} during presentation and movement signals cannot account for changes in Approach-related vS^{NAc} activity following GHSR1a knockdown. (A and B) Estimated β weights for food presentation and velocity for (A) $vS^{NAc::Scrambled}$ and (B) $vS^{NAc::shRNAmir}$ animals. Data represent mean ± sem.

Importantly, within animals, I found that there was no modulation in the Ca^{2+} activity for food presentation and velocity across the PBS and ghrelin conditions in both $vS^{NAc::Scrambled}$ and $vS^{NAc::shRNAmir}$ animals (two-way repeated-measures

ANOVA, $vS^{NAc::Scrambled}$ interaction, p = 0.35; $vS^{NAc::shRNAmir}$ interaction, p = 0.43; **Figure 5.10A–B**). Notably, there was an effect of GHSR1a knockdown on the vS^{NAc} response to food presentation (two-way mixed effects ANOVA of presentation β weight, main effect of virus injected, $F_{1,10}$ = 6.42, p = 0.03), indicating that molecular knockdown of GHSR1a attenuated the Ca^{2+} response to food presentation; this finding suggests that there might be homeostatic plasticity in the vS circuit following GHSR1a knockdown (see Discussion). As an important final check, fibre photometry recording sites were verified to be localised within the vS (**Figure 5.11**).

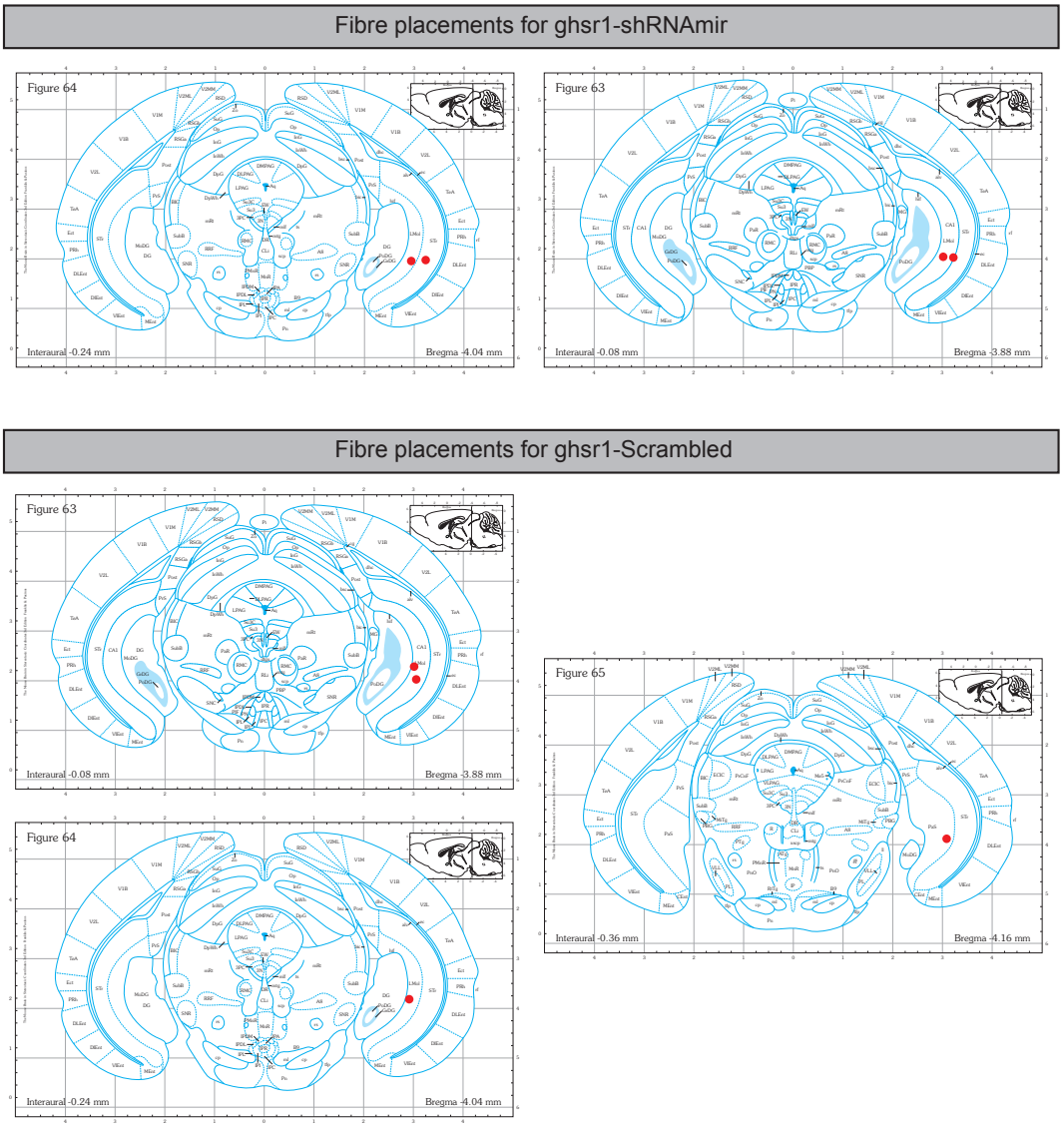

Figure 5.11: Representative fibre locations of RNAi-mediated GHSR1a knockdown experiments.

In summary, I found that GHSR1a knockdown prevented the ghrelin-mediated

inhibition of vS^{NAc} neurons during chow presentation, and specifically diminished the hunger state-dependent encoding of Approach behaviour. This effectively decoupled Approach-related activity from subsequent chow consumption, showing that hunger state sensing in vS^{NAc} neurons is dependent on the GHSR1a.

5.2.4 Bidirectional modulation of approach-to-eat transitions through chemogenetic control of vS^{NAc} activity

The previous data demonstrate that ghrelin recruits an inhibitory plasticity mechanism in the postsynaptic compartment in vS that depends on GHSR1a activity. Furthermore, ghrelin receptor signalling in vS^{NAc} neurons is required for the encoding of food approach behaviour in a hunger-dependent manner. Therefore, one hypothesis is that the activity of the vS^{NAc} circuit influences an animal's strategy during feeding behaviour and, in turn, is capable of controlling the amount of food that it consumes.

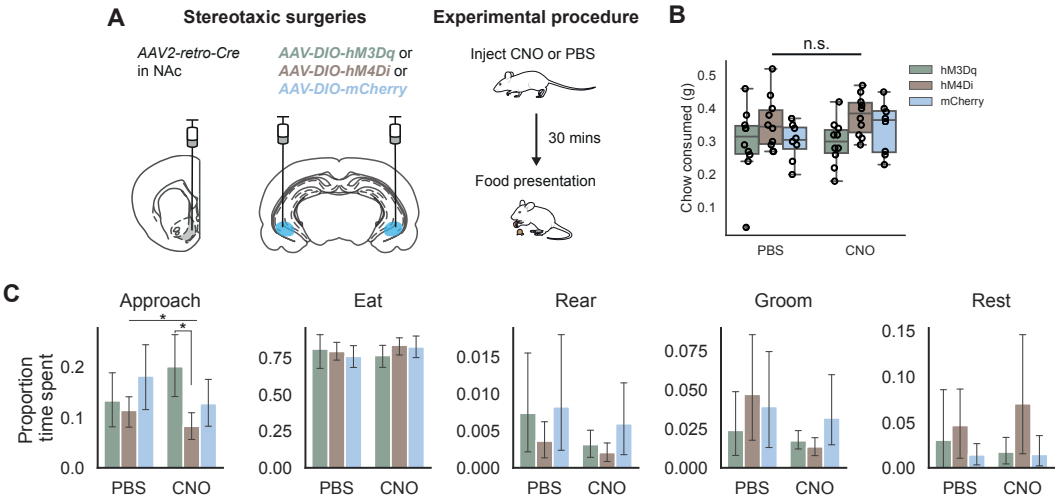

Figure 5.12: Bidirectional manipulation of vS^{NAc} activity governs exploratory Approach behaviour. (A) *Left*: Stereotaxic surgery protocol to virally express DREADDs in vS^{NAc} neurons. *AAV2-retro-Syn-Cre* is first injected into NAc. In the same surgery, Cre-dependent DREADDs is injected into vS. *Right*: At least four weeks later, animals were fasted overnight prior to behavioural testing. On test day, animals were injected with either 1 mg/kg CNO or PBS, allowed to recover for 30 mins in the testing box before presentation of a chow pellet. (B) Amount of chow consumed within 10 minutes of chow presentation. (C) Distributions of time spent (normalised) in each BSS behaviour after animals had been injected with PBS or CNO (n = 10 hM3Dq animals, 10 hM4Di animals, n = 8 mCherry control animals). Data presented as mean ± sem. Illustration downloaded from SciDraw.

To probe whether vS^{NAc} neurons are necessary and/or sufficient to drive food approach during free behaviour under physiological conditions, I virally expressed

the excitatory and inhibitory designer receptors exclusively activated by designer drugs (DREADDs), hM3Dq and hM4Di, respectively, or fluorophore-only control, in vS^{NAc} neurons (**Figure 5.12A**). In this system, the inert ligand clozapine-N-oxide (CNO) binds to the DREADDs and activates or inhibits these neurons *in vivo*. Expression of the DREADDs was targeted to vS^{NAc} neurons by first injecting *AAV2-retro-Syn-Cre* in NAc, and Cre-dependent *AAV8-Syn-DIO-hM3Dq-mCherry*, *AAV8-Syn-DIO-hM4Di-mCherry* or *AAV8-Syn-DIO-mCherry* bilaterally into vS. Four weeks later, I subjected the animals to behavioural testing. Animals were fasted overnight prior to testing; this method was preferred to i.p. injections of ghrelin as both the DREADDs and GHSR1a are GPCRs that might lead to interference in signalling cascades (Mear et al., 2013, see Limitations of experiments under Discussion). On testing day, animals were given i.p. injections of 1 mg/kg CNO or PBS control and allowed 30 mins to recover prior to presentation of a pellet of chow (**Figure 5.12A**).

Firstly, the amount of chow consumed within the 10 minute presentation period did not differ depending on drug and virus (two-way mixed effects model, interaction between drug and virus, $F_{2,25} = 0.327$, $p = 0.724$; **Figure 5.12B**), indicating that manipulating vS^{NAc} activity was not sufficient to influence food consumption at a timescale of 10 minutes. This was initially surprising, given recent reports of the ability of vS^{NAc} neurons in controlling feeding behaviour (Reed et al., 2018; Yang et al., 2019). To examine whether vS^{NAc} manipulation affected the short-term dynamics of feeding behaviour, I next examined how much time animals spent engaging in a particular BSS behaviour (namely, Approach, Eat, Rear, Groom and Rest). Strikingly, the amount of time spent in Approach behaviour was significantly elevated through vS^{NAc} activation in the hM3Dq group compared to the hM4Di group (two-way mixed effects ANOVA for duration of engagement in Approach behaviour, virus as between-subject factor and drug as within-subject factor, interaction between virus and drug injected, $F_{2, 25} = 6.789$, $p = 0.004$; main effect of virus, $F_{1, 25} = 2.627$, $p = 0.092$; main effect of drug injected, $F_{2, 25} = 0.0012$, $p = 0.97$, n = 10 hM3Dq animals, 10 hM4Di animals, 8 mCherry animals; **Figure 5.12C**). This is in keeping with the observed encoding of exploratory Approach behaviour by vS^{NAc} neurons (Chapter 4). Posthoc testing revealed that this difference was driven

largely by differences between the hM3Dq and hM4Di groups in the CNO condition, while the control mCherry group was variable and did not differ from either the hM3Dq and hM4Di groups (proportion time spent in Approach in the CNO group, post-hoc unpaired t-test with Benjamini-Hochberg correction, hM3Dq vs. hM4Di, t = 3.137, p = 0.031; hM4Di vs. mCherry, t = 1.544, p = 0.225; hM3Dq vs. mCherry, t = 1.695, p = 0.218). By contrast, general exploratory (Rear) and consummatory behaviours (Rest, Groom and Eat) were unaltered by these manipulations of vS^{NAc} activity, again consistent with the specific encoding of food Approach behaviour observed in the fibre photometry experiments. This result indicates that vS^{NAc} activation is capable of driving food approach behaviour.

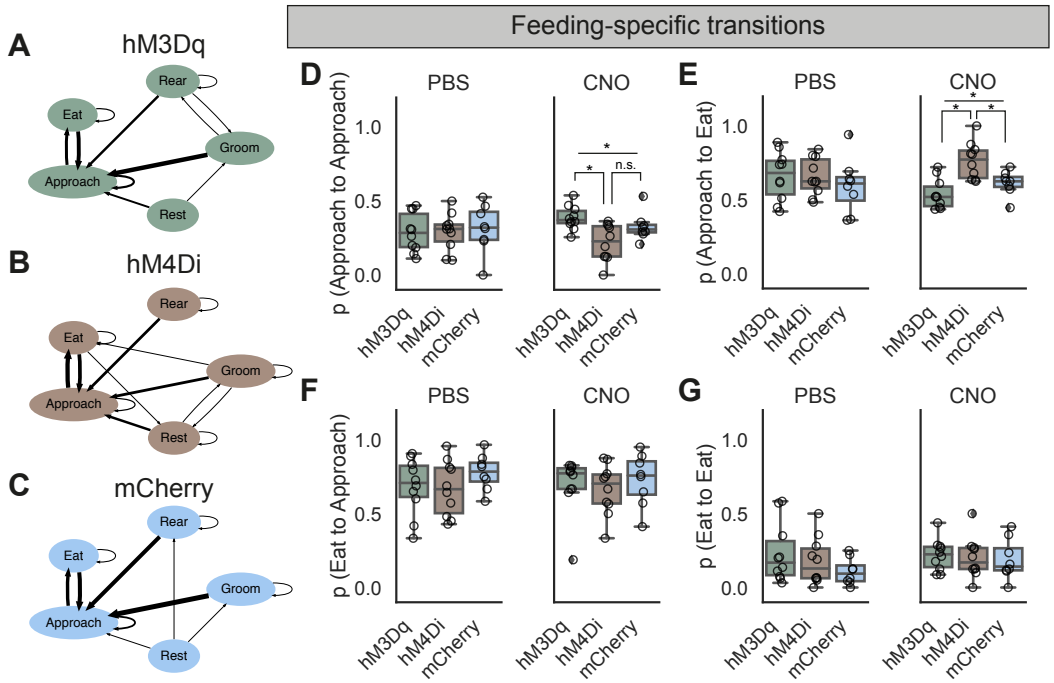

Figure 5.13: Manipulating vS^{NAc} changes the transition dynamics of feeding behaviour. (A–C) Markov graphs in the CNO condition for (A) hM3Dq, (B) hM4Di and (C) mCherry animals. Each node represents a BSS behaviour, and each arrow (edge) indicates a transition. The thickness of each arrow is weighted by the transition probability. (D–G) Markov chain transition probability analysis in both the PBS and CNO condition for (D) Approach-Approach, (E) Approach-Eat, (F) Eat-Approach and (G) Eat-Eat conditions. Approach-Approach and Approach-Eat transition probabilities are significantly modulated by CNO injection. Box plots represent median and the whiskers represent 1.5 times the interquartile range.

To examine whether the moment-to-moment behavioural transitions were affected by vS^{NAc} activity changes, I analysed the dynamics of feeding behaviour as a stochastic Markov process – as described previously – by computing the transition

probabilities from one BSS behaviour to the next (**Figure 5.13A–C**). Predictably, overnight fasted animals engaged mostly in feeding-specific behaviours, i.e. Approach and Eat. Therefore, I focused my analysis specifically on the behavioural dynamics between Approach and Eat. This analysis revealed differences in the Approach-Approach and Approach-Eat transitions (**Figure 5.13D–E**). Firstly, there was a trend of increased Approach-Approach transition probability with the manipulation of vS^{NAc} activity, but this was not significant (two-way mixed effects ANOVA, interaction between drug injection and DREADDs virus, $F_{2,25} = 2.356$, $p = 0.115$; main effect of virus, $F_{2,25} = 2.631$, $p = 0.092$; main effect of drug injection, $F_{1,25} = 0.142$, $p = 0.709$; **Figure 5.13D**). When analysing the CNO condition separately, the Approach-Approach transition probability depended on the virus injected (one-way ANOVA, $F_{2,\ 25} = 7.02$, $p = 0.003$; **Figure 5.13D**). More specifically, vS^{NAc} inhibition with hM4Di produced a lower Approach-Approach probability than vS^{NAc} activation with hM3Dq, while the mCherry condition was variable (Approach-Approach transition probability in the CNO group, post-hoc unpaired t-test with Benjamini-Hochberg correction, hM3Dq vs. hM4Di, $t = 3.602$, $p = 0.01$; hM4Di vs. mCherry, $t = -2.111$, $p = 0.153$; hM3Dq vs. mcherry, $t = 1.435$, $p = 0.347$).

Secondly, for Approach-Eat transitions, inhibiting vS^{NAc} activity promoted the transition from Approach to Eat (two-way mixed effects ANOVA, interaction between Approach-Eat transition probability and DREADDs virus, $F_{2,25} = 3.788$, $p = 0.037$; main effect of drug injection, $F_{1,25} = 1 \times 10^{-6}$, $p = 0.999$; main effect of virus, $F_{2,25} = 4.108$, $p = 0.029$; **Figure 5.13E**). When analysing the CNO group separately, the Approach-Eat transition probability was increased with vS^{NAc} inhibtion but not affected by vS^{NAc} activation (one-way ANOVA, $F_{2,\ 25} = 11.80$, $p = 2.46 \times 10^{-4}$; **Figure 5.13E**). In the hM4Di group, the high Approach-Eat transition probability denoted that once animals began investigating food (Approach), they were more likely to transition towards eating the food (Eat) relative to the mCherry and hM3Dq conditions. Posthoc testing revealed that in the CNO injected group, the main differences in Approach-Eat transitions arose predominantly from the increased Approach-Eat transition probability in the hM4Di group relative to the hM3Dq and mCherry conditions (Approach-Eat transition probability in the CNO group, post-hoc unpaired t-test with Benjamini-Hochberg correction, hM3Dq vs. hM4Di, $t = 4.453$, $p = 0.002$;

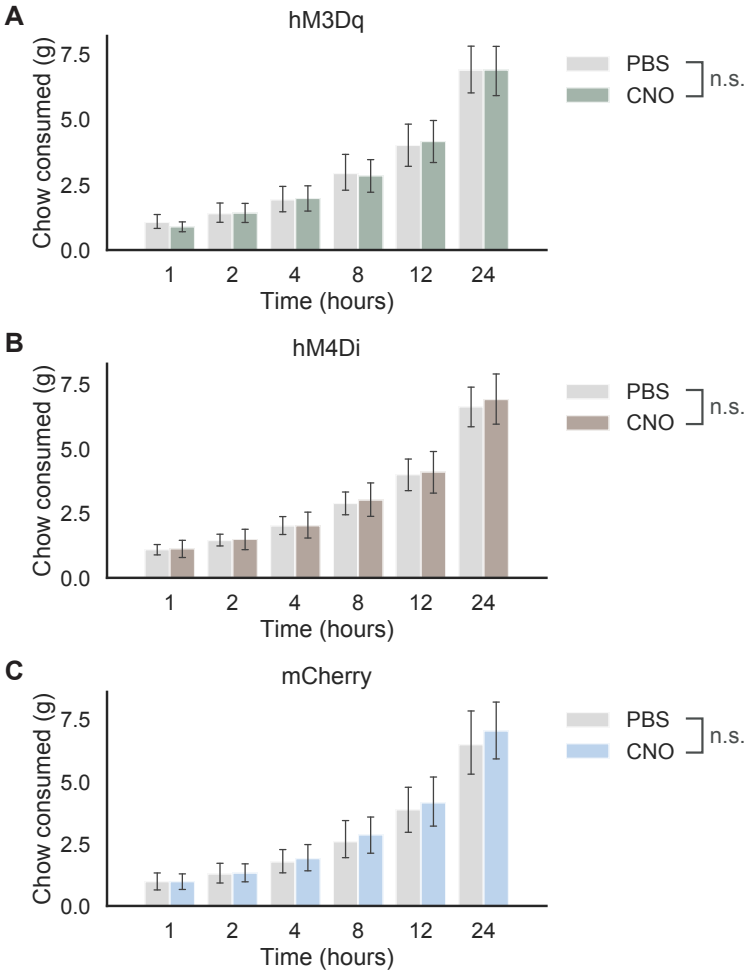

Figure 5.14: Manipulating vS^{NAc} activity does not change overall chow consumption over multiple hours. (A–C) Sequential measurement of chow intake after either PBS or CNO injection in singly housed mice expressing either (A) hM3Dq, (B) hM4Di or (C) mCherry in vS^{NAc} neurons. Data represent mean ± sem.

hM4Di vs. mCherry, t = 3.093, p = 0.021; hM3Dq vs. mcherry, t = 1.726, p = 0.207). No difference was detected in the transition probabilities during Eat-Approach and Eat-Eat transitions (**Figure 5.13F–G**), as well as other non-feeding-specific transitions (data not shown). Collectively, these results indicate that vS^{NAc} activation drives food investigation, while vS^{NAc} inhibition regulates the dynamics of feeding behaviour through changing the transition probabilities between Approach and Eat behaviour.

Does this change in behavioural transition dynamics translate to changes in overall consumption over longer periods of time? To address this question, I singly housed each animal and, following a 16-hour fast, delivered i.p. injections of either

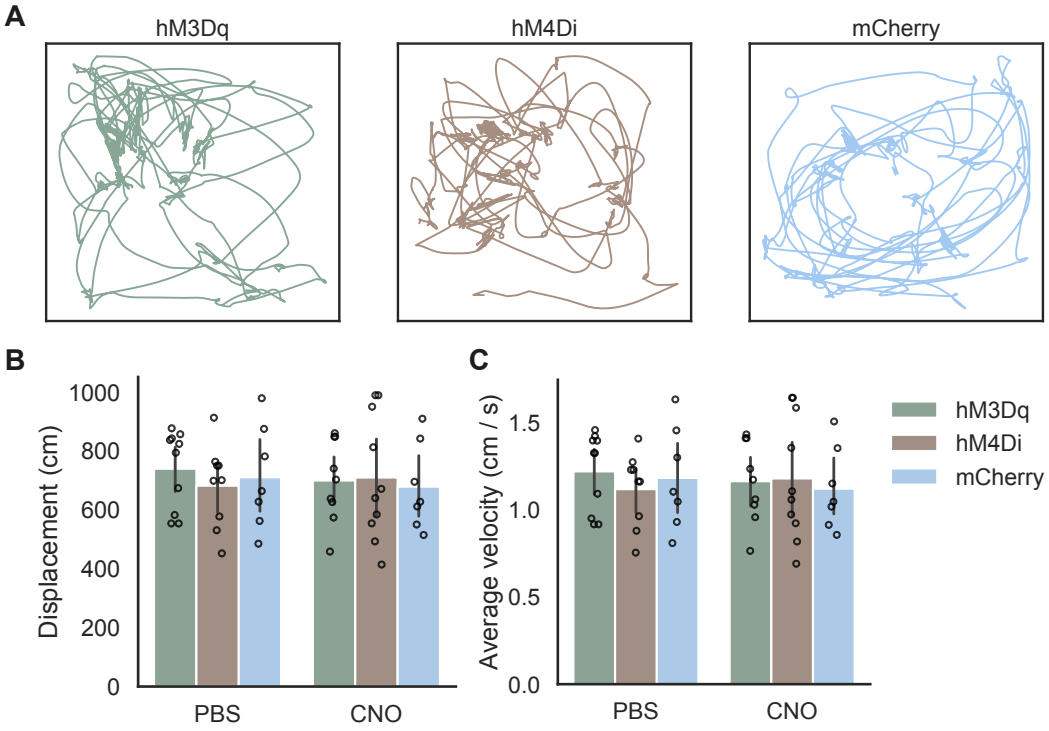

Figure 5.15: Manipulating vS^{NAc} activity does not change locomotion. (A) Example position tracking of animals in the behavioural boxes during presentation of chow. (B) The cumulative displacement of animals across drug and DREADDs virus conditions (Displacement in cm, CNO, hM3Dq = 699.29 ± 46.36, hM4Di = 709.44 ± 67.07, mCherry = 678.31 ± 55.78; PBS, hM3Dq = 739.12 ± 42.24, hM4Di = 681.46 ± 46.59, mCherry = 710.25 ± 66.50). (C) The velocity of the tracked animals across drug and DREADDs virus conditions (average velocity in cm/s, CNO, hM3Dq = 1.16 ± 0.08, hM4Di = 1.18 ± 0.11, mCherry = 1.12 ± 0.09l; PBS, hM3Dq = 1.22 ± 0.07, hM4Di = 1.12 ± 0.07, mCherry = 1.18 ± 0.11). Data represent mean ± sem.

PBS or 1 mg/kg CNO before returning chow into the home cage. I then measured the amount of food consumed across multiple hours (**Figure 5.14A–C**). Surprisingly, this experiment revealed that vS^{NAc} activity was neither necessary nor sufficient to drive food consumption behaviour (two-way repeated-measures ANOVA, hM3Dq: time × drug, $F_{6, 54} = 0.78$, $p = 0.59$; main effect of drug, $F_{1, 9} = 0.001$, $p = 0.975$; hM4Di, time × drug, $F_{6,42} = 0.46$, $p = 0.83$; main effect of drug, $F_{1, 7} = 0.168$, $p = 0.694$; mCherry, time × drug, $F_{6,42} = 2.15$, $p = 0.07$; main effect of drug, $F_{1, 7} = 1.194$, $p = 0.311$; **Figure 5.14A–C**). Thus, vS^{NAc} activity does not influence food consumption, but rather food-seeking behaviour, i.e. the decision to transition from investigating to eating food.

One possibility was that manipulating vS^{NAc} activity could have changed arousal and overall locomotion, thereby increasing the probability of Approach

behaviour by chance. By tracking the animal's position across time, I observed that these DREADDs-mediated manipulation of vS^{NAc} activity did not influence total cumulative distance travelled (two-way mixed-effects ANOVA, displacement in cm, interaction between virus and drug injected, $F_{2,21} = 0.665$, $p = 0.525$; **Figure 5.15A–B**) and average velocity (average velocity in cm/s, interaction between virus and drug injected, $F_{2,21} = 0.708$, $p = 0.503$; **Figure 5.15B**). This control analysis shows that vS^{NAc} activity manipulations did not influence locomotion. Taken together, these data indicate that vS^{NAc} activity promotes increased investigation of food and gates the transition from Approach to Eat behaviour.

5.3 Discussion

Using a combination of approaches, including *in vitro* whole-cell electrophysiology with pharmacology, molecular knockdown with fibre photometry, and pharmacogenetic manipulation, this chapter presented data that demonstrate a ghrelin-mediated increase in inhibitory synaptic transmission. In turn, reducing ghrelin signalling in vS^{NAc} by molecular knockdown of GHSR1a eliminated the behavioural encoding of food approach behaviour, highlighting the relevance of vS ghrelin signalling in food-seeking behaviour. Lastly, manipulating vS^{NAc} acitivity independent of ghrelin signalling showed that inhibition of vS^{NAc} neurons was sufficient to regulate the transition from Approach to Eat, while activation of vS^{NAc} increased overall food investigation time.

5.3.1 Determinants of inhibitory synaptic transmission in vS^{NAc} neurons

In my studies of synaptic tranmission in vS^{NAc} and vS^{LH} neurons, I first showed that incubation of hippocampal acute slices in ghrelin was not sufficient to modulate inhibitory synaptic transmission. Instead, systemic i.p. injections of ghrelin were sufficient to increase mIPSC amplitude, and not frequency, in vS^{NAc} neurons. This suggests that postsynaptic inhibitory plasticity is recruited by ghrelin signalling in a projection-specific manner. To my knowledge, this is the first account of projection-specific ghrelin signalling, and of ghrelin-mediated changes in inhibitory synaptic transmission, within the hippocampus.

Firstly, the lack of an effect of acute ghrelin incubation, and the presence

of an effect with systemic ghrelin, suggests that additional factors may be required to bring about changes in inhibitory plasticity. The most likely candidate for this additional requirement is dopamine, given the observation that GHSR1a heterodimerises with D1 dopamine receptors in hippocampus (Kern et al., 2015; Tian et al., 2019) and elsewhere in the brain (Kern et al., 2014). GHSR1a is also expressed in the ventral tegmental area (VTA) (Abizaid et al., 2006; Skibicka and Kanoski, 2016), and the VTA sends dopaminergic afferents to hippocampus (Rosen et al., 2015; McNamara et al., 2014). Additionally, ghrelin itself is a strong modulator of dopaminergic tone (Cone et al., 2014). Thus, systemic i.p. injections of ghrelin appear well-placed to orchestrate the combined dopaminergic input with ghrelin receptor binding within vS to initiate inhibitory plasticity.

Another possible determinant of hippocampal population activity is cholinergic input arising from the diagonal band and medial septum; incubation in cholinergic agonists like carbachol is sufficient to promote plasticity in hippocampal circuitry, including the re-balancing of excitatory and inhibitory network activity (Colgin, 2016; Colgin et al., 2003; Drever et al., 2011; Hunt et al., 2018). Furthermore, increased cholinergic drive is known to occur during the anticipatory period leading up to food reward (Inglis et al., 1994), and ghrelin receptors are expressed in the laterodorsal tegmental nucleus (Jerlhag et al., 2007), an important source of cholinergic input to the septum which then send cholinergic afferents to hippocampus. Therefore, another hypothesis is that concomitant ghrelin binding to GHSR1a, together with dopaminergic and/or cholinergic input, is required to initiate synaptic plasticity. Future experiments studying the interactions between ghrelin, dopamine and acetylcholine signalling in vS *in vitro*, as well as dopamine and acetylcholine signalling in vS *in vivo* using the dopamine sensor dLight (Patriarchi et al., 2018) or acetylcholine sensor iAChSnFR (Borden et al., 2020) under different states of hunger, would provide deeper insights into the neuromodulatory determinants of inhibitory plasticity in vS.

Secondly, systemic ghrelin modulated inhibitory plasticity specifically in vS^{NAc} neurons, and not vS^{LH} neurons. This was initially surprising, given the mounting evidence supporting the role of vS^{LH} neurons in mediating a ghrelin-dependent increase in motivated feeding behaviour. Recent studies have claimed that ghrelin

signalling within vS^{LH} neurons is sufficient to promote increased feeding behaviour (Hsu et al., 2015; Suarez et al., 2019, 2020). In particular, Hsu et al. (2015) and Suarez et al. (2020) conducted experiments in which infusion of ghrelin into vS is sufficient to increase meal size, and that blocking orexin signalling in downstream regions of vS prevents this behavioural effect. Instead, the findings presented in this chapter show that ghrelin specifically modulates synaptic transmission in vS^{NAc}, and not vS^{LH}, neurons. Together with findings from the previous chapter, and as discussed in Chapter 4, it is more likely that vS^{NAc} neurons are uniquely sensing circulating ghrelin levels and conveying these signals to LH via the NAc.

Lastly, ghrelin signalling appeared to mediate changes in inhibitory transmission. While ghrelin has been reported to modulate excitatory synaptic plasticity (Ribeiro et al., 2014; Diano et al., 2006; Tian et al., 2019), ghrelin has also been implicated in modulating inhibitory synaptic transmission (Cruz et al., 2013; Vergnano et al., 2008). Additionally, this change appeared to be localised to the postsynaptic compartment, since the mIPSC amplitude, but not frequency, was increased. Furthermore, this modulation of inhibitory transmission could be reversed by incubating the slices in the ghrelin receptor antagonist D-lys. Thus, GHSR1a signalling appears to be crucial for mediating changes in inhibitory synaptic transmission within vS^{NAc} neurons. It is known that signalling cascades triggered by GHSR1a activation, involving protein kinase C activation, increases in intracellular Ca^{2+} and activation of kinases such as CamKII (Kullmann et al., 2012; Kern et al., 2015) is capable of modulating $GABA_A$ receptor function and trafficking. Although less well-defined than synaptic plasticity at excitatory synapses, the evidence shown here highlights that one important determinant of inhibitory plasticity within the hippocampus may be circulating peripheral hormones that trigger neuromodulation of cell-type specific hippocampal neurons.

5.3.2 Limitation: sparse mEPSC events

While these experiments focused on the effect of ghrelin on inhibitory synaptic transmission, it is possible that excitatory synaptic transmission may also be modulated by ghrelin. This was technically challenging to study, since the frequency of miniature excitatory postsynaptic currents (mEPSCs) within the vS was extremely low (about 0.1 Hz, data not shown). This could be due to either a problem of detec-

tion (depending on recording noise) or presynaptic mechanisms. First, the peak-to-peak recording noise was consistently $\sim$5 pA, and the sparse mESPC events ranged from -10 to -20 pA, making low detection due to noise unlikely. Increasing the extracellular concentration of KCl from 2.5 mM to 5 mM or Ca^{2+} from 2 mM to 4 mM also did not result in an appreciable increase in mEPSC event rate (data not shown). Furthermore, there are consistent reports in the literature indicating low mESPC event rates in the vS (Sakimoto et al., 2019; Nguyen et al., 2015). Therefore, it is likely that under *in vitro* conditions, there is simply very low mEPSC event rates, which limits the possible experiments that can clarify the potential role of ghrelin on influencing excitatory synaptic transmission in vS.

As an alternate experiment, I chose to use electrode stimulation of a major afferent pathway to CA1 and subiculum: the Schaffer collateral (SC) pathway. Ventral CA1 and subiculum receive dense inputs from CA3 (Ding et al., 2020); thus, this method represents one possible way of studying the effect of ghrelin on excitatory synaptic transmission. This experiment revealed that the level of synaptic excitation did not change with acute incubation of ghrelin, contrary to reports of AMPAR insertion in CA3-CA1 synapses with ghrelin incubation (Ribeiro et al., 2014). This may reflect differences in preparation (i.e. hippocampal cultures vs. acute hippocampal slices) and projection-specificity of hippocampal neurons (as I focused on recording from vS^{LH} and vS^{NAc} neurons).

However, one caveat of this technique, as opposed to mEPSC recordings, is that there may potentially be pathway-specificity in ghrelin's effect on synaptic excitation, for example, in the temporo-ammonic pathway or specific long-range inputs (Wee and MacAskill, 2020). Furthermore, with electrical stimulation of inputs, it remains difficult to assess how systemic ghrelin (e.g. delivered via i.p. injection) influences excitatory synaptic transmission in vS, as the technique is unable to establish a baseline level of synaptic excitation strength since the strength of stimulation is adjusted from slice to slice. One potential experiment that could make use of electrical stimulation of inputs would be to compare the level of synaptic excitation in projection-defined vS neurons in a within-slice, pairwise manner, coupled with systemic i.p. injections of ghrelin prior to perfusion. This would be an important experiment to conduct in the future.

Nevertheless, the collective evidence gathered, which demonstrate an extremely sparse mEPSC event rate that does not change with systemic ghrelin injections and a robust effect of systemic ghrelin on mIPSC amplitude, suggests that one main effect of ghrelin is its influence in promoting increased inhibitory synaptic transmission on vS^{NAc} neurons.

5.3.3 GHSR1a signalling in vS^{NAc} is necessary for the encoding of food approach

Using shRNAmir molecular knockdown of the GHSR1a while simultaneously imaging the activity of vS^{NAc} neurons, I found that the behavioural encoding of food approach behaviour is crucially dependent upon GHSR1a signalling within vS^{NAc} neurons. Not only did inhibition of vS^{NAc} neurons at the time of food presentation and food approach require an intact GHSR1a system, knocking down GHSR1a also appeared to decorrelate the encoding of Approach behaviour in vS^{NAc} activity. These results give rise to a number of interpretations. Firstly, GHSR1a signalling is known to support the learned aspects of feeding behaviour, such as meal entrainment (Kanoski et al., 2013; Hsu et al., 2015). While I did not examine how GHSR1a signalling affected this aspect of feeding, the fact that impairing GHSR1a signalling diminished the behavioural encoding of food approach and anticipation even in an innate ('unlearned') behaviour – i.e. spontaneous investigation with a food item – suggests that GHSR1a signalling is constantly required for the expectation of upcoming food consumption. Moreover, these results imply that the encoding of food anticipation in both innate and learned feeding may engage common mechanisms. In the future, it will be important to causally assess the role of GHSR1a in vS^{NAc} neurons in mediating food-seeking behaviour under different hunger states. Lastly, the requirement of normal GHSR1a signalling in the neural activity of vS^{NAc} neurons during food investigation indicates that the vS is actively engaged in some deliberation over the value of food. Given the strong ties of the hippocampal CA1 and subiculum region to value processing (Lee et al., 2012; Jeong et al., 2018; Ólafsdóttir et al., 2015; Bakkour et al., 2019; Hölscher et al., 2003), one interesting possibility is that ghrelin forms part of a fundamental mechanism in forming associations about food-related value with sensory stimuli in the service of higher-order feeding behaviour.

Additionally, while the present findings indicate specificity of ghrelin signalling in vS^{NAc} neurons, it is still possible that GHSR1a may be expressed in other vS populations, such as projections to PFC or lateral septum that are both implicated in feeding behaviour (Sweeney and Yang, 2015; Kanoski et al., 2016). GHSR1a signalling may also be important in vS^{LH} neurons for reasons other than producing feeding, such as salience processing and arousal (Jimenez et al., 2018; Gonzalez et al., 2016). These projections may play complementary roles in feeding behaviour, and their respective roles could be examined in a similar way by employing simultaneous calcium imaging with molecular knockdown. Furthermore, different hippocampal subfields also express GHSR1a, such as DG (Hornsby et al., 2016) and CA3 (Diano et al., 2006; Ribeiro et al., 2014), potentially modulating circuit function throughout the hippocampus. Thus, as a first step, it will be important to establish if there is vS projection-specificity in the expression of GHSR1a by combining retrograde tracing with RNA or protein labelling by in-situ hybridisation or antibody labelling, respectively. Dense recordings of vS incorporating DG, CA3, CA1 and subiculum could also be studied with newly developed probes that are capable of recording large areas of the brain across different states of hunger (Jun et al., 2017).

One potential effect of the shRNAi-mediated knockdown approach, especially over the course of $>$4 weeks of expression *in vivo*, is the changes in network activity due to homeostatic plasticity (Keck et al., 2013; Barnes et al., 2015). Given the GHSR1a signalling promotes increased inhibitory drive onto vS^{NAc} neurons, an expected effect of GHSR1a knockdown would be compensatory reduction in net excitation in vS^{NAc} projections, therefore promoting reductions in network activity. This may explain why I observed reduced salience-related activation of $vS^{NAc::shRNAmir}$ activity in response to food presentation. Given that neural activity was monitored in these experiments using Ca^{2+} imaging, where the baseline activity (fluorescence) is difficult to establish, it is impossible given the current methodological constraints to determine how impaired GHSR1a signalling might have affected network activity. Thus, future work may incorporate electrophysiological recordings of action potential firing to establish how GHSR1a knockdown may account for potential changes in vS network activity.

Another open question regarding the molecular knockdown approach is the extent to which GHSR1a knockdown impaired either ligand-independent or ligand-dependent GHSR1a, or both these mechanisms. Studies have shown that the GHSR1a receptor displays high constitutive activity *in vivo*, and that either i.c.v. cannulation or peripheral administration of GHSR1a inverse agonists, such as substance P, suppresses feeding more than when a control peptide was cannulated (Petersen et al., 2009). Notably, however, Petersen et al. (2009) did not compare this effect on feeding to an i.c.v. infusion of the GHSR1a antagonist D-lys, which precludes a comparison of the effect of GHSR1a inverse agonism with competitive antagonism.

Although interpretation of the results should be limited in view of potential homeostatic plasticity and other compensatory mechanisms that may arise in the vS population activity following GHSR1a knockdown, the current results favour the interpretation that ghrelin-dependent signalling, as opposed to constitutive activity of GHSR1a, is responsible for changes in vS^{NAc} activity across different states of hunger. If GHSR1a signalled purely constitutively in vS^{NAc} neurons, then i.p. injections of ghrelin would not be able to modulate vS^{NAc} activity. This was not the case, since vS^{NAc} activity during Approach was modulated by ghrelin only in $vS^{NAc::Scrambled}$ and not in $vS^{NAc::shRNAmir}$. This suggests that systemic ghrelin requires intact GHSR1a in vS^{NAc} neurons to promote changes in vS^{NAc} activity. Furthermore, the response of vS^{NAc} to chow presentation in the PBS-injected condition was similar between $vS^{NAc::shRNAmir}$ and $vS^{NAc::Scrambled}$ animals. Therefore, it is likely that ghrelin-dependent signalling is required in vS^{NAc} neurons for the inhibition of vS^{NAc} activity, although future studies employing i.c.v. cannulation of inverse agonists with simultaneous recording of vS^{NAc} neurons will be required to fully address this question.

5.3.4 Requirement of vS^{NAc} activity for feeding behaviour on short and long timescales

Given that ghrelin promotes increased inhibitory drive onto vS^{NAc} neurons and that vS^{NAc} activity *in vivo* is low during food approach, I used pharmacogenetic manipulation of vS^{NAc} activity to address whether vS^{NAc} activity was causal in controlling feeding behaviour. At the short timescale, activation of vS^{NAc} increased food inves-

tigation time and inhibiting vS^{NAc} activity increased the probability of transitioning from Approach to Eat behaviour.

Interestingly, this change in feeding behavioural strategy in the short timescale did not alter overall food consumption, which runs counter to findings in manipulations of hippocampal activity (Azevedo et al., 2019; Henderson et al., 2012; Yang et al., 2019; Reed et al., 2018), as well as earlier findings presented in Chapter 4 where the activity of vS^{NAc} during Approach was highly predictive of subsequent food consumption. However, classic experiments involving lesion of hippocampus observed that feeding behaviour – from the point of view of absolute food consumption – is highly variable. While some studies have shown that lesion to hippocampus increases amount of food consumed and body weight (Henderson et al., 2012), others have reported decreased or no change in food consumption patterns (Clifton and Somerville, 1994; Clifton et al., 1998). Instead, what these classic studies seem to demonstrate is that lesions to either hippocampus or nucleus accumbens made animals appear to take 'small but frequent meals', which overall produced no change in total food consumption. This fits well with our findings, where manipulation of vS^{NAc} activity appeared to change the short-term dynamics of eating, for example, transitions between Approach and Eat, while leaving overall food consumption unchanged. Indeed, others have also shown that lateral septum – one main output target of the vS – is specifically involved in food-seeking behaviour and not food consumption (Carus-Cadavieco et al., 2017). It is also plausible that projections other than vS^{NAc}, such as those to prefrontal cortex or lateral septum (Hsu et al., 2018; Sweeney and Yang, 2015; Azevedo et al., 2019), may be more influential on food consumption. Thus, my findings ascribe a role for the vS^{NAc} in food-seeking and anticipation, rather than as a direct controller of food consumption.

What is the function of the hippocampus and NAc in feeding? Many studies have revealed value-based computations in hippocampus, where the hippocampus is engaged during value deliberation and appraisal (Bakkour et al., 2019; Lee et al., 2012), while NAc is involved in updating the values based on actual outcome (Ito and Doya, 2009; Kim et al., 2009). Furthermore, there is almost a separate literature of the hippocampus' involvement in approach-avoidance conflict and anxiety

(Ito et al., 2008; Bannerman et al., 2012; Jimenez et al., 2018), where hippocampus is involved in behavioural inhibition. The findings in this Chapter fits both views, where inhibition of hippocampus promotes transitions to consumption, while activation leads to increased exploration. Therefore, I speculate that hippocampus is involved in incorporating information about food value, and deliberating over the value of food (which includes simulating or predicting the likely value of eating) while attending to food-related stimuli. Such deliberation about food-related value in hippocampus can then be read out by downstream structures like the NAc to produce behavioural outputs and update the rewards based on the actual outcome (Ito and Doya, 2009; Kim et al., 2009; Roitman et al., 2005; O'Connor et al., 2015).

One limitation of the pharmacogenetic experiments was that the specific effect of ghrelin combined with pharmacogenetic manipulation could not be examined. For one, the ghrelin receptor GHSR1a is a G_q-coupled receptor whose signalling cascade intersects with the hM3Dq system, which is also G_q-coupled (Mear et al., 2013). Injecting ghrelin while activating hM3Dq signalling would presumably lead to competing effects, although this effect remains untested. Consistent with this idea, ghrelin-injected animals showed no difference in investigation time or altered transition dynamics with hM3Dq activation (data not shown). Therefore, the experiments shown in this chapter only include vS^{NAc} activity manipulation in the fasted state, which physiologically and behaviourally mimics the ghrelin-injected state. One possible way of surmounting this drawback is the use of optogenetic activation and/or inhibition, which bypasses signalling cascades to directly depolarise or hyperpolarise neurons. Thus, future studies implementing optogenetic manipulation of vS^{NAc} activity would be able to clarify this question.

5.3.5 Source of inhibitory inputs to vS^{NAc} neurons

Given the increased inhibition of vS^{NAc} neurons, one natural question was where this source of inhibitory inputs onto vS^{NAc} neurons originates from. Either local interneurons within the vS, long-range upstream synaptic inputs or a combination of these two sources may provide the inhibitory inputs that in turn depend on the levels of circulating ghrelin. While other hormones such as the female sex hormone oestradiol have been shown to selectively target GABAergic interneurons within the hippocampus (Weiland et al., 1997), it remains unclear whether ghre-

lin also binds to GHSR1a in local hippocampal interneurons to trigger inhibitory plasticity. Preliminary experiments involving imaging of local vS interneurons revealed that vS interneurons do not change their activity levels after i.p. injections of ghrelin (data not shown). It is possible that more specific interneuronal cell-types, such as parvalbumin-expressing and somatostatin-expressing interneurons, may differentially contribute to the neural processing of feeding behaviour. Additionally, extrahippocampal long-range inputs may signal to vS^{NAc} neurons via interneurons in a feedforward (disynaptic) manner.

Another possibility is that long-range inputs may provide the inhibitory inputs to vS^{NAc}. Regions that contain largely GABAergic neurons and have been implicated in feeding behaviour, such as the diagonal band (Patel et al., 2019; Herman et al., 2016; Cassidy et al., 2019), or neuromodulators that may alter $GABA_A$ function, such as dopamine from VTA and dorsal raphe, may be important in conveying hunger-related signals to vS and modulating synaptic transmission. However, little is known about the input connectivity of projection-defined vS neurons. To begin to address this question, the next chapter will build on the existing anatomical circuitry of vS by mapping brain-wide inputs to projection-defined vS neurons (Wee and MacAskill, 2020). This would form a starting point to comprehensively define the upstream inputs to vS and to understand the potential anatomical basis for the heterogeneous behavioural functions of individual vS projections in response to changes in the hunger state.

In conclusion, systemic ghrelin promotes an increased inhibitory drive in vS^{NAc} neurons, and ghrelin receptor signalling is required for this inhibition of the vS^{NAc} circuit, particularly at the time of food approach. In turn, inhibition of this circuit is sufficient to alter feeding behavioural patterns. Together, these studies highlight the central role of ghrelin signalling in modulating synaptic transmission in vS circuitry and its role in food-seeking behaviour.

Chapter 6

Biased connectivity of brain-wide inputs to ventral subiculum output neurons

Hippocampal pyramidal neurons within the ventral subiculum (vS) coordinate diverse behaviours through targeted projections to multiple downstream brain regions. These principal neurons integrate thousands of local and long-range synaptic inputs to compute action potential output, and their inputs are proposed to connect uniquely with each population. To date, there is a lack of information regarding this unique input targeting of each of the vS projection. In this chapter, I provide evidence for the anatomically and functionally biased input connectivity of projection-defined vS neurons, using a combination of retrograde tracing, monosynaptic rabies tracing with brain-wide input quantification, whole-cell electrophysiology and optogenetics. Specifically, I identified heterogeneity in the input connectivity of vS projections to nucleus accumbens (vS^{NAc}), lateral hypothalamus (vS^{LH}) and prefrontal cortex (vS^{PFC}). These results suggest that one potential mechanism for heterogeneity in the behavioural functions of vS neurons, including the projection-specificity of the effect of hunger on vS neurons, may be due to the unique input connectivity of individual vS projections.

Results published: Wee RWS, MacAskill AF. 2020. Biased Connectivity of Brain-wide Inputs to Ventral Subiculum Output Neurons. Cell Rep 30:3644–3654.e6. doi:10.1016/j.celrep.2020.02.093

6.1 Introduction

The hippocampus coordinates a diverse range of behaviours (Strange et al., 2014), from spatial navigation (O'Keefe and Dostrovsky, 1971) to approach-avoidance behaviours (Ciocchi et al., 2015; Jimenez et al., 2018), including reward processing (Ciocchi et al., 2015; Gauthier and Tank, 2018). In addition to heterogeneity present along the long axis (dorsal-ventral) gradient of the hippocampus (Moser and Moser, 1998; Strange et al., 2014; Fanselow and Dong, 2010), another important hypothesis of how the hippocampus might contribute to such diverse behaviours is the existence of heterogeneous principal neurons that differ in their gene expression (Cembrowski et al., 2016, 2018b; Cembrowski and Spruston, 2019; Strange et al., 2014), electrophysiological properties (Kim and Spruston, 2011) and behavioural function (Cembrowski et al., 2016, 2018b; Ciocchi et al., 2015; Jimenez et al., 2018). In particular, distinct hippocampal projections were shown in Chapters 4 and 5 to be differentially sensitive to hunger and involved in feeding behaviour.

The main ventral hippocampal output region, the ventral subiculum (vS), is composed of multiple neuronal populations that send parallel, long-range projections to distinct brain areas, including prefrontal cortex (vS^{PFC}), lateral hypothalamus (vS^{LH}) and nucleus accumbens shell (vS^{NAc}) (Naber and Witter, 1998). These populations are proposed to integrate a myriad of local and long-range inputs (Wyss et al., 1979; Amaral and Cowan, 1980; Strange et al., 2014) to perform their unique behavioural functions (Adhikari et al., 2010; Cembrowski et al., 2018b; Ciocchi et al., 2015; Trouche et al., 2019; Jimenez et al., 2018; Soltesz and Losonczy, 2018). For example, synaptic transmission to vS^{NAc} and vS^{LH} differed depending on ghrelin levels (as described in Chapter 5). Thus, understanding the input connectivity of individual vS projections would be important to clarify the neural basis of heterogeneity of their behavioural function. However, to date, knowledge of such input connectivity of the vS circuitry is lacking. Further, these vS populations are spatially patterned, in particular along the proximal-distal (PD) axis (ranging from the CA1 to the presubiculum borders; Cembrowski et al., 2018b; Kim and Spruston, 2011), and synaptic input varies dramatically across different spatial locations in vS (Aggleton and Christiansen, 2015; Knierim et al., 2014; Cembrowski et al., 2018b; Masurkar et al., 2017; van Groen et al., 2003). Based on this, I hypothesised that

different vS projection populations receive distinct upstream inputs, and reasoned that the identity and amount of their inputs may in turn depend on the spatial location of postsynaptic neurons (Cembrowski et al., 2016, 2018b), their downstream target (Ciocchi et al., 2015; Jimenez et al., 2018), or a combination of these two factors.

To address this hypothesis, I first studied the anatomical organisation of vS^{NAc}, vS^{LH} and vS^{PFC}; I then applied rabies tracing across these different vS projections occupying distinct spatial locations of vS, and obtained a brain-wide map of inputs to these vS subpopulations. I identified quantitative differences in multiple long-range input regions to vS that depended to different extents on the spatial location and projection target of vS neurons, and used channelrhodopsin-2-assisted circuit-mapping (CRACM; Petreanu et al., 2007) to validate that the observed anatomical bias translated into functional bias in one example input. These results clarify the rules of input connectivity to vS that may form an important neural basis for specialised functions of vS projections during behaviour.

6.2 Results

6.2.1 Hippocampal projection populations are topographically organised in ventral subiculum along the anterior-posterior axis

Each vS projection population is thought to occupy a unique spatial distribution in the hippocampus (Kim and Spruston, 2011), and long-range input into hippocampus has been shown to be highly topographical (Aggleton and Christiansen, 2015; Knierim et al., 2014; Cembrowski et al., 2018b; Masurkar et al., 2017; van Groen et al., 2003). Based on these observations, I reasoned that there are potentially two important determinants of input connectivity: spatial location ("where is the cell located in vS?") and projection target ("where does the cell send axons to?").

Thus, I first wanted to determine the spatial distribution of the different projection populations within vS. To study the anatomical organisation of three different projection populations in vS, namely vS^{NAc}, vS^{LH} and vS^{PFC}, I stereotaxically injected the retrograde tracer cholera toxin subunit-B (CTXβ) into PFC, LH or NAc in a pairwise manner (**Figure 6.1A**). The CTXβ is taken up by presynaptic terminals and retrogradely labels the somas of projection neurons that target the injected

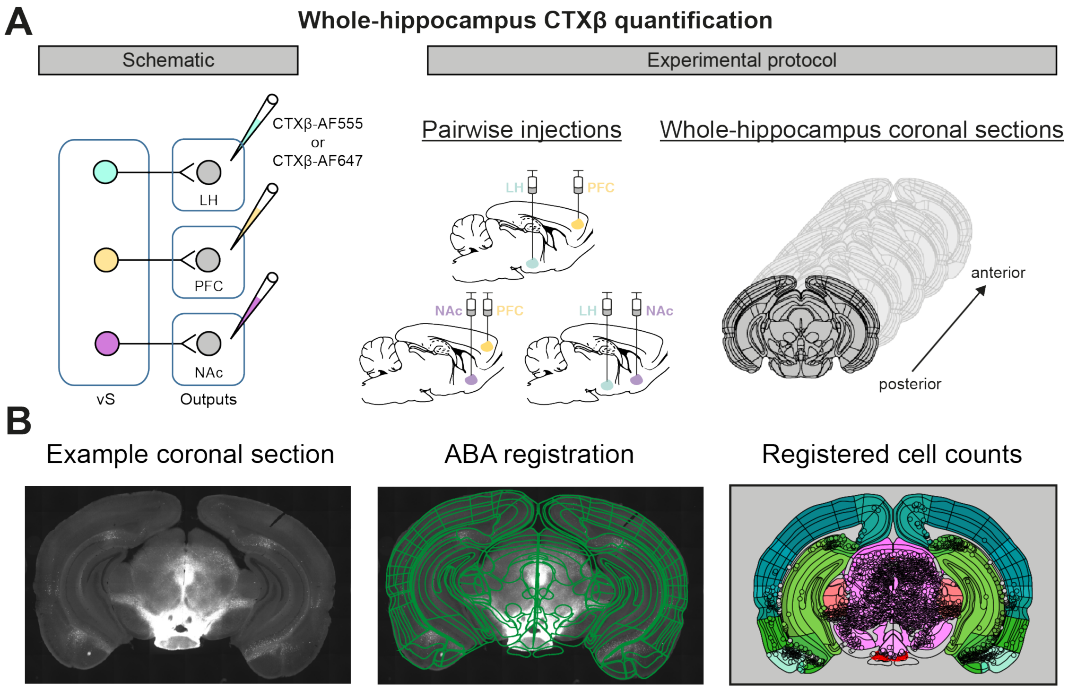

Figure 6.1: CTXβ quantification protocol. (A) *Left*: Protocol for retrograde tracing using CTXβ. CTXβ binds to the ganglioside GM1 receptor and is taken up by the presynaptic terminals; subsequently, it retrogradely labels projection neurons that target the anatomical injection site. CTXβ tagged with Alexa Fluor 555 or 647 (AF555 or AF647, respectively) can be injected in the same brain at different locations to study the anatomical organisation of projection-defined vS neurons. *Right*: To study the organisation of projection-defined vS neurons, CTXβ-AF555 or -647 was injected in a pairwise manner in NAc, LH or PFC. After 2 weeks and brain dissection, coronal brain secions spanning the hippocampus were imaged and analysed. (B) WholeBrain-based neuronal segmentation and anatomical registration to the Allen Brain Atlas (ABA).

site. Next, I collected every second coronal section that spanned the hippocampus (**Figure 6.1A**), and analysed this anatomical dataset by conducting whole-hippocampus cell counts using segmentation and registration of the data to the Allen Brain Atlas (ABA, **Figure 6.1B**, see Methods for analysis pipeline). Briefly, the dataset was analysed using WholeBrain (Fürth et al., 2018), software written in R that enables the semi-automated segmentation of cells and their anatomical registration to the Allen Brain Atlas. The cell counting procedure was applied to 2D sections spanning the hippocampus to allow the reconstruction of the complex 3D structure of the hippocampus (**Figure 6.2A–B**).

After counting all cells within the hippocampus, I first confirmed that vS^{PFC}, vS^{NAc} and vS^{LH} neurons resided predominantly in vS (**Figure 6.2C**), and that the fraction of colocalised cells (neurons that projected to more than one injection site)

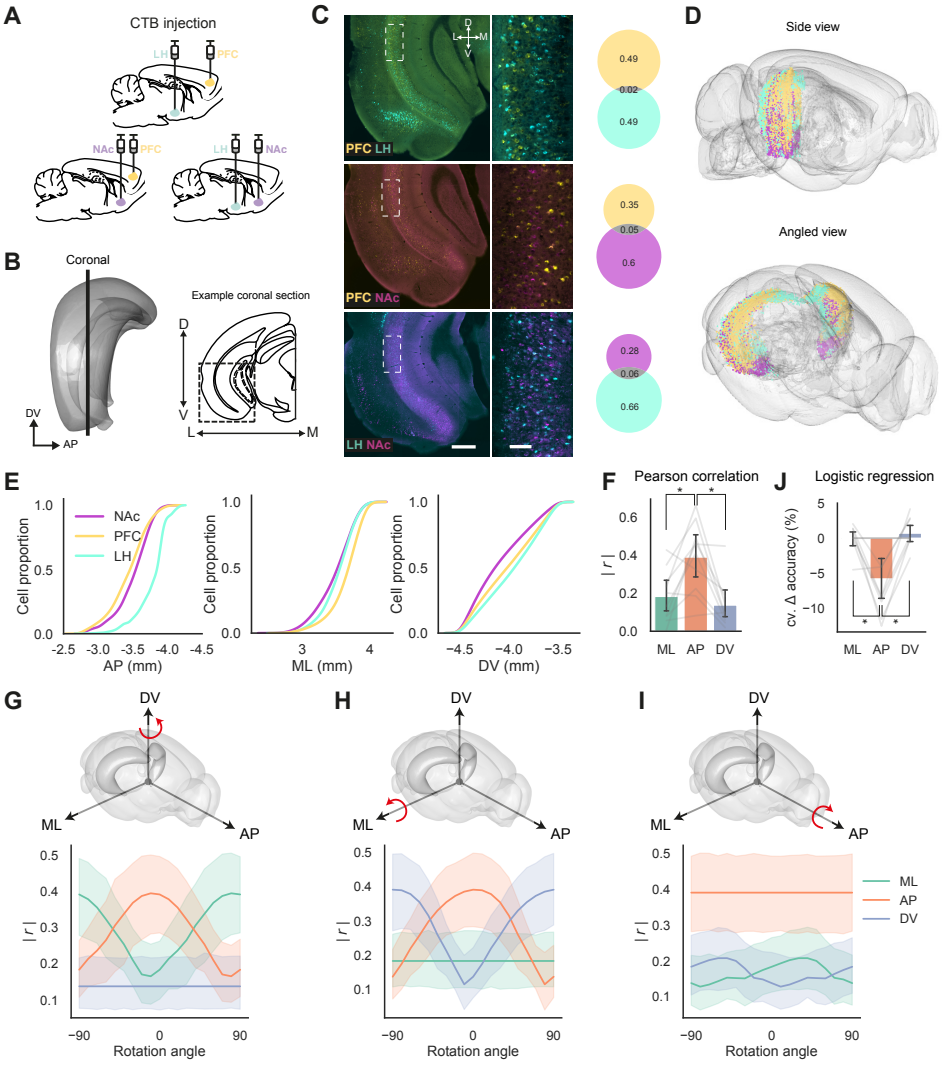

Figure 6.2: Non-overlapping vS neurons occupy distinct spatial sites along the anterior-posterior axis. (A) Experimental protocol of pairwise CTXβ injections into NAc, LH or PFC. (B) *Left*: Side view of a 3D diagram of the hippocampus, with the plane of coronal sectioning shown. *Right*: an example coronal section from the Paxinos atlas with a boxed area indicating the location of retrogradely labelled vS cells. (C) *Left*: Example coronal section images of the vS with retrogradely labelled cells. *Middle*: Zoom-in images of the boxed area from *Left*. Scale bar: 500 µm (right) 50 µm (left). *Right*: Proportion of single and dual-labelled hippocampal neurons. (D) 3D whole-brain diagrams with CTXβ-labelled hippocampal neurons (n = 108,291 hippocampal neurons pooled from 10 hemispheres, 6 animals). (E) Cumulative distribution curves of CTXβ-labelled cells in vH (DV -3.5 to -4.5 mm) along the anterior-posterior (AP), dorso-ventral (DV) and medio-lateral (ML) axes. (F) The highest correlation between projection type and spatial position occurred along AP. (G–I) The correlation between projection type and spatial position was systematically varied by applying a virtual rotation along the (G) DV, (H) ML and (I) AP axes in bins of 10°. Correlation was maximal with AP and varied most with changes in the AP direction. Colors indicate the native DV, AP and DV axes *without* rotation (0°). (J) Logistic regression analysis predicts projection type based on spatial location. Removal of AP as a predictor led to the largest decrease in accuracy. Data are presented as mean ± sem.

ranged from 2 to 6% (Naber and Witter, 1998). The low proportion of colabelling indicated that each projection population largely projected to one downstream target. Using this approach, I found that vS projection populations occupied spatially distinct locations within vS (**Figure 6.2D–E**). The locations of these neurons varied across all three axes (AP, ML and DV), but most notably along the AP axis (**Figure 6.2E**), where vS^{PFC} neurons were located at more anterior locations, vS^{LH} neurons were located at more posterior locations, and vS^{NAc} neurons were spread across the entire range of vS (mean position along AP, vS^{PFC} = -3.46 ± 0.02 mm, vS^{NAc} = -3.55 ± 0.04 mm, vS^{LH} = -3.81 ± 0.03 mm).

As I was interested in studying the organisation of the ventral hippocampus (vH), I focused my analysis on cell counts restricted to the ventral pole of hippocampus (defined as -3.5 to -4.5 mm in DV, **Figure 6.2B–C**). Qualitatively, vS neurons seemed to differ in projection type and have the largest spread most notably along the AP axis compared to DV and ML (standard deviation of cells in mm with bootstrapped 95% confidence interval, AP = 0.171 [0.137, 0.200], ML = 0.089 [0.069, 0.108], DV = 0.121 [0.084, 0.155]; **Figure 6.2D–E**). This larger spread of cell distributions along AP indicated that the AP axis might best correlate with differences in output projection type. To confirm this prediction, I conducted Pearson correlation analysis to quantify how much the projection type of vS neurons covaried with spatial location along each brain axis. I observed that projection type covaried across all axes, but most dramatically with AP position (repeated-measures one-way ANOVA, $F_{2,18}$ = 16.7, p = 0.0001; **Figure 6.2F**).

I next examined how this correlation of projection type along the AP, DV and ML axes changed as the anatomical dataset was virtually rotated along each axis (**Figure 6.2G–I**). Specifically, one axis was held fixed, while allowing the other two axes to shift (e.g. DV held fixed while ML and AP are rotated). If AP was really the axis which best correlated with projection type, then the peak correlation coefficient would occur exactly along the AP axis. This analysis showed that the correlation was indeed maximal along the AP axis before rotation (i.e. at rotation angle = 0°), and that rotating the AP axis led to reductions in the correlation coefficient (**Figure 6.2G–H**). Notably, holding the AP axis constant and rotating the DV and ML axes did not lead to changes in the correlation for either the ML or DV axis (**Figure 6.2I**).

This strong correlation of spatial position of vS neurons with AP position suggested that AP position was a key determinant in the projection identity of vS neurons. I next wondered how much unique information was contained within the AP, ML and DV positions in predicting projection output type. Thus, as a complementary analysis, I trained linear classifiers with information along AP, ML and DV as predictors, and asked how much worse these classifiers performed on classifying unseen data after removing a single axis as a predictor. This decrement in accuracy between the full and reduced models (cv. Δ accuracy) indicates the amount of unique information provided by spatial position along each brain axis in predicting the output projection type of vS neurons. In keeping with the correlation analysis, I found that the spatial position of neurons along AP was most predictive of their output target (repeated-measures one-way ANOVA, within-brain comparison of cv. Δ accuracy across different brain axes, $F_{2,18} = 7.072$, $p = 0.005$, n = 10 hemispheres from 6 brains; **Figure 6.2J**). Taken together, the spatial position along AP appears to best correlate with and predict the output projection type of vS neurons.

6.2.2 The topography of vS projection neurons along AP maps onto the proximal-distal axis

Next, I reasoned that the marked distribution of vS projection populations across the AP axis might be a reflection of the known PD distribution of subiculum projections along the pyramidal cell layer (Cembrowski et al., 2018a). Importantly, the PD axis in vS is oriented approximately along the AP axis (**Figure 6.3A–B**). To visualise the entire PD axis in a single slice, I made horizontal slices of vS with retrogradely labelled projections and observed segregated distributions of vS projections oriented approximately along AP (**Figure 6.3B**). I then quantified the spatial location of vS projections along the PD axis and found that vS projections were organised topographically (**Figure 6.3C**). Specifically, vS^{PFC} neurons were located at more proximal locations, vS^{LH} neurons were located at more distal locations, and vS^{NAc} neurons were spread out across the entire PD axis (**Figure 6.3B–C**). Furthermore, correlation and regression analyses further indicated that projection type varies most along the PD compared to the deep-superficial (DS, which is a approximation of ML in vS) and DV axes (Pearson correlation coefficient, repeated-measures one-way ANOVA, $F_{2,18} = 49.214$, $p = 0.0000$; cv. Δ accuracy, repeated-measures

one-way ANOVA, $F_{2,18}$ = 10.829, p = 0.0008, n = 10 hemispheres from 7 brains; **Figure 6.3D**). Thus, the PD axis is well approximated by the AP axis in vS.

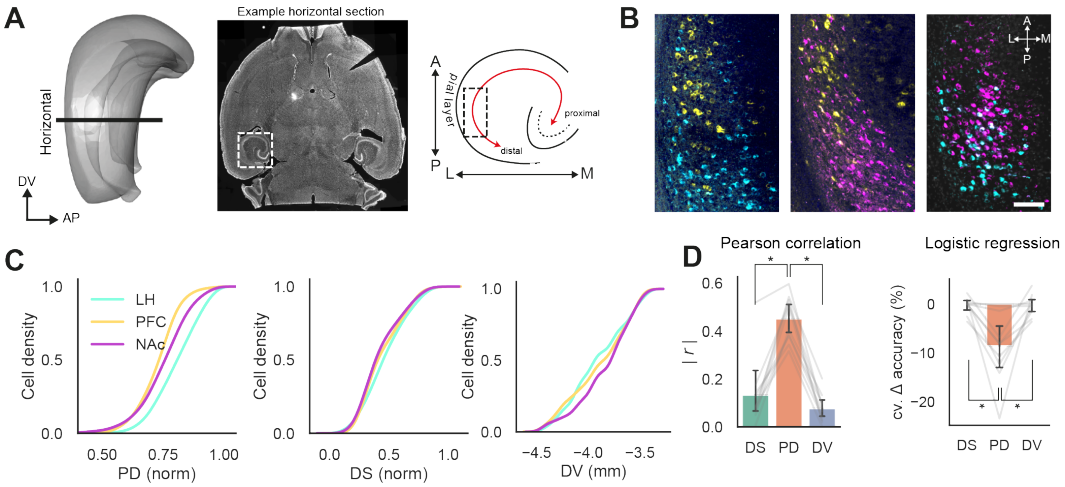

Figure 6.3: Non-overlapping vS neurons occupy distinct spatial sites along the proximal-distal axis. (A) Left: Side view of the 3D hippocampus, with the horizontal cutting plane illustrated. Middle: An example horizontal brain section. The boxed area indicates the location of the vH. Right: outline of vH from Middle, illustrating the PD axis (red). The boxed area is the approximate location of the example images in (B). (B) Example horizontal section images of retrogradely labelled vS neurons. Individual vS projections show distinct spatial patterns most notably along the AP axis. Scale bar: 100 µm. (C) Cumulative distribution curves of cell counts along the proximal-distal axis. (D) Pearson correlation (Left) and logistic regression (Right) analyses analogous to **Figure 6.2F**. The PD axis captures most variation and best predicts the projection type of vS neurons.

One interesting observation of these experiments in the coronal and horizontal planes of vS was that the spatial distributions of the different vS projection populations appeared highly overlapping, including along the AP or PD axis. This is notably different from that observed in dorsal subiculum (Cembrowski et al., 2018a), where a sharp border separates the distinct projection populations along the PD axis. One possibility was that the angle of slicing could have obscured this demarcation between proximal and distal subiculum. To control for this possibility, I carried out linear discriminant analysis (LDA) on the registered, 3D whole-hippocampus neuronal distributions (**Figure 6.4A**). LDA is a supervised dimensionality reduction method that maximises the separability between class groups. When applied to the 3D anatomical dataset, this method unbiasedly identifies a virtual plane (subspace) that best separates the three populations of vS projection neurons. By examining the distribution of neurons in this subspace, I observed that – although there was a clear sub-regional organisation – the spatial distribution of the three populations

in vS still remained highly overlapping (**Figure 6.4A**). Thus, in contrast to dorsal subiculum, vS appears to be organised as a gradient, especially with vS^{NAc} neurons being present at almost every point along the AP axis.

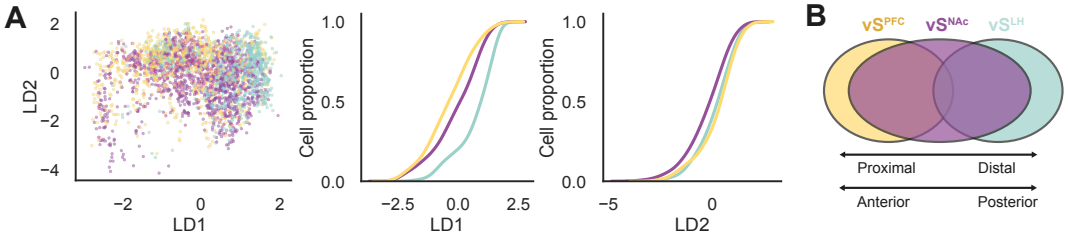

Figure 6.4: Absence of a clear border between vS projection populations.(A) LDA of anatomically registered neurons in vS. *Left*: held-out test dataset projected onto the first and second linear discriminant subspace. The first linear discriminant accounts for 86% of the discriminability across projection populations. Cumulative distribution curves of cells along the first (*Middle*) and second (*Right*) linear discriminant, showing considerable overlap of projection populations. Each dot represents one cell. (B) Schematic of vS topography, where vS neurons are intermingled, vS^{PFC} neurons are located most proximally, vS^{LH} neurons most distally and vS^{NAc} neurons span the area between both vS^{PFC} and vS^{LH}.

Overall, the findings describe an ordered topography of vS projection neurons, where vS^{PFC} neurons are located most proximally and anteriorly, vS^{LH} neurons most distally and posteriorly, and vS^{NAc} neurons occupy the space between vS^{PFC} and vS^{LH} neurons (**Figure 6.4B**); this in turn indicates that vS projection populations are segregated cell types and occupy overlapping yet distinct locations within vS, best separated across the AP axis.

6.2.3 Labelling of hippocampal input dependent on spatial location and projection target

Subsequently, to directly assess the organisation of presynaptic inputs onto each of the three vS projections, I applied tracing the relationship between input-output (TRIO; Beier et al., 2015, 2019; Ren et al., 2018; Schwarz et al., 2015; **Figure 6.5A**). This technique is a rabies virus-based method to trace the monosynaptic inputs from projection-defined neurons. The procedure involved first injecting *AAV2-CAG-retro-Cre* or *AAV2-Syn-retro-Cre* (Tervo et al., 2016) into the output target region to retrogradely express Cre recombinase in vS neurons that project to the target site. Secondly, in the same surgery, a single Cre-dependent helper construct (*AA2/1-synP-FLEX-split-TVA-2A-B19G*, or TVA-G) was injected into vS to express TVA in projection-defined vS neurons. After 2 weeks of TVA-

G expression, G-deleted, pseudotyped rabies virus (*EnvA-RVΔG-H2B-mCherry*) harbouring nuclear-localised mCherry was then injected into vS to infect TVA-G-positive cells. Rabies only infects TVA-G-positive, projection-defined neurons (termed starter cells), and monosynaptically labels the upstream inputs to these starter cells. Following rabies monosynaptic tracing, brain-wide inputs were quantified in consecutive sagittal sections using the WholeBrain software (**Figure 6.5B**). Notably, the sagittal plane was chosen for cell counting to allow accurate quantification of starter cells along the AP axis (the axis of most variation in output-projection type) while allowing for registration to the Allen Brain Atlas (see Discussion).

Importantly, I systematically varied the injection site of TVA-G and rabies within vS (**Figure 6.5A**, see also **Figure 6.6, 6.7B**). Given that I identified the AP axis as the principal brain axis along which vS projection types varied, I chose to stereotaxically inject TVA-G and rabies along a range in the AP axis (from -3.7 to -3.2 mm). This method ensured that, for each projection target, I sampled starter cells (i.e. cells from which rabies virus begins the monosynaptic retrograde tracing) from a range of different AP sites within vS (**Figure 6.6, 6.7A–B**). To quantify the location of starter cells, I determined the centre-of-mass (COM) of the starter cells for a given experiment by calculating their mean AP, DV and ML position. Examining the COM for each experiment, I observed that the distribution of COM along AP, ML and DV across the different experiments were comparable (standard deviation of COM in mm of all experiments pooled together; AP = 0.23; ML = 0.19; DV = 0.28). Despite the similarity in the distribution of COM along the three axes, the AP axis still explained the greatest variance in output projection type (Pearson correlation coefficient of starter cells ± bootstrapped 95% confidence interval after 1000 sampling iterations with replacement, ML = 0.045 ± 0.018, AP = 0.541 ± 0.016, DV = 0.095 ± 0.014). This overall strategy thus provided experimental control over both the starter cell location (COM; by injection location of TVA-G and rabies within vS) and output projection (Projection; by injection location of *AAV2-retro-Cre* in target sites), allowing an assessment of how variations in spatial position of vS neurons (across the AP, ML and DV axes), projection target (across PFC, NAc and LH), and their combination influence input size and identity.

As a series of control analyses, I confirmed qualitatively that the *rAAV-retro-*

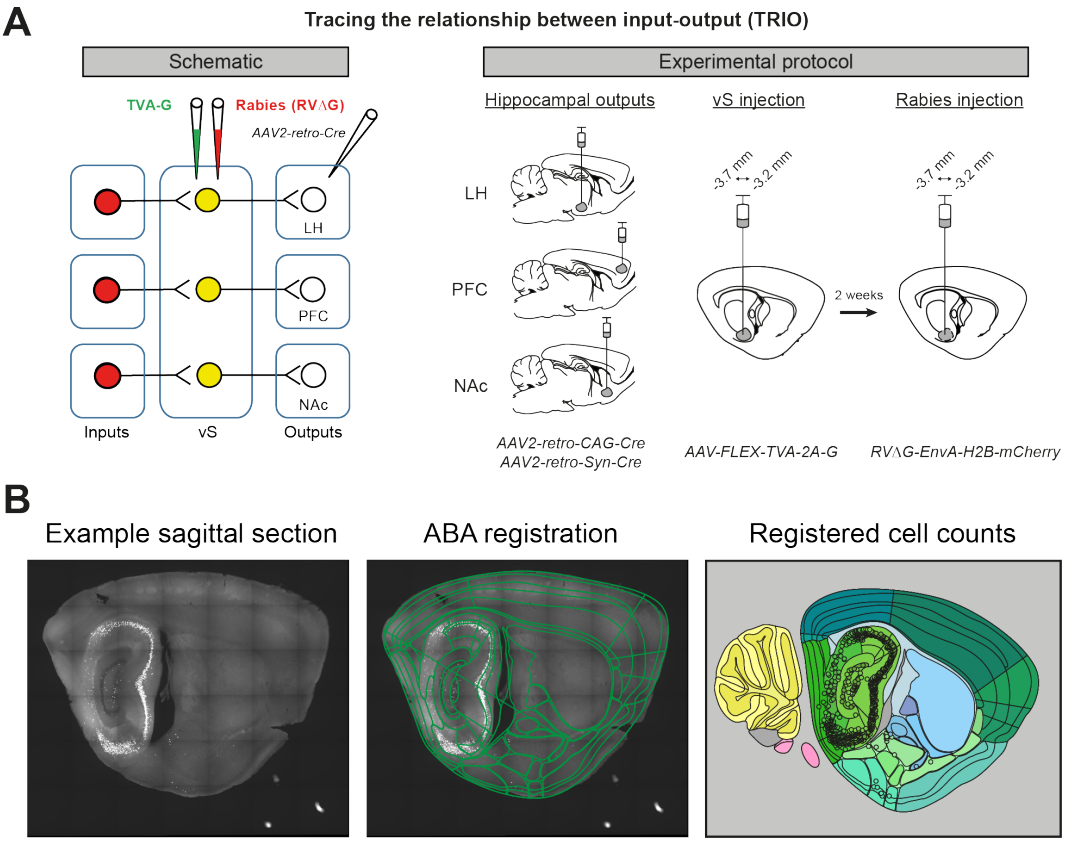

Figure 6.5: TRIO schematic. (A) *Left*: Tracing the input-output relationship (TRIO) schematic. TRIO is a technique to identify the upstream monosynaptic connections of projection-defined neurons. This is achieved through restricting the expression of TVA-G to specific vS projections prior to injection of rabies into the vS. *Right*: To obtain TRIO whole-brain maps for vS^{NAc}, vS^{PFC} and vS^{LH}, the retrograde Cre virus *rAAV2-retro-Cre* was injected into PFC, LH or NAc, and a Cre-dependent, single-construct virus expressing TVA and G was injected into vS. After at least 2 weeks later, rabies was injected into vS for monosynaptic tracing. Note that the coordinates for injection of TVA-G and rabies were varied between -3.2 to -3.7 mm. (B) Analysis pipeline for brainwide quantification using WholeBrain. After preparing serial sagittal brain sections from rabies-injected brains, each section was analysed in a semi-automated manner using WholeBrain (Furth et al, 2018). An example sagittal section is depicted (*Left*), and is anatomically registered to the Allen Brain Atlas plate (*Middle*). Following registration, the annotated cell counts were analysed (*Right*).

Cre injection sites remained localised within the output region of interest (NAc, LH or PFC; **Figure 6.7C–E**) Then, I quantified the starter cell number and spatial distributions in AP, ML and DV for each brain (**Figure 6.7B, F–G**). As expected with rabies virus tracing, there was a linear correlation between the number of starter cells and total number of rabies-labelled inputs (Pearson correlation coefficient = 0.829, $p = 6.38 \times 10^{-6}$; **Figure 6.7F**). I also measured the efficiency of the rabies tracing by analysing the number of inputs innervating one starter cell (total number

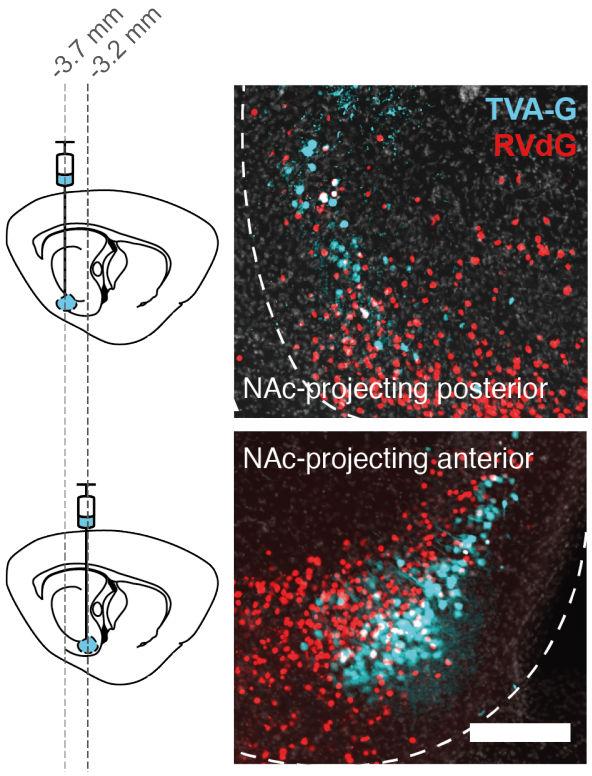

Figure 6.6: Control of starter cell location. Left: Schematic to control for starter cell location by injecting TVA-G and rabies into either a more posterior (AP position: -3.7 mm) or anterior position (AP position: -3.2 mm). Right: Images of distal (top) and proximal (bottom) vS, with starter cell labelling. This strategy allowed us to isolate vS^{NAc} starter cells across different AP positions (see **Figure 6.2** and **Figure 6.3**). Scale bar: 200 µm.

of rabies-labelled inputs divided by the total number of starter cells, i.e. convergent index). I found that individual vS projections received on average similar numbers of inputs (one-way Kruskal-Wallis ANOVA, convergent indices across vS projections $F_{2,18} = 3.769$, $p = 0.152$; **Figure 6.7G**). The COM of starter cells for all experiments were also manually verified to be localised within vS.

Additionally, to exclude the possibility that the rabies virus was indiscriminately tracing from non-Cre-expressing neurons, I performed experiments where either Cre, TVA-G or both Cre and TVA-G were omitted from the injection in the first surgery (**Figure 6.8**); rabies virus was injected into vS in the second surgery for all control conditions. Non-specific rabies-labelling was only detected in the condition where Cre injection into the output site was omitted and TVA-G and rabies were injected into vS (TVA-G+, Cre-, rabies+ condition). In this condition, there were 10.3 ± 4.1 cells mCherry+ cells detected locally within the hippocampus, and no long-range inputs from outside the hippocampus (**Figure 6.8A–B, E**). Crucially,

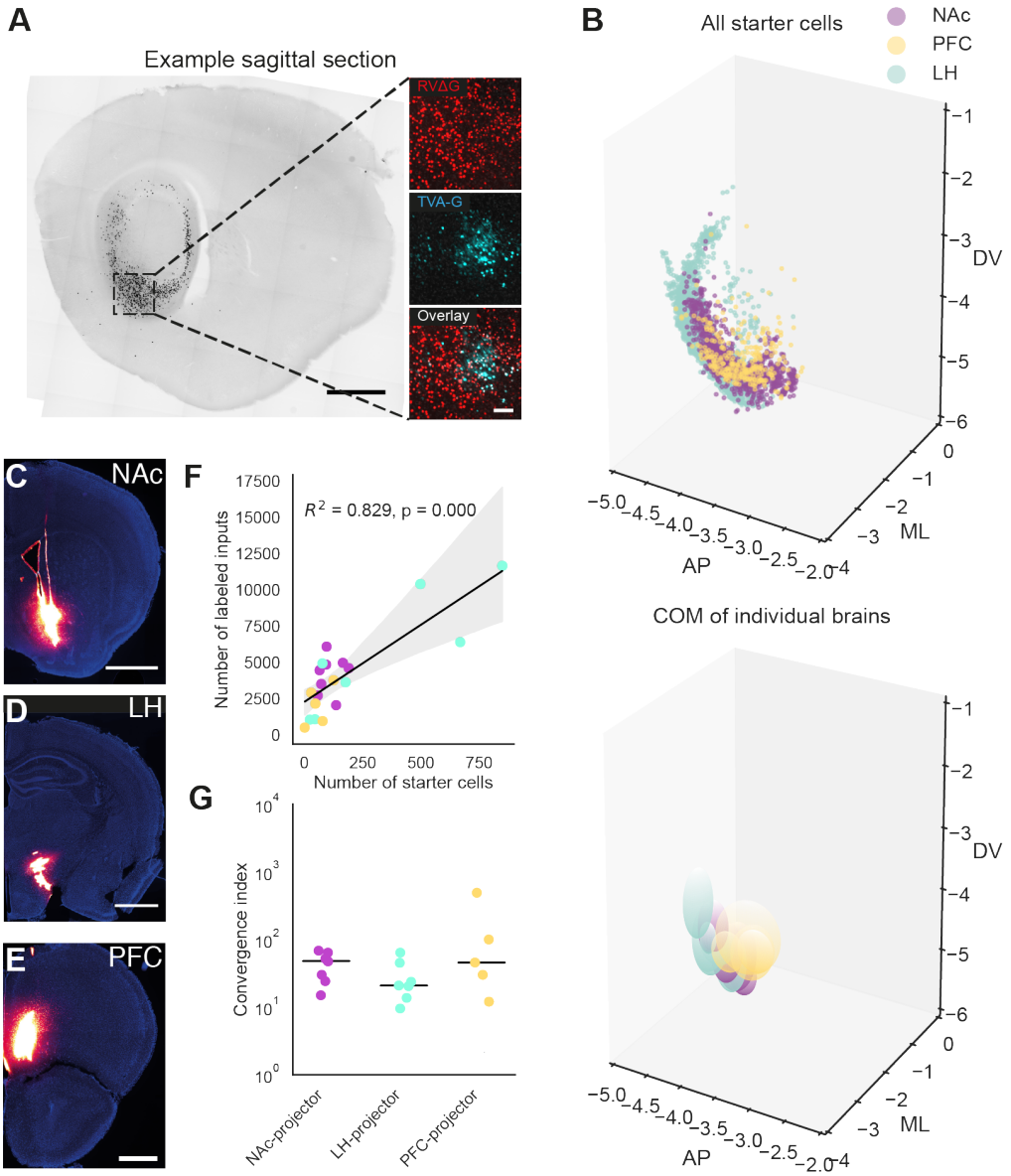

Figure 6.7: Quantification of starter cells. (A) Left: Example sagittal section image with rabies-labelled cells (black) in the hippocampus. Right: Zoom-in images of the boxed area from *Left*. Starter cells (white) colocalise for TVA-G (cyan) and rabies (red). Scale bar: 1000 µm (right), 200 µm (left). (B) 3D scatter plots (*Top*) and geometric COM of individual brain samples (*Bottom*) of starter cells. The geometric COM of individual brains are represented as ellipsoids, where the centre is defined as the mean of the starter cells in AP, ML and DV, and the radii indicate 1 standard deviation of the cell distribution in AP, ML and DV. (C–E) Example injection sites using identical volumes of CTXβ-647 and stereotactic coordinates as for AAV2-retro-Cre injections. All injection sites were localised in the targeted regions. Scale bar: 1000 µm for C and D, 500 µm for E. (F) Scatter plot of the number of starter cells against the total number of labelled inputs counted in each brain sample. Shaded regions represent bootstrapped 95% confidence intervals. (G) Convergent indices (the total number of inputs divided by the number of starter cells) plotted for each projection population. The solid line indicates the median convergent index. Note the log scale.

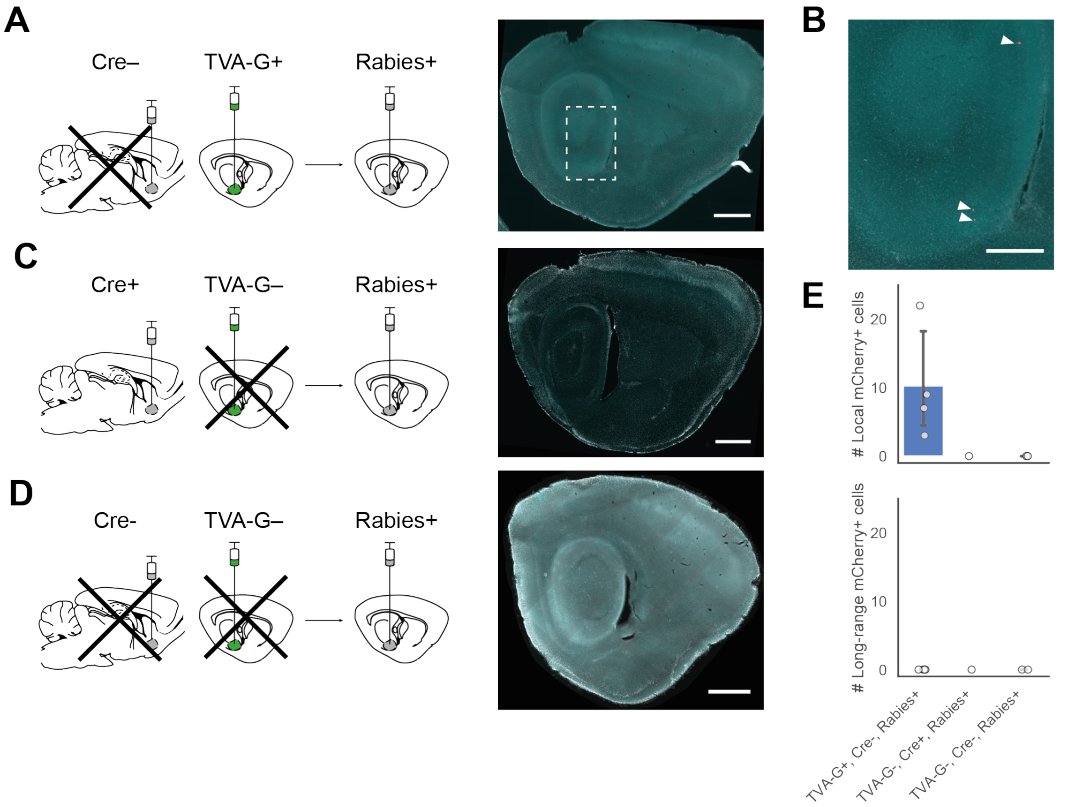

Figure 6.8: TRIO control experiments. (A, C, D) Schematics for control surgeries for TRIO. (A–B) Controls with the single-construct TVA-G virus injected into vS and without AAV2-retro-Cre, with rabies injection 2 weeks later (n = 4 brains). (A) Right: Sagittal brain section from a representative experiment without Cre injection. (B) Zoom-in image of boxed region in (A, *Right*). Arrowheads indicate sparse mCherry+ rabies-labelled cells, likely due to Cre-independent expression of TVA-G and subsequent rabies infection of starter cells. (C–D) No TVA-G (C, n = 1 brain) and no TVA-G and Cre (D, n = 2 brains) controls. No mCherry+ cells were detected in (C) and (D). (E) Quantification of mCherry+ labelled inputs in control conditions. All leaky mCherry+ cells were detected locally within the hippocampal formation, and none were detected in long-range input regions. Bar plots indicate mean ± sem. Scale bars: 1000 µm (A, C, D, *Right*), 500 µm (B, zoomed-in image) The data from one control animal (C) was obtained from experiments done by Karyna Mischanchuk.

there were no local or long-range mCherry+ input cells in the other control conditions (TVA-G-, Cre+, rabies+ and TVA-G-, Cre-, rabies+; **Figure 6.8A,C–E**). These control experiments demonstrate that leaky input labelling by rabies infection was minimal, that input labelling was specific to projection-defined vS neurons and required the presence of both Cre and TVA-G for successful conditional expression.

6.2.4 Brain-wide rabies tracing reveals biased connectivity of vS projection neurons

To quantify input to vS, I implemented the TRIO protocol described above, conducted brain-wide cell counts of rabies-labelled neurons in sagittal sections and registered the data to the ABA (Fürth et al., 2018; Oh et al., 2014). Rabies tracing identified many inputs from a whole host of different regions, including thalamic, striatal, pallidal, cortical, hypothalamic and amygdalar regions (**Figure 6.9, 6.10A**). Examples of regions providing inputs to vS included the nucleus of diagonal band, medial septum, nucleus reuniens, posterior amygdala and preoptic area (**Figure 6.9**). Qualitatively, I observed that there were variations in labelling from these regions when comparing tracing data across different projection targets or positions along the AP axis. Subsequently, I quantified at a coarse level the number of inputs arising from broad anatomical regions. The majority ($\sim$90%) of direct inputs to all vS projection types and spatial locations arose locally within the hippocampal formation, while the remainder came from extrahippocampal sources (**Figure 6.10A**).

Next, I wanted to quantitatively investigate whether long-range input onto vS neurons depended on either projection target (PFC, LH or NAc), spatial location (COM in AP, ML and DV) or their combination (**Figure 6.10B**). To disambiguate the effects of projection and COM on the amount of rabies-labelled input, I used ordinary least-squares (OLS) regression to model the detected rabies-labelled inputs as a linear combination of projection and COM (**Figure 6.10B**). For this OLS modeling analysis, I focused on the brain regions that contributed more than 1% of extrahippocampal input to vS (15 brain regions), and tested the ability of each model to predict the percentage of total extrahippocampal input from that region. Using this method, I found that input from medial preoptic area (MPO), posterior amygdala (PA), nucleus reuniens (RE) and paraventricular thalamus (PVT) provided quantitatively different input sizes to vS depending on either COM, output projection or both predictors (ANOVA of linear models, corrected with the Benjamini-Hochberg method for false-discovery rate < 0.05; MPO, $F_{5,14} = 5.502$, $p = 0.026$; PA, $F_{5,14} = 6.424$, $p = 0.026$; PVT, $F_{5,14} = 4.891$, $p = 0.030$; PVT, $F_{5,14} = 6.023$, $p = 0.026$; $n = 20$ mice; **Figure 6.10C**).

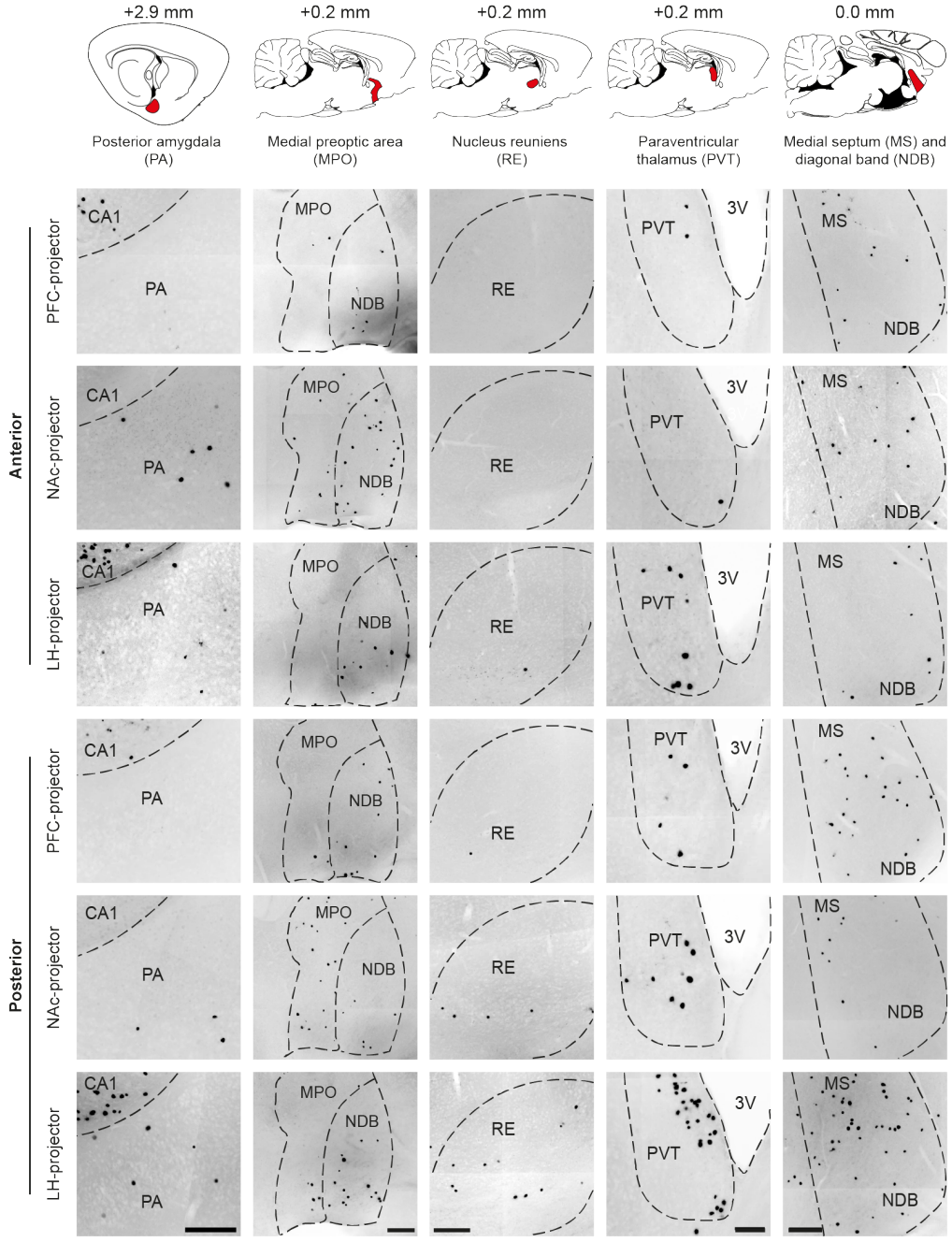

Figure 6.9: Representative long-range monosynaptic inputs to vS neurons by projection type and the centre-of-mass (COM) of the starter cells along the AP axis. Classification of starter cells into anterior and posterior groups was based on the rank order of COM along the AP axis. Approximate sagittal planes are displayed with red-shaded boxes indicating the estimated locations of the corresponding images. The numbers above the sagittal plates are the distance (medial-lateral) from bregma. Note that the COM of the 'posterior' PFC-projector example resides in the anterior 50% percentile of the COM AP, but is the most posterior example available for the PFC-projectors. Error bars represent sem. ac: anterior commissure; 3V: third ventricle. Scale bars: 200 µm (all input regions except PVT); 100 µm (PVT).

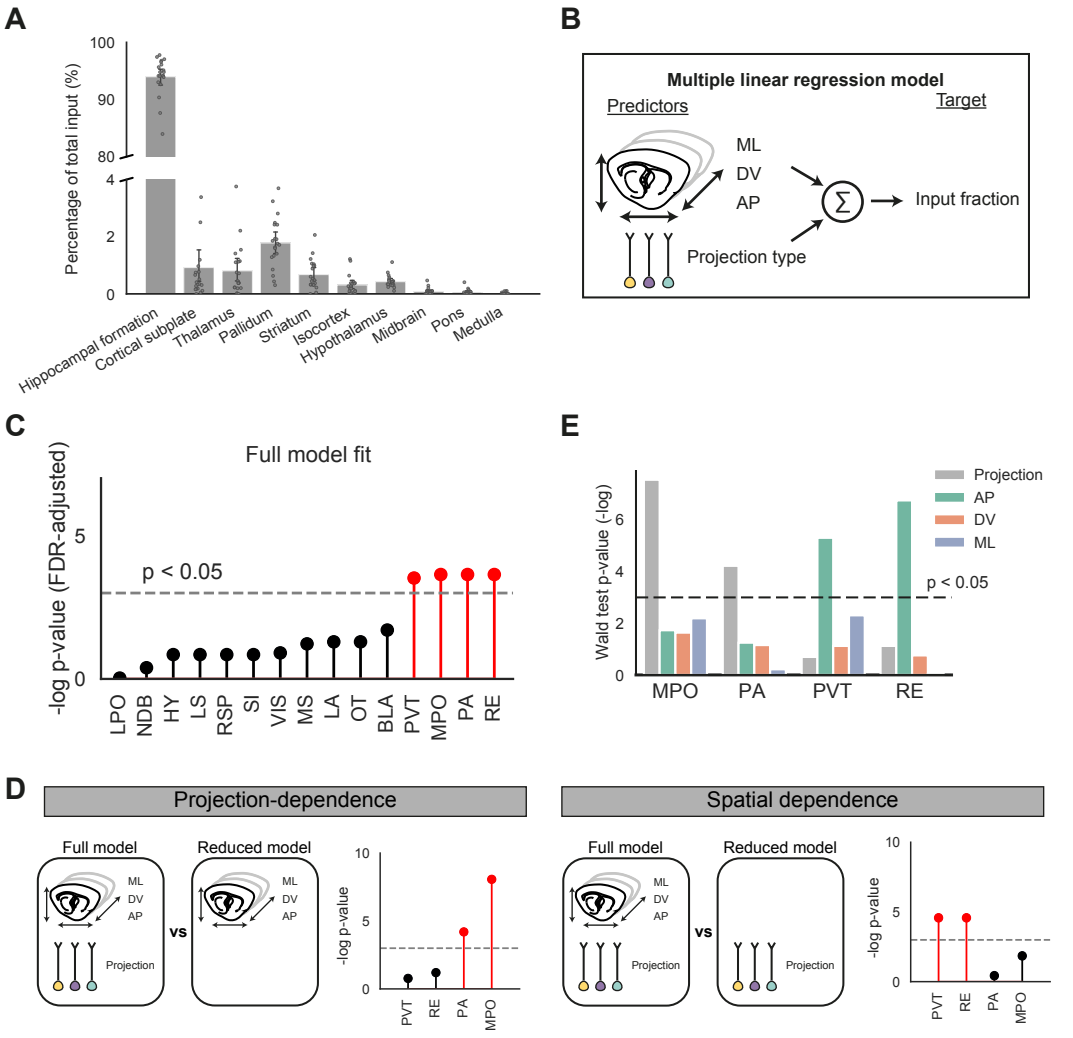

Figure 6.10: TRIO of vS output neurons reveals projection and spatial bias of inputs. (A) Bar plot illustrating the overall inputs from coarse (parent) anatomical structures normalised to the total number of inputs counted in a single brain. Note the break in the y-axis. (n = 20 brains) (B) Schematic of linear regression analysis. Linear models were constructed with COM (ML, AP and DV) and Projection as independent predictors and the extrahippocampal input fraction (log-transformed) as the dependent variable. (C) Full model fits were assessed by computing the F-statistic of full models containing COM and projection as predictors and correcting the associated p-values for multiple comparisons (see Methods). Inputs from PVT, MPO, PA and RE (red) remained statistically significant after correction. (D) Likelihood ratio tests that compare full models (containing both COM and Projection as predictors) to reduced models (containing either COM *or* Projection as a single predictor). (E) The statistical significance of each predictor was tested using the Wald test. MPO and PA are highly projection-specific, signified by a statistically significant Projection predictor. By contrast, PVT and RE inputs are highly spatially dependent with a statistically significant COM (AP) predictor.

To directly investigate the relative contribution of projection type or COM on the amount of RE, PVT, MPO and PA inputs, I compared single-predictor (projection *OR* COM) reduced models with full (projection *AND* COM) models using likelihood ratio

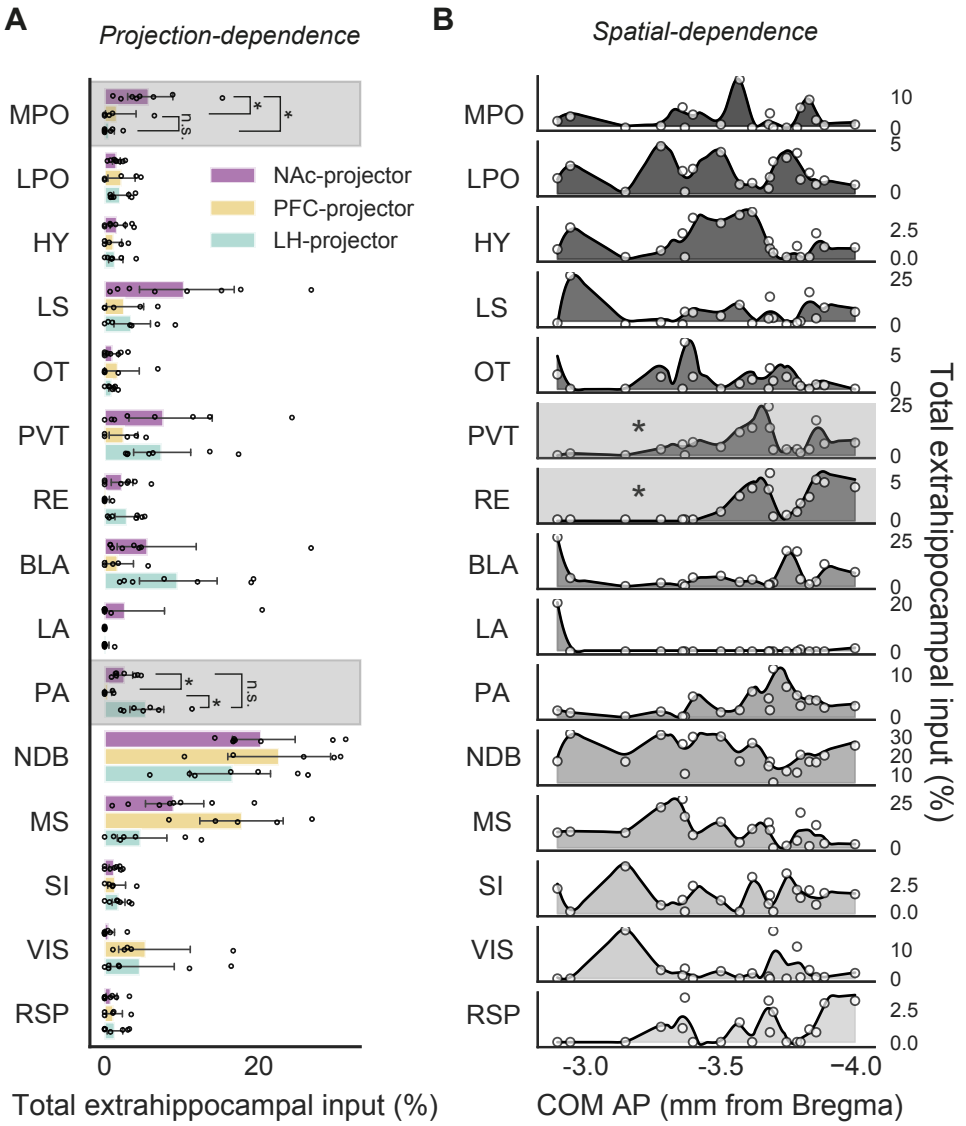

Figure 6.11: Quantification and posthoc testing of vS extrahippocampal inputs. (A) Quantification of extrahippocampal long-range monosynaptic inputs. The number of inputs from a brain region is expressed as a percentage of the total number of extrahippocampal inputs (i.e. inputs from outside the hippocampal formation). Shaded boxes indicate input regions with significant multiple linear regression model fits. Statistically significant model fits were followed up with post-hoc pairwise Tukey multiple comparisons (*$p < 0.05$). (B) Same dataset as in (A) where the input fractions are plotted as a function of COM along the AP axis. The shaded continuous line represents the smoothed input density. The inputs from RE and PVT (*) resulted in model fits with a statistically significant COM AP coefficient.

tests (**Figure 6.10D**). Using this approach, I found that MPO and PA innervated vS dependent solely on the projection target of the postsynaptic neuron, while RE and PVT inputs were dependent on COM (**Figure 6.10D**). More specifically, I also investigated which brain axis – AP, ML or DV – was important for the spatial dependence of PVT and RE inputs, and found that both RE and PVT inputs depended mostly on

COM along the AP axis (**Figure 6.10E**). Importantly, the AP axis emerged as the most important determinant in rabies-labelled input despite the comparable spread of starter cell distributions along AP, ML and DV across experiments (**Figure 6.7B**). Post-hoc testing on the significant model hits revealed that MPO input selectively innervated vS^{NAc} neurons; PA input selectively targeted vS^{LH} and vS^{NAc} neurons; while RE and PVT input targeted vS^{LH} and vS^{NAc} neurons only at posterior locations within vS (**Figure 6.11A–B**).

Subsequently, I obtained a qualitative description of all extrahippocampal inputs supplying at least 0.25% input to vS (35 regions, **Figure 6.12A**) and their relative dependence on COM or projection (**Figure 6.12B–D**). To probe the relative importance of COM and projection on the amount of extrahippocampal input, I compared models containing only COM ('COM model') or projection ('Projection model') information by computing the Bayesian information criterion (BIC) value for each type of model (**Figure 6.12B**). The magnitude of the difference in BIC (ΔBIC) values provides an indication of the likelihood of the model given the observed data. In this analysis, more negative BIC values indicate a higher projection dependence whereas more positive BIC values represent a higher COM dependence. Sorting input brain regions by the ΔBIC revealed a wide range in the relative dependence of different synaptic input on both COM and projection identity (**Figure 6.12C**). This analysis also revealed that 29% of brain regions (10/35) are biased towards COM ($\Delta\text{BIC} > 2$), 37% of regions (13/35) are biased towards projection identity ($\Delta\text{BIC} <$ -2), and 34% of regions (12/35) are equally dependent on COM and projection identity ($-2 < \Delta\text{BIC} < 2$; **Figure 6.12C–D**). By grouping input brain regions into coarser anatomical groups, this analysis also yielded general principles of input connectivity: thalamic inputs such as PVT, RE and anterodorsal thalamic inputs to vS tended to be COM-dependent, while amygdalar, hypothalamic and pallidal inputs such as MPO, PA, MS were more projection-dependent (**Figure 6.12D**).

For spatially-dependent inputs like PVT and RE, the amount of rabies-labelled inputs was highest when the COM was located more posteriorly, and lowest where the COM was positioned more anteriorly. This suggested that the axonal targeting of these inputs within vS might also follow an AP gradient. I hypothesised that for such inputs, the amount of axonal labelling would be strongest in the posterior

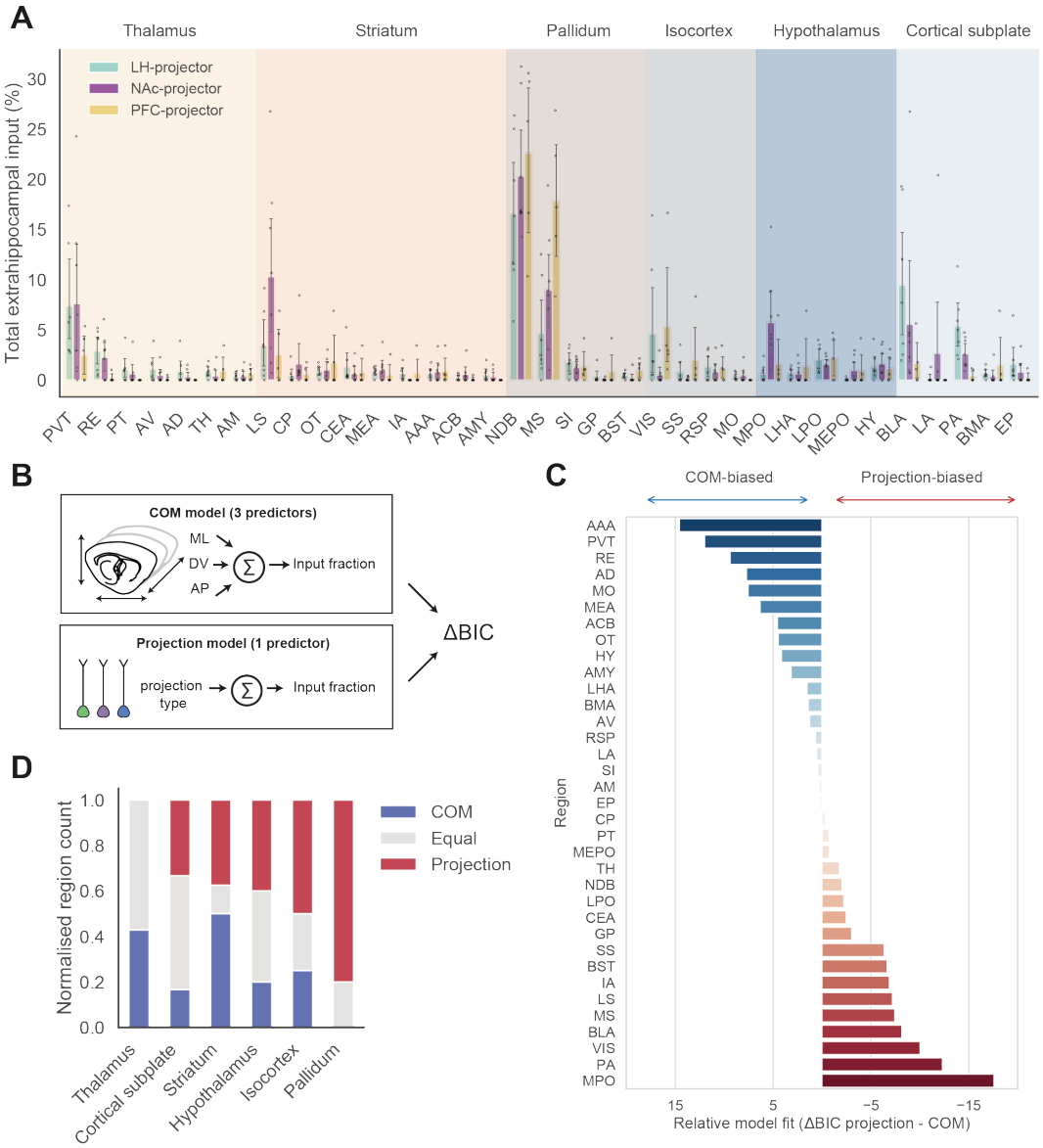

Figure 6.12: Projection and spatial dependence analysis of vS inputs. (A) Unthresholded extrahippocampal inputs. Data for long-range inputs from 35 extrahippocampal brain regions by each projection population. Note that the dataset was preprocessed by including only input regions that generated at least 0.05% of extrahippocampal input. Data expressed as a percentage of total extrahippocampal input cells counted in a single brain sample. Bar plots indicate mean ± sem. (B) Schematic of single-predictor linear models where COM in all 3 brain axes of starter cells or projection identity were used as predictors, and the extrahippocampal input fraction normalised to total input was used as the target variable for each brain region. The two competing models were then compared with BIC as a measure of goodness-of-fit. (B) For each of 35 brain regions that provide input to vS, the relative likelihood (Bayesian information criterion, or BIC, score) was calculated for each the single-predictor COM and projection model, and the absolute difference between these values the BIC of the competing models were plotted as a measure of goodness-of-fit. The more positive the BIC, the more the input size of a given brain region is biased towards COM, while the more negative the BIC, the more the input size is biased towards projection type. Inputs vary widely on their relative spatial- and projection-dependence. (C) Anatomical input regions classified as COM-, projection-, or equally COM- and projection-dependent based on ΔBIC value. Regions with ΔBIC $<$-2 were classified as projection-dependent, -2 $<$ ΔBIC $<$ 2 as equally projection- and COM-dependent, and ΔBIC $>$ 2 as COM-dependent. Thalamic inputs such as PVT and RE tended to be COM or equally dependent, whereas pallidal inputs tended to be projection-dependent.

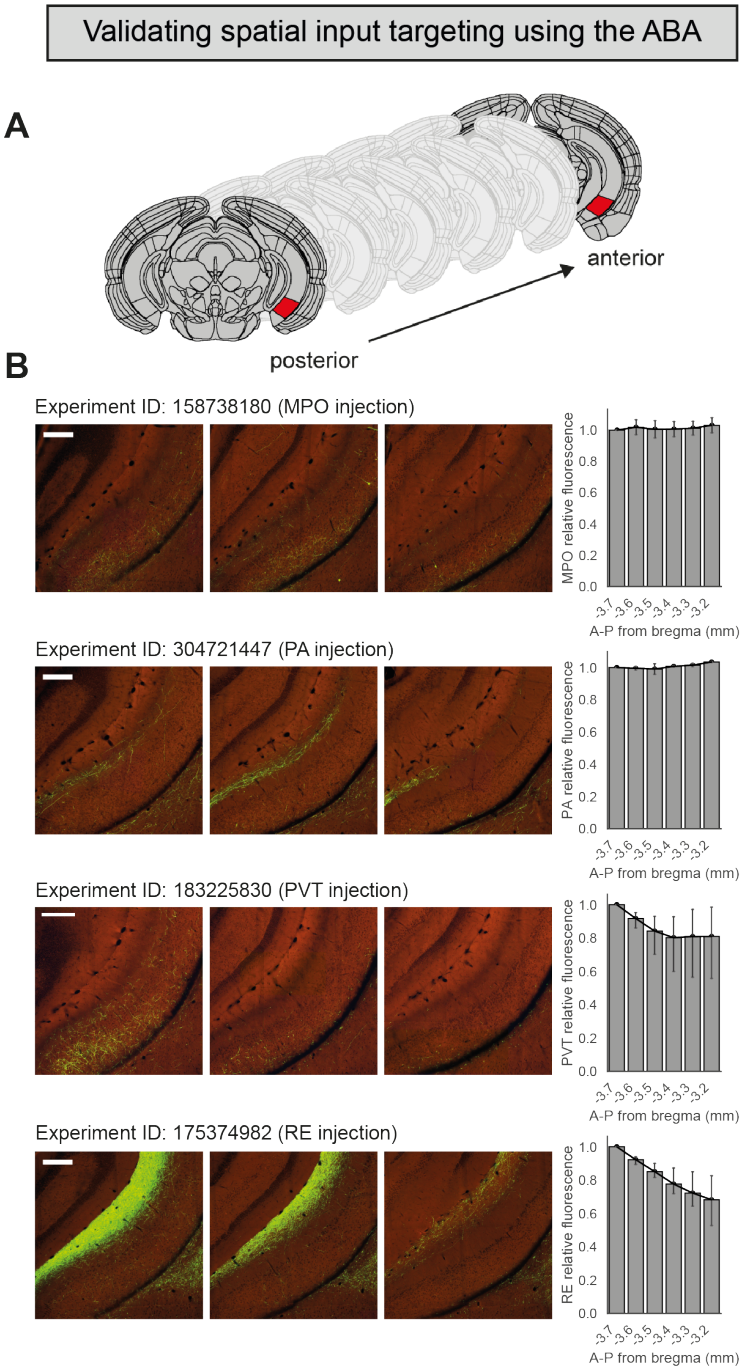

Figure 6.13: 1 Allen Brain Atlas validation of spatial targeting of inputs. (A) Analysis of anterograde tracing experiments from the ABA. Six coronal sections, spaced 100 µm apart and covering the vS region, were downloaded from the ABA and analysed. The region shaded in red were the approximate ROIs which were used to compute the relative intensity of axonal projections. (B) Left: Example consecutive image series (depicting every second section of the six sections) for each experiment showing the vS region. Scale bar: 100 µm. Right: Relative fluorescence intensity of axonal projections in the vS, normalised to the posterior-most section. MPO and PA injection experiments (n = 3 and n = 2 brains, respectively) show consistent axonal projection density across the six sections, while the RE and PVT injection experiments (n = 3 brains each) display prominent spatial targeting along the AP axis. Error bars: 500 µm. Bar plots represent mean ± sem.

vS and weakest in anterior vS, whereas projection-dependent inputs such as PA and MPO would have negligible differences in axonal targeting along the AP axis. Testing these predictions would require anterograde axonal labelling experiments from many brain regions; these are fortunately already available on the Allen Brain Atlas Mouse Connectivity database. Therefore, to test these predictions of the rabies tracing data, I analysed anterograde labelling experiments from different input regions available from the ABA (**Figure 6.13A–B**). Coronal sections of vS were downloaded from approximately -3.7 mm to -3.2 mm (six 100 µm sections) and the fluorescence intensity in vS was analysed. In keeping with the predictions of the TRIO experiments, I observed qualitatively strong spatial dependence of axonal innervation across the AP axis for RE and PVT, but not for MPO or PA input (**Figure 6.13B**). In particular, RE and PVT axonal fluorescence was highest in posterior vS and lowest in anterior vS, whereas fluorescence changed minimally across the AP axis for inputs from MPO and PA. This analysis thus provides a further validation of the TRIO method in detecting the spatial dependence of brain-wide inputs.

Overall, the rabies tracing dataset has identified brain-wide regions that project to vS, including quantitatively biased inputs from MPO, RE, PVT and PA that depend differentially on the location and projection identity of the postsynaptic neuron.

6.2.5 Biased nucleus reuniens input to hippocampal projection neurons

The RE is a thalamic structure that is essential for a range of functions, from contextual learning (Xu and Südhof, 2013) and goal-directed behaviour (Ito et al., 2015) to salience encoding and decision-making (Salay et al., 2018; Vertes, 2006). The circuit model underlying these functions is proposed to be a reciprocal vS-PFC-RE-vS loop, where RE links the PFC and hippocampus (Dolleman-van der Weel et al., 2019; Vertes, 2006). Specifically, it is assumed that, within the hippocampus, vS^{PFC} neurons receive and integrate RE input and transmit these signals back to PFC. Yet surprisingly, I observed that the RE input was anatomically biased to avoid vS^{PFC} neurons (Mann-Whitney U test, U = 12.0, p = 0.013, n = 5 vS^{PFC}, n = 15 non-vS^{PFC}; **Figure 6.14A**).

This finding runs counter to classic models of the vS-PFC-RE-vS circuit where RE functions as a relay between PFC and hippocampus via long-range input to

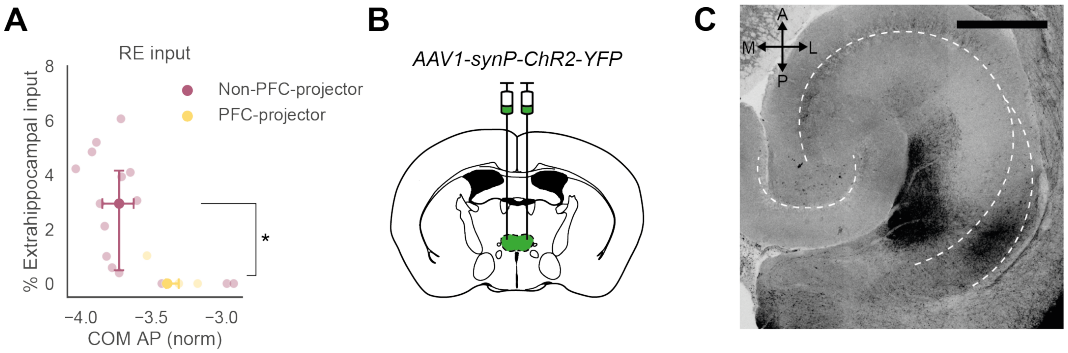

Figure 6.14: Nucleus reuniens inputs to vS projection neurons are functionally biased. (A) Extrahippocampal fractions of RE inputs as a function of COM and projection population. Non-PFC projectors (i.e. pooled vS^{NAc} and vS^{LH}) had overall higher RE inputs than vS^{PFC}. Data points and error bars indicate the median and inter-quartile range. (B) AAV expressing ChR2 under the synapsin promoter was injected bilaterally into RE. (C) Confocal image of a horizontal section of hippocampus. RE axons expressing ChR2 target distal regions of vS.

vS^{PFC} projections (Dolleman-van der Weel et al., 2019; Vertes, 2006). I thus sought to confirm this anatomical bias using channelrhodopsin-2-assisted circuit mapping (CRACM) to ensure that this result was not due to methodological constraints such as viral tropism (Luo et al., 2018) or activity-dependence of viral tracing (Beier et al., 2017; see Discussion). From my tracing data, I hypothesised that RE input was spatially biased, i.e. RE input targets posterior areas where vS^{PFC} neurons are not abundant (COM). In addition, I wanted to ask if RE input formed synaptic connections with the few vS^{PFC} neurons in the most posterior locations (Projection).

To conduct CRACM of RE input, I injected *pAAV-hSyn-hChR2(H134R)-EYFP* to express ChR2 in RE (**Figure 6.14B–C**) and, in the same surgery, red and green retrobeads into either NAc and LH or PFC and LH (**Figure 6.15A,E**). After 2 weeks, acute horizontal slices of vS were prepared for whole-cell electrophysiology. In these slices, I found that ChR2+ axons emanating from RE were observed most densely in the distal, posterior region of vS (**Figure 6.14C**), consistent with the spatial dependence of the rabies tracing data. Under visual guidance, I then targeted pairs of retrogradely labelled neurons within the axon-rich distal region vS to record light-evoked postsynaptic currents using brief pulses of blue light. By recording from pairs of neighbouring neurons within the same slice, this approach allowed me to directly compare the relative strength of RE inputs across projection populations while controlling for spatial position, ChR2 expression and light

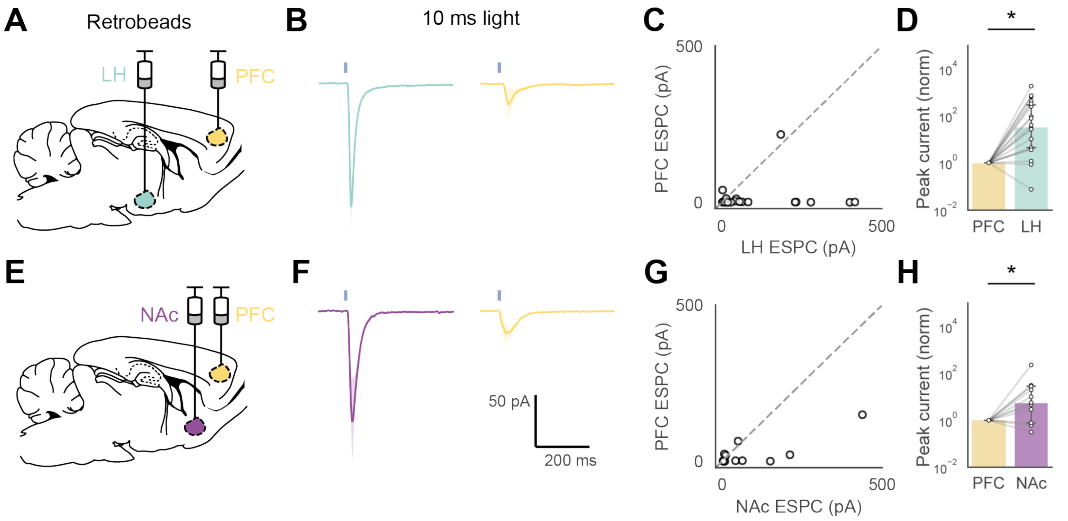

Figure 6.15: (A, E) In the same surgery after ChR2 injection into RE, red and green retrobeads were injected into either NAc and PFC or LH and PFC. (B, F) Light-evoked excitatory postsynaptic currents in pairs of (B) vS^{LH} and vS^{PFC}, or (F) vS^{NAc} and vS^{PFC}. All data represent responses to 10 ms of blue light. Solid line: mean response, shaded region: SEM. (C, G) Scatter plots of light-evoked photocurrents from cell pairs. (D,H) Normalised EPSCs scaled to the photocurrent elicited in vS^{PFC}; the relative amplitudes of light-evoked photocurrents are higher in vS^{LH} and vS^{NAc}. Bar plots and error bars indicate median and 95% bootstrapped confidence intervals.

intensity. I observed that excitatory RE input was indeed much weaker onto vS^{PFC} neurons, whereas it strongly targeted neighbouring vS^{LH} (Light-evoked response in LH-projectors = 123.64 ± 33.46 pA, and PFC-projectors = 18.11 ± 12.91 pA; Wilcoxon signed-rank test, pairs of recorded vS^{PFC} and vS^{LH} neurons, W = 4.0, p = 3.86 × 10^{-4}, n = 18 pairs from 3 animals) and vS^{NAc} neurons (Light-evoked response in NAc-projectors = 96.34 ± 42.10 pA, and in PFC-projectors = 27.52 ± 13.95 pA; Wilcoxon signed-rank test, pairs of recorded vS^{NAc} and vS^{LH} neurons, W = 6.0, p = 0.016, n = 11 pairs from 3 animals; **Figure 6.15B–D, F–H**). Overall, these results demonstrate a functional bias of RE inputs away from vS^{PFC} and towards both vS^{LH} and vS^{NAc}, thus describing a more complex connectivity pattern than the current model of a vS-PFC-RE-vS circuit loop.

6.3 Discussion

Using a combination of retrograde tracing, conditional rabies tracing and optogenetics with whole-cell electrophysiology, the data presented in this chapter demonstrate that the vS output circuitry is comprised of projection-specific, topographically organised populations that receive a range of local and long-range inputs. In turn,

the targeting of these inputs depends to different degrees on the spatial position and projection target of the postsynaptic vS neuron.

6.3.1 Topography of vS projections

I used CTXβ retrograde tracing to reveal the distribution of neurons in vS that project to PFC, NAc and LH and confirmed previous findings that suggest that there are unique populations of neurons in vS that project to each downstream region (Naber and Witter, 1998). However, due to the efficiency of retrograde labelling, significant proportions of neurons projecting to multiple downstream sites cannot be definitively ruled out. For example, if a given retrograde tracer injection labels only a small fraction of the total number of projection-defined neurons, then it is possible that dual-labelled neurons may be under-sampled. Using single-neuron tracing and whole-brain imaging, Winnubst et al. (2019) recently showed that many neurons in dorsal subiculum do indeed project to multiple downstream areas (Winnubst et al., 2019). This multi-region targeting motif appears to also apply in vH (Ciocchi et al., 2015; Kim and Cho, 2017). Thus, an interesting future direction would be to clarify the extent of projection specificity of individual vS neuronal projection neurons.

Consistent with previous findings, I also observed that different vS projections were organised topographically. vS^{PFC} neurons were located most anteriorly and proximally (along AP and PD, respectively), vS^{LH} were found posteriorly and distally, and vS^{NAc} were widely distributed throughout vS (Kim and Spruston, 2011; Cembrowski et al., 2018b). Anatomical analysis conducted in both coronal and horizontal sections demonstrated that this AP gradient is most likely due to the previously described divergence along the PD axis of the pyramidal cell layer (Cembrowski et al., 2018b). Notably, these results are incongruent with findings from dorsal subiculum (dS). Specifically, Cembrowski et al. (2018a) showed that dS neurons projecting to NAc and hypothalamus occupy the proximal and distal regions of subiculum, respectively, with a sharp border separating the two subpopulations. By contrast, I found that vS^{NAc} and vS^{LH} occupied vS in a gradient-like fashion, with a region of considerable anatomical intermingling between the two vS populations. Even with linear discriminant analysis, which found the best plane to anatomically separate the vS projections, the vS projections were still highly intermingled. These

results highlight that the dS and vS may represent fundamentally distinct circuitries, above and beyond their DV locations. This is consistent with recent work that found that the vS complex is formed mainly by prosubiculum, whereas the dS complex is formed mainly by subiculum (Ding et al., 2020). Subiculum and prosubiculum, in turn, have distinct input-output connectivity and gene expression patterns, underscoring the distinctions between vS and dS. Therefore, findings in dS may not necessarily map well to vS given their inherent distinctions in genetic expression, connectivity and function.

6.3.2 Biased input to vS based on projection identity and spatial location

The topography of vS projection neurons within vS prompted us to investigate the contribution of spatial location on the types of afferent inputs that each vS projection receives. To this end, I experimentally varied the injection coordinates during rabies tracing, which enabled me to sample starter cells from different COM positions (**Figure 6.10B**). This strategy allowed me to investigate the relative contribution of both projection identity and COM of vS neurons on the type and amount of rabies-labelled inputs.

Whole-brain and projection-specific rabies tracing identified many inputs to vS, including anterior hypothalamic inputs from MPO, amygdalar inputs from PA and thalamic inputs from RE and PVT. These inputs targeted distinct populations in vS: MPO selectively innervated vS^{NAc}, PA selectively innervated vS^{NAc} and vS^{LH}, and RE and PVT innervated vS^{NAc} and vS^{LH} only in posterior vS. Notably, the consistent MPO inputs to vS^{NAc} have not been previously described in the literature (Wyss et al., 1979; Bienkowski et al., 2018). The specificity in input labelling across different vS projections and spatial positions further raises interesting questions regarding the function of these upstream neurons. For example, the vS is important for relating appetitive social interactions with particular contexts (Okuyama et al., 2016), and MPO input has been shown to be important for integrating social stimuli with hormonal state (McHenry et al., 2017). Thus, inputs signalling ethologically important stimuli may be conveyed to vS, and in particular vS^{NAc} neurons, to coordinate goal-directed behaviour.

More generally, the observed input connectivity of vS supports a model of com-

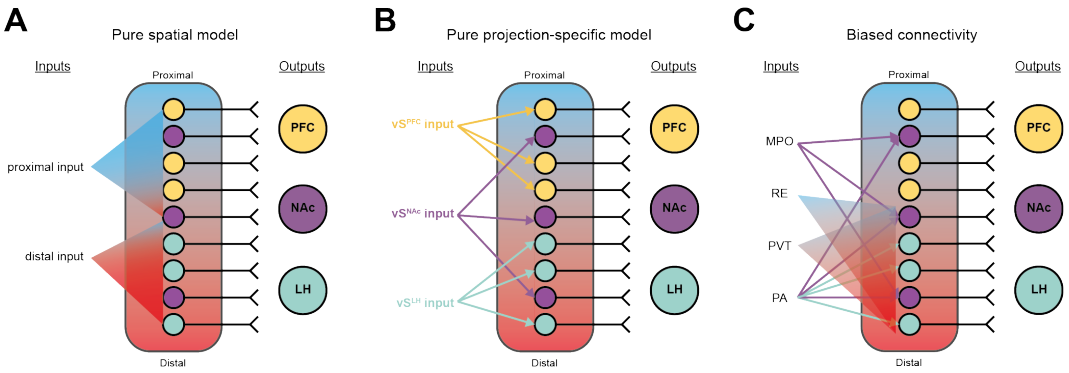

Figure 6.16: (A–C) Models of vS input connectivity based purely on the (A) spatial location or (B) projection identity of the postsynaptic vS neurons. (C) The findings presented in this chapter support a combined model from (A) and (B), where inputs can be projection-, COM- or both projection- and COM-biased.

bined topographical and output-defined connectivity of vS inputs (**Figure 6.16A–C**) where, depending on the upstream region, vS inputs are biased according to the location, projection type or both these attributes of postsynaptic vS neurons. This variation in inputs across space and projection type is in keeping with the known spatial and projection-specific functions of subiculum; across proximal-distal subdivisions, proximal vS is involved in sensory encoding (Knierim et al., 2014) and distal vS supports path integration (Knierim et al., 2014; Cembrowski et al., 2018b), while across projection populations, vS^{PFC} and vS^{LH} encode anxiety (Adhikari et al., 2010; Ciocchi et al., 2015; Jimenez et al., 2018) and vS^{NAc} encodes social memory (Okuyama et al., 2016) and reward-seeking behaviour (Reed et al., 2018; Trouche et al., 2019; LeGates et al., 2018; Britt et al., 2012). Crucially, the joint spatial- and projection-dependence of RE inputs also support the existence of spatial- and projection-specific function. For example, goal-directed locomotion has been proposed to be both specific to vS^{NAc} neurons and distal subiculum (Cembrowski et al., 2018b; Ciocchi et al., 2015; Okuyama et al., 2016). The data presented suggests that the input specificity of vS may be an important axis in producing the distinct activity dynamics of individual projections during free behaviour.

6.3.3 Biased connectivity of RE input away from vS^{PFC} neurons

A surprising result from the dataset was that the RE input did not innervate vS^{PFC} neurons. The RE is essential for bidirectional communication between hippocampus and PFC. This thalamic region is proposed to form an anatomical link between

hippocampus and PFC, thereby closing a PFC-RE-vS-PFC loop. Furthermore, this circuit has been the focus of preclinical models of disorders such as schizophrenia, depression and Alzheimer's disease (Vertes, 2006; Dolleman-van der Weel et al., 2019; Ito et al., 2015). Little information is present about the extent to which the projection-defined vS populations are involved in this circuit loop, and it is generally assumed that RE input is integrated by vS^{PFC} neurons to relay signals from hippocampus to PFC. By demonstrating that vS^{PFC} receive anatomically few and functionally weaker RE inputs, the data challenge this circuit model and instead suggest that RE input is integrated upstream of vS^{PFC} neurons – i.e. either through dorsal hippocampus, entorhinal cortex, local interneurons or local pyramidal cell populations – before being transmitted back to PFC. It will be necessary for future work to investigate in more detail the hippocampal microcircuitry that is involved in integrating RE input, the details of other multi-synaptic routes that may allow reciprocal connectivity between the hippocampus and PFC, such as via entorhinal cortex and amygdala, and how this circuit organisation contributes to behaviour.

Interestingly, RE input is anatomically and functionally biased towards vS^{NAc} and vS^{LH} neurons. This observed circuit connectivity complements previous data that demonstrated key roles for RE in goal-directed planning (Ito et al., 2015) and fear generalisation (Xu and Südhof, 2013) – functions that may be crucial for the proposed roles of vS^{NAc} in reward-seeking and vS^{LH} in anxiety (Cembrowski et al., 2018b; Ciocchi et al., 2015; Jimenez et al., 2018). In Chapters 4 and 5, I showed that vS^{NAc} projections are uniquely sensitive to the hunger state, while vS^{LH} is important for encoding salience. It is possible that RE input is required in the encoding of these behaviours in vS activity. It is also possible that distinct subpopulations of RE may differentially target vS^{NAc} and vS^{LH} and contribute to different behaviours. For example, Salay et al. (2018) demonstrated that midline thalamus neurons comprised projection-defined cell types that subserved different roles in visually evoked escape behaviours (Salay et al., 2018). Therefore, the nature of the RE-vS circuit remains an exciting avenue for further research.

6.3.4 Limitations of the study

Although conditional rabies tracing is now a widely used technique that enables systematic brain-wide mapping of upstream synaptic input (Beier et al., 2015, 2017;

Do et al., 2016; Ren et al., 2018; Ährlund Richter et al., 2019; Sun et al., 2019), there are a number of caveats related to this technique that require caution when interpreting rabies tracing data. One example of this is that the mechanism of trans-synaptic retrograde spread is unclear (Luo et al., 2018), which raises several potential confounds. For example, the efficiency of rabies viral spread may depend on uncontrolled variables such as tropism for certain cell-types and synapses (Luo et al., 2018), the level of upstream circuit activity (Beier et al., 2017), or even non-synaptic transfer (Luo et al., 2018). Indeed, in the TRIO experiments described in this chapter, neuromodulatory inputs such as serotonin from dorsal raphe and dopamine from VTA were poorly labelled by rabies, even though these inputs have been shown to project to vH (Riley and Moore, 1981). In addition, there is conflicting evidence as to whether the quantity of rabies-labelled input neurons correlates with functional synaptic strength (Luo et al., 2018). While multiple studies have shown that the number of input neurons across many brain regions scales with the connection probability and synaptic strength (Lerner et al., 2015; Sun et al., 2014; Kohara et al., 2013), other studies did not reach similar conclusions (Smith et al., 2016; Choi et al., 2019).

To mitigate the potential shortcomings of the technique, I conducted a series of control experiments and analyses. First, I leveraged on publicly available anterograde tracing experiments, such as those from the ABA Mouse Connectivity Atlas (Beier et al., 2019), to not only confirm direct targeting of newly-identified inputs to vS, such as those from MPO, but also validate the spatial targeting of RE and PVT input (Figure 6.13). Second, I conducted CRACM to directly assess the synaptic strength of identified inputs (Lerner et al., 2015). Using this approach, I confirmed that the RE input is stronger at synapses onto vS^{NAc} and vS^{LH} and weaker onto vS^{PFC} (Figure 6.15). In this instance, the functional strength of input correlated with the number of rabies-labelled inputs, but this is not always guaranteed. Thus, using these two approaches enabled me to more conclusively show that inputs to vS are anatomically and functionally biased as suggested by the rabies tracing data.

There are other technical considerations that are important to highlight with the use of whole-brain mapping. The first is the choice of the plane of sectioning, as there is the potential for reduced sampling resolution across the axis of slicing. For

example, in this study, sagittal sectioning did result in reduced resolution of regions defined predominantly in the ML axis, such as the lateral and medial entorhinal cortices. Defining the plane of sectioning is also important as the level of detail in anatomical annotation available in the ABA differs across anatomical axes. For example, the Allen Brain Atlas is more resolved along the coronal (plates spaced in 100 µm intervals) than the sagittal (plates spaced in 200 µm intervals) plane. As a result, the lateral-most regions in the sagittal plane, such as insular cortex which plays a key role in internal state sensing (Livneh et al., 2017, 2020), could not be resolved in this study.

Nevertheless, multiple brain-wide tracing studies have used horizontal, coronal (Bienkowski et al., 2018; Cembrowski et al., 2018b; Sun et al., 2014; Beier et al., 2015; Weissbourd et al., 2014) and sagittal (Wall et al., 2013; Roy et al., 2017; Beier et al., 2011) planes of sectioning successfully. I was motivated to use the sagittal plane of sectioning to allow accurate estimates of AP position within the brain, as this was the principal axis along which vS projection type varied. Even with the presence of this caveat, error associated with axis of sectioning was recently shown to be minimal when detailed registration is carried out (Fürth et al., 2018).

In addition, the use of stereotaxic injections means that - despite small injection volume and controlled rate of injection - the possibility that small amounts of virus or tracer might have leaked into neighbouring regions could not be excluded. Finally, the success of tracing experiments is dependent on the efficiency of the tracing system, and novel variants of the rabies system, such as more efficient glycoproteins (Kim et al., 2016), or more stable rabies virus (Reardon et al., 2016; Ciabatti et al., 2017; Chatterjee et al., 2018) could increase the sampling of more neuronal cell types for whole-brain anatomy experiments in the future.

In summary, this chapter presents data that describes the 3D anatomical organisation of parallel vS projections and their input connectivity. vS projections reside in distinct locations where individual projections are best discriminated along the AP axis. In turn, inputs target vS neurons according to the projection identity or spatial location of the vS postsynaptic neurons, supporting a spatial- and projection-defined rule of input connectivity in vS. These results suggest the intriguing possibility that this underlying biased input connectivity represents a neural

mechanism for the selective control of individual vS projections during behaviour.

Chapter 7

General Discussion

In this Chapter, I summarise the findings presented in Chapters 3 to 6, integrate them with the literature and discuss the potential neural mechanisms of hunger state sensing in the hippocampus. Then, I discuss the implications of such a function, and formulate testable hypotheses that can be addressed in future studies.

7.1 Brief summary of results

From spatial navigation and memories, to motivated behaviour, stress and anxiety, the hippocampus appears to contribute to a wide range of seemingly disparate behaviours. This thesis expands on a lesser-known function of the hippocampus, i.e. motivational state sensing, which is being increasingly recognised as an important contributor to adaptive, flexible behaviour (Davidson and Jarrard, 1993; Kennedy, 2004; Kennedy and Shapiro, 2009; Carey et al., 2019). Below, I provide a brief summary of the key findings described in Chapters 3 to 6 in the context of the original research questions outlined in the Introduction:

- **What are the activity dynamics of the ventral hippocampus (vH) during feeding behaviour across different states of hunger?** Feeding behaviour is built from simpler behaviours, most notably feeding behaviours such as food investigation (Approach) and consumption (Eat) and non-feeding-specific behaviours (Rear, Groom and Rest). Excitatory vS neurons specifically encode food exploratory and investigative behaviour, signalling anticipation of food intake. This occurs even in the simplest of tasks devoid of an explicit task structure, i.e. free-feeding behaviour, as well as a learned operant behaviour.

Hunger reduces vS activity specifically during the approach phase of feeding behaviour.

- **What are the ventral hippocampal circuits specifically involved in encoding feeding behaviour and the hunger state?** The activity of vS projections to the nucleus accumbens (vS^{NAc}), as opposed to projections to the lateral hypothalamus (vS^{LH}), encodes feeding behaviour, and more specifically investigative Approach behaviour. Hunger – through peripheral injections of ghrelin – inhibits vS^{NAc}, and not vS^{LH}, activity during food approach. Additionally, vS^{NAc} activity during food approach is predictive of subsequent food intake and encodes the value of food.

- **What are the circuit and cellular mechanisms supporting this hunger sensitivity in vH?** At the cellular level, systemic ghrelin enhances inhibitory synaptic transmission specifically in vS^{NAc} neurons, and this effect can be reversed with the ghrelin receptor antagonist D-lys. At the circuit level, ghrelin receptor signalling is required for this inhibition of vS^{NAc} circuit activity at the time of food approach. Importantly, the vS^{NAc} circuit regulates food-seeking behaviour, as pharmacogenetic inhibition of vS^{NAc} *in vivo* promotes an increase in transitioning from food approach to consumption, while vS^{NAc} activation increases the time spent investigating food.

- **What is the input connectivity of the vS that might explain functional heterogeneity in the vS circuit?** The vS is made up of topographical projections to distinct downstream regions. This topography, in combination with the identity of their downstream target, dictates the type and amount of inputs that vS neurons receive, providing a potential neural basis for heterogeneous function in vS.

These findings of a hunger, and specifically ghrelin-sensitive vS circuit that mediates food-seeking behaviour, provides one of the first mechanistic descriptions of how the hippocampus may sense an internal state like hunger *in vivo*. Such a hormonal signalling mechanism may also interact dynamically with the heterogeneous inputs that vS receives, producing a complex interplay of synaptic and hormonal input integration within vS to guide behaviour. In the next sections, I discuss

what these findings imply for integrative hippocampal computations, including how hunger and more generally motivational state sensing may be used as schemas (i.e. relationships between distinct external and/or internal cues) to support flexible behaviour, how disruption of these processes may give rise to disease, and propose outstanding questions remaining as avenues for further research.

7.2 Role of ghrelin in motivation-related neural circuitry

Although ghrelin has been commonly referred to as the 'hunger hormone' that mimics fasting (Chapter 3; see also Tschöp et al., 2000; Wren et al., 2001), several observations make it more likely that ghrelin mediates food anticipation rather than food consumption. First, the concentration profile of circulating ghrelin accurately reflects the anticipation of an upcoming meal, where ghrelin levels ramp towards the onset of food consumption over a timescale of hours (Drazen et al., 2006; Cummings et al., 2004). This anticipatory increase in ghrelin levels prior to food consumption may be an important determinant in shaping ramping neural activity observed in hippocampus and a multitude of other brain regions (see below for discussion on ramping signals in hippocampus). Consistent with this idea, my data demonstrate that ghrelin inhibits vS activity specifically during food anticipation, and studies employing genetic knockouts of GHSR1a show that mice have disrupted anticipatory locomotion during the time period preceding a meal (Blum et al., 2009; Verhagen et al., 2011). Furthermore, GHSR1a-null mice have normal body weight (Sun et al., 2008), indicating that ghrelin is dispensable in homeostatic food intake regulation. Collectively, these observations prompt a re-examination of the function of ghrelin as supporting food consumption alone, and suggest a more nuanced role in anticipatory feeding behaviour and planning.

Second, beyond the hypothalamus and hippocampus, receptors for ghrelin are expressed in brain structures known to support goal-directed feeding behaviour. For example, the basal amygdala, which encodes the utility of goals (both rewards and punishments) (Gore et al., 2015; Gründemann et al., 2019; Paton et al., 2006; Belova et al., 2008) expresses GHSR1a (Alvarez-Crespo et al., 2012) and is acutely sensitive to the hunger state (Calhoon et al., 2018). The mesolimbic dopaminergic pathway, comprising the projection from ventral tegmental area (VTA) to nucleus accumbens (NAc), is also involved in ghrelin signalling; cannulation of ghrelin into

the lateral ventricles increases dopamine concentrations in striatum (Cone et al., 2014), while direct cannulation into regions like LH and VTA promote food intake and the effort expended to retrieve food (Skibicka and Kanoski, 2016; Skibicka et al., 2011; Naleid et al., 2005). This expression pattern of ghrelin receptors in regions supporting goal-directed behaviour further suggest that the behavioural effect of ghrelin may be more complex than as a simple controller of food consumption.

Third, at the neural level, ghrelin appears to be a key factor in modulating synaptic plasticity and learning. In my experiments, I showed that ghrelin modulates inhibitory plasticity in vS^{NAc} neurons. Other previous experiments have shown that ghrelin promotes functional (Ribeiro et al., 2014; Diano et al., 2006; Cruz et al., 2013; Yang et al., 2011) and structural (Berrout and Isokawa, 2012; Diano et al., 2006) plasticity, with important ramifications for learning and memory. For example, peripheral injections of ghrelin produced robust LTP in hippocampus and improved spatial working memory in mice (Diano et al., 2006). These reports of ghrelin-dependent changes in synaptic plasticity and hippocampal-dependent behavioural functions strongly suggest that ghrelin may also have influences on the learning of associations. For example, ghrelin increases prediction error-related signals in hippocampus and value-related signals in striatum in a food odour-conditioning task, which may be used to promote the learning of food-cue associations (Han et al., 2018). During this task, there was also increased hippocampal-striatum coupling when human participants were injected with ghrelin compared to saline control. Thus, it appears that ghrelin plays a role in value computations between the hippocampus and striatum in the learning of food-related associations, suggesting a higher-order function of ghrelin than simply driving food intake.

More generally, it is becoming increasingly understood that the hippocampus not only encodes the relationships between distinct cues in the environment (Cohen and Eichenbaum, 1993), but also the value of outcomes (Lee et al., 2012). For example, the hippocampal-to-NAc projection has been proposed to be important for the learning of value associations in physical and abstract dimensions (Trouche et al., 2019; LeGates et al., 2018; Wimmer and Shohamy, 2012; Duncan et al., 2018; Ito et al., 2008), and to relay these signals to ventral striatum (Pennartz et al., 2011b). In rodents, a spatial context paired with reward will lead to expression of

reward-seeking behaviour, manifested as an increased place preference; this behaviour is crucially dependent on an intact hippocampus to NAc projection (Trouche et al., 2019; LeGates et al., 2018). In more abstract domains, human subjects can use a form of learning called configural learning – i.e. learning that the configuration of cues leads to one outcome, while individual (elemental) cues each predict a different outcome. This sort of learning is also highly dependent on the projection from hippocampus to NAc (Duncan et al., 2018), suggesting that the binding of distinct elements to rewarding outcomes is a principal function of hippocampal projections to NAc. Thus, the learning of value associations, including food-related associations, appears to engage a general hippocampus-NAc circuit that is capable of learning associations that span physical and abstract domains.

One key feature of a flexible, relational system for learning value associations, and especially food-related value, is the multiplexing of distinct sensory inputs, for example, the sensory properties of food such as taste and odour, within hippocampal activity. Sensory inputs converge in hippocampus likely through relays from well-established sensory pathways via perirhinal, postrhinal and entorhinal cortices (Kanoski and Grill, 2017), and through mono- and disynaptic pathways from olfactory cortex to hippocampus via amygdala and entorhinal cortex. In dorsal CA1, pyramidal neurons and interneurons are known to multiplex signals relating spatial location and taste within single neurons (Herzog et al., 2019, 2020), giving rise to hypotheses about conjunctive space-food availability codes that might be read out by downstream brain regions to guide behaviour.

An intriguing possibility is that this multiplexing of signals enables relational binding of associations and the learning of sensory cue-internal state associations. Based on one main finding of this thesis – i.e. that the hormone ghrelin can modulate the activity of hippocampal projections to NAc – I propose that hormone-based, hunger state signals can also be integrated within vS with conjunctive sensory cues. Such an integration would be possible given the role of the hippocampus in relational encoding, and may be used to guide feeding behaviour under appropriate conditions. A further speculation is that such a hunger state-sensory cue association would also be linked with the value of actions, akin to model-based reinforcement learning (see below for discussion about planning), such that partic-

ular hunger state-cue associations can be used to predict the amount of reward-outcomes. If this is true, then such a relational encoding between hunger and feeding behaviour may be a fundamental mechanism or schema (Tse et al., 2007; McKenzie et al., 2014) for relating food-related cues under different hunger states to varying levels of value. Thus, in this view, one prime role of ghrelin signalling within the hippocampus may be its role in forming value associations (i.e. by constructing a model-based value landscape) and sending this information to NAc to guide behaviour (see below for experiments to directly test this idea).

Together, these studies prompt a re-conceptualisation of ghrelin's role not simply as a reporter for hunger, but rather as a hormonal mechanism to directly regulate circuitry involved in food-seeking behaviour.

7.3 Interacting motivational systems within hippocampus

The hippocampus has been proposed to support the sensing of multiple, orthogonal motivational systems, ranging from thirst and hunger to pain and stress. These related and interacting motivations are mediated by circulating peptides such as vasopressin and angiotensin II (thirst), insulin (glucose metabolism), glucagon-like peptide 1 and leptin (satiety), oestrogen and testosterone (sex-related), oxytocin (prosocial behaviour) and so on. In turn, the hippocampus densely expresses receptors recognising these ligands (Lathe, 2001; Lathe et al., 2020). The dense expression of receptors in hippocampus for circulating hormones is in agreement with the long history of work showing the ability of circulating hormones, such as glucocorticoids and oestrogen, in modulating the structural and functional plasticity of hippocampal neurons (Woolley, 1998; McEwen et al., 2015). One speculation is that, given the common evolution of the hippocampus and olfactory circuit from chemosensory epithelium, a prominent function of the hippocampus would be the sensing of many internal circulating molecules, much like how the olfactory bulb and cortex sense external odorant molecules (Lathe, 2001). Consistent with this idea, a recent survey of of endocrine receptor expression found that 30% of receptors encompassing stress, hormonal, hunger, thirst, infection/inflammation-related genes, were expressed at higher levels in hippocampus compared to cortex and cerebellum (Lathe et al., 2020).

There is evidence that motivational systems, primarily hunger and thirst, have

orthogonal representations in the hippocampus. The earliest work documenting that motivation can be separately used to learn about outcomes was an experiment in which rats were trained to approach one goal if hungry and another goal if thirsty. Lesioning the hippocampus impaired the ability of rats to learn to use the internal state to choose the appropriate goal, as well as cause perseverance in inappropriate goal approach (Hsiao and Isaacson, 1971); however, this study was confounded by the fact that the animals received hippocampal lesions prior to learning and thus could have had deficits in spatial processing, as well as used alternative strategies to solve the task, such as the formation of compound reward-arm cues, rather than relying on internal state cues.

Kennedy (2004) improved upon this initial finding by showing that the hippocampus – independent of spatial processing – was required in a contextual-retrieval task where compound internal state (hunger vs. thirst) and sensory cue information guided the animal's choice of the correct box containing the correct goal (water or food). Later, the same group showed than when recording from hippocampal place assemblies, place cell remapping occurred with motivational shifts from thirsty to hungry (Kennedy and Shapiro, 2009). Lastly, Carey et al. (2019) showed that hippocampal replay activity occurred in sequences in a manner that was dependent on hunger and thirst state (Carey et al., 2019), i.e. the trajectory of quiet awake replay appears to be biased by multiple motivational systems. Together, this indicated that hunger and thirst could act as distinct internal contexts in the service of planning and goal-directed behaviour. Thus, one interesting possibility is that the signalling of the hunger state by ghrelin within vS does not occur in a vacuum, but rather interacts dynamically with other motivational states.

The sensitivity of the hippocampus to motivational states, coupled with the role of the vH in forming value associations, suggests that motivational states may act as relational schemas to enable flexible behaviour (Behrens et al., 2018; Cohen and Eichenbaum, 1993). This generalisation of interoceptive motivational states to support behaviour other than feeding behaviour was hinted at from early work by Davidson and Jarrard (1993), who described the ability of rats to use their hunger states to predict an upcoming footshock. This raised the exciting prospect that motivational states are able to shape the internal model generated by the hippocam-

pus, possibly served by distinct hippocampal representations of hunger and thirst (Carey et al., 2019; Kennedy and Shapiro, 2009). Indeed, motivational states such as hunger can affect decision-making; for example, hunger encourages exploration in mice, and they are more likely to enter 'anxiogenic' areas such as the open arms of the elevated plus maze when hungry (Burnett et al., 2016), while humans subjects make more risky decisions in a gambling task in the fasted compared to the fed state (Symmonds et al., 2010). This effect of hunger on non-feeding related behaviour, such as approach-avoidance under uncertainty, in a variety of organisms in fish, rodents and humans (Filosa et al., 2016; Burnett et al., 2016; Symmonds et al., 2010) provides evidence that motivational states may be factored into the internal models generated by the hippocampus to enable flexible behaviour.

7.4 Anticipatory neural signals in hippocampus

One of the most common observations of anticipatory brain activity is a signal preceding the onset of a behaviourally relevant event. This feature has been observed in cortical regions such as prefrontal cortex (Narayanan, 2016), subcortical regions such as the mesolimbic dopamine circuitry (Hamid et al., 2016; Howe et al., 2013; Kim et al., 2019) and the CA1 and subicular regions in hippocampus (Deadwyler et al., 1996; Aronov et al., 2017). These signals are often interpreted as being predictive of an upcoming goal. In cortex, these signals are thought to be involved in the planning of motor actions (Chen et al., 2017; Li et al., 2016). Another equally plausible interpretation of such preemptive signals is the encoding of elapsed time, for example in CA1 hippocampal neurons, to bridge temporal gaps between relevant stimuli (MacDonald et al., 2011; Paton and Buonomano, 2018; Soares et al., 2016).

The vS activity observed in my operant feeding task experiments (Chapter 3) increased slowly from the onset of cue light to food delivery. This ramp-like signal is reminiscent of other anticipatory, value-related signals that have been reported in the mesolimbic dopamine circuitry (Hamid et al., 2016; Howe et al., 2013; Kim et al., 2019) which have been hypothesised to track the proximity towards a goal (Howe et al., 2013) and reflect the value of effort expended (Hamid et al., 2016). Such anticipatory signals indicate a degree of prospection for the upcoming reward, which have interesting implications for the underlying behavioural strategy in goal-

directed behaviour. Mechanistically, at the single-cell level, neuronal activity could potentially be organised as a sequential activation pattern that tiles the period from the onset to the end of a trial (MacDonald et al., 2011); alternatively, co-activation of neural ensembles, as in an attractor network, could account for this preemptive increase in activity preceding food intake.

Notably, there is increasing evidence in both humans and rodents that model-based behaviour is supported by the hippocampus (Vikbladh et al., 2019; Miller et al., 2017; Johnson and Redish, 2007; Pfeiffer and Foster, 2013). This view is supported by the hippocampus' role in flexibly relating distinct features of the environment in forming episodic memory (Cohen and Eichenbaum, 1993) and in simulating futures (Bakkour et al., 2019; Stachenfeld et al., 2017; Kay et al., 2020; Johnson and Redish, 2007; Ólafsdóttir et al., 2015). One study recently found that a major determinant for the evolution of anticipatory ramping signal – at least within the mesolimbic dopaminargic pathway – is the use of an internal model, e.g. time-keeping or tracking of distance already covered in relation to goals (Guru et al., 2020). Thus, one interesting hypothesis is that the anticipatory ramping signals may originate in the hippocampus, which are then relayed to downstream areas like the midbrain dopaminergic circuit (Lisman and Grace, 2005).

In my experiments, the predictive ramp-like signal was observed even during the operant feeding task where the delivery of food was deterministic (i.e. 100% probability of reward), whereas tasks measuring model-based behaviour usually utilise probabilitistic reward schedules to introduce uncertainty and engagement in model-based learning. One potential explanation for this observation is the use of even a small temporal delay (50-250 ms in the operant task) is sufficient to use time-keeping to expect an upcoming food reward; alternatively, it is possible that the nature of hunger signals – i.e. their continuous fluctuations in circulating levels daily – means that food-related value is always probabilistic and requires inference based on the sampled level of circulating hormones within the hippocampus and elsewhere in the brain. As these explanations are not mutually exclusive, it is possible that both these descriptions can account for vS ramping activity during the anticipation of upcoming food intake.

The predictive nature of vS activity – i.e. the increased vS activity preceding

actual food consumption or delivery seen in my experiments – is in keeping with current ideas about hippocampal function. That is, the hippocampus is increasingly thought to signal the likelihood of occupying future spatial or non-spatial states (Stachenfeld et al., 2017), representing future choices (Kay et al., 2020) and active deliberation about the value of choices in the run up to decision time (Bakkour et al., 2018). Indeed, many studies have observed anticipatory increases in hippocampal activity prior to outcome (Lee et al., 2012; Ciocchi et al., 2015), and this thesis further demonstrates that such an anticipatory signal applies to food-related rewards in a hunger-dependent manner.

On the other hand, the data presented in this thesis is also consistent with the idea that the hippocampus is involved in behavioural inhibition (Gray and McNaughton, 2003; Bannerman et al., 2012), where high activity in vH (e.g. in the sated state) suppresses consummatory behaviour, while low activity promotes transitions towards eating. How can the vH support seemingly distinct psychological processes – i.e. food investigation and behavioural inhibition? One idea is that these two processes could occur simultaneously; while anticipating upcoming food or deciding whether to eat or not, animals may suppress task-unrelated behaviour until receiving the food reward. What occurs during this suppression of behaviour may be either increased information seeking (i.e. attending to salient external or internal cues; Gray and McNaughton, 2003) or active deliberation about available options (Bakkour et al., 2019; Biderman et al., 2020). In the latter case, the hippocampus is particularly important to arbitrate between value-based decisions as the hippocampus is important in determining the value of present options based on past learnt associations (Barron et al., 2013; Behrens et al., 2018). Consistent with this idea, value-based deliberation among competing options correlates with hippocampal activity (Bakkour et al., 2019). In this way, perhaps deciding to eat or not is similar to deciding between two options of differing value, where the deliberation over the decision to eat is accompanied by increased attention and suppression of ongoing behaviour.

7.5 Does ghrelin directly bind to ventral hippocampal neurons?

Given the tight regulation of substance entry across the blood-brain barrier (BBB), one important question is whether ghrelin and other hormones mediate their effects on vS circuitry by directly binding hippocampal neurons, or are signalled via upstream synaptic inputs. This question remains highly debated. On the one hand, the hippocampus is situated adjacent to circulating cerebrospinal fluid (CSF) in the ventricles, and has a rich surrounding blood supply from the choroid plexus (Lathe, 2001). Substances used to assess BBB integrity, such as Evans blue, have been shown to readily pass through the BBB surrounding the hippocampus, and be taken up by hippocampal neurons (Hamasaki et al., 2020). On the other hand, others have argued that peptide hormones like ghrelin are unable to cross the BBB except at circumventricular organs or regions with fenestrated capillaries (Fry and Ferguson, 2010; Kern et al., 2014, 2015; Furness et al., 2011; Schaeffer et al., 2013). This is because while steroid hormones such as oestrogen and testerone are highly non-polar and readily cross the BBB by diffusion, peptide hormones like ghrelin, insulin and leptin are highly polar due to to their charged side chain groups, and thus cannot cross the BBB without specialised mechanisms (Banks, 2012); yet, multiple studies have shown that ghrelin is able to cross the BBB by saturable mechanisms, albeit at a low level (Banks et al., 2002; Diano et al., 2006; Rhea et al., 2018), and that radioactive-labeled ghrelin injected peripherally can directly bind to hippocampal neurons (Diano et al., 2006). Recently, one study also found that the hippocampus expresses the ghrelin O-acyltransferase (GOAT) enzyme – the key enzyme that switches on the biological activity of unacylated circulating ghrelin by serine-3 octanoylation (Murtuza and Isokawa, 2018). This suggests alternative routes for multiple isoforms of ghrelin, each having distinct BBB penetrability (Banks et al., 2002; Rhea et al., 2018), to reach the hippocampus and bind to GHSR1a. Furthermore, the hippocampus expresses functional receptors for peptide hormones like ghrelin (Zigman et al., 2006; Guan et al., 1997), leptin (Harvey, 2013) and insulin (Soto et al., 2019), suggesting that these hormones are capable of binding to hippocampal neurons to affect their function.

One argument that ghrelin does not bind to hippocampal neurons is that re-

ceptors like GHSR1a exhibit high constitutive activity at baseline (i.e. without ligand binding) (Petersen et al., 2009). Yet this is hard to reconcile with past experiments showing peripheral ghrelin binding to hippocampal neurons (Diano et al., 2006). Furthermore, the GHSR1a knockdown experiments in Chapter 5 showed that there was a GHSR1a-dependent response to peripherally injected ghrelin in vS^{NAc} activity. Given these observations, this makes it unlikely that GHSR1a in vS^{NAc} is signalling purely constitutively. Rather, it is more likely that there is some combination of ligand-dependent and ligand-independent activity within the GHSR1a system in hippocampus.

Additionally, the effect of ghrelin could potentially be mediated by upstream neuromodulatory signalling, such as dopamine D1 receptor signalling in tandem with GHSR1a (Kern et al., 2015). For example, ghrelin could activate ghrelin-sensing LH neurons that then promotes VTA activity (Cone et al., 2016) to provide the dopaminergic source to hippocampus. Other potential neuromodulators or neuropeptides that could act as co-agonists to ghrelin signalling in vH include acetylcholine from septal areas (Colgin et al., 2003), serotonin from raphe (Yang et al., 2019) or melanin concentrating hormone from hypothalamus (Noble et al., 2019). Alternatively, others have also proposed that there may be a source of brain-derived ghrelin, although there is growing consensus that this is unlikely based on observations of reporter mice expressing GFP under the ghrelin promoter and immunohistochemical findings (Sakata et al., 2009; Furness et al., 2011; Cabral et al., 2017). Finally, the BBB is not a static structure, and its permeability varies as a function of several variables; for example, accessibility of ghrelin is dependent on the hunger state (Langlet et al., 2013; Banks et al., 2008).

On the balance of the evidence, it appears difficult to square the discrepancies surrounding the ability of ghrelin to cross the BBB to bind to hippocampal neurons or through some other alternate mechanism between studies. Thus, a parsimonious account of the results described within this thesis would therefore be that the vH senses ghrelin in a ghrelin receptor-dependent manner; whether ghrelin directly modulates hippocampal activity by direct binding or through upstream synaptic inputs remains an open question.

7.6 Implications of hippocampus and hunger sensing for psychiatric disease

The vH, given its wide-ranging roles in ambiguity resolution and approach-avoidance conflict processing, is implicated in many psychiatric diseases, including drug addiction (Cooper et al., 2006), depression (Bagot et al., 2015) and schizophrenia (Mukherjee et al., 2019). A common symptom of affective disorders is maladaptive feeding behaviour, including changes in weight and appetite (American Psychiatric Association, 2013). One possibility is that impaired hippocampal function in these conditions may result in insensitivity to the internal hunger state, and consequently the inability to use hunger state-related associations. In turn, the hunger insensitivity would lead to inappropriate feeding behaviour, as has been observed in human patients (Hebben et al., 1985; Rozin et al., 1998) and rodents with hippocampal lesions (Henderson et al., 2012; Hannapel et al., 2017). This possibility also has precedence as damage to hippocampus impairs adaptive decision-making, as assessed by performance on the Iowa Gambling task (Gupta et al., 2009; Gutbrod et al., 2006).

There is some experimental support that the lack of interoceptive awareness of the hunger state is a hallmark of psychiatric and developmental disorders (Khalsa et al., 2018). For example, in Prader-Willi syndrome, a developmental disorder characterised by excessive eating and severe obesity from an early age, patients are unable to report their satiety levels (Holland et al., 1995). Additionally, major depressive disorder is associated with reduced sensitivity of insular cortex – a region that is critical for interoception (Livneh et al., 2020) – to changes in the metabolic state (Simmons et al., 2016). Conversely, in eating disorders like anorexia nervosa – characterised by excessive food restriction, anxiety and purging behaviour – hypersensitivity to the hunger state sensing has been reported in insular cortex, and some have suggested that this hypersensitivity underlies the food-related anxiety and subsequent food avoidance behaviour seen in anorexia nervosa (Khalsa et al., 2015).

These observations from the clinical literature and the increasing appreciation of vH as a neural substrate for emotional processing suggest the possibility of hippocampal involvement in disorders linked to metabolic dysregulation. Mechanistic

studies focusing on the links between hippocampal function and feeding disorders in preclinical animal models will likely provide key insights into how impaired hippocampal function might give rise to maladaptive behaviour.

7.7 Future research directions

In addition to future experiments outlined in the Discussion section of the individual Results chapters, below I outline several future experiments that can address outstanding questions arising from the preceding discussion:

1. **Can hippocampal ghrelin signalling be flexibly incorporated into more abstract rules and value computations?**

   One interesting idea is the potential role of hippocampal ghrelin signalling in forming separate value associations and signalling this information for reinforcement via vS projections to NAc. Given the relational nature of hippocampal function, one prediction is that hunger – via hippocampal ghrelin signalling – is capable of acting as an internal context to be associated with a particular contingency. This could be tested in an operant task where animals are trained to press a **right** lever for reward when ghrelin levels are **high**, or press a **left** lever for reward when ghrelin levels are **low**. To maintain roughly equivalent motivational levels, the animals could be alternatively injected with ghrelin (hunger) or sodium chloride (to simulate thirst) (Zimmerman et al., 2017), where the hunger rule denotes that right lever leads to reward, thirst rule denotes that left lever leads to reward, and vice versa. If animals can be successfully trained in this task, then perturbation of ghrelin receptor signalling in hippocampus during this task might lead to impaired rule performance. Such an experiment would directly address the role of ghrelin signalling in forming value associations, and suggest that one mechanism underlying feeding behaviour is a general, relational association between hormonal state, value and action within the hippocampal projection to NAc.

2. **What is the extent of hippocampal BBB permeability under different states of hunger?**

   As it remains unclear whether the vH is actually permeable to blood-borne circulating factor, one experiment that can be easily conducted is to assess

BBB integrity in the vH (after 24 hours fasting or following i.p. injection of ghrelin) to Evans blue – the dye that is routinely used to assess BBB permeability (Hamasaki et al., 2020). This experiment can be combined with retrograde tracing of subpopulations of vS neurons – e.g. vS projections to NAc – to determine if Evans blue localises specifically to subpopulations of projection neurons, or is more diffuse across hippocampal regions. The findings of this study would be informative of the extent of hippocampal exposure to circulating hormones in the bloodstream.

3. **What is the unique role of TRIO-identified inputs in relaying hunger-related signals to vS?**

   Crucially, the inputs identified by TRIO may represent important neural determinants for the effect of ghrelin on vS^{NAc} neurons. For example, the paraventricular thalamus (PVT) targets posterior vS where vS^{NAc} neurons are abundant, and both inhibition (Stratford and Wirtshafter, 2013; Zhang and van den Pol, 2017) and excitation (Betley et al., 2013) of PVT promotes feeding behaviour. The PVT encodes the salience of stimuli by integrating internal states like thirst and hunger and external cues to support goal-seeking behaviour (Kelley et al., 2005; Hua et al., 2018; Otis et al., 2019; Zhu et al., 2018; Gao et al., 2020), and therefore represents a strong candidate for providing hunger state signals to vS. Another example is the diagonal band nucleus (NDB) and septal area, cholinergic basal forebrain areas that bidirectionally modulate feeding behaviour in response to external cues (Patel et al., 2019; Herman et al., 2016; Cassidy et al., 2019). Indeed, preliminary evidence from the lab (data not shown) suggest that GABAergic neurons in these regions project to vS. Other regions like the preoptic area (Yu et al., 2017; McHenry et al., 2017), nucleus reuniens (Ito et al., 2015), basal amygdala (Calhoon et al., 2018; Namburi et al., 2015; Kim et al., 2017; Gründemann et al., 2019) and insular cortex (Gehrlach et al., 2020; Livneh et al., 2017, 2020) all provide input to vS (Wee and MacAskill, 2020) and control different aspects of internal state sensing and goal-directed behaviour. These inputs represent potential sources of hunger-related signals to vS whose individual roles can be clarified with projection-specific activity recordings and perturbation techniques.

In summary, this thesis describes a hunger-sensitive hippocampal circuit – with distinct synaptic, anatomical and behavioural properties – that may act as a neural mechanism for utilising hunger state signals within the hippocampus. Understanding how this circuit integrates internal states and sensory stimuli into value computations to support goal-directed behaviour, and how disruption of this process may give rise to disease, will be important topics of future study.

Bibliography

Abizaid, A., Liu, Z.-W., Andrews, Z. B., Shanabrough, M., Borok, E., Elsworth, J. D., Roth, R. H., Sleeman, M. W., Picciotto, M. R., Tschöp, M. H., Gao, X.-B., and Horvath, T. L. (2006). Ghrelin modulates the activity and synaptic input organization of midbrain dopamine neurons while promoting appetite. *The Journal of clinical investigation*, 116(12):3229–3239.

Adhikari, A., Topiwala, M. A., and Gordon, J. A. (2010). Synchronized activity between the ventral hippocampus and the medial prefrontal cortex during anxiety. *Neuron*, 65(2):257–269.

Aggleton, J. P. and Christiansen, K. (2015). *The subiculum: the heart of the extended hippocampal system*, volume 219. Elsevier B.V., 1 edition.

Allcroft, D. J., Tolkamp, B. J., Glasbey, C. A., and Kyriazakis, I. (2004). The importance of 'memory' in statistical models for animal feeding behaviour. *Behavioural processes*, 67(1):99–109.

Alvarez-Crespo, M., Skibicka, K. P., Farkas, I., Molnár, C. S., Egecioglu, E., Hrabovszky, E., Liposits, Z., and Dickson, S. L. (2012). The amygdala as a neurobiological target for ghrelin in rats: neuroanatomical, electrophysiological and behavioral evidence. *PloS one*, 7(10):e46321.

Amaral, D. G. and Cowan, W. M. (1980). Subcortical afferents to the hippocampal formation in the monkey. *Journal of Comparative Neurology*, 189(4):573–591.

Andermann, M. L. and Lowell, B. B. (2017). Toward a Wiring Diagram Understanding of Appetite Control. *Neuron*, 95(4):757–778.

Aronov, D., Nevers, R., and Tank, D. W. (2017). Mapping of a non-spatial dimension by the hippocampal–entorhinal circuit. *Nature*, 543(7647):719–722.

Association, A. P. (2013). *Diagnostic and statistical manual of mental disorders (DSM-5®)*.

Augustine, V., Gokce, S. K., Lee, S., Wang, B., Davidson, T. J., Reimann, F., Gribble, F., Deisseroth, K., Lois, C., and Oka, Y. (2018). Hierarchical neural architecture underlying thirst regulation. *Nature*, pages 1–20.

Augustine, V., Lee, S., and Oka, Y. (2020). Neural Control and Modulation of Thirst, Sodium Appetite, and Hunger. *Cell*, 180(1):25–32.

Azevedo, E. P., Pomeranz, L., Cheng, J., Schneeberger, M., Vaughan, R., Stern, S. A., Tan, B., Doerig, K., Greengard, P., and Friedman, J. M. (2019). A Role of Drd2 Hippocampal Neurons in Context-Dependent Food Intake. *Neuron*, 102(4):873–886.e5.

Bach, D. R., Hoffmann, M., Finke, C., Hurlemann, R., and Ploner, C. J. (2019). Disentangling Hippocampal and Amygdala Contribution to Human Anxiety-Like Behavior. *Journal of Neuroscience*, 39(43):8517–8526. Publisher: Society for Neuroscience _eprint: https://www.jneurosci.org/content/39/43/8517.full.pdf.

Bagot, R. C., Parise, E. M., Peña, C. J., Zhang, H.-X., Maze, I., Chaudhury, D., Persaud, B., Cachope, R., Bolaños-Guzmán, C. A., Cheer, J. F., Cheer, J., Deisseroth, K., Han, M.-H., and Nestler, E. J. (2015). Ventral hippocampal afferents to the nucleus accumbens regulate susceptibility to depression. *Nature communications*, 6:7062.

Baimel, C., McGarry, L. M., and Carter, A. G. (2019). The Projection Targets of Medium Spiny Neurons Govern Cocaine-Evoked Synaptic Plasticity in the Nucleus Accumbens. *Cell Reports*, 28(9):2256–2263.e3.

Bakkour, A., Palombo, D. J., Zylberberg, A., Kang, Y. H., Reid, A., Verfaellie, M., Shadlen, M. N., and Shohamy, D. (2019). The hippocampus supports deliberation during value-based decisions. *eLife*, 8:227.

Bakkour, A., Zylberberg, A., Shadlen, M. N., and Shohamy, D. (2018). Value-based decisions involve sequential sampling from memory. *bioRxiv*, page 269290.

Banks, W. A. (2012). Brain meets body: the blood-brain barrier as an endocrine interface. *Endocrinology*, 153(9):4111–4119.

Banks, W. A., Burney, B. O., and Robinson, S. M. (2008). Effects of triglycerides, obesity, and starvation on ghrelin transport across the blood-brain barrier. *Peptides*, 29(11):2061–2065.

Banks, W. A., Tschöp, M., Robinson, S. M., and Heiman, M. L. (2002). Extent and direction of ghrelin transport across the blood-brain barrier is determined by its unique primary structure. *The Journal of pharmacology and experimental therapeutics*, 302(2):822–827.

Bannerman, D. M., Bus, T., Taylor, A., Sanderson, D. J., Schwarz, I., Jensen, V., Hvalby, , Rawlins, J. N. P., Seeburg, P. H., and Sprengel, R. (2012). Dissecting spatial knowledge from spatial choice by hippocampal NMDA receptor deletion. *Nature Neuroscience*, 15(8):1153–1159.

Bannerman, D. M., Deacon, R. M. J., Offen, S., Friswell, J., Grubb, M., and Rawlins, J. N. P. (2002). Double dissociation of function within the hippocampus: spatial memory and hyponeophagia. *Behavioral Neuroscience*, 116(5):884–901.

Bannerman, D. M., Sprengel, R., Sanderson, D. J., McHugh, S. B., Rawlins, J. N. P., Monyer, H., and Seeburg, P. H. (2014). Hippocampal synaptic plasticity, spatial memory and anxiety. *Scientific Reports*, 15(3):181–192.

Barnes, S. J., Sammons, R. P., Jacobsen, R. I., Mackie, J., Keller, G. B., and Keck, T. (2015). Subnetwork-Specific Homeostatic Plasticity in Mouse Visual Cortex In Vivo. *Neuron*, 86(5):1290–1303.

Barron, H. C., Dolan, R. J., and Behrens, T. E. J. (2013). Online evaluation of novel choices by simultaneous representation of multiple memories. *Nature Neuroscience*, 16(10):1492–1498.

Behrens, T. E. J., Muller, T. H., Whittington, J. C. R., Mark, S., Baram, A. B., Stachenfeld, K. L., and Kurth-Nelson, Z. (2018). What Is a Cognitive Map? Organizing Knowledge for Flexible Behavior. *Neuron*, 100(2):490–509.

Beier, K. T., Gao, X. J., Xie, S., DeLoach, K. E., Malenka, R. C., and Luo, L. (2019). Topological Organization of Ventral Tegmental Area Connectivity Revealed by Viral-Genetic Dissection of Input-Output Relations. *Cell Reports*, 26(1):159–167.e6.

Beier, K. T., Kim, C. K., Hoerbelt, P., Hung, L. W., Heifets, B. D., DeLoach, K. E., Mosca, T. J., Neuner, S., Deisseroth, K., Luo, L., and Malenka, R. C. (2017). Rabies screen reveals GPe control of cocaine-triggered plasticity. *Nature*, pages 1–22.

Beier, K. T., Saunders, A., Oldenburg, I. A., Miyamichi, K., Akhtar, N., Luo, L., Whelan, S. P. J., Sabatini, B., and Cepko, C. L. (2011). Anterograde or retrograde transsynaptic labeling of CNS neurons with vesicular stomatitis virus vectors. *Proceedings of the National Academy of Sciences of the United States of America*, 108(37):15414–15419.

Beier, K. T., Steinberg, E. E., DeLoach, K. E., Xie, S., Miyamichi, K., Schwarz, L. A., Gao, X. J., Kremer, E. J., Malenka, R. C., and Luo, L. (2015). Circuit Architecture of VTA Dopamine Neurons Revealed by Systematic Input-Output Mapping. *Cell*, 162(3):622–634.

Belova, M. A., Paton, J. J., and Salzman, C. D. (2008). Moment-to-moment tracking of state value in the amygdala. *The Journal of neuroscience : the official journal of the Society for Neuroscience*, 28(40):10023–10030.

Benoit, S. C. and Davidson, T. L. (1996). Interoceptive sensory signals produced by 24-hr food deprivation, pharmacological glucoprivation, and lipoprivation. *Behavioral Neuroscience*, 110(1):168–180.

Berman, G. J., Choi, D. M., Bialek, W., and Shaevitz, J. W. (2014). Mapping the stereotyped behaviour of freely moving fruit flies. *Journal of the Royal Society, Interface*, 11(99):20140672.

Berrout, L. and Isokawa, M. (2012). Ghrelin promotes reorganization of dendritic spines in cultured rat hippocampal slices. *Neuroscience Letters*, 516(2):280–284.

Betley, J. N., Cao, Z. F. H., Ritola, K. D., and Sternson, S. M. (2013). Parallel, Redundant Circuit Organization for Homeostatic Control of Feeding Behavior. *Cell*, 155(6):1337–1350.

Biderman, N., Bakkour, A., and Shohamy, D. (2020). What Are Memories For? The Hippocampus Bridges Past Experience with Future Decisions. *Trends in cognitive sciences*.

Bienkowski, M. S., Bowman, I., Song, M. Y., Gou, L., Ard, T., Cotter, K., Zhu, M., Benavidez, N. L., Yamashita, S., Abu-Jaber, J., Azam, S., Lo, D., Foster, N. N., Hintiryan, H., and Dong, H.-W. (2018). Integration of gene expression and brain-wide connectivity reveals the multiscale organization of mouse hippocampal networks. *Nature Neuroscience*, 21(11):1628–1643.

Blum, I. D., Patterson, Z., Khazall, R., Lamont, E. W., Sleeman, M. W., Horvath, T. L., and Abizaid, A. (2009). Reduced anticipatory locomotor responses to scheduled meals in ghrelin receptor deficient mice. *Neuroscience*, 164(2):351–359.

Borden, P. M., Zhang, P., Shivange, A. V., Marvin, J. S., Cichon, J., Dan, C., Podgorski, K., Figueiredo, A., Novak, O., Tanimoto, M., Shigetomi, E., Lobas, M. A., Kim, H., Zhu, P. K., Zhang, Y., Zheng, W. S., Fan, C., Wang, G., Xiang, B., Gan, L., Zhang, G.-X., Guo, K., Lin, L., Cai, Y., Yee, A. G., Aggarwal, A., Ford, C. P., Rees, D. C., Dietrich, D., Khakh, B. S., Dittman, J. S., Gan, W.-B., Koyama, M., Jayaraman, V., Cheer, J. F., Lester, H. A., Zhu, J. J., and Looger, L. L. (2020). A fast genetically encoded fluorescent sensor for faithful in vivo acetylcholine detection in mice, fish, worms and flies. *bioRxiv*, page 2020.02.07.939504.

Bouton, M. E. (1993). Context, time, and memory retrieval in the interference paradigms of Pavlovian learning. *Psychological bulletin*, 114(1):80–99.

Britt, J. P., Benaliouad, F., McDevitt, R. A., Stuber, G. D., Wise, R. A., and Bonci, A. (2012). Synaptic and behavioral profile of multiple glutamatergic inputs to the nucleus accumbens. *Neuron*, 76(4):790–803.

Brog, J. S., Salyapongse, A., Deutch, A. Y., and Zahm, D. S. (1993). The patterns of afferent innervation of the core and shell in the "accumbens" part of the rat ventral striatum: immunohistochemical detection of retrogradely transported fluoro-gold. *Journal of Comparative Neurology*, 338(2):255–278.

Buckner, R. L. (2010). The Role of the Hippocampus in Prediction and Imagination. *Annual Review of Psychology*, 61(1):27–48.

Burnett, C. J., Funderburk, S. C., Navarrete, J., Sabol, A., Liang-Guallpa, J., Desrochers, T. M., and Krashes, M. J. (2019). Need-based prioritization of behavior. *eLife*, 8:140.

Burnett, C. J., Li, C., Webber, E., Tsaousidou, E., Xue, S. Y., Brüning, J. C., and Krashes, M. J. (2016). Hunger-Driven Motivational State Competition. *Neuron*, 92(1):187–201.

Buzsáki, G. (2015). Hippocampal sharp wave-ripple: A cognitive biomarker for episodic memory and planning. *Hippocampus*, 25(10):1073–1188.

Cabral, A., López Soto, E. J., Epelbaum, J., and Perelló, M. (2017). Is Ghrelin Synthesized in the Central Nervous System? *International journal of molecular sciences*, 18(3).

Calhoon, G. G., Sutton, A. K., Chang, C.-J., Libster, A. M., Glober, G. F., Leveque, C. L., Murphy, G. D., Namburi, P., Leppla, C. A., Siciliano, C. A., Wildes, C. P., Kimchi, E. Y., Beyeler, A., and Tye, K. M. (2018). Acute Food Deprivation Rapidly Modifies Valence-Coding Microcircuits in the Amygdala. *bioRxiv*, page 285189.

Calhoon, G. G. and Tye, K. M. (2015). Resolving the neural circuits of anxiety. *Nature Neuroscience*, 18(10):1394–1404.

Carey, A. A., Tanaka, Y., and van der Meer, M. A. A. (2019). Reward revaluation biases hippocampal replay content away from the preferred outcome. *Nature Neuroscience*, 22(9):1450–1459.

Carlini, V. P., Martini, A. C., Schiöth, H. B., Ruiz, R. D., Fiol de Cuneo, M., and de Barioglio, S. R. (2008). Decreased memory for novel object recognition in

chronically food-restricted mice is reversed by acute ghrelin administration. *Neuroscience*, 153(4):929–934.

Carlini, V. P., Monzon, M. E., Varas, M. M., Cragnolini, A. B., Schiöth, H. B., Scimonelli, T. N., and de Barioglio, S. R. (2002). Ghrelin increases anxiety-like behavior and memory retention in rats. *Biochemical and Biophysical Research Communications*, 299(5):739–743.

Carlini, V. P., Varas, M. M., Cragnolini, A. B., Schiöth, H. B., Scimonelli, T. N., and de Barioglio, S. R. (2004). Differential role of the hippocampus, amygdala, and dorsal raphe nucleus in regulating feeding, memory, and anxiety-like behavioral responses to ghrelin. *Biochemical and Biophysical Research Communications*, 313(3):635–641.

Carola, V., Mirabeau, O., and Gross, C. T. (2011). Hidden Markov model analysis of maternal behavior patterns in inbred and reciprocal hybrid mice. *PLoS ONE*, 6(3):e14753.

Carus-Cadavieco, M., Gorbati, M., Ye, L., Bender, F., van der Veldt, S., Kosse, C., Börgers, C., Lee, S. Y., Ramakrishnan, C., Hu, Y., Denisova, N., Ramm, F., Volitaki, E., Burdakov, D., Deisseroth, K., Ponomarenko, A., and Korotkova, T. (2017). Gamma oscillations organize top-down signalling to hypothalamus and enable food seeking. *Nature*, 542(7640):232–236.

Cassidy, R. M., Lu, Y., Jere, M., Tian, J.-B., Xu, Y., Mangieri, L. R., Felix-Okoroji, B., Selever, J., Xu, Y., Arenkiel, B. R., and Tong, Q. (2019). A lateral hypothalamus to basal forebrain neurocircuit promotes feeding by suppressing responses to anxiogenic environmental cues. *Science Advances*, 5(3):eaav1640.

Cembrowski, M. S., Bachman, J. L., Wang, L., Sugino, K., Shields, B. C., and Spruston, N. (2016). Spatial Gene-Expression Gradients Underlie Prominent Heterogeneity of CA1 Pyramidal Neurons. *Neuron*, 89(2):351–368.

Cembrowski, M. S., Phillips, M. G., DiLisio, S. F., Shields, B. C., Winnubst, J., Chandrashekar, J., Bas, E., and Spruston, N. (2018a). Dissociable Structural and Functional Hippocampal Outputs via Distinct Subiculum Cell Classes. *Cell*.

Cembrowski, M. S. and Spruston, N. (2019). Heterogeneity within classical cell types is the rule: lessons from hippocampal pyramidal neurons. *Nature Reviews Neuroscience*, 20(4):193–204.

Cembrowski, M. S., Wang, L., Lemire, A. L., Copeland, M., DiLisio, S. F., Clements, J., and Spruston, N. (2018b). The subiculum is a patchwork of discrete subregions. *eLife*, 7.

Cenquizca, L. A. and Swanson, L. W. (2006). Analysis of direct hippocampal cortical field CA1 axonal projections to diencephalon in the rat. *Journal of Comparative Neurology*, 497(1):101–114.

Cenquizca, L. A. and Swanson, L. W. (2007). Spatial organization of direct hippocampal field CA1 axonal projections to the rest of the cerebral cortex. *Brain Research Reviews*, 56(1):1–26.

Cetin, A., Komai, S., Eliava, M., Seeburg, P. H., and Osten, P. (2007). Stereotaxic gene delivery in the rodent brain. *Nature Protocols*, 1(6):3166–3173.

Chatterjee, S., Sullivan, H. A., MacLennan, B. J., Xu, R., Hou, Y., Lavin, T. K., Lea, N. E., Michalski, J. E., Babcock, K. R., Dietrich, S., Matthews, G. A., Beyeler, A., Calhoon, G. G., Glober, G., Whitesell, J. D., Yao, S., Cetin, A., Harris, J. A., Zeng, H., Tye, K. M., Reid, R. C., and Wickersham, I. R. (2018). Nontoxic, double-deletion-mutant rabies viral vectors for retrograde targeting of projection neurons. *Scientific Reports*, pages 1–16.

Chen, T.-W., Li, N., Daie, K., and Svoboda, K. (2017). A Map of Anticipatory Activity in Mouse Motor Cortex. *Neuron*, 94(4):866–879.e4.

Chen, Y., Lin, Y.-C., Kuo, T.-W., and Knight, Z. A. (2015). Sensory Detection of Food Rapidly Modulates Arcuate Feeding Circuits. *Cell*, 160(5):829–841.

Chen, Y., Lin, Y.-C., Zimmerman, C. A., Essner, R. A., and Knight, Z. A. (2016). Hunger neurons drive feeding through a sustained, positive reinforcement signal. *eLife*, 5:1202.

Choi, K., Holly, E. N., Davatolhagh, M. F., Beier, K. T., and Fuccillo, M. V. (2019).

Integrated anatomical and physiological mapping of striatal afferent projections. *The European journal of neuroscience*, 49(5):623–636.

Ciabatti, E., González-Rueda, A., Mariotti, L., Morgese, F., and Tripodi, M. (2017). Life-Long Genetic and Functional Access to Neural Circuits Using Self-Inactivating Rabies Virus. *Cell*, 170(2):382–392.e14.

Ciocchi, S., Passecker, J., Malagon-Vina, H., Mikus, N., and Klausberger, T. (2015). Selective information routing by ventral hippocampal CA1 projection neurons. *Science*, 348(6234):560–563.

Clements, J. D. and Bekkers, J. M. (1997). Detection of spontaneous synaptic events with an optimally scaled template. *Biophysical Journal*, 73(1):220–229.

Clifton, P. G. and Somerville, E. M. (1994). Disturbance of meal patterning following nucleus accumbens lesions in the rat. *Brain Research*, 667(1):123–128.

Clifton, P. G., Vickers, S. P., and Somerville, E. M. (1998). Little and often: Ingestive behavior patterns following hippocampal lesions in rats. *Behavioral Neuroscience*, 112(3):502–511.

Cohen, N. J. and Eichenbaum, H. B. (1993). *Memory, amnesia, and the hippocampal system.* Memory, amnesia, and the hippocampal system. The MIT Press, Cambridge, MA, US.

Colgin, L. L. (2016). Rhythms of the hippocampal network. 17(4):239–249.

Colgin, L. L., Kubota, D., and Lynch, G. (2003). Cholinergic plasticity in the hippocampus. *Proceedings of the National Academy of Sciences of the United States of America*, 100(5):2872–2877.

Colgin, L. L., Moser, E. I., and Moser, M.-B. (2008). Understanding memory through hippocampal remapping. *Trends in Neurosciences*, 31(9):469–477.

Compan, V., Walsh, B. T., Kaye, W., and Geliebter, A. (2015). How Does the Brain Implement Adaptive Decision Making to Eat? *The Journal of neuroscience : the official journal of the Society for Neuroscience*, 35(41):13868–13878.

Cone, J. J., Fortin, S. M., McHenry, J. A., Stuber, G. D., McCutcheon, J. E., and Roitman, M. F. (2016). Physiological state gates acquisition and expression of mesolimbic reward prediction signals. *Proceedings of the National Academy of Sciences*, 113(7):1943–1948.

Cone, J. J., McCutcheon, J. E., and Roitman, M. F. (2014). Ghrelin Acts as an Interface between Physiological State and Phasic Dopamine Signaling. *Journal of Neuroscience*, 34(14):4905–4913.

Cooper, D. C., Klipec, W. D., Fowler, M. A., and Ozkan, E. D. (2006). A role for the subiculum in the brain motivation/reward circuitry. *Behavioural Brain Research*, 174(2):225–231.

Corcoran, K. A. and Maren, S. (2001). Hippocampal inactivation disrupts contextual retrieval of fear memory after extinction. *Journal of Neuroscience*, 21(5):1720–1726. ISBN: 0270-6474 Publisher: Soc Neuroscience.

Cruz, M. T., Herman, M. A., Cote, D. M., Ryabinin, A. E., and Roberto, M. (2013). Ghrelin increases GABAergic transmission and interacts with ethanol actions in the rat central nucleus of the amygdala. *Neuropsychopharmacology : official publication of the American College of Neuropsychopharmacology*, 38(2):364–375.

Cummings, D. E., Frayo, R. S., Marmonier, C., Aubert, R., and Chapelot, D. (2004). Plasma ghrelin levels and hunger scores in humans initiating meals voluntarily without time- and food-related cues. *American journal of physiology. Endocrinology and metabolism*, 287(2):E297–304.

Damian, M., Marie, J., Leyris, J.-P., Fehrentz, J.-A., Verdié, P., Martinez, J., Banères, J.-L., and Mary, S. (2012). High constitutive activity is an intrinsic feature of ghrelin receptor protein: a study with a functional monomeric GHS-R1a receptor reconstituted in lipid discs. *The Journal of biological chemistry*, 287(6):3630–3641.

Davidson, T. J., Kloosterman, F., and Wilson, M. A. (2009a). Hippocampal replay of extended experience. *Neuron*, 63(4):497–507.

Davidson, T. L. (1998). Hunger cues as modulatory stimuli. In *Occasion setting: Associative learning and cognition in animals.*, pages 223–248. American Psychological Association, Washington.

Davidson, T. L. and Benoit, S. C. (1996). The learned function of food-deprivation cues: A role for conditioned modulation. *Animal Learning & Behavior*, 24(1):46–56.

Davidson, T. L., Chan, K., Jarrard, L. E., Kanoski, S. E., Clegg, D. J., and Benoit, S. C. (2009b). Contributions of the hippocampus and medial prefrontal cortex to energy and body weight regulation. *Hippocampus*, 19(3):235–252.

Davidson, T. L. and Jarrard, L. E. (1993). A role for hippocampus in the utilization of hunger signals. *Behavioral and neural biology*, 59(2):167–171.

Davidson, T. L. and Jarrard, L. E. (2004). The hippocampus and inhibitory learning: a 'Gray' area? *Neuroscience and Biobehavioral Reviews*, 28(3):261–271.

Davidson, T. L., Kanoski, S. E., Chan, K., Clegg, D. J., Benoit, S. C., and Jarrard, L. E. (2010). Hippocampal lesions impair retention of discriminative responding based on energy state cues. *Behavioral Neuroscience*, 124(1):97–105.

Davidson, T. L., Kanoski, S. E., Schier, L. A., Clegg, D. J., and Benoit, S. C. (2007). A potential role for the hippocampus in energy intake and body weight regulation. *Current Opinion in Pharmacology*, 7(6):613–616.

Davidson, T. L., Sample, C. H., and Swithers, S. E. (2014). An application of Pavlovian principles to the problems of obesity and cognitive decline. *Neurobiology of Learning and Memory*, 108(C):172–184.

Davis, J. F., Choi, D. L., Clegg, D. J., and Benoit, S. C. (2011). Signaling through the ghrelin receptor modulates hippocampal function and meal anticipation in mice. *Physiology & Behavior*, 103(1):39–43.

Deacon, R. M., Bannerman, D. M., and Rawlins, N. P. (2001). Conditional discriminations based on external and internal cues in rats with cytotoxic hippocampal lesions. *Behavioral Neuroscience*, 115(1):43–57.

Deadwyler, S. A., Bunn, T., and Hampson, R. E. (1996). Hippocampal ensemble activity during spatial delayed-nonmatch-to-sample performance in rats. *Journal of Neuroscience*, 16(1):354–372.

Delgado, J. M. R. and Anand, B. K. (1953). Increase of food intake induced by electrical stimulation of the lateral hypothalamus. *The American journal of physiology*, 172(1):162–168.

Diano, S., Farr, S. A., Benoit, S. C., McNay, E. C., da Silva, I., Horvath, T. L., Gaskin, F. S., Nonaka, N., Jaeger, L. B., Banks, W. A., Morley, J. E., Pinto, S., Sherwin, R. S., Xu, L., Yamada, K. A., Sleeman, M. W., and Tschöp, M. H. (2006). Ghrelin controls hippocampal spine synapse density and memory performance. *Nature Neuroscience*, 9(3):381–388.

Dickinson, A. and Balleine, B. (1994). Motivational control of goal-directed action. *Animal Learning & Behavior*, 22(1):1–18.

Ding, S.-L., Yao, Z., Hirokawa, K. E., Nguyen, T. N., Graybuck, L. T., Fong, O., Bohn, P., Ngo, K., Smith, K. A., Koch, C., Phillips, J. W., Lein, E. S., Harris, J. A., Tasic, B., and Zeng, H. (2020). Distinct Transcriptomic Cell Types and Neural Circuits of the Subiculum and Prosubiculum along the Dorsal-Ventral Axis. *Cell Reports*, 31(7):107648.

Do, J. P., Xu, M., Lee, S.-H., Chang, W.-C., Zhang, S., Chung, S., Yung, T. J., Fan, J. L., Miyamichi, K., Luo, L., and Dan, Y. (2016). Cell type-specific long-range connections of basal forebrain circuit. *eLife*, 5:4746.

Doll, B. B., Duncan, K. D., Simon, D. A., Shohamy, D., and Daw, N. D. (2015a). Model-based choices involve prospective neural activity. *Nature Neuroscience*, 18(5):767–772.

Doll, B. B., Shohamy, D., and Daw, N. D. (2015b). Multiple memory systems as substrates for multiple decision systems. *Neurobiology of Learning and Memory*, 117:4–13.

Dolleman-van der Weel, M. J., Griffin, A. L., Ito, H. T., Shapiro, M. L., Witter, M. P., Vertes, R. P., and Allen, T. A. (2019). The nucleus reuniens of the thalamus sits at

the nexus of a hippocampus and medial prefrontal cortex circuit enabling memory and behavior. *Learning & memory (Cold Spring Harbor, N.Y.)*, 26(7):191–205.

Dong, H.-W., Swanson, L. W., Chen, L., Fanselow, M. S., and Toga, A. W. (2009). Genomic-anatomic evidence for distinct functional domains in hippocampal field CA1. *Proceedings of the National Academy of Sciences of the United States of America*, 106(28):11794–11799.

Drazen, D. L., Vahl, T. P., D'Alessio, D. A., Seeley, R. J., and Woods, S. C. (2006). Effects of a fixed meal pattern on ghrelin secretion: evidence for a learned response independent of nutrient status. *Endocrinology*, 147(1):23–30.

Drever, B. D., Riedel, G., and Platt, B. (2011). The cholinergic system and hippocampal plasticity. *Behavioural Brain Research*, 221(2):505–514.

Duncan, K. D., Doll, B. B., Daw, N. D., and Shohamy, D. (2018). More Than the Sum of Its Parts: A Role for the Hippocampus in Configural Reinforcement Learning. *Neuron*.

Eichenbaum, H. B. and Cohen, N. J. (2014). Can we reconcile the declarative memory and spatial navigation views on hippocampal function? *Neuron*, 83(4):764–770.

Fanselow, M. S. and Dong, H.-W. (2010). Are the Dorsal and Ventral Hippocampus Functionally Distinct Structures? *Neuron*, 65(1):7–19.

Ferrini, F., Salio, C., Lossi, L., and Merighi, A. (2009). Ghrelin in central neurons. *Current neuropharmacology*, 7(1):37–49. Publisher: Bentham Science Publishers Ltd.

File, S. E. and Gonzalez, L. E. (1996). Anxiolytic effects in the plus-maze of 5-HT1A-receptor ligands in dorsal raphé and ventral hippocampus. *Pharmacology, biochemistry, and behavior*, 54(1):123–128.

Filosa, A., Barker, A. J., Dal Maschio, M., and Baier, H. (2016). Feeding State Modulates Behavioral Choice and Processing of Prey Stimuli in the Zebrafish Tectum. *Neuron*, 90(3):596–608.

Fry, M. and Ferguson, A. V. (2010). Ghrelin: central nervous system sites of action in regulation of energy balance. *International journal of peptides*, 2010(5):1–8.

Furness, J. B., Hunne, B., Matsuda, N., Yin, L., Russo, D., Kato, I., Fujimiya, M., Patterson, M., McLeod, J., Andrews, Z. B., and Bron, R. (2011). Investigation of the presence of ghrelin in the central nervous system of the rat and mouse. *Neuroscience*, 193(C):1–9.

Fürth, D., Vaissière, T., Tzortzi, O., Xuan, Y., Märtin, A., Lazaridis, I., Spigolon, G., Fisone, G., Tomer, R., Deisseroth, K., Carlén, M., Miller, C. A., Rumbaugh, G., and Meletis, K. (2018). An interactive framework for whole-brain maps at cellular resolution. *Nature Neuroscience*, 21(1):139–149.

Gao, C., Leng, Y., Ma, J., Rooke, V., Rodriguez-Gonzalez, S., Ramakrishnan, C., Deisseroth, K., and Penzo, M. A. (2020). Two genetically, anatomically and functionally distinct cell types segregate across anteroposterior axis of paraventricular thalamus. *Nature Neuroscience*, 23(2):217–228.

Gauthier, J. L. and Tank, D. W. (2018). A Dedicated Population for Reward Coding in the Hippocampus. *Neuron*.

Gehrlach, D. A., Gaitanos, T. N., Klein, A. S., Weiand, C., Hennrich, A. A., Conzelmann, K.-K., and Gogolla, N. (2020). A whole-brain connectivity map of mouse insular cortex. *bioRxiv*, 214(5–6):2020.02.10.941518.

Gershman, S. J. (2017). Context-dependent learning and causal structure. *Psychonomic bulletin & review*, 24(2):557–565.

Goldstone, A. P., Prechtl, C. G., Scholtz, S., Miras, A. D., Chhina, N., Durighel, G., Deliran, S. S., Beckmann, C., Ghatei, M. A., Ashby, D. R., Waldman, A. D., Gaylinn, B. D., Thorner, M. O., Frost, G. S., Bloom, S. R., and Bell, J. D. (2014). Ghrelin mimics fasting to enhance human hedonic, orbitofrontal cortex, and hippocampal responses to food. *The American journal of clinical nutrition*, 99(6):1319–1330.

Gonzalez, J. A., Iordanidou, P., Strom, M., Adamantidis, A., and Burdakov, D. (2016). Awake dynamics and brain-wide direct inputs of hypothalamic MCH and orexin networks. *Nature Communications*, 7:1–9.

González, J. A., Jensen, L. T., Iordanidou, P., Strom, M., Fugger, L., and Burdakov, D. (2016). Inhibitory Interplay between Orexin Neurons and Eating. *Current Biology*, 26(18):2486–2491.

Good, M. and Honey, R. C. (1991). Conditioning and contextual retrieval in hippocampal rats. *Behavioral neuroscience*, 105(4):499. ISBN: 1939-0084 Publisher: American Psychological Association.

Gooley, J. J., Schomer, A., and Saper, C. B. (2006). The dorsomedial hypothalamic nucleus is critical for the expression of food-entrainable circadian rhythms. *Nature Neuroscience*, 9(3):398–407.

Gore, F., Schwartz, E. C., Brangers, B. C., Aladi, S., Stujenske, J. M., Likhtik, E., Russo, M. J., Gordon, J. A., Salzman, C. D., and Axel, R. (2015). Neural Representations of Unconditioned Stimuli in Basolateral Amygdala Mediate Innate and Learned Responses. *Cell*, 162(1):134–145.

Gray, J. A. and McNaughton, N. (2003). *The Neuropsychology of Anxiety*. An Enquiry Into the Function of the Septo-hippocampal System. Oxford University Press.

Grossman, S. P., Dacey, D., Halaris, A. E., Collier, T., and Routtenberg, A. (1978). Aphagia and adipsia after preferential destruction of nerve cell bodies in hypothalamus. *Science*, 202(4367):537–539.

Grupe, D. W. and Nitschke, J. B. (2013). Uncertainty and anticipation in anxiety: an integrated neurobiological and psychological perspective. *Nature Reviews Neuroscience*, 14(7):488–501.

Gründemann, J., Bitterman, Y., Lu, T., Krabbe, S., Grewe, B. F., Schnitzer, M. J., and Lüthi, A. (2019). Amygdala ensembles encode behavioral states. *Science*, 364(6437):eaav8736.

Guan, X. M., Yu, H., Palyha, O. C., McKee, K. K., Feighner, S. D., Sirinathsinghji, D. J., Smith, R. G., Van der Ploeg, L. H., and Howard, A. D. (1997). Distribution of mRNA encoding the growth hormone secretagogue receptor in brain and peripheral tissues. *Brain research. Molecular brain research*, 48(1):23–29.

Gupta, R., Duff, M. C., Denburg, N. L., Cohen, N. J., Bechara, A., and Tranel, D. (2009). Declarative memory is critical for sustained advantageous complex decision-making. *Neuropsychologia*, 47(7):1686–1693.

Guru, A., Seo, C., Post, R. J., Kullakanda, D. S., Schaffer, J. A., and Warden, M. R. (2020). Ramping activity in midbrain dopamine neurons signifies the use of a cognitive map. *bioRxiv*, 542:2020.05.21.108886.

Gutbrod, K., Krouzel, C., Hofer, H., Müri, R., Perrig, W., and Ptak, R. (2006). Decision-making in amnesia: do advantageous decisions require conscious knowledge of previous behavioural choices? *Neuropsychologia*, 44(8):1315–1324.

Hafting, T., Fyhn, M., Molden, S., Moser, M.-B., and Moser, E. I. (2005). Microstructure of a spatial map in the entorhinal cortex. *Nature*, 436(7052):801–806.

Hahn, J. D. and Swanson, L. W. (2012). Connections of the lateral hypothalamic area juxtadorsomedial region in the male rat. *Journal of Comparative Neurology*, 520(9):1831–1890.

Halford, J. C. G., Wanninayake, S. C. D., and Blundell, J. E. (1998). Behavioral Satiety Sequence (BSS) for the Diagnosis of Drug Action on Food Intake. *Pharmacology, biochemistry, and behavior*, 61(2):159–168.

Hamasaki, S., Mukuda, T., Koyama, Y., Nakane, H., and Kaidoh, T. (2020). Constitutive accessibility of circulating proteins to hippocampal neurons in physiologically normal rats. *Brain and Behavior*, 10(3):443.

Hamid, A. A., Pettibone, J. R., Mabrouk, O. S., Hetrick, V. L., Schmidt, R., Vander Weele, C. M., Kennedy, R. T., Aragona, B. J., and Berke, J. D. (2016). Mesolimbic dopamine signals the value of work. *Nature Neuroscience*, 19(1):117–126.

Hampson, R. E. and Deadwyler, S. A. (2003). Temporal firing characteristics and the strategic role of subicular neurons in short-term memory. *Hippocampus*, 13(4):529–541.

Hampson, R. E., Hedberg, T., and Deadwyler, S. A. (2000). Differential information processing by hippocampal and subicular neurons. *Annals of the New York Academy of Sciences*, 911:151–165.

Han, J. E., Frasnelli, J. A., zeighami, y., Larcher, K., Boyle, J. A., McConnell, T., Malik, S., Jones-Gotman, M., and Dagher, A. (2018). Ghrelin enhances food odor conditioning in healthy humans: an fMRI study.

Hannapel, R. C., Henderson, Y. O., Nalloor, R., Vazdarjanova, A., and Parent, M. B. (2017). Ventral hippocampal neurons inhibit postprandial energy intake. *Hippocampus*, 27(3):274–284.

Harvey, J. (2013). Leptin regulation of neuronal morphology and hippocampal synaptic function. pages 1–7.

Hebben, N., Corkin, S., Eichenbaum, H. B., and Shedlack, K. (1985). Diminished ability to interpret and report internal states after bilateral medial temporal resection: Case H.M. *Behavioral Neuroscience*, 99(6):1031–1039.

Henderson, Y. O., Smith, G. P., and Parent, M. B. (2012). Hippocampal neurons inhibit meal onset. *Hippocampus*, 23(1):100–107.

Herman, A. M., Ortiz-Guzman, J., Kochukov, M., Herman, I., Quast, K. B., Patel, J. M., Tepe, B., Carlson, J. C., Ung, K., Selever, J., Tong, Q., and Arenkiel, B. R. (2016). A cholinergic basal forebrain feeding circuit modulates appetite suppression. *Nature*, 538(7624):253–256.

Herzog, L. E., Katz, D. B., and Jadhav, S. P. (2020). Refinement and Reactivation of a Taste-Responsive Hippocampal Network. *Current Biology*, 30(7):1306–1311.e4.

Herzog, L. E., Pascual, L. M., Scott, S. J., Mathieson, E. R., Katz, D. B., and Jadhav, S. P. (2018). Interaction of taste and place coding in the hippocampus. *bioRxiv*, page 431353.

Herzog, L. E., Pascual, L. M., Scott, S. J., Mathieson, E. R., Katz, D. B., and Jadhav, S. P. (2019). Interaction of Taste and Place Coding in the Hippocampus. *The*

Journal of neuroscience : the official journal of the Society for Neuroscience, 39(16):3057–3069.

Higgs, S., Williamson, A. C., Rotshtein, P., and Humphreys, G. W. (2008). Sensory-Specific Satiety Is Intact in Amnesics Who Eat Multiple Meals. *Psychological Science*, 19(7):623–628.

Hirsh, R. (1974). The hippocampus and contextual retrieval of information from memory: a theory. *Behavioral biology*, 12(4):421–444.

Hock, B. J. and Bunsey, M. D. (1998). Differential effects of dorsal and ventral hippocampal lesions. *Journal of Neuroscience*, 18(17):7027–7032.

Holland, A. J., Treasure, J., Coskeran, P., and Dallow, J. (1995). Characteristics of the eating disorder in Prader-Willi syndrome: implications for treatment. *Journal of intellectual disability research : JIDR*, 39 (Pt 5)(5):373–381.

Holland, P. C., Lamoureux, J. A., Han, J. S., and Gallagher, M. (1999). Hippocampal lesions interfere with Pavlovian negative occasion setting. *Hippocampus*, 9(2):143–157.

Hornsby, A. K. E., Redhead, Y. T., Rees, D. J., Ratcliff, M. S. G., Reichenbach, A., Wells, T., Francis, L., Amstalden, K., Andrews, Z. B., and Davies, J. S. (2016). Short-term calorie restriction enhances adult hippocampal neurogenesis and remote fear memory in a Ghsr-dependent manner. *Psychoneuroendocrinology*, 63:198–207.

Howe, M. W., Tierney, P. L., Sandberg, S. G., Phillips, P. E. M., and Graybiel, A. M. (2013). Prolonged dopamine signalling in striatum signals proximity and value of distant rewards. *Nature*, 500(7464):575–579.

Hsiao, S. and Isaacson, R. L. (1971). Learning of food and water positions by hippocampus damaged rats. *Includes a Special Section on Chronobiology Aspects of the Sleep–Wake Cycle and Thermoreregulation*, 6(1):81–83.

Hsu, T. M., Hahn, J. D., Konanur, V. R., Lam, A., and Kanoski, S. E. (2014). Hippocampal GLP-1 Receptors Influence Food Intake, Meal Size, and Effort-Based

Responding for Food through Volume Transmission. *Neuropsychopharmacology*, 40(2):327–337.

Hsu, T. M., Hahn, J. D., Konanur, V. R., Noble, E. E., Suarez, A. N., Thai, J., Nakamoto, E. M., and Kanoski, S. E. (2015). Hippocampus ghrelin signaling mediates appetite through lateral hypothalamic orexin pathways. *eLife*, 4:e46321.

Hsu, T. M., Noble, E. E., Liu, C. M., Cortella, A. M., Konanur, V. R., Suarez, A. N., Reiner, D. J., Hahn, J. D., Hayes, M. R., and Kanoski, S. E. (2018). A hippocampus to prefrontal cortex neural pathway inhibits food motivation through glucagon-like peptide-1 signaling. *Molecular psychiatry*, 23(7):1555–1565.

Hsu, T. M., Suarez, A. N., and Kanoski, S. E. (2016). Ghrelin: A link between memory and ingestive behavior. *Physiology & Behavior*, 162(C):10–17.

Hua, R., Wang, X., Chen, X., Wang, X., Huang, P., Li, P., Mei, W., and Li, H. (2018). Calretinin Neurons in the Midline Thalamus Modulate Starvation-Induced Arousal. *Current Biology*, 28(24):3948–3959.e4.

Hull, C. L. (1943). *Principles of behavior*, volume 422. Appleton-century-crofts New York.

Hunt, D. L., Linaro, D., Si, B., Romani, S., and Spruston, N. (2018). A novel pyramidal cell type promotes sharp-wave synchronization in the hippocampus. *Nature Neuroscience*, 21(7):985–995.

Hölscher, C., Jacob, W., and Mallot, H. A. (2003). Reward modulates neuronal activity in the hippocampus of the rat. *Behavioural Brain Research*, 142(1-2):181–191.

Inagaki, H. K., Fontolan, L., Romani, S., and Svoboda, K. (2019). Discrete attractor dynamics underlies persistent activity in the frontal cortex. *Nature*, 34:1.

Inglis, F. M., Day, J. C., and Fibiger, H. C. (1994). Enhanced acetylcholine release in hippocampus and cortex during the anticipation and consumption of a palatable meal. *Neuroscience*, 62(4):1049–1056.

Ito, H. T., Zhang, S.-J., Witter, M. P., Moser, E. I., and Moser, M.-B. (2015). A prefrontal–thalamo–hippocampal circuit for goal-directed spatial navigation. *Nature*, 522(7554):50–55.

Ito, M. and Doya, K. (2009). Validation of decision-making models and analysis of decision variables in the rat basal ganglia. *The Journal of neuroscience : the official journal of the Society for Neuroscience*, 29(31):9861–9874.

Ito, R., Everitt, B. J., and Robbins, T. W. (2005). The hippocampus and appetitive Pavlovian conditioning: effects of excitotoxic hippocampal lesions on conditioned locomotor activity and autoshaping. *Hippocampus*, 15(6):713–721.

Ito, R. and Lee, A. C. H. (2016). The role of the hippocampus in approach-avoidance conflict decision-making: Evidence from rodent and human studies. *Behavioural Brain Research*, 313:345–357.

Ito, R., Robbins, T. W., Pennartz, C. M. A., and Everitt, B. J. (2008). Functional Interaction between the Hippocampus and Nucleus Accumbens Shell Is Necessary for the Acquisition of Appetitive Spatial Context Conditioning. *Journal of Neuroscience*, 28(27):6950–6959.

Jennings, J. H., Rizzi, G., Stamatakis, A. M., Ung, R. L., and Stuber, G. D. (2013). The inhibitory circuit architecture of the lateral hypothalamus orchestrates feeding. *Science*, 341(6153):1517–1521.

Jennings, J. H., Ung, R. L., Resendez, S. L., Stamatakis, A. M., Taylor, J. G., Huang, J., Veleta, K., Kantak, P. A., Aita, M., Shilling-Scrivo, K., Ramakrishnan, C., Deisseroth, K., Otte, S., and Stuber, G. D. (2015). Visualizing Hypothalamic Network Dynamics for Appetitive and Consummatory Behaviors. *Cell*, 160(3):516–527.

Jeong, Y., Huh, N., Lee, J., Yun, I., Lee, J. W., Lee, I., and Jung, M. W. (2018). Role of the hippocampal CA1 region in incremental value learning. *Nature Reviews Neuroscience*, 8(1):9870–15.

Jerlhag, E., Egecioglu, E., Dickson, S. L., Douhan, A., Svensson, L., and Engel, J. A. (2007). Ghrelin administration into tegmental areas stimulates locomotor activity and increases extracellular concentration of dopamine in the nucleus accumbens. *Addiction biology*, 12(1):6–16.

Jimenez, J. C., Su, K., Goldberg, A. R., Luna, V. M., Biane, J. S., Ordek, G., Zhou, P., Ong, S. K., Wright, M. A., Zweifel, L., Paninski, L., Hen, R., and Kheirbek, M. A. (2018). Anxiety Cells in a Hippocampal-Hypothalamic Circuit. *Neuron*, 97(3):670–683.e6.

Johnson, A. and Redish, A. D. (2007). Neural ensembles in CA3 transiently encode paths forward of the animal at a decision point. *The Journal of neuroscience : the official journal of the Society for Neuroscience*, 27(45):12176–12189.

Jonas, P., Major, G., and Sakmann, B. (1993). Quantal components of unitary EPSCs at the mossy fibre synapse on CA3 pyramidal cells of rat hippocampus. *The Journal of Physiology*, 472(1):615–663.

Jun, J. J., Steinmetz, N. A., Siegle, J. H., Denman, D. J., Bauza, M., Barbarits, B., Lee, A. K., Anastassiou, C. A., Andrei, A., Aydın, , Barbic, M., Blanche, T. J., Bonin, V., Couto, J., Dutta, B., Gratiy, S. L., Gutnisky, D. A., Häusser, M., Karsh, B., Ledochowitsch, P., Lopez, C. M., Mitelut, C., Musa, S., Okun, M., Pachitariu, M., Putzeys, J., Rich, P. D., Rossant, C., Sun, W.-L., Svoboda, K., Carandini, M., Harris, K. D., Koch, C., O'Keefe, J., and Harris, T. D. (2017). Fully integrated silicon probes for high-density recording of neural activity. *Nature*, 551(7679):232–236.

Jung, M., Wiener, S., and McNaughton, B. (1994). Comparison of spatial firing characteristics of units in dorsal and ventral hippocampus of the rat. *The Journal of Neuroscience*, 14(12):7347.

Kanoski, S. E., Fortin, S. M., Ricks, K. M., and Grill, H. J. (2013). Ghrelin Signaling in the Ventral Hippocampus Stimulates Learned and Motivational Aspects of Feeding via PI3K-Akt Signaling. *Biological Psychiatry*, 73(9):915–923.

Kanoski, S. E. and Grill, H. J. (2017). Hippocampus Contributions to Food Intake Control: Mnemonic, Neuroanatomical, and Endocrine Mechanisms. *Biological Psychiatry*, 81(9):748–756.

Kanoski, S. E., Hayes, M. R., and Skibicka, K. P. (2016). GLP-1 and weight loss: unraveling the diverse neural circuitry. *American Journal of Physiology-Regulatory, Integrative and Comparative Physiology*, 310(10):R885–R895.

Kanoski, S. E., Walls, E. K., and Davidson, T. L. (2007). Interoceptive "satiety" signals produced by leptin and CCK. *Peptides*, 28(5):988–1002.

Kay, K., Chung, J. E., Sosa, M., Schor, J. S., Karlsson, M. P., Larkin, M. C., Liu, D. F., and Frank, L. M. (2020). Constant Sub-second Cycling between Representations of Possible Futures in the Hippocampus. *Cell*, pages 1–42.

Keck, T., Keller, G. B., Jacobsen, R. I., Eysel, U. T., Bonhoeffer, T., and Hübener, M. (2013). Synaptic scaling and homeostatic plasticity in the mouse visual cortex in vivo. *Neuron*, 80(2):327–334.

Kelley, A. E., Baldo, B. A., and Pratt, W. E. (2005). A proposed hypothalamic-thalamic-striatal axis for the integration of energy balance, arousal, and food reward. *The Journal of comparative neurology*, 493(1):72–85.

Kennedy, P. J. (2004). Retrieving Memories via Internal Context Requires the Hippocampus. *Journal of Neuroscience*, 24(31):6979–6985.

Kennedy, P. J. and Shapiro, M. L. (2009). Motivational states activate distinct hippocampal representations to guide goal-directed behaviors. *Proceedings of the National Academy of Sciences of the United States of America*, 106(26):10805–10810.

Kern, A., Grande, C., and Smith, R. G. (2014). Apo-Ghrelin Receptor (apo-GHSR1a) Regulates Dopamine Signaling in the Brain. *Frontiers in endocrinology*, 5:129.

Kern, A., Mavrikaki, M., Ullrich, C., Albarran-Zeckler, R., Brantley, A. F., and Smith, R. G. (2015). Hippocampal Dopamine/DRD1 Signaling Dependent on the Ghrelin Receptor. *Cell*, 163(5):1176–1190.

Khalsa, S. S., Adolphs, R., Cameron, O. G., Critchley, H. D., Davenport, P. W., Feinstein, J. S., Feusner, J. D., Garfinkel, S. N., Lane, R. D., Mehling, W. E., Meuret, A. E., Nemeroff, C. B., Oppenheimer, S., Petzschner, F. H., Pollatos, O., Rhudy, J. L., Schramm, L. P., Simmons, W. K., Stein, M. B., Stephan, K. E., Van den Bergh, O., Van Diest, I., von Leupoldt, A., Paulus, M. P., and Interoception Summit 2016 participants (2018). Interoception and Mental Health: A Roadmap. *Biological psychiatry. Cognitive neuroscience and neuroimaging*, 3(6):501–513.

Khalsa, S. S., Craske, M. G., Li, W., Vangala, S., Strober, M., and Feusner, J. D. (2015). Altered interoceptive awareness in anorexia nervosa: Effects of meal anticipation, consumption and bodily arousal. *The International journal of eating disorders*, 48(7):889–897.

Kheirbek, M. A., Drew, L. J., Burghardt, N. S., Costantini, D. O., Tannenholz, L., Ahmari, S. E., Zeng, H., Fenton, A. A., and Hen, R. (2013). Differential control of learning and anxiety along the dorsoventral axis of the dentate gyrus. *Neuron*, 77(5):955–968.

Kim, E. J., Jacobs, M. W., Ito-Cole, T., and Callaway, E. M. (2016). Improved Monosynaptic Neural Circuit Tracing Using Engineered Rabies Virus Glycoproteins. *Cell Reports*, 15(4):692–699.

Kim, H., Sul, J. H., Huh, N., Lee, D., and Jung, M. W. (2009). Role of striatum in updating values of chosen actions. *The Journal of neuroscience : the official journal of the Society for Neuroscience*, 29(47):14701–14712.

Kim, H. R., Malik, A. N., Mikhael, J. G., Bech, P., Tsutsui-Kimura, I., Sun, F., Zhang, Y., Li, Y., Watabe-Uchida, M., Gershman, S. J., and Uchida, N. (2019). A unified framework for dopamine signals across timescales. *bioRxiv*, 9:803437.

Kim, J., Zhang, X., Muralidhar, S., LeBlanc, S. A., and Tonegawa, S. (2017). Basolateral to Central Amygdala Neural Circuits for Appetitive Behaviors. *Neuron*, 93(6):1464–1479.e5.

Kim, W. B. and Cho, J.-H. (2017). Synaptic Targeting of Double-Projecting Ventral CA1 Hippocampal Neurons to the Medial Prefrontal Cortex and Basal Amygdala. *The Journal of neuroscience : the official journal of the Society for Neuroscience*, 37(19):4868–4882.

Kim, Y. and Spruston, N. (2011). Target-specific output patterns are predicted by the distribution of regular-spiking and bursting pyramidal neurons in the subiculum. *Hippocampus*, 22(4):693–706.

Kjelstrup, K. B., Solstad, T., Brun, V. H., Hafting, T., Leutgeb, S., Witter, M. P., Moser, E. I., and Moser, M.-B. (2008). Finite scale of spatial representation in the hippocampus. *Science (New York, N.Y.)*, 321(5885):140–143.

Knierim, J. J., Neunuebel, J. P., and Deshmukh, S. S. (2014). Functional correlates of the lateral and medial entorhinal cortex: objects, path integration and local-global reference frames. *Philosophical transactions of the Royal Society of London. Series B, Biological sciences*, 369(1635):20130369–20130369.

Kohara, K., Pignatelli, M., Rivest, A. J., Jung, H.-Y., Kitamura, T., Suh, J., Frank, D., Kajikawa, K., Mise, N., Obata, Y., Wickersham, I. R., and Tonegawa, S. (2013). Cell type–specific genetic and optogenetic tools reveal hippocampal CA2 circuits. *Nature Neuroscience*, 17(2):269–279.

Komorowski, R. W., Garcia, C. G., Wilson, A., Hattori, S., Howard, M. W., and Eichenbaum, H. B. (2013). Ventral Hippocampal Neurons Are Shaped by Experience to Represent Behaviorally Relevant Contexts. *Journal of Neuroscience*, 33(18):8079–8087.

Krause, M., German, P. W., Taha, S. A., and Fields, H. L. (2010). A Pause in Nucleus Accumbens Neuron Firing Is Required to Initiate and Maintain Feeding. *The Journal of Neuroscience*, 30(13):4746.

Kullmann, D. M., Moreau, A. W., Bakiri, Y., and Nicholson, E. (2012). Plasticity of Inhibition. *Neuron*, 75(6):951–962.

Langlet, F., Levin, B. E., Luquet, S., Mazzone, M., Messina, A., Dunn-Meynell, A. A., Balland, E., Lacombe, A., Mazur, D., Carmeliet, P., Bouret, S. G., Prevot, V., and Dehouck, B. (2013). Tanycytic VEGF-A boosts blood-hypothalamus barrier plasticity and access of metabolic signals to the arcuate nucleus in response to fasting. *Cell metabolism*, 17(4):607–617.

Lathe, R. (2001). Hormones and the hippocampus. *The Journal of endocrinology*, 169(2):205–231.

Lathe, R., Singadia, S., Jordan, C., and Riedel, G. (2020). The interoceptive hippocampus: Mouse brain endocrine receptor expression highlights a dentate gyrus (DG)-cornu ammonis (CA) challenge-sufficiency axis. *PLoS ONE*, 15(1):e0227575.

Lee, H., Ghim, J.-W., Kim, H., Lee, D., and Jung, M. (2012). Hippocampal neural correlates for values of experienced events. *The Journal of neuroscience : the official journal of the Society for Neuroscience*, 32(43):15053–15065.

LeGates, T. A., Kvarta, M. D., Tooley, J. R., Francis, T. C., Lobo, M. K., Creed, M. C., and Thompson, S. M. (2018). Reward behaviour is regulated by the strength of hippocampus–nucleus accumbens synapses. *Nature*, 76:1.

Lerner, T. N., Shilyansky, C., Davidson, T. J., Evans, K. E., Beier, K. T., Zalocusky, K. A., Crow, A. K., Malenka, R. C., Luo, L., Tomer, R., and Deisseroth, K. (2015). Intact-Brain Analyses Reveal Distinct Information Carried by SNc Dopamine Subcircuits. *Cell*, 162(3):635–647.

Lever, C., Burton, S., Jeewajee, A., O'Keefe, J., and Burgess, N. (2009). Boundary vector cells in the subiculum of the hippocampal formation. *The Journal of neuroscience : the official journal of the Society for Neuroscience*, 29(31):9771–9777.

Lever, C., Burton, S., and O'Keefe, J. (2006). Rearing on Hind Legs, Environmental Novelty, and the Hippocampal Formation. *Reviews in the Neurosciences*, 17(1-2):9626.

Li, N., Daie, K., Svoboda, K., and Druckmann, S. (2016). Robust neuronal dynamics in premotor cortex during motor planning. *Nature*, 532(7600):459–464.

Lisman, J. E. and Grace, A. A. (2005). The hippocampal-VTA loop: controlling the entry of information into long-term memory. *Neuron*, 46(5):703–713. Place: United States.

Livneh, Y., Ramesh, R. N., Burgess, C. R., Levandowski, K. M., Madara, J. C., Fenselau, H., Goldey, G. J., Diaz, V. E., Jikomes, N., Resch, J. M., Lowell, B. B., and Andermann, M. L. (2017). Homeostatic circuits selectively gate food cue responses in insular cortex. *Nature*, 546(7660):611–616.

Livneh, Y., Sugden, A. U., Madara, J. C., Essner, R. A., Flores, V. I., Sugden, L. A., Resch, J. M., Lowell, B. B., and Andermann, M. L. (2020). Estimation of Current and Future Physiological States in Insular Cortex. *Neuron*.

Lopes, G., Bonacchi, N., Frazão, J., Neto, J. P., Atallah, B. V., Soares, S., Moreira, L., Matias, S., Itskov, P. M., Correia, P. A., Medina, R. E., Calcaterra, L., Dreosti, E., Paton, J. J., and Kampff, A. R. (2015). Bonsai: an event-based framework for processing and controlling data streams. *Frontiers in neuroinformatics*, 9(10):7.

Luo, L., Callaway, E. M., and Svoboda, K. (2018). Genetic Dissection of Neural Circuits: A Decade of Progress. *Neuron*, 98(2):256–281.

MacAskill, A. F., Cassel, J. M., and Carter, A. G. (2014). Cocaine exposure reorganizes cell type- and input-specific connectivity in the nucleus accumbens. *Nature Neuroscience*, 17(9):1198–1207.

MacAskill, A. F., Little, J. P., Cassel, J. M., and Carter, A. G. (2012). Subcellular connectivity underlies pathway-specific signaling in the nucleus accumbens. *Nature Neuroscience*, 15(12):1624–1626.

MacDonald, C. J., Lepage, K. Q., and Eden, U. T. (2011). Hippocampal "time cells" bridge the gap in memory for discontiguous events. 71(4):737–749.

Maldonado-Irizarry, C. S., Swanson, C. J., and Kelley, A. E. (1995). Glutamate receptors in the nucleus accumbens shell control feeding behavior via the lateral hypothalamus. *Journal of Neuroscience*, 15(10):6779–6788.

Malik, S., McGlone, F., Bedrossian, D., and Dagher, A. (2008). Ghrelin modulates brain activity in areas that control appetitive behavior. *Cell Metabolism*, 7(5):400–409.

Mani, B. K., Walker, A. K., Lopez Soto, E. J., Raingo, J., Lee, C. E., Perelló, M., Andrews, Z. B., and Zigman, J. M. (2014). Neuroanatomical characterization of a growth hormone secretagogue receptor-green fluorescent protein reporter mouse. *Journal of Comparative Neurology*, 522(16):3644–3666.

Maren, S. (1999). Neurotoxic or electrolytic lesions of the ventral subiculum produce deficits in the acquisition and expression of Pavlovian fear conditioning in rats. *Behavioral Neuroscience*, 113(2):283–290.

Markowitz, J. E., Gillis, W. F., Beron, C. C., Neufeld, S. Q., Robertson, K., Bhagat, N. D., Peterson, R. E., Peterson, E., Hyun, M., Linderman, S. W., Sabatini, B. L.,

and Datta, S. R. (2018). The Striatum Organizes 3D Behavior via Moment-to-Moment Action Selection. *Cell*, 174(1):44–58.e17.

Masurkar, A. V., Srinivas, K. V., Brann, D. H., Warren, R., Lowes, D. C., and Siegelbaum, S. A. (2017). Medial and Lateral Entorhinal Cortex Differentially Excite Deep versus Superficial CA1 Pyramidal Neurons. *Cell Reports*, 18(1):148–160.

Mathis, A., Mamidanna, P., Cury, K. M., Abe, T., Murthy, V. N., Mathis, M. W., and Bethge, M. (2018). DeepLabCut: markerless pose estimation of user-defined body parts with deep learning. *Nature Neuroscience*, 21(9):1281–1289.

McEwen, B. S., Bowles, N. P., Gray, J. D., Hill, M. N., Hunter, R. G., Karatsoreos, I. N., and Nasca, C. (2015). Mechanisms of stress in the brain. *Nature Neuroscience*, 18(10):1353–1363.

McHenry, J. A., Otis, J. M., Rossi, M. A., Robinson, J. E., Kosyk, O., Miller, N. W., McElligott, Z. A., Budygin, E. A., Rubinow, D. R., and Stuber, G. D. (2017). Hormonal gain control of a medial preoptic area social reward circuit. *Nature Neuroscience*, 20(3):449–458.

McKenzie, S., Frank, A. J., Kinsky, N. R., Porter, B., and Rivière, P. D. (2014). Hippocampal representation of related and opposing memories develop within distinct, hierarchically organized neural schemas. 83(1):202–215.

McNamara, C. G., Tejero-Cantero, , Trouche, S., Campo-Urriza, N., and Dupret, D. (2014). Dopaminergic neurons promote hippocampal reactivation and spatial memory persistence. *Nature Neuroscience*, 17(12):1658–1660.

McNay, E. C. (2007). Insulin and ghrelin: peripheral hormones modulating memory and hippocampal function. *Current Opinion in Pharmacology*, 7(6):628–632.

Mear, Y., Enjalbert, A., and Thirion, S. (2013). GHS-R1a constitutive activity and its physiological relevance. *Frontiers in neuroscience*, 7:87–87.

Mickelsen, L. E., Bolisetty, M., Chimileski, B. R., Fujita, A., Beltrami, E. J., Costanzo, J. T., Naparstek, J. R., Robson, P., and Jackson, A. C. (2019). Single-cell transcriptomic analysis of the lateral hypothalamic area reveals molecularly dis-

tinct populations of inhibitory and excitatory neurons. *Nature Neuroscience*, 22(4):642–656.

Miller, K. J., Botvinick, M. M., and Brody, C. D. (2017). Dorsal hippocampus contributes to model-based planning. *Nature Neuroscience*, 20(9):1269–1276.

Min, D. K., Tuor, U. I., and Chelikani, P. K. (2011). Gastric distention induced functional magnetic resonance signal changes in the rodent brain. *Neuroscience*, 179:151–158.

Mitchell, V. r., Bouret, S., Beauvillain, J.-C., Schilling, A., Perret, M., Kordon, C., and Epelbaum, J. (2000). Comparative distribution of mRNA encoding the growth hormone secretagogue-receptor (GHS-R) inMicrocebus murinus (Primate, Lemurian) and rat forebrain and pituitary. *Journal of Comparative Neurology*, 429(3):469–489.

Momennejad, I., Otto, A. R., Daw, N. D., and Norman, K. A. (2018). Offline replay supports planning in human reinforcement learning. *eLife*, 7.

Morris, R. G. M., Garrud, P., Rawlins, J. N. P., and O'Keefe, J. (1982). Place navigation impaired in rats with hippocampal lesions. *Nature*, 297(5868):681–683.

Morton, G. J., Meek, T. H., and Schwartz, M. W. (2014). Neurobiology of food intake in health and disease. *Scientific Reports*, 15(6):367–378.

Moser, M.-B. and Moser, E. I. (1998). Functional differentiation in the hippocampus. *Hippocampus*, 8(6):608–619.

Mukherjee, A., Carvalho, F., Eliez, S., and Caroni, P. (2019). Long-Lasting Rescue of Network and Cognitive Dysfunction in a Genetic Schizophrenia Model. *Cell*.

Murtuza, M. I. and Isokawa, M. (2018). Endogenous ghrelin-O-acyltransferase (GOAT) acylates local ghrelin in the hippocampus. *Journal of neurochemistry*, 144(1):58–67.

Müller, T. D., Nogueiras, R., Andermann, M. L., Andrews, Z. B., Anker, S. D., Argente, J., Batterham, R. L., Benoit, S. C., Bowers, C. Y., Broglio, F., Casanueva, F. F., D'Alessio, D., Depoortere, I., Geliebter, A., Ghigo, E., Cole, P. A., Cowley,

M., Cummings, D. E., Dagher, A., Diano, S., Dickson, S. L., Diéguez, C., Granata, R., Grill, H. J., Grove, K., Habegger, K. M., Heppner, K., Heiman, M. L., Holsen, L., Holst, B., Inui, A., Jansson, J. O., Kirchner, H., Korbonits, M., Laferrère, B., LeRoux, C. W., Lopez, M., Morin, S., Nakazato, M., Nass, R., Perez-Tilve, D., Pfluger, P. T., Schwartz, T. W., Seeley, R. J., Sleeman, M., Sun, Y., Sussel, L., Tong, J., Thorner, M. O., van der Lely, A. J., van der Ploeg, L. H. T., Zigman, J. M., Kojima, M., Kangawa, K., Smith, R. G., Horvath, T. L., and Tschöp, M. H. (2015). Ghrelin. *Molecular Metabolism*, 4(6):437–460.

Naber, P. A. and Witter, M. P. (1998). Subicular efferents are organized mostly as parallel projections: a double-labeling, retrograde-tracing study in the rat. *Journal of Comparative Neurology*, 393(3):284–297.

Naleid, A. M., Grace, M. K., Cummings, D. E., and Levine, A. S. (2005). Ghrelin induces feeding in the mesolimbic reward pathway between the ventral tegmental area and the nucleus accumbens. *Peptides*, 26(11):2274–2279.

Namburi, P., Beyeler, A., Yorozu, S., Calhoon, G. G., Halbert, S. A., Wichmann, R., Holden, S. S., Mertens, K. L., Anahtar, M., Felix-Ortiz, A. C., Wickersham, I. R., Gray, J. M., and Tye, K. M. (2015). A circuit mechanism for differentiating positive and negative associations. *Nature*, 520(7549):675–678.

Narayanan, N. S. (2016). Ramping activity is a cortical mechanism of temporal control of action. *Current Opinion in Behavioral Sciences*, 8:226–230.

Natalucci, G., Riedl, S., Gleiss, A., Zidek, T., and Frisch, H. (2005). Spontaneous 24-h ghrelin secretion pattern in fasting subjects: maintenance of a meal-related pattern. *European journal of endocrinology*, 152(6):845–850.

Nguyen, H.-B., Bagot, R. C., Diorio, J., Wong, T. P., and Meaney, M. J. (2015). Maternal care differentially affects neuronal excitability and synaptic plasticity in the dorsal and ventral hippocampus. *Neuropsychopharmacology*, 40(7):1590–1599.

Nieh, E. H., Matthews, G. A., Allsop, S. A., Presbrey, K. N., Leppla, C. A., Wichmann, R., Neve, R., Wildes, C. P., and Tye, K. M. (2015). Decoding Neural Circuits that Control Compulsive Sucrose Seeking. *Cell*, 160(3):528–541.

Nieh, E. H., Vander Weele, C. M., Matthews, G. A., Presbrey, K. N., Wichmann, R., Leppla, C. A., Izadmehr, E. M., and Tye, K. M. (2016). Inhibitory Input from the Lateral Hypothalamus to the Ventral Tegmental Area Disinhibits Dopamine Neurons and Promotes Behavioral Activation. *Neuron*, 90(6):1286–1298.

Noble, E. E., Wang, Z., Liu, C. M., Davis, E. A., Suarez, A. N., Stein, L. M., Tsan, L., Terrill, S. J., Hsu, T. M., Jung, A.-H., Raycraft, L. M., Hahn, J. D., Darvas, M., Cortella, A. M., Schier, L. A., Johnson, A. W., Hayes, M. R., Holschneider, D. P., and Kanoski, S. E. (2019). Hypothalamus-hippocampus circuitry regulates impulsivity via melanin-concentrating hormone. *Nature communications*, 10(1):4923.

Oh, S. W., Harris, J. A., Ng, L., Winslow, B., Cain, N., Mihalas, S., Wang, Q., Lau, C., Kuan, L., Henry, A. M., Mortrud, M. T., Ouellette, B., Nguyen, T. N., Sorensen, S. A., Slaughterbeck, C. R., Wakeman, W., Li, Y., Feng, D., Ho, A., Nicholas, E., Hirokawa, K. E., Bohn, P., Joines, K. M., Peng, H., Hawrylycz, M. J., Phillips, J. W., Hohmann, J. G., Wohnoutka, P., Gerfen, C. R., Koch, C., Bernard, A., Dang, C., Jones, A. R., and Zeng, H. (2014). A mesoscale connectome of the mouse brain. *Nature*, 508(7495):207–214.

O'Keefe, J. and Dostrovsky, J. (1971). The hippocampus as a spatial map. Preliminary evidence from unit activity in the freely-moving rat. *Brain Research*, 34(1):171 – 175.

O'Keefe, J. and Nadel, L. (1978). *The hippocampus as a cognitive map*. Oxford: Clarendon Press.

Okuyama, T., Kitamura, T., Roy, D. S., Itohara, S., and Tonegawa, S. (2016). Ventral CA1 neurons store social memory. *Science*, 353(6307):1536.

Olds, J. (1958). Self-stimulation of the brain; its use to study local effects of hunger, sex, and drugs. *Science*, 127(3294):315–324.

O'Neil, E. B., Newsome, R. N., Li, I. H. N., Thavabalasingam, S., Ito, R., and Lee, A. C. H. (2015). Examining the Role of the Human Hippocampus in Approach-Avoidance Decision Making Using a Novel Conflict Paradigm and Multivariate Functional Magnetic Resonance Imaging. *The Journal of neuroscience : the official journal of the Society for Neuroscience*, 35(45):15039–15049.

Otis, J. M., Zhu, M., Namboodiri, V. M. K., Cook, C. A., Kosyk, O., Matan, A. M., Ying, R., Hashikawa, Y., Hashikawa, K., Trujillo-Pisanty, I., Guo, J., Ung, R. L., Rodriguez-Romaguera, J., Anton, E. S., and Stuber, G. D. (2019). Paraventricular Thalamus Projection Neurons Integrate Cortical and Hypothalamic Signals for Cue-Reward Processing. *Neuron*, 103(3):423–431.e4.

O'Connor, E. C., Kremer, Y., Lefort, S., Harada, M., Pascoli, V., Rohner, C., and Lüscher, C. (2015). Accumbal D1R Neurons Projecting to Lateral Hypothalamus Authorize Feeding. *Neuron*, 88(3):553–564.

Padilla-Coreano, N., Bolkan, S. S., Pierce, G. M., Blackman, D. R., Hardin, W. D., Garcia-Garcia, A. L., Spellman, T. J., and Gordon, J. A. (2016). Direct Ventral Hippocampal-Prefrontal Input Is Required for Anxiety-Related Neural Activity and Behavior. *Neuron*, 89(4):857–866.

Patel, J. M., Swanson, J., Ung, K., Herman, A., Hanson, E., Ortiz-Guzman, J., Selever, J., Tong, Q., and Arenkiel, B. R. (2019). Sensory perception drives food avoidance through excitatory basal forebrain circuits. *eLife*, 8:5163.

Paton, J. J., Belova, M. A., Morrison, S. E., and Salzman, C. D. (2006). The primate amygdala represents the positive and negative value of visual stimuli during learning. *Nature*, 439(7078):865–870.

Paton, J. J. and Buonomano, D. V. (2018). The Neural Basis of Timing: Distributed Mechanisms for Diverse Functions. *Neuron*, 98(4):687–705.

Patriarchi, T., Cho, J. R., Merten, K., Howe, M. W., Marley, A., Xiong, W.-H., Folk, R. W., Broussard, G. J., Liang, R., Jang, M. J., Zhong, H., Dombeck, D., von Zastrow, M., Nimmerjahn, A., Gradinaru, V., Williams, J. T., and Tian, L. (2018). Ultrafast neuronal imaging of dopamine dynamics with designed genetically encoded sensors. *Science*, 360(6396):eaat4422.

Pennartz, C. M. A., Ito, R., Verschure, P. F. M. J., Battaglia, F. P., and Robbins, T. W. (2011a). The hippocampalâ€“striatal axis in learning, prediction and goal-directed behavior. *Trends in Neurosciences*, 34(10):548–559.

Pennartz, C. M. A., Verschure, P. F. M. J., Battaglia, F. P., and Robbins, T. W. (2011b). The hippocampal-striatal axis in learning, prediction and goal-directed behavior. *Trends in neurosciences*, 34(10):548–559.

Petersen, P. S., Woldbye, D. P. D., Madsen, A. N., Egerod, K. L., Jin, C., Lang, M., Rasmussen, M., Beck-Sickinger, A. G., and Holst, B. (2009). In vivo characterization of high Basal signaling from the ghrelin receptor. *Endocrinology*, 150(11):4920–4930.

Petreanu, L., Huber, D., Sobczyk, A., and Svoboda, K. (2007). Channelrhodopsin-2–assisted circuit mapping of long-range callosal projections. *Nature Neuroscience*, 10(5):663–668.

Petrovich, G. D., Canteras, N. S., and Swanson, L. W. (2001). Combinatorial amygdalar inputs to hippocampal domains and hypothalamic behavior systems. *Brain research. Brain research reviews*, 38(1-2):247–289.

Pfeiffer, B. E. and Foster, D. J. (2013). Hippocampal place-cell sequences depict future paths to remembered goals. *Nature*, 497(7447):74–79.

Reardon, T. R., Murray, A. J., Turi, G. F., Wirblich, C., Croce, K. R., Schnell, M. J., Jessell, T. M., and Losonczy, A. (2016). Rabies Virus CVS-N2cΔG Strain Enhances Retrograde Synaptic Transfer and Neuronal Viability. *Neuron*, 89(4):711–724.

Reed, S. J., Lafferty, C. K., Mendoza, J. A., Yang, A. K., Davidson, T. J., Grosenick, L., Deisseroth, K., and Britt, J. P. (2018). Coordinated Reductions in Excitatory Input to the Nucleus Accumbens Underlie Food Consumption. *Neuron*.

Ren, J., Friedmann, D., Xiong, J., Liu, C. D., Ferguson, B. R., Weerakkody, T., DeLoach, K. E., Ran, C., Pun, A., Sun, Y., Weissbourd, B., Neve, R. L., Huguenard, J., Horowitz, M. A., and Luo, L. (2018). Anatomically Defined and Functionally Distinct Dorsal Raphe Serotonin Sub-systems. *Cell*, 175(2):472–487.e20.

Reppucci, C. J. and Petrovich, G. D. (2016). Organization of connections between the amygdala, medial prefrontal cortex, and lateral hypothalamus: a single and double retrograde tracing study in rats. *Brain structure & function*, 221(6):2937–2962.

Resendez, S. L., Jennings, J. H., Ung, R. L., Namboodiri, V. M. K., Zhou, Z. C., Otis, J. M., Nomura, H., McHenry, J. A., Kosyk, O., and Stuber, G. D. (2016). Visualization of cortical, subcortical and deep brain neural circuit dynamics during naturalistic mammalian behavior with head-mounted microscopes and chronically implanted lenses. *Nature Protocols*, 11(3):566–597.

Rhea, E. M., Salameh, T. S., Gray, S., Niu, J., Banks, W. A., and Tong, J. (2018). Ghrelin transport across the blood-brain barrier can occur independently of the growth hormone secretagogue receptor. *Molecular Metabolism*, 18:88–96.

Riaz, S., Schumacher, A., Sivagurunathan, S., Van Der Meer, M., and Ito, R. (2017). Ventral, but not dorsal, hippocampus inactivation impairs reward memory expression and retrieval in contexts defined by proximal cues. *Hippocampus*, 27(7):822–836.

Ribeiro, L. F., Catarino, T., Santos, S. D., Benoist, M., van Leeuwen, J. F., Esteban, J. A., and Carvalho, A. L. (2014). Ghrelin triggers the synaptic incorporation of AMPA receptors in the hippocampus. *Proceedings of the National Academy of Sciences of the United States of America*, 111(1):E149–58.

Riley, J. N. and Moore, R. Y. (1981). Diencephalic and brainstem afferents to the hippocampal formation of the rat. *Brain research bulletin*, 6(5):437–444.

Risold, P. Y. and Swanson, L. W. (1996). Structural evidence for functional domains in the rat hippocampus. *Science (New York, N.Y.)*, 272(5267):1484–1486.

Roitman, M. F., Wheeler, R. A., and Carelli, R. M. (2005). Nucleus accumbens neurons are innately tuned for rewarding and aversive taste stimuli, encode their predictors, and are linked to motor output. *Neuron*, 45(4):587–597.

Rolls, E. T. (2013). The mechanisms for pattern completion and pattern separation in the hippocampus. *Frontiers in Systems Neuroscience*, 7:74.

Rosas, J. M., Todd, T. P., and Bouton, M. E. (2013). Context change and associative learning. *Wiley interdisciplinary reviews. Cognitive science*, 4(3):237–244.

Rosen, Z. B., Cheung, S., and Siegelbaum, S. A. (2015). Midbrain dopamine

neurons bidirectionally regulate CA3-CA1 synaptic drive. *Nature Neuroscience*, 18(12):1763–1771.

Rossi, M. A., Basiri, M. L., McHenry, J. A., Kosyk, O., Otis, J. M., van den Munkhof, H. E., Bryois, J., Hübel, C., Breen, G., Guo, W., Bulik, C. M., Sullivan, P. F., and Stuber, G. D. (2019). Obesity remodels activity and transcriptional state of a lateral hypothalamic brake on feeding. *Science*, 364(6447):1271.

Roy, D. S., Kitamura, T., Okuyama, T., Ogawa, S. K., Sun, C., Obata, Y., Yoshiki, A., and Tonegawa, S. (2017). Distinct Neural Circuits for the Formation and Retrieval of Episodic Memories. pages 1–33.

Royer, S., Sirota, A., Patel, J., and Buzsáki, G. (2010). Distinct representations and theta dynamics in dorsal and ventral hippocampus. *The Journal of neuroscience : the official journal of the Society for Neuroscience*, 30(5):1777–1787.

Rozin, P., Dow, S., Moscovitch, M., and Rajaram, S. (1998). What Causes Humans to Begin and End a Meal? A Role for Memory for What Has Been Eaten, as Evidenced by a Study of Multiple Meal Eating in Amnesic Patients. *Psychological Science*, 9(5):392–396.

Sakata, I., Nakano, Y., Osborne-Lawrence, S., Rovinsky, S. A., Lee, C. E., Perelló, M., Anderson, J. G., Coppari, R., Xiao, G., Lowell, B. B., Elmquist, J. K., and Zigman, J. M. (2009). Characterization of a novel ghrelin cell reporter mouse. *Regulatory Peptides*, 155(1-3):91–98.

Sakimoto, Y., Mizuno, J., Kida, H., Kamiya, Y., Ono, Y., and Mitsushima, D. (2019). Learning Promotes Subfield-Specific Synaptic Diversity in Hippocampal CA1 Neurons. *Cerebral cortex (New York, N.Y. : 1991)*, 29(5):2183–2195.

Salay, L. D., Ishiko, N., and Huberman, A. D. (2018). A midline thalamic circuit determines reactions to visual threat. *Nature*, 557(7704):183–189.

Saper, C. B., Chou, T. C., and Elmquist, J. K. (2002). The need to feed: homeostatic and hedonic control of eating. *Neuron*, 36(2):199–211.

Schaeffer, M., Langlet, F., Lafont, C., Molino, F., Hodson, D. J., Roux, T., Lamarque, L., Verdié, P., Bourrier, E., Dehouck, B., Banères, J.-L., Martinez, J., Méry, P.-F.,

Marie, J., Trinquet, E., Fehrentz, J.-A., Prévot, V., and Mollard, P. (2013). Rapid sensing of circulating ghrelin by hypothalamic appetite-modifying neurons. *Proceedings of the National Academy of Sciences of the United States of America*, 110(4):1512–1517.

Schellekens, H., De Francesco, P. N., Kandil, D., Theeuwes, W. F., McCarthy, T., van Oeffelen, W. E. P. A., Perelló, M., Giblin, L., Dinan, T. G., and Cryan, J. F. (2015). Ghrelin's Orexigenic Effect Is Modulated via a Serotonin 2C Receptor Interaction. *ACS Chemical Neuroscience*, 6(7):1186–1197. Publisher: American Chemical Society.

Schepers, S. T. and Bouton, M. E. (2017). Hunger as a Context: Food Seeking That Is Inhibited During Hunger Can Renew in the Context of Satiety. *Psychological Science*, 28(11):1640–1648.

Schumacher, A., Vlassov, E., and Ito, R. (2015). The ventral hippocampus, but not the dorsal hippocampus is critical for learned approach-avoidance decision making. *Hippocampus*, 26(4):530–542.

Schwarz, L. A., Miyamichi, K., Gao, X. J., Beier, K. T., Weissbourd, B., DeLoach, K. E., Ren, J., Ibanes, S., Malenka, R. C., Kremer, E. J., and Luo, L. (2015). Viral-genetic tracing of the input–output organization of a central noradrenaline circuit. *Nature*, 524(7563):88–92.

Scoville, W. B. and Milner, B. (1957). *Loss of recent memory after bilateral hippocampal lesions*, volume 12 of *Patient H. M.* American Psychiatric Publishing.

Scudder, S. L., Baimel, C., Macdonald, E. E., and Carter, A. G. (2018). Hippocampal-Evoked Feedforward Inhibition in the Nucleus Accumbens. *Journal of Neuroscience*, 38(42):9091–9104.

Shi, L., Bian, X., Qu, Z., Ma, Z., Zhou, Y., Wang, K., Jiang, H., and Xie, J. (2013). Peptide hormone ghrelin enhances neuronal excitability by inhibition of Kv7/KCNQ channels. *Nature Communications*, 4(1):1435–12.

Simmons, W. K., Burrows, K., Avery, J. A., Kerr, K. L., Bodurka, J., Savage, C. R., and Drevets, W. C. (2016). Depression-Related Increases and Decreases in

Appetite: Dissociable Patterns of Aberrant Activity in Reward and Interoceptive Neurocircuitry. *American Journal of Psychiatry*, 173(4):418–428.

Simon, J. J., Wetzel, A., Sinno, M. H., Skunde, M., Bendszus, M., Preissl, H., Enck, P., Herzog, W., and Friederich, H.-C. (2017). Integration of homeostatic signaling and food reward processing in the human brain. *JCI insight*, 2(15):e92970.

Skibicka, K. P., Hansson, C., Alvarez-Crespo, M., Friberg, P. A., and Dickson, S. L. (2011). Ghrelin directly targets the ventral tegmental area to increase food motivation. *Neuroscience*, 180:129–137.

Skibicka, K. P. and Kanoski, S. E. (2016). Food Hedonics. In *Neuroendocrinology of Appetite*, pages 90–111. John Wiley & Sons, Ltd, Chichester, UK.

Smith, J. B., Klug, J. R., Ross, D. L., Howard, C. D., Hollon, N. G., Ko, V. I., Hoffman, H., Callaway, E. M., Gerfen, C. R., and Jin, X. (2016). Genetic-Based Dissection Unveils the Inputs and Outputs of Striatal Patch and Matrix Compartments. *Neuron*, 91(5):1069–1084.

Soares, S., Atallah, B. V., and Paton, J. J. (2016). Midbrain dopamine neurons control judgment of time. *Science*, 354(6317):1273.

Soltesz, I. and Losonczy, A. (2018). CA1 pyramidal cell diversity enabling parallel information processing in the hippocampus. *Scientific Reports*, pages 1–10.

Soto, M., Cai, W., Konishi, M., and Kahn, C. R. (2019). Insulin signaling in the hippocampus and amygdala regulates metabolism and neurobehavior. *Proceedings of the National Academy of Sciences of the United States of America*, 116(13):6379–6384.

Stachenfeld, K. L., Botvinick, M. M., and Gershman, S. J. (2017). The hippocampus as a predictive map. *Scientific Reports*, pages 1–22.

Sterling, P. (2012). Allostasis: a model of predictive regulation. *Physiology & Behavior*, 106(1):5–15.

Strange, B. A., Witter, M. P., Lein, E. S., and Moser, E. I. (2014). Functional organization of the hippocampal longitudinal axis. *Scientific Reports*, 15(10):655–669.

Stratford, T. R. and Kelley, A. E. (1997). GABA in the nucleus accumbens shell participates in the central regulation of feeding behavior. *Journal of Neuroscience*, 17(11):4434–4440.

Stratford, T. R. and Wirtshafter, D. (2013). Injections of muscimol into the paraventricular thalamic nucleus, but not mediodorsal thalamic nuclei, induce feeding in rats. *Brain research*, 1490:128–133.

Stuber, G. D. and Wise, R. A. (2016). Lateral hypothalamic circuits for feeding and reward. *Nature Neuroscience*, 19(2):198–205.

Suarez, A. N., Liu, C. M., Cortella, A. M., Noble, E. E., and Kanoski, S. E. (2020). Ghrelin and Orexin Interact to Increase Meal Size Through a Descending Hippocampus to Hindbrain Signaling Pathway. *Biological Psychiatry*, 87(11):1001–1011.

Suarez, A. N., Noble, E. E., and Kanoski, S. E. (2019). Regulation of Memory Function by Feeding-Relevant Biological Systems: Following the Breadcrumbs to the Hippocampus. *Frontiers in Molecular Neuroscience*, 12:101.

Sun, Q., Li, X., Ren, M., Zhao, M., Zhong, Q., Ren, Y., Luo, P., Ni, H., Zhang, X., Zhang, C., Yuan, J., Li, A., Luo, M., Gong, H., and Luo, Q. (2019). A whole-brain map of long-range inputs to GABAergic interneurons in the mouse medial prefrontal cortex. *Nature Neuroscience*, 22(8):1357–1370.

Sun, Y., Butte, N. F., Garcia, J. M., and Smith, R. G. (2008). Characterization of adult ghrelin and ghrelin receptor knockout mice under positive and negative energy balance. *Endocrinology*, 149(2):843–850.

Sun, Y., Nguyen, A. Q., Nguyen, J. P., Le, L., Saur, D., Choi, J., Callaway, E. M., and Xu, X. (2014). Cell-Type-Specific Circuit Connectivity of Hippocampal CA1 Revealed through Cre-Dependent Rabies Tracing. *Cell Reports*, 7(1):269–280.

Swanson, L. W. and Cowan, W. (1975). Hippocampo-hypothalamic connections: origin in subicular cortex, not ammon's horn. 189(4199):303–304.

Sweeney, P. and Yang, Y. (2015). An excitatory ventral hippocampus to lateral septum circuit that suppresses feeding. *Nature Communications*, 6:1–11.

Symmonds, M., Emmanuel, J. J., Drew, M. E., Batterham, R. L., and Dolan, R. J. (2010). Metabolic state alters economic decision making under risk in humans. *PLoS ONE*, 5(6):e11090.

Taha, S. A. and Fields, H. L. (2006). Inhibitions of nucleus accumbens neurons encode a gating signal for reward-directed behavior. *The Journal of neuroscience : the official journal of the Society for Neuroscience*, 26(1):217–222. Publisher: Society for Neuroscience.

Taube, J. S., Muller, R. U., and Ranck, J. B. (1990). Head-direction cells recorded from the postsubiculum in freely moving rats. I. Description and quantitative analysis. *The Journal of neuroscience : the official journal of the Society for Neuroscience*, 10(2):420–435.

Tervo, D. G. R., Hwang, B.-Y., Viswanathan, S., Gaj, T., Lavzin, M., Ritola, K. D., Lindo, S., Michael, S., Kuleshova, E., Ojala, D., Huang, C.-C., Gerfen, C. R., Schiller, J., Dudman, J. T., Hantman, A. W., Looger, L. L., Schaffer, D. V., and Karpova, A. Y. (2016). A Designer AAV Variant Permits Efficient Retrograde Access to Projection Neurons. *Neuron*, 92(2):372–382.

Tian, J., Guo, L., Sui, S., Driskill, C., Phensy, A., Wang, Q., Gauba, E., Zigman, J. M., Swerdlow, R. H., Kroener, S., and Du, H. (2019). Disrupted hippocampal growth hormone secretagogue receptor 1 interaction with dopamine receptor D1 plays a role in Alzheimer's disease. *Science translational medicine*, 11(505):eaav6278.

Toates, F. M. (1981). The control of ingestive behaviour by internal and external stimuli–a theoretical review. *Appetite*, 2(1):35–50.

Trask, S., Thrailkill, E. A., and Bouton, M. E. (2017). Occasion setting, inhibition, and the contextual control of extinction in Pavlovian and instrumental (operant) learning. *Behavioural processes*, 137:64–72.

Trouche, S., Koren, V., Doig, N. M., Ellender, T. J., El-Gaby, M., Lopes-dos Santos, V., Reeve, H. M., Perestenko, P. V., Garas, F. N., Magill, P. J., Sharott, A., and Dupret, D. (2019). A Hippocampus-Accumbens Tripartite Neuronal Motif Guides Appetitive Memory in Space. *Cell*.

Tschöp, M., Smiley, D. L., and Heiman, M. L. (2000). Ghrelin induces adiposity in rodents. *Nature*, 407(6806):908–913.

Tse, D., Langston, R. F., Kakeyama, M., Bethus, I., Spooner, P. A., Wood, E. R., Witter, M. P., and Morris, R. G. M. (2007). Schemas and memory consolidation. *Science*, 316(5821):76–82.

Uchida, A., Zigman, J. M., and Perelló, M. (2013). Ghrelin and eating behavior: evidence and insights from genetically-modified mouse models. *Frontiers in neuroscience*, 7:121.

Valenstein, E. S., Cox, V. C., and Kakolewski, J. W. (1968). Modification of motivated behavior elicited by electrical stimulation of the hypothalamus. *Science*, 159(3819):1119–1121.

van der Meer, M. A. A. and Redish, A. D. (2011). Ventral striatum: a critical look at models of learning and evaluation. *Current Opinion in Neurobiology*, 21(3):387–392.

van Groen, T., Miettinen, P., and Kadish, I. (2003). The entorhinal cortex of the mouse: organization of the projection to the hippocampal formation. *Hippocampus*, 13(1):133–149.

Vargha-Khadem, F., Gadian, D. G., Watkins, K. E., Connelly, A., Van Paesschen, W., and Mishkin, M. (1997). Differential effects of early hippocampal pathology on episodic and semantic memory. *Science*, 277(5324):376–380.

Vergnano, A. M., Ferrini, F., Salio, C., Lossi, L., Baratta, M., and Merighi, A. (2008). The gastrointestinal hormone ghrelin modulates inhibitory neurotransmission in deep laminae of mouse spinal cord dorsal horn. *Endocrinology*, 149(5):2306–2312.

Verhagen, L. A. W., Egecioglu, E., Luijendijk, M. C. M., Hillebrand, J. J. G., Adan, R. A. H., and Dickson, S. L. (2011). Acute and chronic suppression of the central ghrelin signaling system reveals a role in food anticipatory activity. *European Neuropsychopharmacology*, 21(5):384–392.

Vertes, R. P. (2006). Interactions among the medial prefrontal cortex, hippocampus and midline thalamus in emotional and cognitive processing in the rat. *Neuroscience*, 142(1):1–20.

Vikbladh, O. M., Meager, M. R., King, J., Blackmon, K., Devinsky, O., Shohamy, D., Burgess, N., and Daw, N. D. (2019). Hippocampal Contributions to Model-Based Planning and Spatial Memory. *Neuron*, 102(3):683–693.e4.

Vinogradova, O. S. (2001). Hippocampus as comparator: Role of the two input and two output systems of the hippocampus in selection and registration of information. *Hippocampus*, 11(5):578–598.

Voorn, P., Vanderschuren, L. J. M. J., Groenewegen, H. J., Robbins, T. W., and Pennartz, C. M. A. (2004). Putting a spin on the dorsal-ventral divide of the striatum. *Trends in Neurosciences*, 27(8):468–474.

Voss, J. L., Gonsalves, B. D., Federmeier, K. D., Tranel, D., and Cohen, N. J. (2011). Hippocampal brain-network coordination during volitional exploratory behavior enhances learning. *Nature neuroscience*, 14(1):115–120.

Walker, A. K., Ibia, I. E., and Zigman, J. M. (2012). Disruption of cue-potentiated feeding in mice with blocked ghrelin signaling. *Physiology & behavior*, 108:34–43.

Wall, N. R., De La Parra, M., Callaway, E. M., and Kreitzer, A. C. (2013). Differential innervation of direct- and indirect-pathway striatal projection neurons. *Neuron*, 79(2):347–360.

Wallner-Liebmann, S., Koschutnig, K., Reishofer, G., Sorantin, E., Blaschitz, B., Kruschitz, R., Unterrainer, H. F., Gasser, R., Freytag, F., Bauer-Denk, C., Schienle, A., Schäfer, A., and Mangge, H. (2010). Insulin and hippocampus activation in response to images of high-calorie food in normal weight and obese adolescents. *Obesity (Silver Spring, Md.)*, 18(8):1552–1557.

Wang, G.-J., Yang, J., Volkow, N. D., Telang, F., Ma, Y., Zhu, W., Wong, C. T., Tomasi, D., Thanos, P. K., and Fowler, J. S. (2006). Gastric stimulation in obese subjects activates the hippocampus and other regions involved in brain reward circuitry. *Proceedings of the National Academy of Sciences*, 103(42):15641–15645.

Wee, R. W. S. and MacAskill, A. F. (2020). Biased Connectivity of Brain-wide Inputs to Ventral Subiculum Output Neurons. *Cell Reports*, 30(11):3644–3654.e6.

Weiland, N. G., Orikasa, C., Hayashi, S., and McEwen, B. S. (1997). Distribution and hormone regulation of estrogen receptor immunoreactive cells in the hippocampus of male and female rats. *Journal of Comparative Neurology*, 388(4):603–612.

Weissbourd, B., Ren, J., DeLoach, K. E., Guenthner, C. J., Miyamichi, K., and Luo, L. (2014). Presynaptic Partners of Dorsal Raphe Serotonergic and GABAergic Neurons. *Neuron*, 83(3):645–662.

Wills, T. J., Lever, C., Cacucci, F., Burgess, N., and O'Keefe, J. (2005). Attractor dynamics in the hippocampal representation of the local environment. *Science*, 308(5723):873–876.

Wimmer, E. and Shohamy, D. (2012). Preference by Association: How Memory Mechanisms in the Hippocampus Bias Decisions. *Science*, 338(6104):267–270.

Winnubst, J., Bas, E., Ferreira, T. A., Wu, Z., Economo, M. N., Edson, P., Arthur, B. J., Bruns, C., Rokicki, K., Schauder, D., Olbris, D. J., Murphy, S. D., Ackerman, D. G., Arshadi, C., Baldwin, P., Blake, R., Elsayed, A., Hasan, M., Ramirez, D., Dos Santos, B., Weldon, M., Zafar, A., Dudman, J. T., Gerfen, C. R., Hantman, A. W., Korff, W., Sternson, S. M., Spruston, N., Svoboda, K., and Chandrashekar, J. (2019). Reconstruction of 1,000 Projection Neurons Reveals New Cell Types and Organization of Long-Range Connectivity in the Mouse Brain. *Cell*, 179(1):268–281.e13.

Wood, E. R., Dudchenko, P. A., and Eichenbaum, H. B. (1999). The global record of memory in hippocampal neuronal activity. *Nature*, 397(6720):613–616.

Woolley, C. S. (1998). Estrogen-mediated structural and functional synaptic plasticity in the female rat hippocampus. *Hormones and behavior*, 34(2):140–148.

Wren, A. M., Seal, L. J., Cohen, M. A., Brynes, A. E., Frost, G. S., Murphy, K. G., Dhillo, W. S., Ghatei, M. A., and Bloom, S. R. (2001). Ghrelin enhances appetite and increases food intake in humans. *The Journal of clinical endocrinology and metabolism*, 86(12):5992.

Wyss, J. M., Swanson, L. W., and Cowan, W. M. (1979). A study of subcortical afferents to the hippocampal formation in the rat. *Neuroscience*, 4(4):463–476.

Xu, C., Krabbe, S., Gründemann, J., Botta, P., Fadok, J. P., Osakada, F., Saur, D., Grewe, B. F., Schnitzer, M. J., Callaway, E. M., and Lüthi, A. (2016). Distinct Hippocampal Pathways Mediate Dissociable Roles of Context in Memory Retrieval. *Cell*, 167(4):961–972.e16.

Xu, W. and Südhof, T. C. (2013). A neural circuit for memory specificity and generalization. *Science*, 339(6125):1290–1295.

Yang, A. K., Mendoza, J. A., Lafferty, C. K., Lacroix, F., and Britt, J. P. (2019). Hippocampal Input to the Nucleus Accumbens Shell Enhances Food Palatability. *Biological Psychiatry*.

Yang, Y., Atasoy, D., Su, H. H., and Sternson, S. M. (2011). Hunger States Switch a Flip-Flop Memory Circuit via a Synaptic AMPK-Dependent Positive Feedback Loop. *Cell*, 146(6):992–1003.

Yiin, Y.-M., Ackroff, K., and Sclafani, A. (2005). Food deprivation enhances the expression but not acquisition of flavor acceptance conditioning in rats. *Appetite*, 45(2):152–160.

Yoon, T., Graham, L. K., and Kim, J. J. (2011). Hippocampal lesion effects on occasion setting by contextual and discrete stimuli. *Neurobiology of learning and memory*, 95(2):176–184.

Yoshida, K., Drew, M. R., Mimura, M., and Tanaka, K. F. (2019). Serotonin-mediated inhibition of ventral hippocampus is required for sustained goal-directed behavior. *Nature Neuroscience*, 422:1.

Yu, K., Ahrens, S., Zhang, X., Schiff, H., Ramakrishnan, C., Fenno, L. E., Deisseroth, K., Zhao, F., Luo, M.-H., Gong, L., He, M., Zhou, P., Paninski, L., and Li, B. (2017). The central amygdala controls learning in the lateral amygdala. *Scientific Reports*, pages 1–12.

Zeltser, L. M., Seeley, R. J., and Tschöp, M. H. (2012). Synaptic plasticity in neuronal circuits regulating energy balance. *Nature Neuroscience*, 15(10):1336–1342.

Zhang, X. and van den Pol, A. N. (2017). Rapid binge-like eating and body weight gain driven by zona incerta GABA neuron activation. *Science*, 356(6340):853–859.

Zhu, Y., Nachtrab, G., Keyes, P. C., Allen, W. E., Luo, L., and Chen, X. (2018). Dynamic salience processing in paraventricular thalamus gates associative learning. *Science*, 362(6413):423–429.

Zigman, J. M., Jones, J. E., Lee, C. E., Saper, C. B., and Elmquist, J. K. (2006). Expression of ghrelin receptor mRNA in the rat and the mouse brain. *Journal of Comparative Neurology*, 494(3):528–548.

Zimmerman, C. A., Leib, D. E., and Knight, Z. A. (2017). Neural circuits underlying thirst and fluid homeostasis. *Scientific Reports*, 18(8):459–469.

Ährlund Richter, S., Xuan, Y., van Lunteren, J. A., Kim, H., Ortiz, C., Pollak Dorocic, I., Meletis, K., and Carlén, M. (2019). A whole-brain atlas of monosynaptic input targeting four different cell types in the medial prefrontal cortex of the mouse. *Nature Neuroscience*, 22(4):657–668.

Ólafsdóttir, H. F., Barry, C., Saleem, A. B., Hassabis, D., and Spiers, H. J. (2015). Hippocampal place cells construct reward related sequences through unexplored space. *eLife*, 4:e06063.